The Influence of the Physical Characteristics of Particulate Materials on their Conveyability in Pneumatic Transport Systems

by

Svein Erlend Martinussen

A thesis submitted in partial fulfilment of the
requirements of the University of Greenwich
for the Degree of Doctor of Philosophy

The University of Greenwich

in collaboration with

Telemark Technological Research and Development Centre
and
Telemark College, Norway

December 1996

The Effect of the Physical Characteristics of Particulate Materials on their Conveyability in Pneumatic Transport Systems

Svein Erlend Martinussen

Abstract

The aim of the investigation has been to establish a link between the physical characteristics of particulate materials, measurable on small samples in a laboratory, and the conveyability of these materials in a pneumatic conveying line. The focus of the investigation has been on conveying velocity limits, and the problem has been approached by comparing own experimentally obtained values against existing models for the prediction of such limits. A quantitative analysis shows that the accuracy of these models range from 77% under prediction to 116% over prediction at certain operating conditions within the area in which they are claimed to be valid.

The pressure data obtained in the experimental investigation have been subjected to various methods of analysis to identify typical behaviour of the pressure fluctuations along the pipeline when changes in the mode of flow, or blockage, is approached. The results of this analysis show that the change from stratified flow (or partially settled suspension flow) to unstable flow, often also referred to as the saltation limit, is associated with the occurrence of coherent structures moving along the pipeline.

To investigate the possibility of applying a fluid dynamic model to understand these phenomena, experiments with wave propagation and damping have been carried out in a channel with fluidized powders. This investigation shows that the wave propagation velocity at large wave length to bed depth ratios for a fluidized powder is identical to that expected from theory on fluid dynamics. The fluid dynamic model is then applied to establish a model for the prediction of maximum obtainable feed rate of solids in a given pipeline. It is also used to establish a model to predict the limit of stable conveying, in suspended or partially suspended flow, based on the Kelvin Helmholz instability for stratified flow of liquids in closed pipelines. The models are purely mechanistic and require no empirical fitting.

Acknowledgements

It is my opinion that the co-operation between the Department of Powder Science and Technology at Telemark Technological Research and Development Centre, and the Wolfson Centre at the University of Greenwich, which has allowed me to change environment from time to time, is particularly positive for the creativity that is needed when doing research.

A special thanks to my supervisors: Prof. Sunil R. deSilva, for employing me in the first instance and for providing experienced every day guidance. Dr. Stephen R. Woodhead, for friendly help and advice, and asking critical questions when necessary. Prof. Alan R. Reed for accurate guidance when time allowed.

I would also like to express my thanks :
To my colleagues at POSTEC and the Wolfson Centre, for all help and support during the work.

To Prof. Kim Esbensen, who introduced me to chemometric data analysis, and to the students carrying out final year projects at Telemark College, Vibeke Yström, Paul Erling Lia and Arild Saudland, for their inquisitive attitude, and producing interesting results with relevance to pneumatic conveying, which I have freely used in my work.

To students carrying out their industrial practice at POSTEC : Hans Toebes for help with the design of the mechanical return system of the test rig, Parminder Singh Nandhra for help with characterisation and conveying tests, and Mitsuhiro Wada for design of the wave tank and help with test work.

To the Norwegian Research Council and members of the POSTEC programme for financial support, and to Telemark College for providing me access to their facilities.

Til Anne, Mari og Eva,
Ljosa i mitt liv, og hjarto i mitt hjarta.

Author's Note

All of the work in this thesis is the sole and original work of the author, except where stated otherwise by acknowledgement or reference.

Table of Contents

Nomenclature

a	Amplitude for surface wave.
A	Pipeline cross section.
c	Surface wave propagation velocity.
C_v	Volume concentration.
d	Particle diameter.
D	Pipeline diameter.
d_p	Particle diameter.
f	Frequency of surface wave.
Fr	Froude number.
f_r	Wall friction factor.
F_{xy}	Fourier transform of cross correlation function.
g	Gravitational acceleration.
h	Bed depth.
K	Correction factor for the flow of solids into the sending tank.
p_1	Pressure at the beginning of the pipeline.
p_L	Pressure in the air supply.
p_N	$1.013 \cdot 10^5$ Pa.
R	Gas constant 286.94 J/(kg K).
R_p	Particle Reynolds number.
R_{xy}	Cross correlation function.
s_Δ	Parameter for ratio between saltation velocities and particle diameters.
T_N	273.15 K.
u_0	Saltation velocity for single particle.
u_0^*	Friction velocity at infinite dilution.
u_c^*	Friction velocity at minimum conveying conditions.
u_{sm}	Superficial air velocity at minimum conveying conditions.
u_{sps}	Superficial air velocity at the limit of stable plug or slug flow.
u_{spu}	Superficial air velocity at minimum pickup conditions.
u_{ss}	Superficial air velocity at saltation.
u_t	Terminal velocity of a free falling particle.
v_s	Superficial air velocity.

v_{xy}	Velocity from cross correlation.
$\dot{V}_{aL}$	Volumetric flow in the air supply.
$\dot{V}_{aN}$	Volumetric flow of air at normal conditions.
$\dot{V}_{a1}$	Volumetric flow of air at the beginning of the pipeline.
$\dot{V}_{s}$	Volumetric flow of solids.
W	The total wave energy per unit surface area of a surface wave.
W'	Time derivative of the total wave energy per unit surface area for a surface wave.
Δt	Time delay of phase information.
ε	Voidage.
η	Apparent viscosity.
θ_{xy}	Phase information of Fourier transform of cross correlation function.
λ	Mean free path / Wave length.
μ	Solids loading ratio.
ν	Kinematic viscosity.
ρ	Density of the suspension / density of fluid.
ρ_a	Gas density.
ρ_p	Particle density.
ρ_s	Solid particle density.
Φ	Flux of solids.
ϕ	Volume fraction of solids.

$Index_b$	Bulk property of the powder.
$Index_g$	Property of the gas.
$Index_L$	Property of the liquid.

1. Introduction

This research program has been undertaken at HiT (Telemark College, Department of Technology) and Telemark Technological Research and Development Centre, in collaboration with the University of Greenwich. The project has mainly been experimental in nature, and the aim of the investigation has been to establish a link between the physical characteristics of a particulate material, measurable on small samples in a laboratory, and the conveyability of the material in a pneumatic conveying line.

The flow in pneumatic transport systems is immensely complex. Unlike single phase systems (gas and liquid) particulate materials frequently are composed of entities which may have sizes ranging over several orders of magnitude. Current models for simulating such systems, by means of computers, resort to simplifying this to a small number of species of particles with different size, that may be viewed as separate "phases" in a multi phase system [1]. For certain materials encountered in "real life" this may be a very coarse simplification. One may hope that the "phases" are chosen so that each of them represent size classes that dominate the behaviour of the flow. Frequently the size classes are lumped together and called the disperse phase.

Several factors therefore have to be considered when investigating the conveyability of particulate materials. First of all it is necessary to define what is meant by conveyability. It is also necessary to consider which mechanisms influence the single particle and the collective behaviour of the material transported in an air flow. Furthermore it is desirable to determine which physical characteristics of the material influence these mechanisms

In the summary of the minutes of the first workshop-meeting on pneumatic conveying held in Karlsruhe in 1991 [2] questions regarding various aspects of conveyability are raised.

- Are there limitations in the conveying mode due to powder characteristics?
- Is there a limitation in the mass flow rate for different powders?
- Can pressure gradients be estimated on the basis of powder characteristics?

- What is the minimum conveying velocity for fine materials?

These questions are all directly associated with conveyability. If the mode of flow is not suitable (for reasons of stability in the mass flow), the necessary flow rate can not be obtained, the pressure gradient is too high for the air supply with the given pipe length or, the air velocity falls below the minimum velocity, this has direct influence on the regularity of the transport of material in the pneumatic conveying pipeline. These aspects can be quantified in the form of a conveying characteristic, which provides a relationship between the pressure gradient, the mass flow of solids, and the conveying velocity. Other aspects of conveyability such as the explosivity, the abrasivity, or the cohesivity of the material may also be considered. But these aspects are difficult to incorporate into design equations for pneumatic conveying equipment, although such aspects may be investigated in separate tests. In this work, the prediction of minimum conveying velocities, based on material characteristics forms the main subject of the investigation.

The motivation for starting the work has been to enable evaluation, and improvement, of existing models for predicting pneumatic transport system performance. The design of pneumatic conveying systems is not only subject to the risk of under-dimensioning with regard to capacity, as for gas or liquid flow systems, it is also subject to the risk of total failure in the form of blockage. As will be shown in this thesis, the current state of the art in engineering formulae does not allow safe design to be carried out. Therefore the design of pneumatic conveying systems is, at present, largely based on experimentally obtained data, in the form of conveying characteristics, displaying the relation between mass flow of solids, air velocity and pressure drop for a given material. Obtaining a conveying characteristic is a time consuming procedure. The possibility of obtaining usable models for computing the design parameters from laboratory test data of the characteristic properties of the material transported, is therefore a major incitement for the work.

The existing design equations for pneumatic conveying systems can be divided into two groups dealing with pressure drop computations and conveying limits respectively. A lot of work has been, and is being, carried out on the prediction of pressure drops in pneumatic conveying pipelines. It has therefore been chosen to focus on conveying limits specifically, and the limit of stable conveying in suspended or partially suspended flow in

particular. Both types of design equations are required to enable the design of a pneumatic conveying system. The conveying limit prediction is dependent on the start pressure in the pipeline, and the pressure drop depends on the conveying velocity chosen. The solution of the set of equations therefore results in an iterative process. Accurate prediction of the conveying limit is particularly important in that it enables the evaluation of the performance of existing transport systems to promote more economical operation by adjusting the air flow.

The approach taken in this investigation has been to carry out an extensive literature survey on minimum conveying velocity in horizontal pneumatic transport. Thereafter the main focus of the research program was on obtaining data for the seven different materials (polyethylene pellets, rape seed, sand, PVC granules, alumina, micronized dolomite and cement) included in the investigation. A series of measurements were then made to identify minimum conveying conditions for these seven materials. To eliminate the effect of pipeline geometry, these investigations were carried out in a straight horizontal pipeline with no flow hindrances. Several kinds of data analysis have been used to identify the nature of the mechanisms that govern the change in mode of flow, or blockage. This was considered to be necessary to improve modelling of the phenomena, and to identify the factors that influence the conveying limits of a material.

2. A Review of the Influence of Material Characteristics and Solids Loading Ratio in Current Methods for Predicting Conveying Limits.

This chapter gives a review of the current state of the art for prediction of conveying limits in pneumatic transport systems. Because of the variety in concepts and approaches towards the problem of predicting conveying limits that can be found in literature about the topic, it has been found necessary, initially in the chapter, to discuss a few basic concepts. The review of existing models is presented thereafter.

2.1 Discussion of Some Important Aspects of Two-Phase Gas-Solids Flow

A scientific description of two-phase gas-solids flow was first presented by Bagnold [3] in an attempt to understand the physics of blowing desert sand. Similar theory is used to understand the behaviour of falling and drifting snow [4], as well as transportation of dust particles in the atmosphere [5]. Technical applications of two-phase gas-solids flow in pneumatic transport, ventilation and dust prevention, have created a need for accurate design equations for such flow in pipelines. The early works on two-phase gas-solids flow, such as those of Zenz [6] and Thomas[7], rely heavily on theories for single particle movement in gases, such as Newtonian drag and Magnus force due to rotation, when mechanisms influencing the flow of solids are discussed. Very few works have been found that incorporate the collective behaviour of the suspension of particles, which becomes increasingly important at higher concentrations of solids.

In the remaining part of section 2.1 the influence of concentration or solids loading ratio will be discussed, to enable quantification of when single particle behaviour is dominant for gas-solids flow.

2.1.1 Single Particle Versus Collective Behaviour of Particulate Materials

As mentioned above, a good indication of the relative dominance of single particle behaviour and collective behaviour can be found by considering the concentration of solid particles in the suspension. As a first approximation it is possible to assume only one size

class of particles to be found in the suspension. The volumetric concentration in the pipeline can be expressed as:

$$C_V = \frac{V_s}{V_a} = \frac{\dot{V}_s \Delta t_s}{\dot{V}_a \Delta t_a} = \frac{\dot{V}_s L v_a}{\dot{V}_a L v_s} = \frac{\dot{V}_s \rho_s v_a \rho_s}{\dot{V}_a \rho_a v_s \rho_a} \cdot \frac{\rho_a}{\rho_s} = \frac{\dot{m}_s}{\dot{m}_a} \frac{v_a \rho_a}{v_s \rho_s}$$

At no-slip conditions between particles and air this gives:

$$C_V = \mu \frac{\rho_a}{\rho_s}$$

Where the variables are defined as:

C_V	Volumetric concentration of solids.
μ	Solids loading ratio.
ρ_a , ρ_s	Air and particle density.
L	Pipeline length.
Δt_a, Δt_s	Time in the pipeline for air and particles.
v_a, v_s	Velocity of air and particles in the pipeline.
$\dot{m}_a$, $\dot{m}_s$	Mass flow rate of air and solids.
V_a, V_s	Volume occupied in the pipeline by air and solids.
$\dot{V}_a$, $\dot{V}_s$	Volumetric flowrate of air and solids.

The volumetric concentration can also be found by determining the volume that a particle, that moves freely in the gas without colliding with another particle, traces in relation to its own volume [8]. As one can see from Figure 2.1 the volumetric concentration is then expressed as:

$$C_V = \frac{4/3\pi(d/2)^3}{\lambda\pi(d)^2} = \frac{d}{6\lambda}$$

Where the variables are defined as:

λ	Mean free path.	d	Particle diameter.

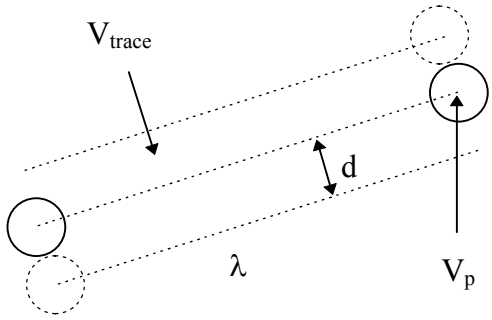

Figure 2.1 Effective volume traced by a particle travelling the mean free distance, in relation to its own volume.

Combining these equations gives an expression for the mean free path.

$$\lambda = \frac{d\rho_s}{6\mu\rho_a}$$

This can now be used as a criterion to determine whether particle-particle interactions are important or not. When particles on the average move a distance that is longer than the cross section of the pipeline without colliding (λ>D), the individual particle trajectory will mainly be that of a single particle moving through the pipeline. In an inertial system following the average axial velocity of a single particle, the particle will bounce on the pipeline wall and be subject to velocity fluctuations in the axial, tangential and radial directions. In this order of magnitude estimate, no slip between air and particles in the axial direction has been assumed. If one then, for simplicity, assumes that the velocity distribution is isotropic in the axial and radial directions, and neglecting the tangential component, one can use the superficial air velocity and the pipeline diameter directly in the estimate. Under the given assumptions collective effects will be negligible and single particle behaviour will be dominant when the solids loading ratio is lower than:

$$\mu < \frac{d\rho_s}{6D\rho_a} \tag{2.1}$$

For most operating conditions in pneumatic conveying equipment this is not the case. There are, of course, differences between materials. A fine material like alumina, with a particle density of 3399kg/m^3, and an average particle diameter of 87μm, will have a limiting solids loading ratio of 0.8 at atmospheric conditions in a 50mm diameter pipeline. A coarse material like polyethylene pellets, with a particle density of 913kg/m^3, and an average particle diameter of 3700μm, will have a limiting solids loading ratio of 9.3 at atmospheric conditions in a 50mm diameter pipeline. When conveying through larger pipeline diameters, or at higher pressures, this solids loading limitation will decrease. The solids loading ratio will also decrease when a slip velocity larger than zero is considered. This means that single particle effects for most materials encountered in industry are dominant only at very low solids loading ratios. A summary of the limiting values for the materials in this test work is shown in Table 2.1.

Table 2.1 Limiting solids loading values for the materials included in the test work (at atmospheric conditions in a 50mm diameter pipeline).

Material tested	Particle density [kg/m3]	Mean particle size [μm]	Limiting value for solids loading ratio below which single particle effects are dominant
Polyethylene pellets	913	3667	9.3
Rape seed	1164	1650	5.3
Sand	2645	687	5.0
PVC granules	1414	472	1.9
Alumina	3399	87	0.8
Microdol 100	2865	91	0.7
Cement	3095	15	0.1

2.1.2 The Saltation Velocity Limit

The work by Bagnold [3] is frequently cited in papers dealing with conveying limits in pneumatic conveying systems. As one will see in the discussion of the different models

below, this is due to the fact that Bagnold was the first to define saltation in two-phase gas-solids flow. His definition is valid for flow of air and sand grains in open land. Saltation is, in this case, described by the jumping or bouncing motion of sand grains along the surface of the desert.

However, what is meant by saltation in a closed pipeline is not straightforward. As one will se later, most authors adopt a definition of the saltation velocity that implies that the material or particles starts to fall out of suspension (or stops jumping into suspension) and a layer forms. This is contradictory to Bagnold's original definition [3] where the layer of solids is a requirement for saltated flow, and where saltation starts when some particles starts to jump.

Suspension flow is defined by Mainwaring and Reed [9] as all modes of flow above the limit where a layer forms. Other authors [6,10,11,12] also adopt a definition where the saltation limit is where a layer forms. It seems more appropriate to adopt a definition where the saltation limit is where the saltation stops, which would be more in accordance with Bagnolds initial definition [3]. In this case suspension flow, according to Mainwarings definition[9], would be, at least at low air flow rates where the solids are partially suspended, identical to saltation flow (where particles jump or bounce along a settled surface of solids).

It is clear from Bagnolds work [3] that the onset of saltation is triggered by sand grains hitting the settled sand and knocking new sand grains from the surface. In this case the concept of a single particle saltation velocity is meaningless, even though this concept is used by some authors [6,7] when investigating conveying limits.

At a given air velocity one would expect the feed rate of solids to influence the amount of saltating particles directly by introducing new ones. This means that the limiting air velocities when turning down the air flow of a saltating flow, and turning up the air flow over a layer of solids where no particles are in suspension, are not identical. This could explain the discrepancy between experimental data obtained in this investigation and the model of Cabrejos [12] for prediction of minimum pickup velocity, since he uses an

experimental setup where the air velocity is decreased by the gradual erosion of a prepared layer of solids in the pipeline.

In addition to the contradictory definitions of the phenomenon, saltation is difficult to observe visually at high feed rates. This may be understood by applying the concept of a mean free path from Secton 2.1.1. At high feed rates or solids loading ratios the mean free path of a particle in the suspension will be too short to allow jumping and bouncing motion. The concept of saltation therefore only applies to low feed rates and low air velocities, and is a typical property associated with flow dominated by single particle behaviour.

2.1.3 Flow Dominated by Single Particle Behaviour

A typical measured viscosity for a gas-solids suspension is, as shown in Section 8.2.2, of the order of 10^{-2} Pa s (see also [13,14]). Under such conditions, the Reynolds number of the suspension in a 50mm diameter pipeline starts out in the laminar region of the Moody diagram [15], moving through the critical, the transient and into the turbulent region as it is conveyed. At the beginning of the pipeline, where the powder is accelerated from initially being at rest up to a higher velocity, the velocity of the suspension of powder is low. If the solids loading ratio condition mentioned in Equation 2.1 is not satisfied, one would expect a laminar flow layer to form, due to the dominance of particle-particle interactions. This layer would then dissipate into a well mixed turbulent flow towards the end of the pipeline. Alternatively, if the solids loading condition in Equation 2.1 is satisfied, we would have a mode of flow dominated by single particle behaviour. Models based on single particle drag force, Magnus force and single particle wall collisions would be best used in attempting to predict these flow conditions.

2.1.4 Flow Dominated by Particle-Particle and Particle-Wall Interaction

As shown in Section 8.2.2 the energy dissipation of a wave travelling on a fluidized bed of alumina has its largest contribution from wall interaction at duct widths below approximately 70mm. Wirth [16], in his model for predicting the behaviour of a moving bed flow, assumes that all the energy dissipation comes from the sliding of the moving bed

against the wall of the pipe, and that the moving bed can be considered to be a rigid body moving through the pipeline. The forces acting should, in this case, be the friction forces between gas and moving bed as well as between the wall and the gas and moving bed. Mi et. al. [17] also consider friction forces to be of great importance when modelling plug flow. Models incorporating these forces together with the liquid like behaviour of a moving bed, or the mechanical properties of a plug, are likely to provide the most useful results when attempting to model or predict such modes of flow.

2.2 Conveyability and Physical Characteristics

It is commonly known that the physical characteristics of a material transported have a great influence on the conveying limits of the material. All models for predicting conveying limits incorporate some physical characteristics of the material. It is not obvious though, which characteristics should be included in such models. This partly relates to the problem of identifying what physical characteristics are involved in the mechanisms described above. For the single particle behaviour we would expect individual particle properties to play a dominant role. Particle density, particle size and shape together with the physical characteristics of the conveying gas and the pipeline should therefore be included in models for predicting conveyability in a suspension flow mode. For the modes of flow with strong particle-particle and particle-wall interactions we would expect collective behaviour dealing with the interaction between the gas and the solids, the interaction between the solids and the pipeline, and the interaction between the particles, to play an important role. Among these physical characteristics we have the permeability of the powder, the air retention characteristics, the wall friction, the internal angle of friction, the viscosity of the bulk of powder, and the bulk density.

The existing models that will be presented later in this chapter use these characteristics, and the type of characteristics considered reflect the experimental data upon which they have been based, as well as what mode of flow they try to predict. In the light of this knowledge it may be easier to understand the background and limitations of existing models.

2.3 Introduction to Various Conveying Velocity Limits and Possible Prediction Methods

The conveying velocity limit is one of the most important aspects of conveyability. Together with pressure drop it defines the limitation for the operating point of a pneumatic conveying system. With a knowledge of these values, an operating point with sufficient safety margin can be selected to avoid blockage, and the required mass flow rate of solids can be obtained. Provided that problems with cohesion, explosibility and erosion are dealt with separately, this will ensure safe and reliable operation of pneumatic conveying systems.

Several correlations for predicting minimum conveying velocity have been developed [6,7,10,11,12,16,18,19,20,21,22,23]. There are great differences in the accuracy of these models, and in general they do not have the accuracy to enable safe design of pneumatic conveying systems [24,25,26], as can also be seen in Chapter 6. The existing models also differ in the type of minimum conveying velocity they predict, since the minimum conveying velocity can be defined in several ways.

All conveying limits are, for a given particulate material, dependent on a combination of the conveying air velocity and the solids feed rate. The terms that have been found useful and objective and will be used throughout this work are listed below. They may be defined in the following way:

- The blockage limit is the limit at which no flow of solids takes place. It is determined by monitoring the mass flow rate of solids.

- The limit of stable conveying in plug or slug flow, and the limit of stable conveying in suspended or partially suspended modes of flow (from now on called the limits of stable conveying) must be defined by choosing some stability criteria either for the pressure or the mass flow of air or solids. This is discussed thoroughly in Section 5.3 on identification of conveying limits.

- The pressure minimum curve is unambiguously defined through the interpolation of constant mass flow curves in the conveying characteristic.

2.3.1 Possible Methods of Prediction

Several methods may be considered when embarking on the task of attempting to predict minimum conveying velocity limits in pneumatic conveying systems. The classical approach would be to establish a theoretical model of the mechanisms involved in limiting the flow of solids. This method was used by Newton [27] to understand gravity and planetary motion, and later by Einstein [28] to refine the understanding of gravity and planetary motion by the general theory of relativity. Very few researchers working with two-phase gas-solids flow and conveying limits have applied this method. It would require knowledge of which parameters are relevant, and about their interaction.

When the complexity of the process to be modelled presents an obstacle to the developement of a theoretical model, it is still possible to establish an empirical model for the relationship between a value that needs to be predicted, and the variables that are considered to be relevant. By considering which characteristics might be relevant to the prediction of the minimum conveying velocity, one can undertake a dimensional analysis, to obtain dimensionless groups that can be related to one another. This technique was used by Darcy [15] to predict pressure losses for flow of liquids and gases through pipes with different roughness factors. Dimensional analysis has been applied by many researchers in the field of two-phase gas-solids flow, as will be shown later in this chapter.

Finally a new potential method for predicting minimum conveying limits should be mentioned. Since the methods mentioned previously rely on some understanding of the underlying process of blockage, or on a selection of a small number of parameters that are believed to be of relevance to it, they are either difficult to use, or may result in unreliable predictions. If one could incorporate a large number of parameters into a statistical analysis of factors that might have an influence on the minimum conveying velocity, this problem could be overcome. Multivariate analysis [29] has the potential to do this. In addition to including traditional static powder characteristics, such as particle density and size, it also

can include results of dynamic tests like fluidization and deaeration in the form of large arrays containing the characteristics in digitalized form. These types of characteristics have previously been condensed down to a few numerical values. In the case of the fluidization characteristics these values have been minimum fluidization velocity and deaeration rate. With multivariate analysis one can include the whole fluidization characteristic, along with other dynamic test results, into a model that predicts conveying behaviour.

These different methods tend to be used for different problems and at different stages of the development of knowledge about the phenomena under investigation.

2.4 Existing Models and Correlations

Several relationships describing the different limiting conditions have been proposed in the literature. They usually describe a relationship between the air velocity, very often in the form of a Froude number, the feed rate of solids or solids loading ratio and different characteristic powder properties.

In addition to the models mentioned above, several simplified approaches exist, which are mainly based on experience. One of these approaches should be mentioned specifically even though it has not been included in the following review. This is the method of Jones [30], which is based on the observation that the materials that are conveyed can be classified in three groups according to their vibrated deaeration constant. The first group, which mainly consists of fine materials with a low vibrated deaeration constant, can be conveyed in moving bed flow, and have been identified by Jones to have minimum conveying velocities of approximately 3m/s. The second group, which consists of materials that have vibrated deaeration constants in an intermediate range, can not be conveyed in dense phase, and are claimed to have minimum conveying velocities of approximately 15m/s. The last group consists of materials, which have high deaeration constants, and can be conveyed in plug flow, again at minimum conveying velocities of approximately 3m/s. Excluding diameter effects, this should leave a sufficient safety margin for all the materials investigated here, even though the original data of Jones show that the method may give

large errors, for fine materials with wide size distributions, and for materials lying on the border line between the middle zone and the zone with low vibrated deaeration constants.

A selection of the most relevant models proposed in the literature is presented in the following sections.

2.4.1 Thomas

D. G. Thomas [7] proposed a model for describing the particle transport mechanism which is based on only two forces balancing the gravitational force. These are the Magnus force and the drag force. The Magnus force is then neglected because it is assumed to be much smaller than the drag force. By using dimensional analysis he then obtained an expression for the minimum transport velocity at infinite dilution, Equation 2.2.

$$\frac{u_t}{u_0^*} = 4.90 \frac{d_p u_0^*}{\nu} \left(\frac{\nu}{D u_0^*} \right)^{0.60} \left(\frac{(\rho_p - \rho)}{\rho} \right)^{0.23} \tag{2.2}$$

$$\frac{u_c^*}{u_0^*} = 1 + 2.8 \left(\frac{u_t}{u_0^*} \right)^{1/3} \phi^{1/2} \tag{2.3}$$

$$\frac{u_{sm}}{u_c^*} = \left(5 \log Re_p - 3.90 \right) \tag{2.4}$$

Where the variables are defined as:

ρ_p	Particle density.	u_c^*	Friction velocity at minimum. conveying conditions.
ρ	Fluid density.		
ν	Kinematic viscosity.	d_p	Particle diameter.
u_t	Terminal velocity of a free falling particle.	D	Pipeline diameter.
		u_{sm}	Superficial air velocity at minimum conveying conditions.
u_0^*	Friction velocity at infinite dilution.		
R_p	Particle Reynolds number.	ϕ	Volume fraction of solids.

This expression contains three coefficients that have to be determined experimentally. He also introduces an experimentally obtained correlation for compensating for the concentration of particles in the suspension, Equation 2.3. Equation 2.3 gives what Thomas calls a friction velocity and an additional calculation, using Equation 2.4 has to be made to obtain u_s which is the superficial air velocity in the pipeline. The data presented in his report includes both water-solids, and air-solids suspensions. There is an obvious error in the correlations, which he also points out himself. For gas-solid suspensions they do not predict the velocity minimum that is found experimentally at a certain concentration of solids in the pipeline.

In his paper, however, he makes several important observations. He identifies clearly that there is no sharp transition between suspension and non-suspension flow. He selects a somewhat arbitrary way of defining this transition. When the ratio between the terminal velocity and what he calls the friction velocity approaches a certain value, he identifies this as the transition between suspension flow and non-suspension flow. This would correspond to what other authors term the saltation velocity. His results also point out the effect the concentration of particles in the air stream has on the ability of the air stream to transport solids.

2.4.2 Barth

Barth [31] presents measurements of pickup rate and settling rate of solids in a pipeline. The experiments were carried out in an 8m long pipeline with a diameter of 40 mm. By filling a short section of the pipeline with a layer of particles he was able to determine the pickup rate at different air velocities by instantaneously measuring the flow of solids at the pipeline outlet. Settling rate was found by feeding the pipeline at a fixed air velocity and solids feed rate until a constant layer of particles was established. He then assumes that the pick up rate and the settling rate balance out at this point. The materials conveyed were coarse polyethylene particles, alumina and pulverised fuel ash. All the experiments took place at very low feed rates, relative to conditions normally found in industrial conveying systems.

These experiments show pickup rates varying with transport air velocity. For the alumina, a maximum pick up rate was reached. At air velocities higher than approximately 6m/s there is no change in the pick up rate. Barth interprets this to be due to the existence of a maximum limit for the solid loading ratio. He also shows that the height of the layer in the pipeline is dependent on both the feed rate and the air velocity.

In his theoretical considerations, he defines three different modes of conveying. They range from one which has all the particles equally distributed across the pipeline cross section, through moving bed flow and stationary layered flow. He considers the transitions between the two first modes of flow to be governed by the equilibrium between the mass of particles bouncing off the pipeline wall and the mass of particles being moved out towards the wall. This is, again, dependent on the drag coefficient of the particles, which will limit the distance the particle travels after bouncing off the wall. The last transition is considered to take place when the momentum transferred to the moving bed by settling particles matches the momentum taken from the moving bed by the friction with the pipeline.

2.4.3 Zenz

Zenz [6] uses the traditional rearranging of the dimensionless groups describing the free fall of a particle in a gas to plot his experimental findings of single particle saltation velocities in a horizontal pipeline. When both the saltation velocity and the terminal velocity are plotted, the difference is shown to be large at low Reynolds numbers. His data also indicate a diameter effect and a effect of the angularity of the particles.

To be able to take into consideration the size distribution of the material that is transported, he uses the minimum and maximum particle diameters of the particle distribution and finds an approximation to the functional relationship between single particle saltation velocity and particle diameter for the distribution. This is then incorporated into the correlation for saltation velocity and solids feed rate he has found, which is shown in Equation 2.5. The constant in the equation originally proposed by Zenz is not dimensionless and has been converted to SI units in Equation 2.5.

$$u_{ss} = \frac{\Phi u_0}{0.21\rho_p\left(s_\Delta\right)^{1.5}} + u_0 \tag{2.5}$$

Where the variables are defined as:

u_{ss}	Superficial air velocity at saltation.	Φ	Flux of solids.
u_0	Saltation velocity for single particle.	ρ_p	Particle density.
s_Δ	Parameter for ratio between saltation velocities and particle diameters.		

The experiments carried out include solids feed rates up to 2 t/h for the coarse sand material. The equipment used consisted of 32 and 63 mm diameter pipelines of 4.6 and 2.7 m length. Both systems were vacuum systems. A wide variety of materials were tested.

2.4.4 Doig and Roper

The correlation developed by Doig and Roper [10] is based on experimental data taken from other authors. By plotting the Froude number of the pipeline against solids loading ratio they identify a relationship between these two parameters. When the terminal velocity is also taken into consideration a graphical analysis of the data yields the correlation. Their correlation also contains constants which are not dimensionless. These constants have been converted to SI units in Equation 2.6.

$$u_{ss} = \sqrt{gD}\mu^{0.25}10^{\left(\frac{u_t - 0.61}{8.54}\right)} \tag{2.6}$$

Where the variables are defined as:

u_{ss}	Superficial air velocity at saltation.	μ	Solids loading ratio.
u_t	Terminal velocity of a free falling particle.	D	Pipeline diameter.
		g	Gravitational acceleration.

2.4.5 Rose and Duckworth

In a series of articles, Rose and Duckworth [18] give a complete model of the pneumatic conveying of materials. They base their model on an experimental correlation of dimensionless parameters, obtained from dimensional analysis, with different macroscopic properties of the flow. The correlations are based both on experiments with water-solids and air-solids suspensions.

The experimental equipment used consisted of two short pipelines, 3.66 m for the test with water and 9.75 m for air, with a diameter of 32 mm. An extensive investigation of different approximately spherically shaped particulate materials and their flow properties in water and air was carried out to achieve these correlations. The particles used in the air-solids experiments were between 960μm and 3.2 mm in diameter, and the size distribution is reported to be quite narrow for each material. Only the experimental correlations are given, as no background data can be found in the report. The experiments were carried out without visual observations of the modes of flow in the pipeline.

Rose and Duckworth define the minimum transport velocity as the point at which the flow of solids becomes unstable. The dimensional analysis of the minimum transport velocity includes the air and solids densities, settling velocity, pipe and particle diameter, shape factor for the particles, mass flow rate of solids, gravitational acceleration and a parameter derived from the spread in the size distribution. The model is purely one dimensional, for steady state flow of an incompressible fluid.

$$u_{ss} = 3.2u_t\left(\mu^{0.2}\left(\frac{D}{d_p}\right)^{0.6}\left(\frac{\rho_p}{\rho}\right)^{-0.7}(gD)^{-0.25}\right) \tag{2.7}$$

Where the variables are defined as:

u_{ss}	Superficial air velocity at saltation.	d_p	Particle diameter.
u_t	Terminal velocity of a free falling particle.	D	Pipeline diameter.
ρ_p	Particle density.	μ	Solids loading ratio.
ρ	Air density.	g	Gravitational acceleration.

The authors make no distinction between saltation and minimum transport velocity. They also report that no pressure minimum point can be found for air solid suspensions in horizontal pipelines. For pipelines that are not horizontal they report this minimum to occur.

2.4.6 Rizk

In his papers [19] and [20] Rizk establishes a simple correlation between the solids loading ratio and the superficial air velocity at saltation.

$$\mu = \frac{1}{10^{\delta}} \left(\frac{u_{ss}}{\sqrt{gD}} \right)^{\chi} \tag{2.8}$$

Where the variables are defined as:

u_{ss}	Superficial air velocity at saltation.	μ	Solids loading ratio.
D	Pipeline diameter.	χ	Determined graphically.
g	Gravitational acceleration.	δ	Determined graphically.

The parameters δ and χ are determined graphically depending on the particle diameter. The correlation is based on experiments on styropor and polystyrol, and as a consequence its validity is limited to coarse, granular materials with low density.

2.4.7 Matsumoto et. al.

Matsumoto et. al. [11] present correlations for minimum conveying velocity and saltation velocity in horizontal conveying. The correlations have been found by first minimising a pressure drop function giving the saltation velocity, shown in Equation 2.9. A parallel is then made to the minimum conveying velocity, and it is determined using the same functional relationship by experimental correlation, shown in Equation 2.10. The experiments were carried out for particles greater than 200 μm. Special care was taken to

avoid end effects in the pipeline, like bends at the end of the horizontal section. In general all their experiments were carried out at very low solid loading ratios.

$$u_{ss} = 3.4\sqrt{gD}\mu^{1/3}\left(\frac{\rho}{\rho_p}\right)^{0.167}\left(\frac{u_t}{\sqrt{gd_p}}\right)^{0.583} \tag{2.9}$$

$$u_{sm} = 3.4\sqrt{gD}\mu^{0.277}\left(\frac{\rho}{\rho_p}\right)^{0.294}\left(\frac{u_t}{\sqrt{gd_p}}\right)^{1.02} \tag{2.10}$$

Where the variables are defined as:

u_{sm}	Minimum superficial air velocity.	u_{ss}	Superficial air velocity at saltation.
d_p	Particle diameter.		
u_t	Terminal velocity of a free falling particle.	D	Pipeline diameter.
ρ_p	Particle density.	μ	Solids loading ratio.
ρ	Air density.	g	Gravitational acceleration.

Their definition of the minimum conveying velocity is the point at which the particles begin to settle on the bottom of the pipeline and a stationary layer is formed. They also identify this as being the point at which the flow of solids is saturated when gradually reducing the air flow. The saltation velocity is identified indirectly as the velocity at which the constant solid flow rate curve reaches a pressure minimum. At the same time they point out the discrepancy between this definition and the visual observations of particles settling on the bottom of the pipeline.

Matsumoto et.al. make several interesting observations on the settling of solids in the pipeline. For particles having low terminal velocities they identified no stationary layers building, even when going past the minimum pressure point. This means passing the saltation velocity without any settling of particles. On the other hand, they report settling to take place even before going below the minimum pressure point for particles having large terminal velocities.

When analysing the saltation or minimum pressure drop problem the authors make several simplifying assumptions. It is assumed that the friction factors for both solids and air flow are constant with regard to air velocity. This is equivalent to assuming that the flow takes place in the completely turbulent region, where the friction factor for air only flow is close to constant with regard to air velocity. Matsumoto et. al. do not define the friction factor specifically, they only give the above mentioned relation between air velocity and friction factor. In addition they also assume that the ratio between the solid and air velocity is constant and a constant relation exists between the terminal velocity and velocity of suspension, which has to be passed to suspend the particles in the air stream. This set of assumptions is consistent when viewed together with frequently cited friction factor correlations such as that of Hinkle [32] , which include the slip velocity between the particles and the air, because the assumption of a fixed ratio between particle velocity and air velocity has been included.

Matsumoto et. al. also assume that there is a close relationship between the saltation velocity and the minimum conveying velocity. They therefore proceed by correlating the minimum conveying velocity to the same parameters and in the same functional relation as for the saltation velocity. The experimentally determined parameters are, of course, slightly changed for the case of the minimum conveying condition.

2.4.8 Cabrejos et. al.

In two articles Cabrejos et. al. [12], [21] have investigated the pickup and saltation velocity of different powders in a specially designed test rig. The test rig and procedure are quite similar to those described by Barth. The rig consists of a section for inserting a layer of powder for pickup velocity measurements, and a closed loop for saltation experiments. In their last report they present results from pickup and saltation velocity measurements for coarse materials (above 100μm) in pipelines of different diameter using air and CO_2 at different pressures.

The saltation experiments were carried out in a 14.5 m long pipeline with a diameter of 50 mm. Saltation was determined visually 7 m downstream of the feed point. During the

saltation experiments the feed rate was kept very low, corresponding to a maximum solid loading ratio of 5. The pickup velocity was determined by filling a 1 m long section of the pipeline with a layer of powder. If the fixed air velocity is slightly above the minimum pickup velocity, Cabrejos claims that the particles on the layer will gradually be blown off, thus increasing the free cross section of the pipeline and decreasing the air velocity until it stabilise at minimum pickup velocity.

Cabrejos conducted a dimensional analysis of the parameters involved in the saltation and pickup mechanisms. The experiments were then used to determine the coefficients for the two expressions by experimental correlation. Only the pickup velocity expression, shown in Equation 2.11, has a practical form and can be used for design purposes.

$$u_{spu} = 0.0428\sqrt{gd_p}\,\mathrm{Re}_p^{0.175}\left(\frac{D}{d_p}\right)^{0.25}\left(\frac{\rho_p}{\rho}\right)^{0.75} \tag{2.11}$$

Where the variables are defined as:

u_{spu}	Superficial air velocity at minimum pickup conditions.	d_p	Particle diameter.
		D	Pipeline diameter.
ρ_p	Particle density.	μ	Solids loading ratio.
ρ	Air density.	g	Gravitational acceleration.
Re_p	Particle Reynolds number		

The saltation expression contains two other unknown, or difficult to determine velocities, i.e. particle velocity and single particle saltation velocity, and as a result, cannot be used directly.

2.4.9 Wirth

In his Dr.Ing. thesis [16] Wirth establishes a model for the prediction of additional pressure drop from transported material. He then uses this expression to identify an expression for the conveying limit. It is valid for moving bed flow, and is based on several simplifications. First of all he considers the moving bed to be a rigid body sliding along the

bottom of the pipe. This is correct if the internal angle of friction is larger than the wall friction angle (and if the material is not fluidized). Secondly he considers the air to be incompressible, which is only valid for short sections of pipeline. The expression for the additional pressure drop due to mass flow of solids is found by using force and mass balances on the moving layer and on the region above it. By doing a separate stability analysis on this expression Wirth finds a criterion for when the mode of flow changes from moving bed flow to unstable flow. His definition of unstable flow is based on visual observations that incorporate flow over a settled layer of solids, blowing dunes and plug flow.

The limit of stable conveying obtained in this way can be displayed in the form of an approximate Equation 2.12. It is limited by an expression for the maximum ratio of volumetric flow between the solids and the gas shown in Equation 2.13

$$u_{sm} = \sqrt[4]{56\mu \frac{\rho}{\rho_p}\left(\frac{\rho_p}{\rho} - 1\right)^2 (1-\varepsilon) f_r^{\,2} D^2 g^2} \tag{2.12}$$

$$\left(\frac{\rho\mu}{\rho_p(1-\varepsilon)}\right)_{max} = 0.27 \tag{2.13}$$

Where the variables are defined as:

u_{sm}	Superficial air velocity at minimum pickup conditions.	ε	Voidage.
		D	Pipeline diameter.
ρ_p	Particle density.	μ	Solids loading ratio.
ρ	Air density.	g	Gravitational acceleration.
f_r	Wall friction factor		

These equations now define the area in which stable moving bed flow is obtainable. In addition Wirth identifies an area in with stable flow over a settled layer of solids. This is when the superficial air velocity is below the value given by equation 2.12, and when the ratio of volumetric flow of solids and the gas is below 0.019.

2.4.10 Pan et. al.

In two articles Pan et. al. [22,23] address, for the first time, the problem of predicting the two velocity limits of stable conveying. No other article has been found that predicts the limit of stable conveying in plug or slug flow, which is the upper velocity limit at which powders are transported in stable plug flow. The correlation of Pan et. al. is empirical, based on the Froude number at the material inlet, and on dimensional analysis of the parameters likely to influence the limiting conveying condition. The dimensional analysis is quite similar to that of Cabrejos et. al. and Rose and Duckworth, but differs in the choice of density dependence. The bulk density of the powder is introduced. The expression for the limit of stable conveying in suspension or partially suspended flow is shown in Equation 2.14 and the expression for the limit of stable conveying in plug flow is shown in Equation 2.15.

$$u_{sm} = 3.151\mu^{-0.018}\left(\frac{d_p}{D}\right)^{0.213}\left(\frac{\rho}{\rho_b}\right)^{-0.254}(gD)^{-0.5} \tag{2.14}$$

$$u_{sps} = 2.959\mu^{0.097}\left(\frac{d_p}{D}\right)^{0.069}\left(\frac{\rho}{\rho_b}\right)^{-0.219}(gD)^{-0.5} \tag{2.15}$$

Where the variables are defined as:

u_{sm}	Minimum superficial air velocity.	u_{sps}	Superficial air velocity at the limit of stable plug or slug flow.
μ	Solids loading ratio.		
d_p	Particle density.		
D	Pipeline diameter.	g	Gravitational acceleration.
ρ_b	Bulk density.	ρ	Air density.

2.4.11 Summary of the Models

Several of the models are Froude number correlations, but it is not clear why limiting values for flow in circular ducts should be correlated by means of Froude numbers. These

numbers are generally related to flow involving free surfaces in open ducts. Since these correlations seem to be the most successful in determining the minimum conveying velocity, one may be justified in concluding that the state of the free surface might be correlated to the blockage of a pipeline. The visual observations of Matsumoto et. al. give indications that the formation of a free surface (saltation) does not correlate with the minimum pressure limit. Even so, it might be possible to correlate the state of the moving bed to the minimum velocity of stable conveying. If a correlation between the state of the moving bed and the limit of stable conveying could be made, the transition from supercritical to sub-critical flow of the moving bed is a likely parameter to investigate. This transition is characterised by the Froude number, which in this case should include a length dimension between the pipeline diameter and the particle diameter. The correlations of Matsumoto et. al. and Rose and Duckworth are in fact similar to Froude number correlations containing this intermediate length dimension.

The procedure Matsumoto et. al. used to compute the pressure drop required to suspend the particles in the air stream is highly simplified. Their assumptions for the model of the saltation velocity are very approximate. However, their analytical treatment of the pressure drop problem, leading to a saltation velocity correlation, is unique in that it establishes a simple mechanistic model for how the gas solids suspension behaves in a pneumatic conveying pipeline. As a consequence there should be room for improvements in this model, and thus also in the resulting correlation.

Barth's pick up rate measurements give some indications that a minimum pickup velocity does exist. For the experiments at constant feed rate he shows that the balance between settling rate and pickup rate, above a velocity of a few meters per second, also depends on the feed rate of solids. Correcting his velocity vs. bed height data for actual air velocity over the settled layer of powder does not give a constant air velocity. One might wonder if the method of Cabrejos et. al., which is similar to Barth's, is influenced by the higher solids loading ratios that occur before stabilisation of the bed height.

A summary of the various models and the underlying data upon which they are based is presented in Table 2.2. A quantitative comparison of the different models is conducted in

Chapter 6, where the experimental data obtained in the investigation described in this thesis are compared to the predictions of the models. Several authors have previously made comparisons between existing models for predicting minimum conveying velocity [24],[25],[26],[33]. These reports show poor agreement between the models and experiments, as well as large discrepancies between the different models. This can also be seen in Tables 6.1 and 6.2, where the difference between the predictions of the models and the actual minimum conveying velocity varies between -77% and 116% of the conveying limit value inside the area of validity for the models.

As one can see from Section 2.4, empirical models so far dominate when it comes to prediction of minimum conveying velocities. The goal of this work will therefore be to utilise the large amount of information obtained through empirical investigations , together with own observations, to enable a thorough evaluation of existing models, and to enable a mechanistic model of blockages in a pipeline to be made.

Table 2.2 Extracts of information about what methods and data the different models for determining conveying limits has been based upon.

Author	Type of model	Name of limit	Definition (Velocity at which:)	Area of validity [particle diameter, or as specified]	Materials tested and maximum solids loading ratio	Length of test pipeline [m]	Diameter of test pipeline [mm]
Thomas	Experimental correlation.	Minimum transport velocity	A layer of solids forms on the bottom of the pipeline	97 - 2000 μm	From other authors : rape seed, glass beads, sand, cress seed, mustard seed, own water/glass bead experiments		16 - 44
Doig and Roper	Comparison of existing models and data, which leads to a new correlation.	Saltation velocity	A layer of solids forms at the bottom of the pipeline	150 μm - 6 mm	From other authors : rape seed, glass beads, salt, sand, wheat, tenite, soya beans.		
Matsumoto et. al.	Pressure drop model and minimalization	Pressure minimum / Saltation velocity Minimum conveying velocity	A pressure minimum is reached on the constant mass flow curve A layer of solids forms on the bottom of the pipeline	290 - 2600 μm $1.0 \leq \rho_p \leq 8.7$ $5 \leq Fr \leq 30$	Spherical particles of: glass, copper and polystyrene up to a solids loading ratio of 5 in 50mm pipeline and 10 in 26mm pipeline	11 and 26	26 and 49
Rose and Duckworth	Dimensional analysis and experimental correlation	Minimum conveying velocity	Particles fall out of suspension and block the pipeline	0.96 - 3.2 mm	Mustard seed, glass, steel and lead up to a solids loading ratio of 10	3.66 and 9.75	32

Table 2.2 Continued.

Author	Type of model	Name of limit	Definition (Velocity at which:)	Area of validity [particle diameter, or as specified]	Materials tested and maximum solids loading ratio	Length of test pipeline [m]	Diameter of test pipeline [mm]
Cabrejos et. al.	Dimensional analysis and experimental correlation	Minimum pickup velocity Saltation velocity	Particles stop being picked up from a settled layer in a PVC pipeline Particles fall out of suspension	25<Re<5000 8<D/dp<1340 700<ρ_p/ρ<4240	Glass beads, alumina, iron oxides, polyester, PVC	1 and 6	50 and 200
Rizk	Experimental correlation.	Pressure minimum	A pressure minimum is reached on the constant mass flow curve	0.7-6 mm $\rho_p \approx 1000$ kg/m^3	Polystyrol and styropor up to a solids loading ratio of 15.		50-400
Zenz	Parallel to free fall velocity, experimental correlation.	Saltation velocity	Particle are skimming along the pipeline almost without touching the bottom of the pipeline	50 μm - several mm	Rice Krispies, rape seed, glass beads, sand, salt, cracking catalyst, soybeans, tenite up to a solids loading ratio of 20.	4.6 and 2.7	32 and 63
Wirth	Stability analysis of pressure drop	Stability limit	Moving bed flow turns unstable	90 μm - 3300 μm	Glass beads, sand, polystyrol, wheat up to a solids loading ratio of 20.	12	10 to 40
Pan et. al.	Dimension Analysis	Stability limit	Plugs form	390 μm - 3760 μm	Plastic pellets, duralina, wheat up to a solids loading ratio of 35.	96 to 137	52.5 to 105

3. Experimental Facilities Used in this Investigation

The test rig used in this investigation with its current instrumentation, is shown in Figure 3.1. Its main components are the blow tank, the pipeline and the receiving tank. The recharging of the blow tank is facilitated by a movable hopper carried by an overhead crane.

The feeding section of the blow tank can be seen in detail in Figure 3.2. It consists of a fluidized cone, a slide valve and a section interfacing the blow tank with the pipeline. Fluidizing air is supplied through a Vyon cloth on the inside of the blow tank skin. The slide valve is DN100 with a slightly reduced aperture, and is used to control the solids flow for free flowing materials.

The conveying air is supplied from a 1000Nm^3/h screw compressor delivering air at 8bar. The air is subsequently dried to approximately 30% relative humidity in an air cooler and drier. At the inlet of the pipeline an array of control valves allows the control of the air supply to the system. Flow rate is controlled by globe valves, and monitored by turbine flow meters. Humidity, temperature and pressure are also monitored on the air supply side.

Ten pressure transducers are positioned along the conveying line. These allow the monitoring of pressure profiles. They also enable measurements of the pressure fluctuations along the pipeline and, in particular, cross correlation measurements, conditional averaging, and frequency analysis. Flow rate, temperature and humidity of the exhaust air from the receiving tank are also measured. The receiving tank itself is located on three load cells enabling average mass flow rate measurements to be made for the conveyed solids. All signals from the different instruments are sampled, digitized and stored in a computer.

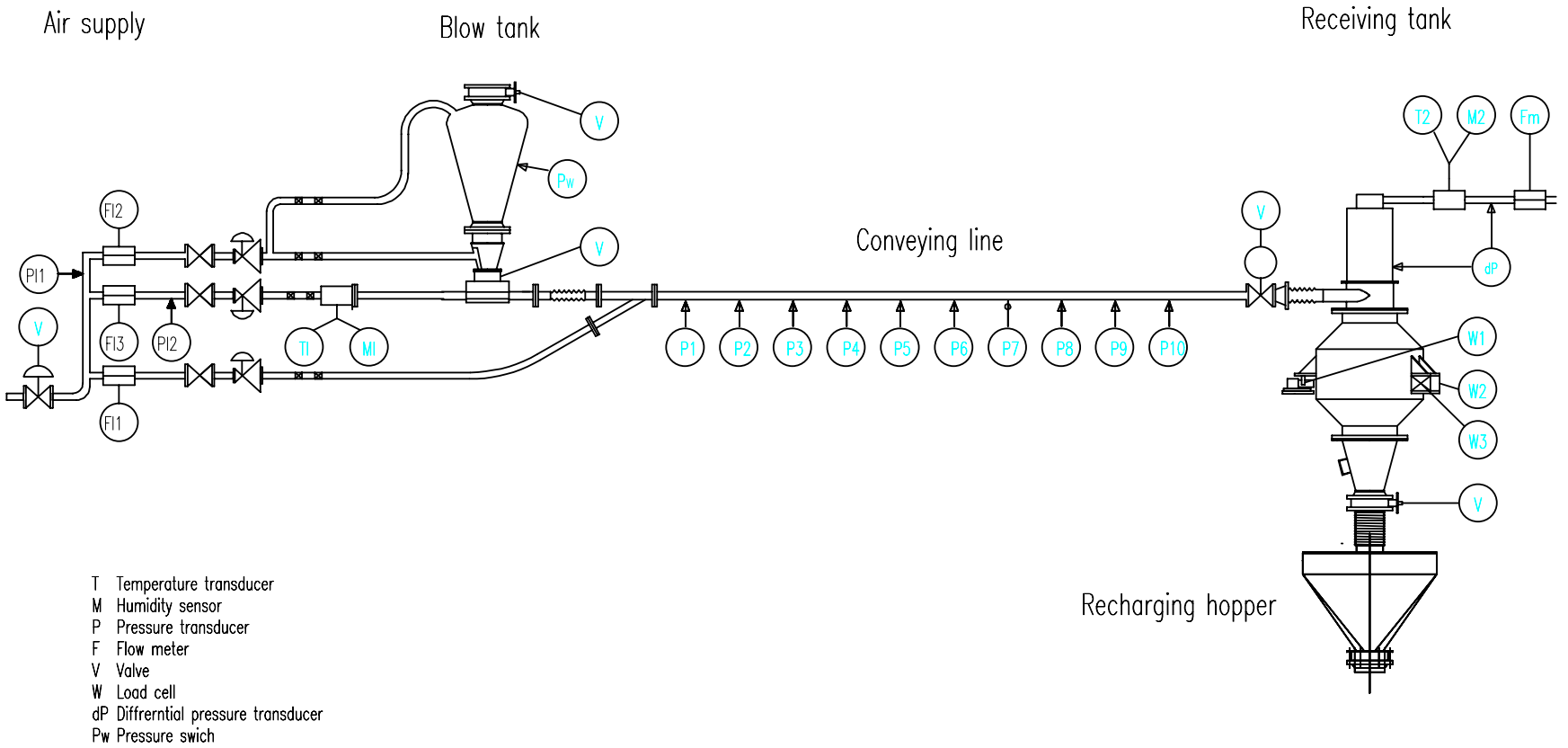

Figure 3.1 The test rig and its current instrumentation.

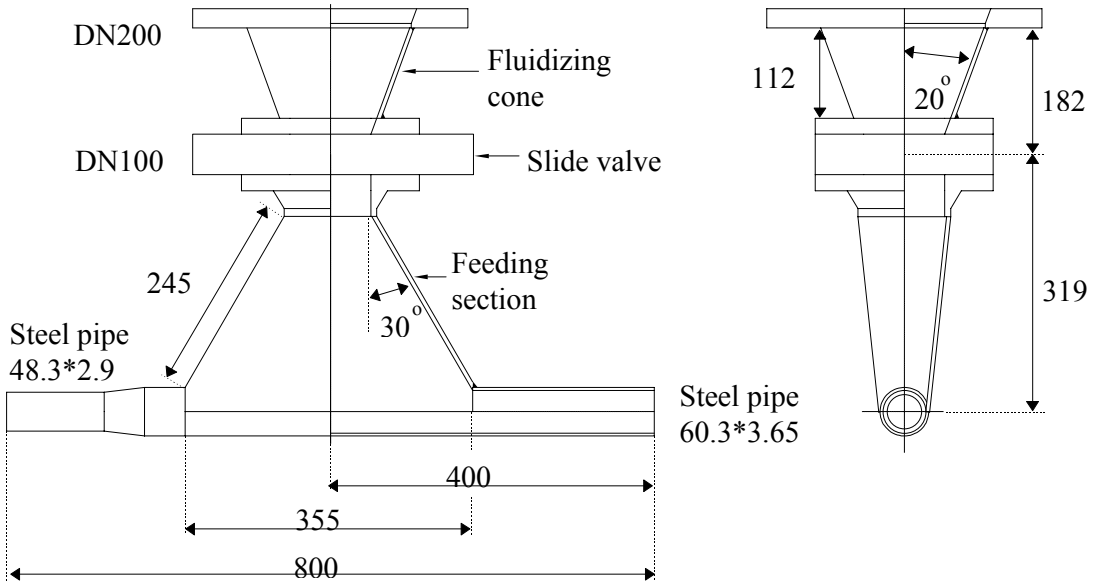

Figure 3.2 The feeding section of the blow tank, all numbers in mm.

The signals from the different transducers are 4-20mA current loop. The signals are measured as a voltage across a 500Ω high precision resistor, with an accuracy of 1%. To reduce aliasing effects from high frequency components in the signal from the pressure transducers, simple first order RC filters are used.

The analogue to digital conversion card is an RTI 800/815. It has 16 differential input channels or 32 single ended channels. Single ended input, and common zero, has been used. Its resolution is 0.02% of full scale reading, which in this case is 10V. Sampling of data in the time domain has been carried out with the internal clock as a reference, and the time base accuracy is 0.01%.

A diagram of one of the pressure transducer circuits is shown in Figure 3.3. With the given values we obtain a cut-off frequency of 90Hz. This was observed to reduce the noise coming from mechanical vibrations in the screw compressor system.

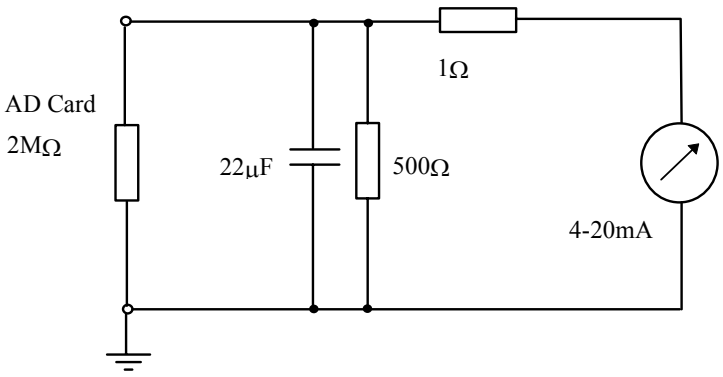

Figure 3.3 The current loop of a pressure transducer circuit.

3.1 General Considerations

The current experimental set-up was designed based on earlier experiments using a more complicated line geometry. Initial experiments gave indications that the geometry of the pipeline might have some influence on the blockage of the pipeline. Blockage of the pipeline was often observed to take place in the section after the first horizontal-to-horizontal bend in the pipeline. At the time, the instrumentation of the test facility was too sparse to determine actually where the blockage occurred in this section, but since the blockage did not seem to take place at the material inlet, it was decided that the geometry of the pipeline might have some influence on the result. Therefore, in the first instance, it was decided to build a conveying line with a very simple geometry, to isolate the effect of this parameter on the experiments. As a result a completely horizontal pipeline was built. The level of the pipeline was adjusted horizontally by using a levelling telescope, which gives an accuracy of approximately ±5mm. Details of the actual layout of the pipeline are given in Figure 3.4. To investigate the effect of a bend in the pipeline, the system was prepared with a possibility of having two different discharge points. These are marked as point B and C in Figure 3.4. Discharge of material at point B gives a 15m long straight pipeline, and discharge at point C gives a 21m long pipeline with one horizontal bend.

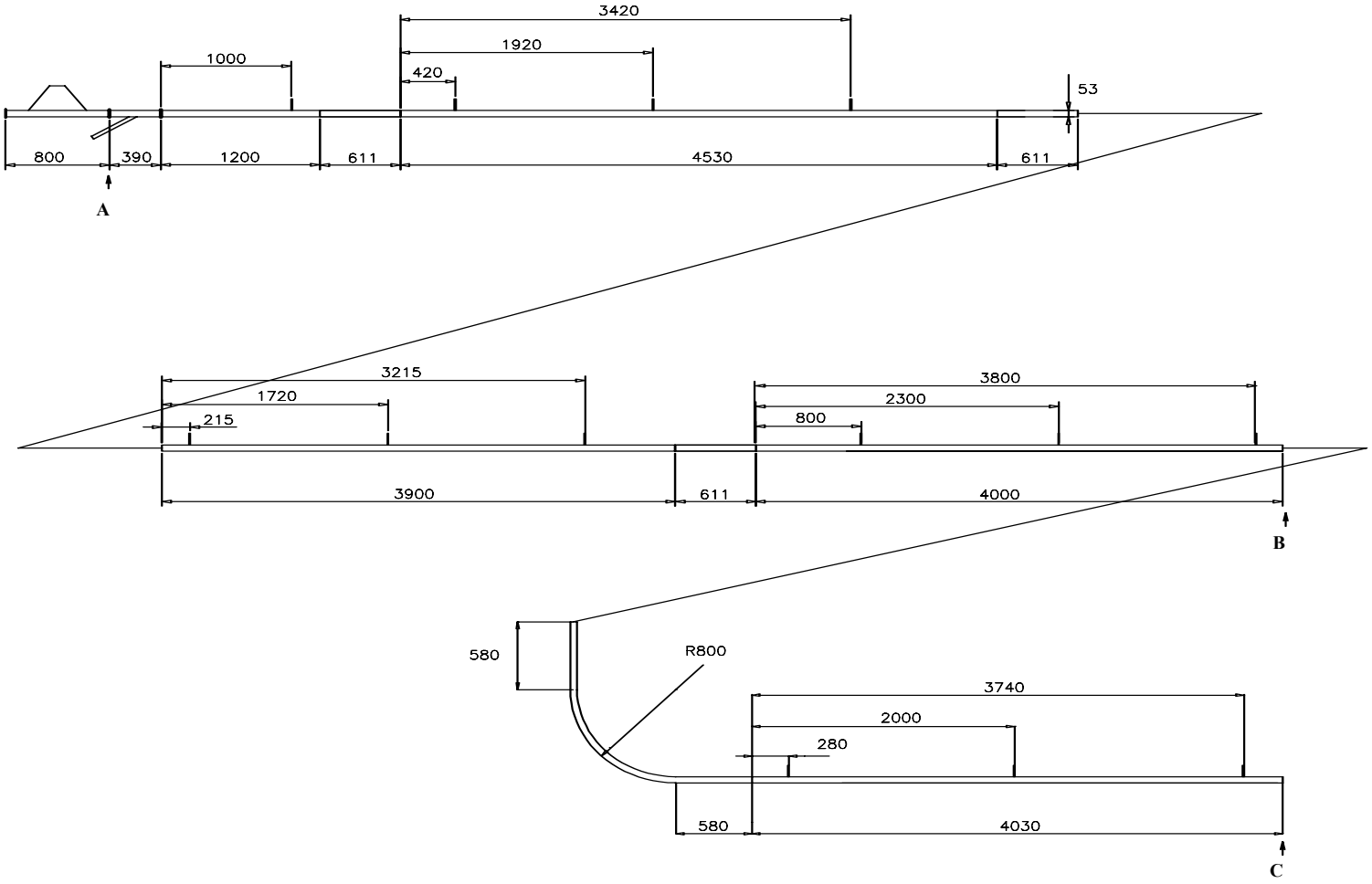

Figure 3.4 The layout of the pipeline, all dimensions on the drawing are shown in mm, total length 21.05m, diameter 53 mm.

3.2 Calibration of Instruments

Some of the instruments used require special attention. All the instruments that have been used have been subjected to calibration and quality control at the factory, but for some of them the performance is likely to change with time and use. For this reason the pressure transducers, have been calibrated several times during the test program, using a Beamex PCS 105 calibrator [34]. In addition to these calibrations the pipeline was closed at the end and the pressure was set to different levels for internal comparison between the transducers. This was done at regular time intervals to identify failures among the pressure transducers.

It was also found to be necessary to recalibrate the turbine flow meters used in the air supply. Since these flow meters were originally calibrated for use at atmospheric conditions, they could not be expected to perform properly at pressures up to 40 KPa. The calibration was carried out according to the ISO 5167-1 standard using an orifice meter.

Finally the load cells were calibrated whenever the receiving tank was moved. This procedure was adopted to detect possible changes in the performance of the cells due to physical damage. Mechanical and electrical connections to the receiving vessel were also modified when it was moved and could cause changes in the hysteresis of the load cell characteristics.

3.3 The Overall Accuracy of the Data Sampling System.

The total error of measurement when sampling from each of the transducers is the sum of errors from several sources. An overview of the transducers used in this investigation together with the nominal and measured accuracies is shown in Table 3.1. The calibration of load cells and pressure transducers has been carried out several times, the worst case results being shown in Table 3.1.

Table 3.1 Specification of transducers and their accuracies.

Name	Type of Tranduser	Range	Nominal accuracy [% of full scale]	Measured accuracy [% of reading]	Supplier	Position without and with bend
Fl1	Flow	2.5..102 m3/h	1.0 %		Flow Technology	
Fl2	Flow	1.7..42 m3/h	0.1 %		Flow Technology	
Fl3	Flow	2.5..102 m3/h	1.0 %		Flow Technology	
Pl1	Pressure	0..15 barg	0.5 %		KMK	
Pl2	Pressure	0..6 barg	0.5 %		Philips	
Tl	Temperature	-10..90 deg C	±0.5 °C		Endress and Hauser	
Ml	Humidity	0..100 % RH	2 %		Endress and Hauser	
P1	Pressure	0..1 barg	0.1 %	0.4%	Keller	0m / 0m
P2	Pressure	0..1 barg	0.1 %	0.3%	Keller	1.23m / 2.73m
P3	Pressure	0..1 barg	0.1 %	0.4%	Keller	2.73m / 6.17m
P4	Pressure	0..1 barg	0.1 %	0.4%	Keller	4.23m / 9.17m
P5	Pressure	0..1 barg	0.1 %	0.1%	Keller	6.17m / 11.26m
P6	Pressure	0..1 barg	0.1 %	0.1%	Keller	7.67m / 12.76m
P7	Pressure	0..1 barg	0.1 %	0.2%	Keller	9.17m / 14.26m
P8	Pressure	0..1 barg	0.1 %	0.7%	Keller	11.26m / 15.92m
P9	Pressure	0..1 barg	0.1 %	0.2%	Keller	12.76m / 17.64m
P10	Pressure	0..1 barg	0.1 %	0.2%	Keller	14.26m / 19.38m
T2	Temperature	-10..90 deg C	±0.5 °C		Endress and Hauser	
M2	Humidity	0..100 % RH	2 %		Endress and Hauser	
W1	Loadcell	0..500 kg	0.25 %	⎫	Nobel	
W2	Loadcell	0..500 kg	0.25 %	⎬ 5.7%	Nobel	
W3	Loadcell	0..500 kg	0.25 %	⎭	Nobel	
Fm	Flow	280 m3/h	0.2 %		Endres and Hauser	

4. The Test Program and the Characteristics of the Materials used in the Investigation

The objective of the investigation reported in this thesis has been to compare physical characteristics of powders with their conveyability in pneumatic transport systems. Characterisation of the different powders, and conveying tests are therefore the two main tasks of the test programme. The physical characteristics of the granular materials included in the test work have been determined using equipment that is either commercially available, or which were built according to suggestions made by previous workers in the field. In addition to these, a tester for viscosity measurements and surface wave propagation has been built and tested based on new principles. The pneumatic conveying test work have been carried out in a completely horizontal rig. Its design was selected after a careful study of literature on the subject, and after preliminary test work in a pipeline with a more complex geometry.

4.1 Test Procedure for Pneumatic Conveying Tests

The bulk of the experiments carried out, consist of pneumatic conveying tests for a number of particulate materials. The data are extracted from the part of the conveying cycle where stable conveying conditions exist, i.e. where mass flow is constant and pressure drop is stable. The stability of the pressure signal is assesed by looking for pressure peaks in the recorded signal, differing from the small fluctuations that are present at stable flow conditions. The start-up procedure of the conveying system had to be adapted to each individual material. A number of different techniques have been developed to identify minimum conveying velocity conditions.

After having set the solids feed rate (by adjusting the opening of the slide valve at the bottom of the sending tank) and air flow rate, the air flow is switched off and the blow tank filled with test material. The setting of the solids feed rate initially had to be done without any prior knowledge about the relation between slide valve opening and solids flow rate. After a few initial test runs it was then possible to select a desired solids flow rate, approximately, by setting the slide valve to a predetermined opening.

Some of the materials tested (cement, micronised dolomite, alumina and sand) had a tendency to flow out into the pipeline if the slide valve controlling the flow of solids was left open. So for these materials the slide valve was kept shut during filling and opened last during start-up. Since the slide valve does not open immediately, because of the speed of the electrical actuator, the initial conveying of material took place at lower feed rates than during stable conveying. The other materials (polyethylene pellets, rape seed and PVC granules) did not flood the pipeline during filling, so the slide valve was kept at a predetermined partially open position, corresponding to the desired discharge rate, at all times.

A set of test runs were then undertaken at a fixed solids feed rate with the air flow gradually reduced in successive tests. The first of these was carried out in the minimum pressure drop region for the powder, so that both minimum pressure drop velocity and minimum stable conveying velocity could be found. To find the minimum pressure drop velocity at a fixed feed rate it is sufficient to interpolate between data points. The limit of stable conveying, however, has to be found by repeated tests, because it is not possible to obtain stable data points beyond the conveying limit.

4.2 The Conveying Cycle

As mentioned earlier, the average data used as a basis for the developement of the conveying characteristic of the material, has to be obtained in the part of the conveying cycle where the pressure is stable and the mass flow rate is constant. In Figure 4.1 a typical plot of pressure on transducer 1 and mass reading on the load cells is shown. There is an initial part of the conveying cycle where the mass flow gradually increases and the pressure at transducer 1 stabilises. After approximately 20s stable conveying takes place. The flow is stable for about 30s. It is in this part of the conveying cycle that average values can be taken. The last 40s of the conveying cycle show the blow tank running empty and the pipeline being blown free of material. This part is also discarded when the average values are computed.

There are several ways to expand the stable part of the conveying cycle. By pressurising the blow tank, or by using a larger blow tank we could have obtained longer periods of stable conveying. Assuming that the pressure signal is normally distributed, and that the

sampling of data is independent and random, one can estimate the probability that the mean of the sample lies within 0.2σ of the sample average of a similar infinitely large sample by applying the t probability distribution [35]. With a sample size of 30, this probability is 96%. Accepting this accuracy means that, with a sampling frequency of 5Hz, only 6s of stable conveying conditions are necessary. It is more likely that low frequency phenomena related to the mode of flow in the pipeline causes pressure variations that makes it necessary to average over a longer period of time. In this case the assumption of random sampling is not valid. This had to be considered in each case.

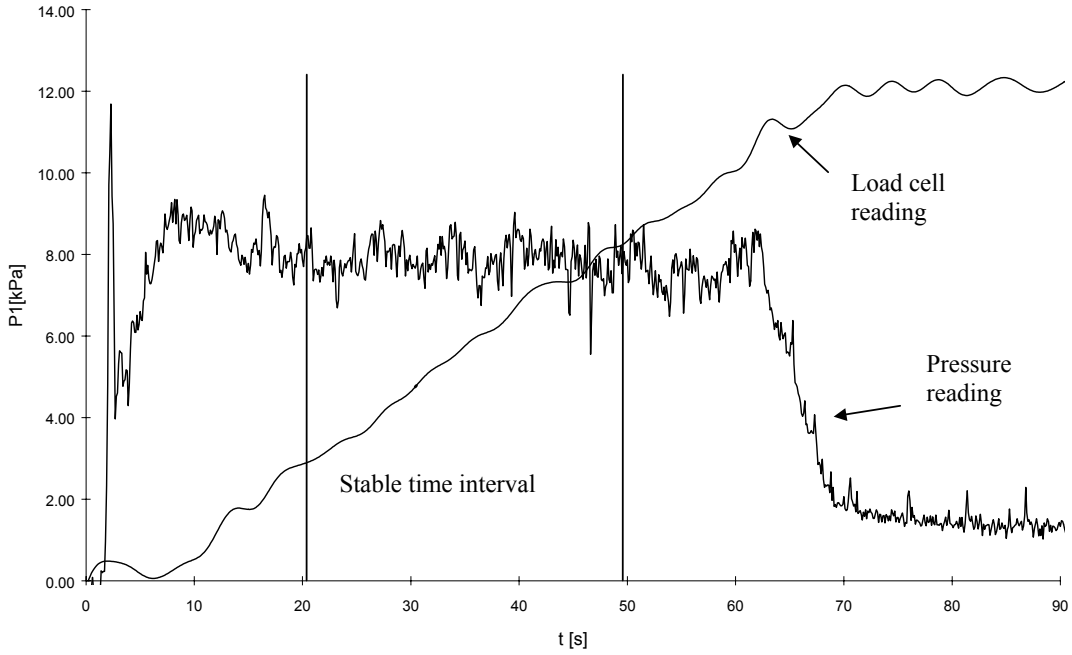

Figure 4.1 The conveying cycle for rape seed test run (RS0207), close to the limit of stable conveying. Stable interval between 20 and 50 seconds marked with lines.

4.3 Computation of Relevant Values

As mentioned in Section 4.1 the average values on which the conveying characteristics are based have been computed from data taken in the stable region of the conveying cycle. The values that are measured directly are pressure, temperature, mass of the receiving hopper, and volumetric flow rate of air. A complete view of where these values are taken can be

found in Figure 3.1 and 3.4. Other values including air velocity, solids loading ratio and pressure gradient have to be computed from the measured values.

First of all a correction factor to compensate for the air that runs into the blow tank to replace the volume of material flowing out of the blow tank has to be computed.

$$K = 1 - \frac{\dot{V}_s}{\dot{V}^*_{a1}} \approx 1 - \frac{\dot{m}}{\dot{V}_{aL} p_L} \cdot \frac{p_1}{\rho_s}$$ where * denotes the uncorrected value.

Where the variables are defined as:

$\dot{V}_s$	Volumetric flow of solids.	$\dot{V}_{a1}$	Volumetric flow of air at the beginning of the pipeline.
$\dot{V}_{aL}$	Volumetric flow in the air supply.	p_1	Pressure at the beginning of the pipeline.
R	Gas constant.	ρ_s	Particle density.
p_L	Pressure in the air supply.		
$\dot{m}$	Mass flow rate of solids.		

The mass flow of solids ($\dot{m}$) is computed as the linear least square fit to the receiving hopper mass, in the time interval where stable conveying is obtained. Linear least square fit is also used for the computation of the pressure gradient (dp/dl). This is done by using the 4 last pressure transducers in the first horizontal pipeline section. Acceleration effects after the feed inlet, and after the bend (for the pipeline configuration with a bend) can thereby be avoided. Other values of interest are computed as follows:

$$v_s = K \frac{\dot{V}_{aL} p_L}{A p_1} \qquad \mu = K^{-1} \frac{\dot{m} R T_L}{\dot{V}_{aL} \cdot p_L} \qquad \dot{V}_{aN} = K \cdot \dot{V}_{aL} \cdot \frac{p_L T_N}{p_N T_L}$$

Where the variables are defined as:

v_s	Superficial air velocity at the start of the pipeline.	K	Correction factor for volume loss in the blow tank.
$\dot{V}_{aL}$	Volumetric flow in the air supply.	p_L	Pressure in the air supply.

A	Pipeline cross section.	p_1	Pressure at the start of the pipeline.
μ	Solids loading ratio.		
R	The gas constant 286.94 J/(kg K).	$\dot{m}$	Mass flow rate of solids.
T_L	Air temperature in the air supply.	p_L	Pressure in the air supply.
$\dot{V}_{aN}$	Volumetric flow of air at normal conditions.	T_N	273.15 K.
		p_N	$1.013 \cdot 10^5$ Pa.

Determination of the actual conveying characteristic was carried out by interpolation of data obtained by the measurements and calculations shown above. The interpolation procedure used was a standard Kriging procedure contained in the software package SURFER® for Windows [36], and described in detail by Cressie in his textbook "Statistics for Spatial Data" [37]. The interpolated contour plot is then used for determining the pressure minimum curve. For the determination of conveying limits several conventions exist, and these are discussed in Section 5.3.

4.4 The Materials and their Characteristics

The original reason for carrying out this investigation was to improve the existing design equations for conveying velocity limits of industrial size pneumatic transport systems. When selecting test materials it was therefore decided to choose from common materials used in the process industry. Seven materials , polyethylene pellets (LDPE), rape seed, Leighton Buzzard sand, PVC granules, alumina, micronised dolomite, and cement were tested in the experimental facility described in the previous chapter. These materials were additionally selected to cover the whole range of materials included in Geldardt's [38] classification for fluidization as shown in Figure 4.2. The materials have been placed in the diagram according to their average particle size, obtained by the various methods of size measurement used, as an approximation to the mean surface to volume diameter. For all these powders a size analysis, an auto pycnometer density measurement, a fluidization test, an angle of repose test and a Jenike test were carried out.

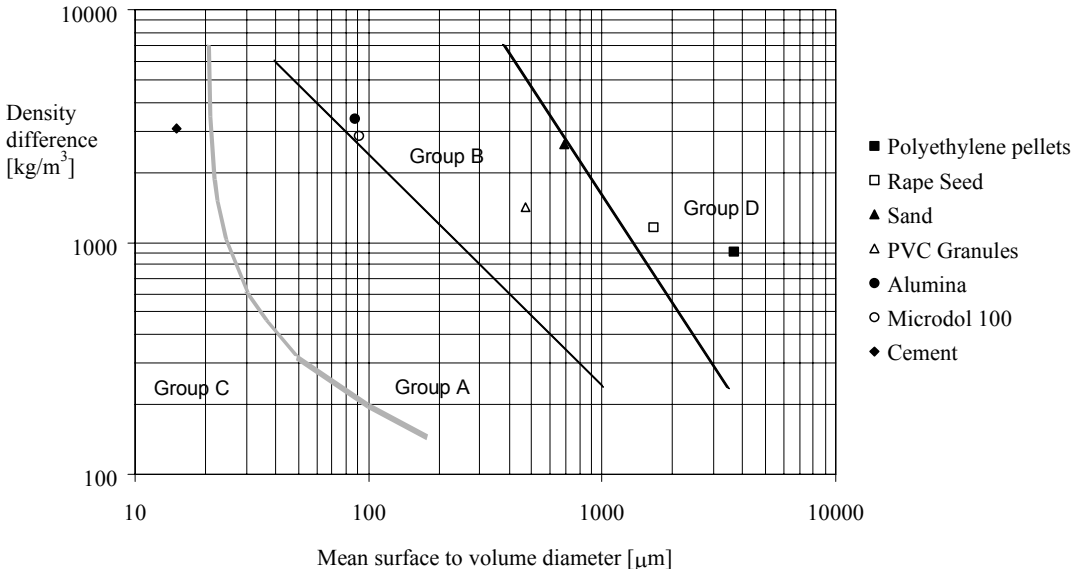

Figure 4.2 The test materials plotted in Geldart's diagram.

The size distributions of micronised dolomite and cement have been obtained in a sedimentation cell (SEDIGRAPH) [39] to allow identification of the smallest size classes contained in these fine powders. The size distribution of the alumina has been found in a laser diffraction unit (HELOS) [40]. The other size distributions have been found by sieving through a column of woven wire cloth sieves according to "Test Sieving-part 1, Methods using Test Sieves of Woven Wire Cloth and Perforated Metal Plate" ISO 2591-1. Granulated PVC required wet sieving to avoid the strong triboelectric charging that would otherwise make this material stick to any surface in its proximity (the walls and the roof of the sieve). Fluidization tests were carried out in a tester designed and manufactured at POSTEC [41]. Details of the fluidisation tester can be seen in Appendix E. The Jenike tests were carried out in a standard Jenike tester [42].

The physical characteristics of the particulate materials, obtained as described above, are presented in Table 4.1. Only the physical characteristics that were determined for all materials have been included. This is to enable a comparison of characteristic properties, that are obtainable for all of the materials, with conveying properties. The complete set of data for the characteristics, including fluidization characteristics and particle size distributions, are presented in Appendix B .

4.5 Degradation of the Material During Conveying Tests

In general a small amount of degradation took place for each of the materials during the conveying tests. This effect is greatest for the fine materials such as cement and micronized dolomite, with a reduction in the median particle size of 10% being typical. The aluminium oxide seems to demonstrate an increase in large particles as well as fines. This is probably due to the fact that some fines were lost each time the sending tank was filled, due to an escape of dust. Even for the coarse materials, polyethylene pellets and rape seed, a small reduction in the median particle size can be seen. All size distributions are shown in Appendix B.1.

Table 4.1 Physical characteristics of materials.

	Particle density [kg/m^3]	Poured bulk density [kg/m^3]	Median particle size [μm]	Mean particle size [μm]	Minimum fluidization velocity [m/s]	Permeability prior to fluidization [m^2/(Pa*s)]	Wall friction angle against ST37 [Deg]	Static angle of repose [Deg]	Dynamic angle of repose [Deg]
Polyethylene Pellets	913	555	3654	3667	1.0	$1.1.10^{-4}$	14.8°	38°	37°
Rape Seed	1164	687	1660	1650	$4.3.10^{-1}$	$3.2.10^{-5}$	18.7°	30°	30°
Sand	2645	1590	622	687	$2.5.10^{-1}$	$1.9.10^{-5}$	16.3°	36°	33°
PVC Granules	1414	518	444	472	$8.1.10^{-2}$	$1.1.10^{-7}$	19.7°	37°	35°
Alumina	3399	939	78	87	$3.1.10^{-3}$	$4.0.10^{-7}$	22.8°	47°	34°
Microdol 100	2865	1212	66	91	$3.0.10^{-4}$	$4.0.10^{-8}$	26.1°	63°	39°
Cement	3095	734	11	15	$3.2.10^{-4}$	$1.0.10^{-7}$	29.3°	65°	33°

5. The Conveying Characteristics of the Materials and Determination of Conveying Limits

The conveying characteristic of a material is a contour plot of three of the variables describing its time averaged behaviour in a pneumatic conveying pipeline. The variables included in the plot are air flow rate, solids flow rate and pressure drop. These are the values of interest for design purposes, since they allow the selection of the air mover, and the pipeline.

A number of combinations exist for selecting the air mover and the pipeline diameter. By increasing the pipeline diameter and the volumetric flow rate of the air mover, a reduced pressure drop can be obtained. The most economic combination of air mover and pipeline must be evaluated individually, and several limitations have to be taken into account. The conveying limit, the maximum pressure drop with a given air mover and the necessary mass flow of solids are such limitations, and the conveying characteristic contains information about all of them.

Since experimental data for the transportation of a material is usually only obtained for one specific conveying pipeline, this set of data needs to be transformed to be valid for a new pipeline configuration. A review of methods for scaling test data has been published by Wypych et. al. [43]. These methods rely on the use of equivalent horizontal length for pipelines of different geometry. This means that bends and vertical sections have to be recomputed to equivalent horizontal length. Recently a new method for predicting pressure drop in pneumatic conveying systems has been developed, that is based on identifying the specific pressure drop for each individual construction element of the pipeline [44]. This removes the necessity of computing equivalent length. Data presented in this investigation have been obtained in a purely horizontal section.

The determination of conveying limits, which is an important part of this investigation, to some extent relies on observing the dynamic behaviour of the flow of solids in the pipeline. Whereas we only need the time averaged values to generate the conveying

characteristic, we need the complete set of pressure and mass flow data to identify conveying limitations. Alternative ways of doing this will be discussed in the Section 5.3.

5.1 Types of Conveying Characteristics

There are several alternative ways of plotting air flow, solids flow and pipeline pressure drop. Different variables representing air flow may be selected, such as volumetric flow rate at normal atmospheric conditions, air velocity at the start of the pipeline, or mass flow rate of air. For solids flow rate, one can either select mass flow rate of solids or solids loading ratio. The pressure drop can be represented by the total pressure drop, or by the specific pressure drop or pressure gradient. The pressure gradient may also be found in several ways, but should preferably be computed from pressure transducers positioned a distance downstream of a bend or a feeding section that is longer than the acceleration length for the material under the given conditions. Typical pressure drop curves will be shown later, and as mentioned in the previous section the pressure gradients reported in this investigation are computed from the last four pressure transducers in the first horizontal pipeline section (se Fig 3.4). In this way acceleration effects were avoided for all materials under all conditions, because the acceleration length was never observed to be larger than 9m (which is the distance to the first of the transducers used for obtaining the pressure gradient)

One may also choose to plot these values using either of them as ordinate, abscissa and contour. The two most commonly used methods both use air flow as abscissa, and only differ in which variable they plot as ordinate. The technique which uses solids flowrate as ordinate is commonly attributed to Mills [45]. The one using pressure drop as ordinate is attributed to Zenz [6]. Two typical conveying characteristics of these kinds can be seen in Figures 5.1 and 5.2 respectively. They both display the same set of data, and can be compared directly.

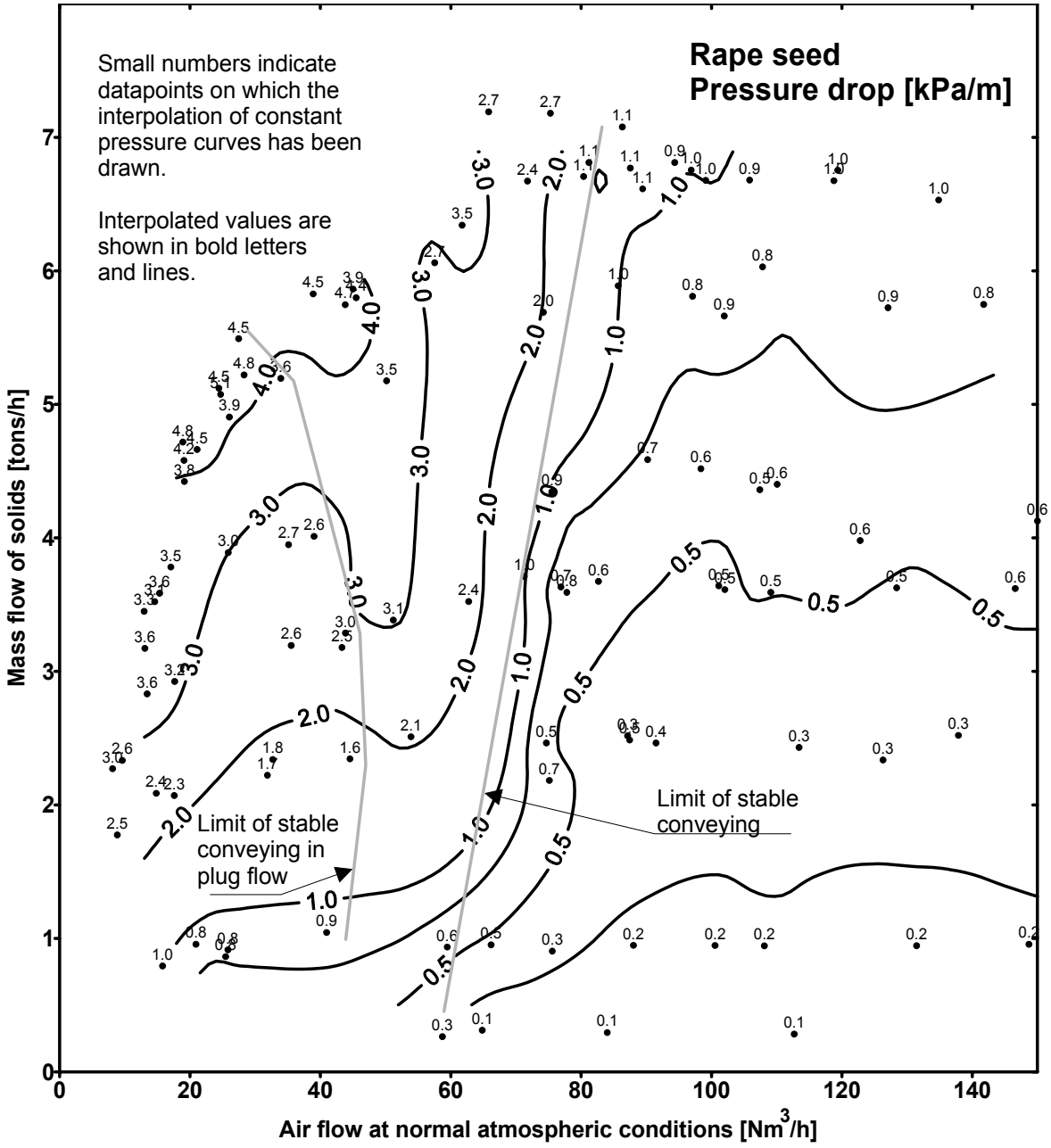

Figure 5.1 Conveying characteristic of the Mills type.

As one can see from the examples, the Mills type diagram has a clear advantage in that it displays the data more homogeneously distributed over the plot area. This may be important for some powders which have extreme variations in the pressure drop with conveying velocity.

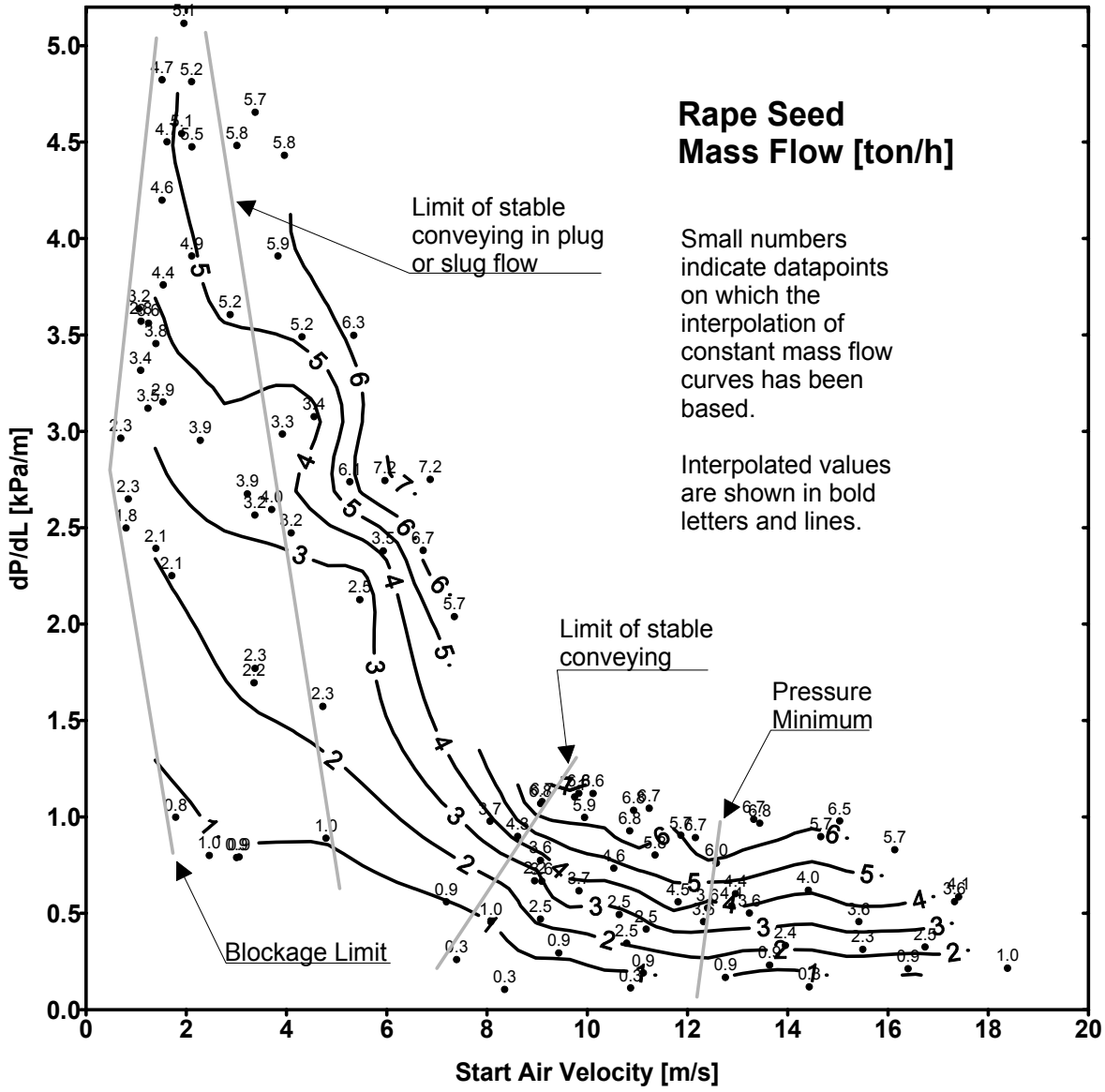

Figure 5.2 Conveying characteristic of the Zenz type.

A second advantage of the Mills diagram is that it displays the data with independent variables, air flow and solids flow, on the axes, and the dependent variable, pressure drop, as a response surface to the two previous variables. This gives a clear picture of the interrelation between these variables, which is advantageous for engineers and students reading conveying characteristics for the first time. The most important advantage of the Zenz type plot is that it is easier to interprete for our purpose because it displays the start velocity of the air which is considered to be of direct relevance to minimum conveying conditions.

In both of the plots, two important conveying limits have been indicated. To the left lies the limit between stable plug flow and unstable modes of flow, and to the right lies the limit between unstable modes of flow and stable suspension or partially suspended flow. The pressure minimum curve seems to be easier to identify for the Zenz type diagram.
For the Zenz type plot it has been customary to display the solids loading ratio instead of the mass flow of solids. This is not considered to be useful since for some materials (e.g. aluminium oxide) it inhibits the observation of the pressure minimum curve. For Alumina the pressure minimum cannot be observed because the constant solids loading curves are all increasing functions of start air velocity. The pressure minimum in this case coincides with the limit of stable conveying, which is not the case for the mass flow plot. When applying conveying characteristics for design of new conveying systems it is also the actual mass flow of solids that is of interest. The use of solids loading ratio in a conveying characteristic will in this case only result in reduced readability.

5.2 Conveying Characteristics Obtained in the Test Program

For the reasons given in the previous section the decision was made to plot the conveying characteristics as Zenz type plots. For the abscissa, the superficial start air velocity has been selected. For the ordinate, the pressure gradient in the steady conveying part of the pipeline has been selected. And finally the constant mass flow rate curves have been drawn in this co-ordinate system. The conveying limits have been drawn according to the guidelines developed in Section 5.3. The accuracy that has been obtained when identifying conveying limits is treated in Section 5.5.

The conveying characteristics represent seven very different materials, the physical characteristics of which were presented in Table 4.1. As a result there are great differences in the conveying characteristics displayed in Figure 5.3. The types of conveying characteristic generally falls into three different categories:

- The first exhibit no “dense phase” conveying.
- The second exhibit a discontinuous change into “plug or slug” flow.
- The third has a continuous change into “moving bed” flow.

The categories correlate with the classifications of Geldart [36], Dixon[46], Mainwaring[47] and Jones[48].

The two materials that exhibit slugging/plug flow are polyethylene pellets and rape seed. A quick inspection of the two characteristics show that the conveying limits of rape seed in general are lower than those for polyethylene pellets. Mass flow of solids and pressure drop are higher for rape seed than for polyethylene pellets for a fixed value of air velocity.

The characteristics that exhibit no "dense phase" conveying are those of alumina, PVC granules and sand. In addition to the variation in conveying limits, mass flow of solids and pressure drop, these characteristics also vary in shape. One interesting point of note is the change in the distance between curves of constant mass flow towards increasing mass flow of solids for alumina and PVC.

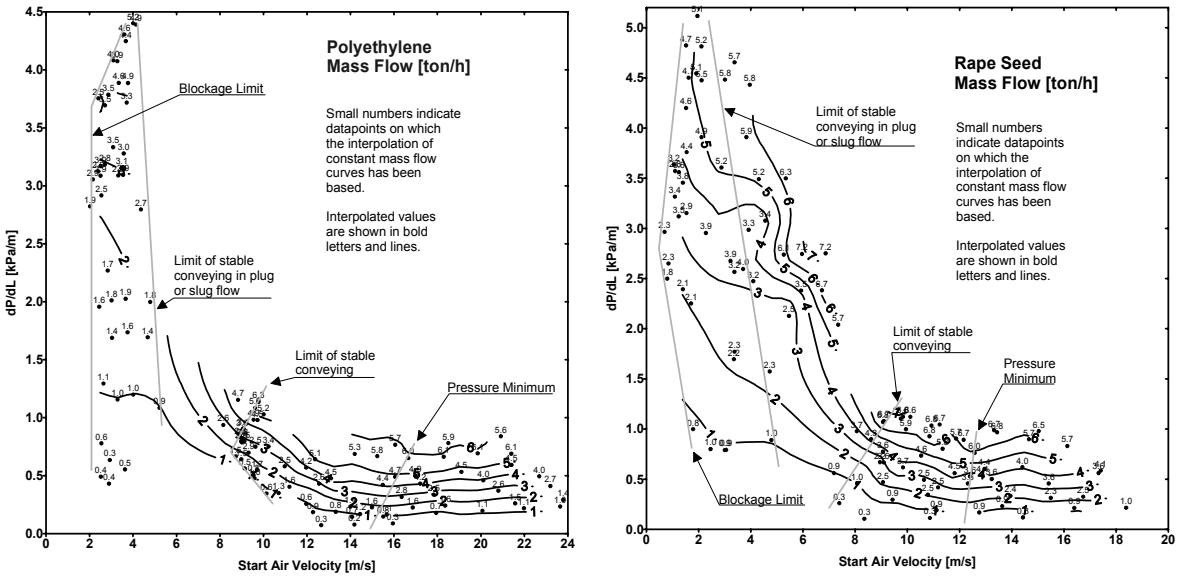

Figure 5.3 Conveying characteristics for all the materials included in the test work

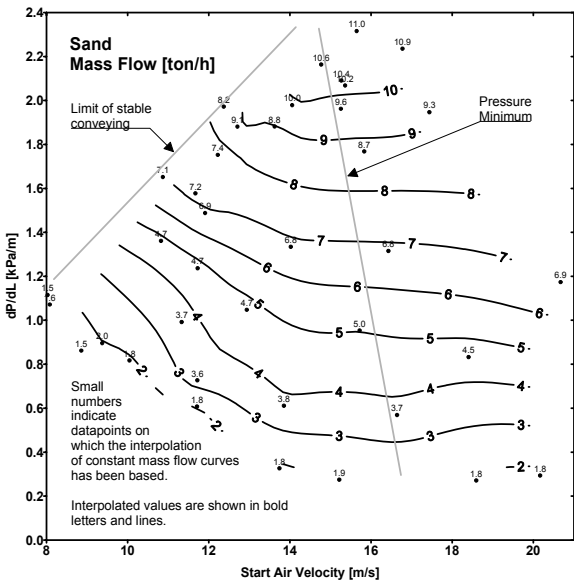

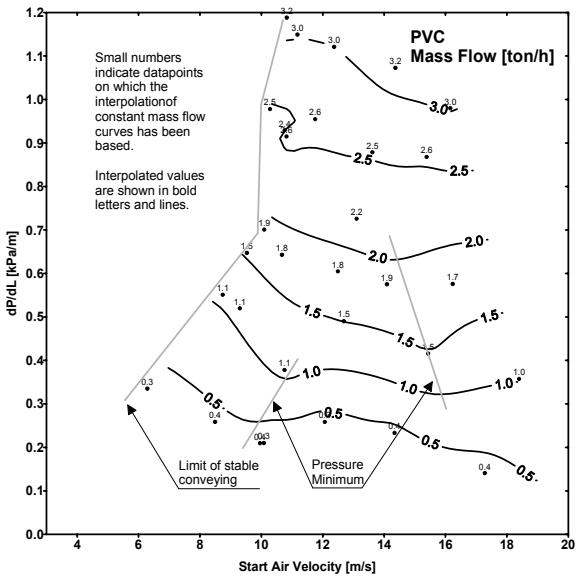

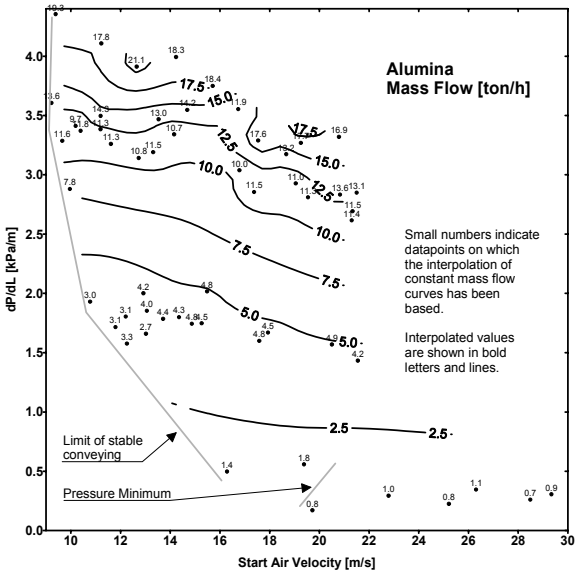

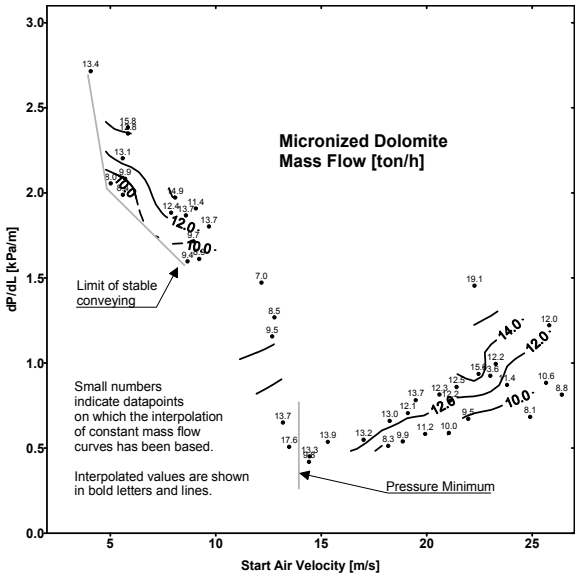

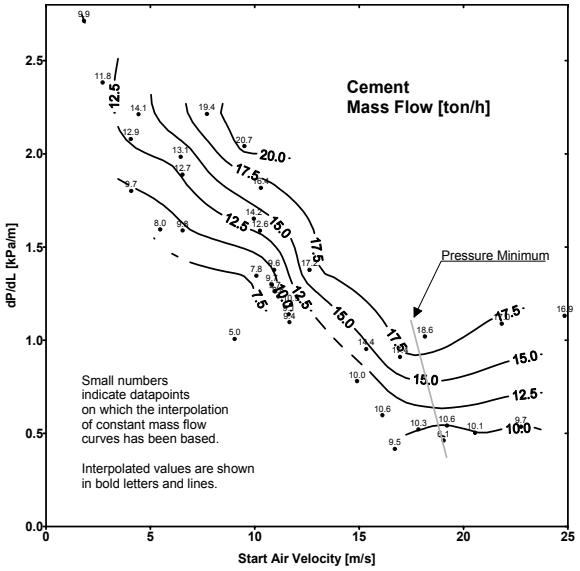

Figure 5.3 (continued) Conveying characteristics for all the materials included in the test work

The materials that can be conveyed in moving bed flow have mass flows and pressure drops that are similar. Maximum mass flow obtained is slightly higher for cement than for micronized dolomite. But the largest differences lie in the shape of the characteristics. The constant mass flow curves for micronized dolomite converge towards the pressure minimum.

An overview of all the conveying data on which the characteristics have been based can be found in Appendix D. The conveying characteristics can be found in Appendix C.

5.3 Identification of Conveying Limits

A conveying characteristic displays time averaged values taken in a interval of stable conveying conditions, where the mass flow rate of solids and pressure drop is stable. It is not possible to read from the conveying characteristics any information about the dynamic behaviour of the system. The introduction of a conveying limit requires some information about the dynamic behaviour of the flow of solids and air, since it is the instability of these values that characterises a blockage or unstable flow. This additional information may come from visual observations of the flow pattern at some point in the pneumatic conveying line, or from observation of the dynamics of measured pressure, air flow or mass flow.

Visual observation has been used by several authors. There are many problems with visual observation. First of all the method relies on the subjective judgement of the observer, and it is difficult to give precise definitions of the flow patterns that occur since granular materials behave differently. Secondly, the flow pattern changes dramatically along the pneumatic conveying pipeline, especially close to the conveying limit. This was observed for all the materials discussed in the previous section. The point at which observations are made will therefore influence the result.

A very simple way of determining the minimum conveying velocity limit visually has been used by Zenz [6]. He makes observations of single particle movement, and identifies the conveying limit as the velocity limit when particles start rolling or bouncing along the

pipeline wall. Matsumoto[11] and Cabrejos[12] make observations of the same type, but use higher concentrations of solids in the pipeline.

Several methods that are not based on visual observation also exist. Rose and Duckworth [18] consider the conveying limit to be the point at which the flow of solids becomes unstable. They do not define what they mean by unstable flow, so it is difficult to relate their data to other data for minimum conveying velocity conditions. A simple and precise way of defining a conveying limit is to identify the pressure minimum curve from the conveying characteristic. This method is used both by Matsumoto [11] and by Rizk [19]. As Matsumoto points out, however, this method, even though it is simple and objective, does not correlate to observations of saltation, or to observations of the limit for stable flow.

A number of other techniques for identifying the conveying limits of a material, based on using objective criteria have been considered/utilized by the author of this thesis. These methods are:

- Measurement of different statistical properties of the pressure fluctuations in the pipeline.
- Direct registration of peaks in the pressure at the beginning of the pipeline and in the air flow at the exit of the pipeline.
- Visual observations of flow pattern at three points along the pipeline supplemented by pressure peak observations.

5.3.1 Visual Observations and Pressure Peaks.

The method of visual observation used was based on observing rapid changes in the flow pattern. This was found to correlate reasonably well with observations of peaks occurring in the pressure at the beginning of the pipeline. Since immediate information about the condition of the flow could be obtained by visual observation, this method was used as a screening for assessing the results of a test run. Since changes in the flow pattern in some cases was difficult to observe, especially when the test run came close to the conveying

limit, additional inspection of the pressure plot was used. The conveying limits drawn in the conveying characteristics in section 5.2 have been identified by this method.

Two plots of the pressure at the beginning of the pipeline can be found in Figure 5.4. Both are for a conveying condition close to the limit of stable conveying, but one displays a peak in the pressure attributed to incipient blockage. For longer pipelines and more complex geometries the method of observing peaks in the pressure does not work. In a M.Sc. project at Telemark College Yström [49] concludes that observation of air flow at the exit of the pipeline is a better solution for these situations.

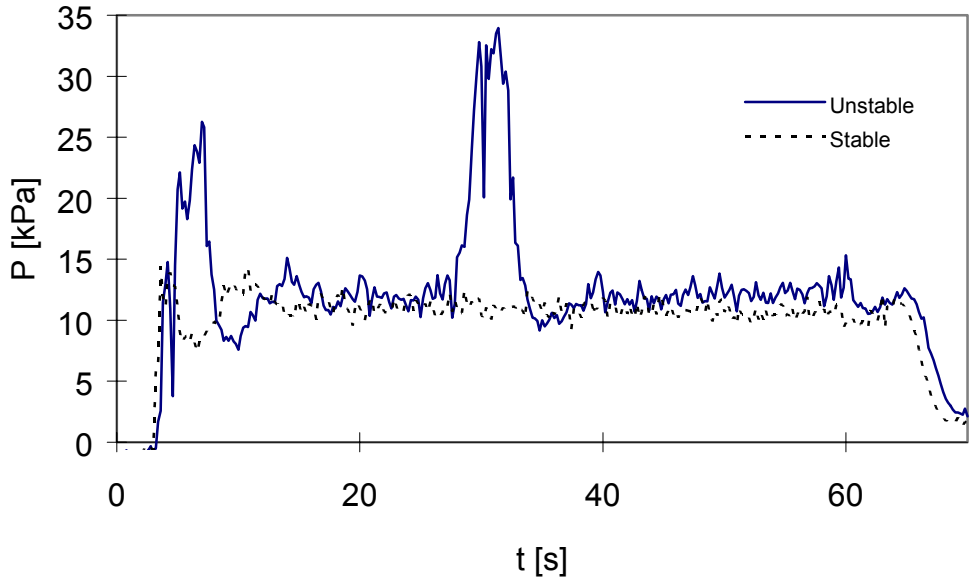

Figure 5.4 Two plots of the pressure at the beginning of the pipeline.

5.3.2 Statistical Analysis of Pressure Fluctuations

As detailed in the previous section, observations of peaks in the pressure plot proved to be useful as a supplement to visual observations when identifying conveying limits. In an attempt to standardise this procedure the standard deviation and the kurtosis [50] of the pressure on the different transducers were computed and mapped onto the conveying characteristic. The peaks in the pressure were then expected to contribute to the increased standard deviation and kurtosis of the pressure signals, and regions of unstable flow were expected to show as areas with high standard deviation and kurtosis. The standard

deviation and kurtosis for rape seed are presented in Figures 5.5 and 5.6. As one can see, both methods give increased values in the region of unstable conveying: i.e. between stable suspension flow and stable plug flow. It is also easy to see that the standard deviation plot gives the clearest distinction between stable suspension flow and unstable flow. The same is the case for the limit between stable plug flow and unstable flow. For all the materials tested, the standard deviation gives the clearest distinction.

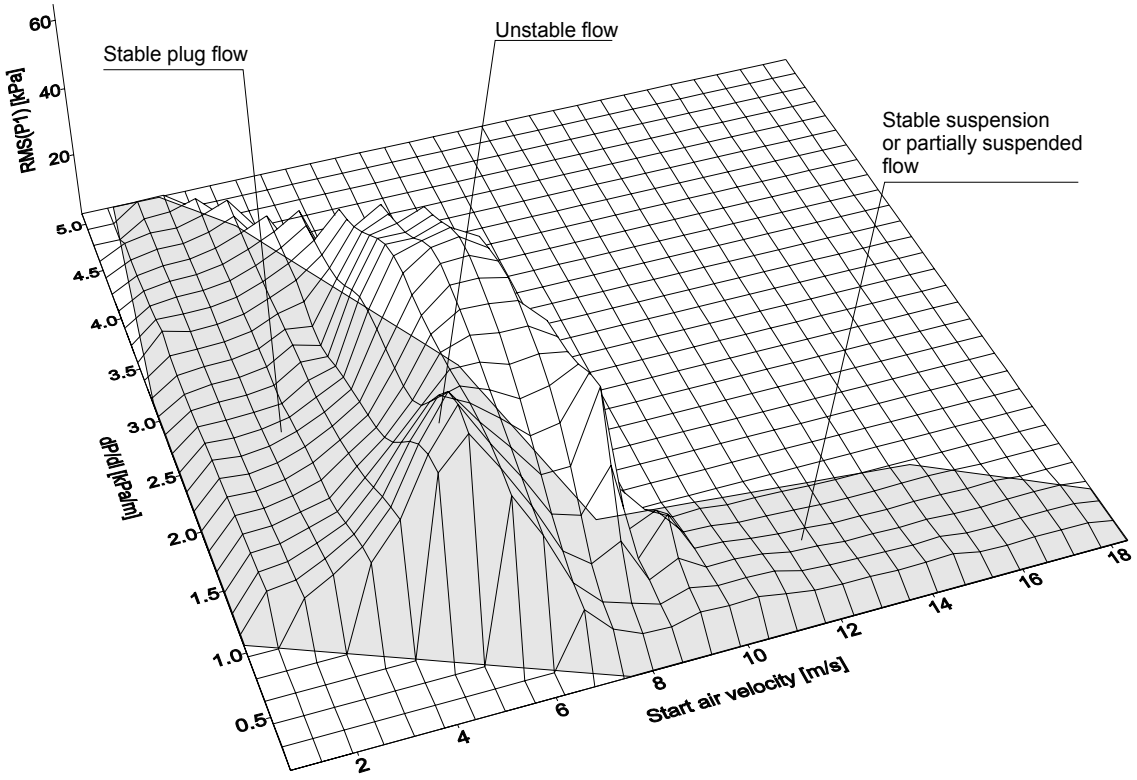

Figure 5.5 Standard deviation map of pressure on transducer 1 relative to start pressure for rape seed.

There may be several reasons for why it is difficult to use the statistical properties of the pressure signal to identify the conveying limit. The occurrence of blockages close to the conveying limit must be dependent on some perturbation of the flow. A perturbation could come from inhomogeneties in the material fed into the pipeline, bulk density variations, size variations or variations in the mass flow of solids into the pipeline. The most likely candidate is flow rate variation, which for coarse granular materials might be increased at low feed rates due to mechanical bridging of the slide valve controlling the mass flow of

solids. For fine materials exhibiting cohesion, bridging might contribute to perturbations of the flow of solids. The occurrence of such perturbations is stochastic in nature and can be expected to be more pronounced close to the limit of stable conveying.

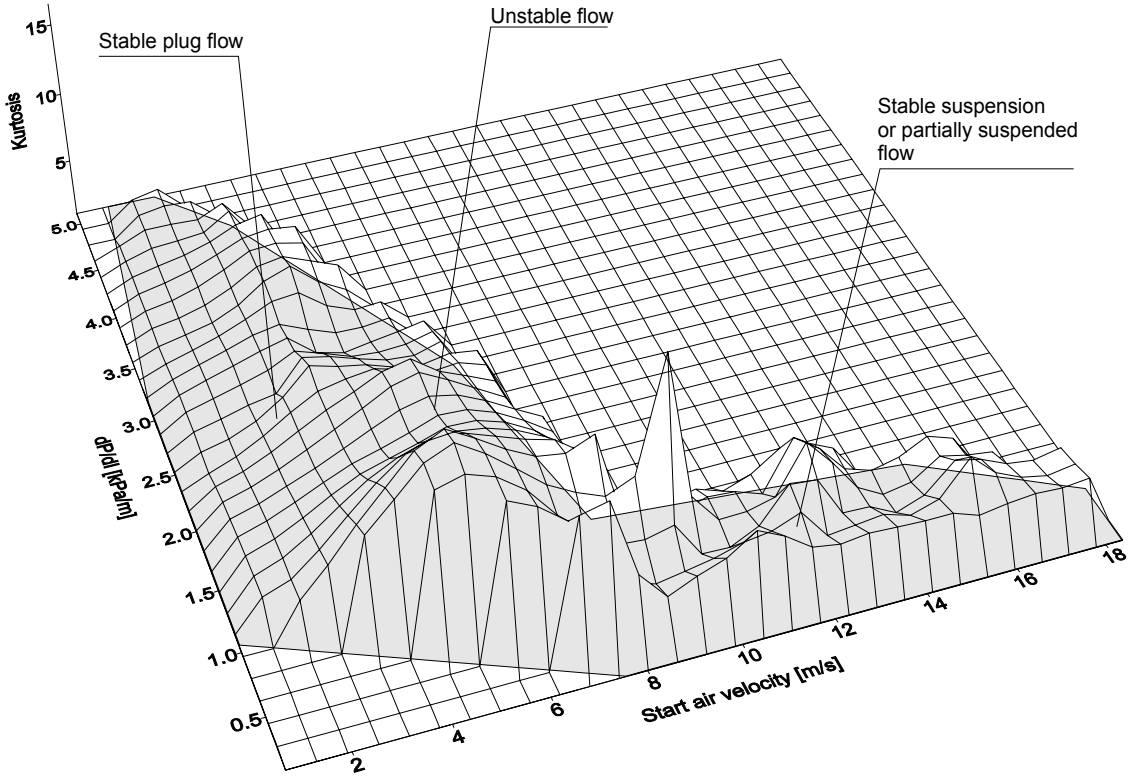

Figure 5.6 Kurtosis map of pressure on transducer 1 for rape seed.

With the length of the time series of data that are available with the test facilities described here, the stochastic nature of incipient blockage will make it more difficult to use statistics for identification of blockage limits.

Direct observation of unstable modes in the pressure fluctuation can also be made. For the polyethylene pellets it was possible to set the airflow so close to the conveying limit that low frequency pressure fluctuations could be observed to turn unstable. An example can be seen in Figure 5.7. In this case the air flow is first set to give marginally stable conditions (and the initial low frequency pressure fluctuation is damped), at approximately 40s the airflow is slightly reduced whereafter the low frequency pressure fluctuations can be seen to be undamped or slightly increasing (which means that it is marginally unstable). So it is

not difficult to quantify what is meant by unstable flow (the flow is unstable when a perturbation in the flow leads to growing fluctuations), and the limit of stable flow can be found directly by watching the pressure plot of the test runs.

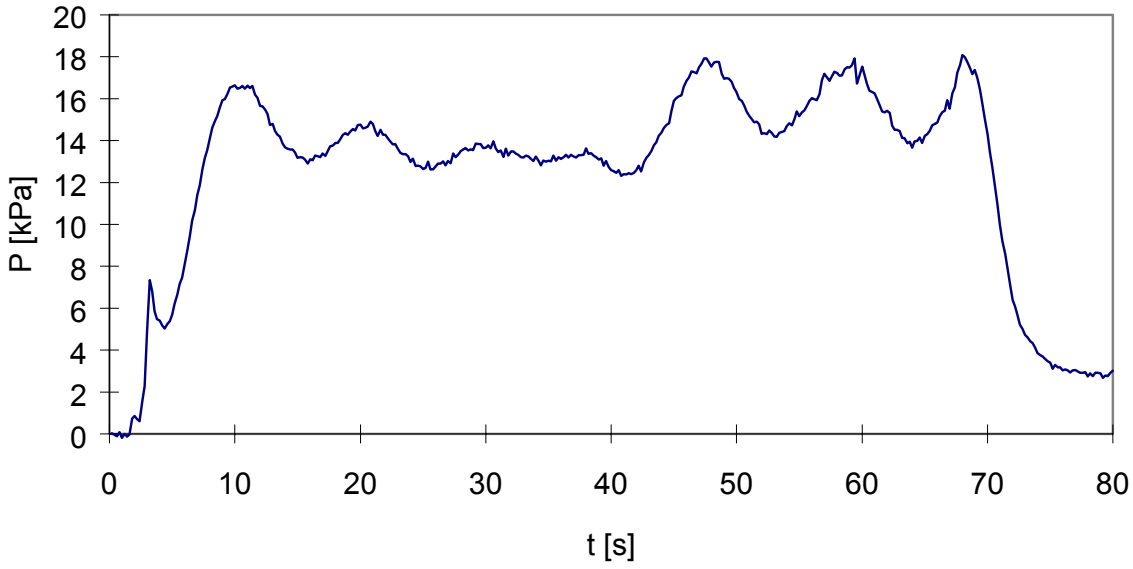

Figure 5.7 Pressure plot for polyethylene pellets

One might wonder why these low frequency fluctuations are present for polyethylene pellets and for none of the other materials. A possible explanation may be that the whole conveying system can be regarded as a dynamic system. The easiest way to understand this phenomenon is to use the mechanical equivalent of a mass on a spring driven by an oscillatory force and damped by friction. The dynamics of the pneumatic conveyor is driven by the air supply. The volume of the blow tank and the pipelines constitutes an inertial effect, and friction loss is associated with the air and solids flowing out of the system. In this case the low frequency seen in Figure 5.7 may well be associated with an eigen frequency of the system. It is therefore possible that it is the dynamics of the pneumatic conveying system itself that influences the stability.

5.4 The Minimum Conveying Velocity and Changes After Introducing a Horizontal to Horizontal Bend

Preliminary experiments, using a more complicated line geometry not described in this thesis, gave indications that the geometry of the pipeline might have some influence on the blockage of the pipeline. Blockage of the pipeline was often observed to take place in the section after the first horizontal-to-horizontal bend in the pipeline. At the time, the instrumentation of the test facilities was too sparse to determine where exactly the blockage occurred, but since the blockage did not seem to take place at the material inlet, it was decided that the geometry of the pipeline might have some influence on the result. The literature survey of velocity limits in horizontal gas-solids flow has shown that no experiments have been carried out to investigate the effects of bends on minimum velocity conditions.

After having carried out the conveying tests in the straight horizontal pipeline, these tests were repeated for three of the materials in a pipeline with a horizontal to horizontal 90° bend. The materials selected for repetition were of type A,B, and D according to Geldarts classification, to cover a broad range of physical properties. The conveying characteristics obtained in this way are shown in Figure 5.8. For each case the corresponding characteristics without a bend (from Figure 5.3) are plotted to the right.

Comparison with the characteristics obtained without a bend, shows two differences worthy of note. In the low mass flow rate part of the conveying characteristics for PVC granules and rape seed the limit of stable conveying in suspension flow seems to have changed.

The conveying velocity limit for PVC seems to have been reduced with a bend, but with the limited accuracy of the conveying limit in this part of the characteristics no definitive conclusion can be made. Judging from the raw data, the last point of stable conveying without a bend is further from the actual limit than the last point of stable conveying with a bend. In this case the difference is just a result of the poor accuracy in deciding the conveying limit in this part of the characteristic.

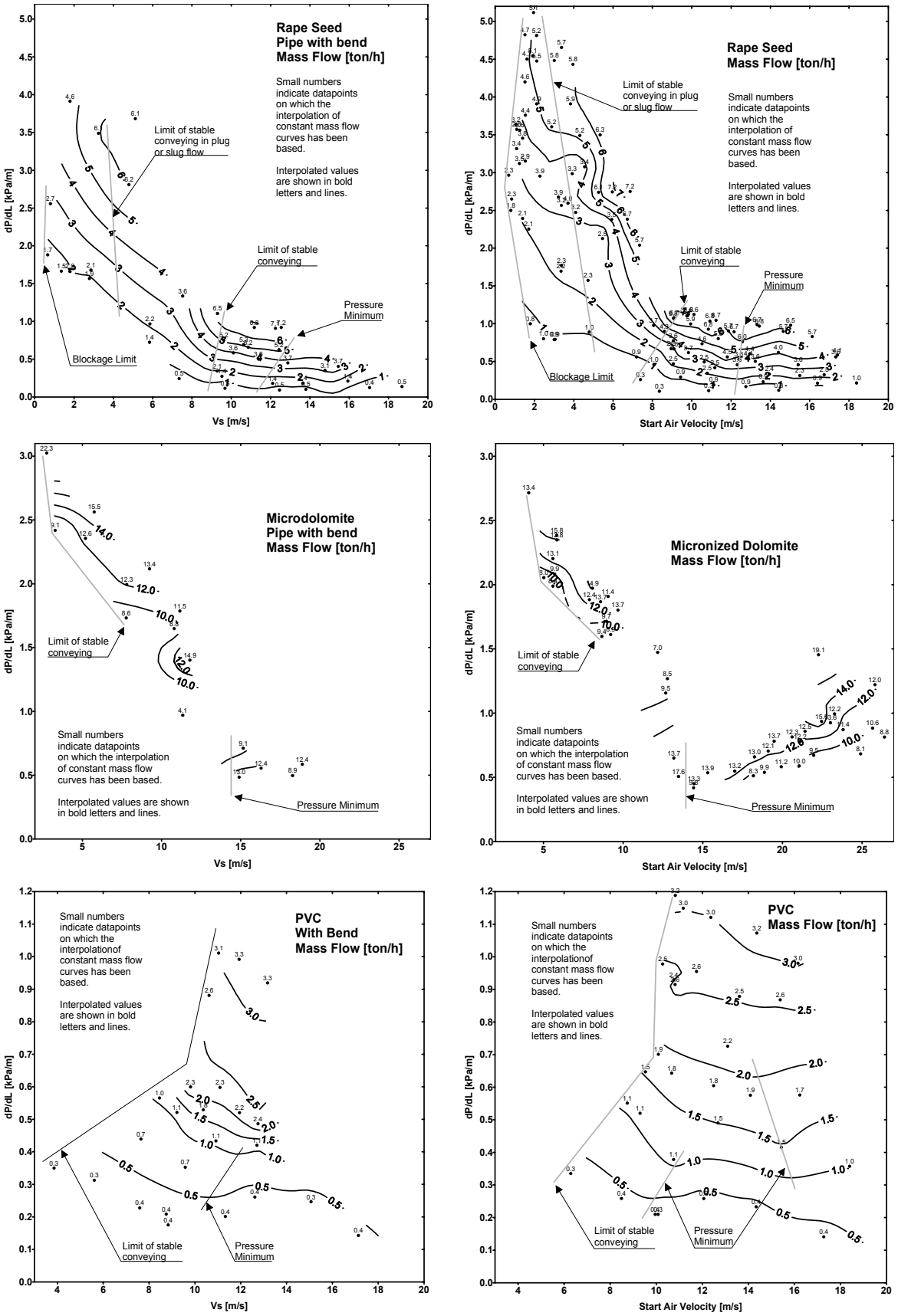

Figure 5.8 Conveying characteristics for three materials with and without a horizontal to horizontal bend

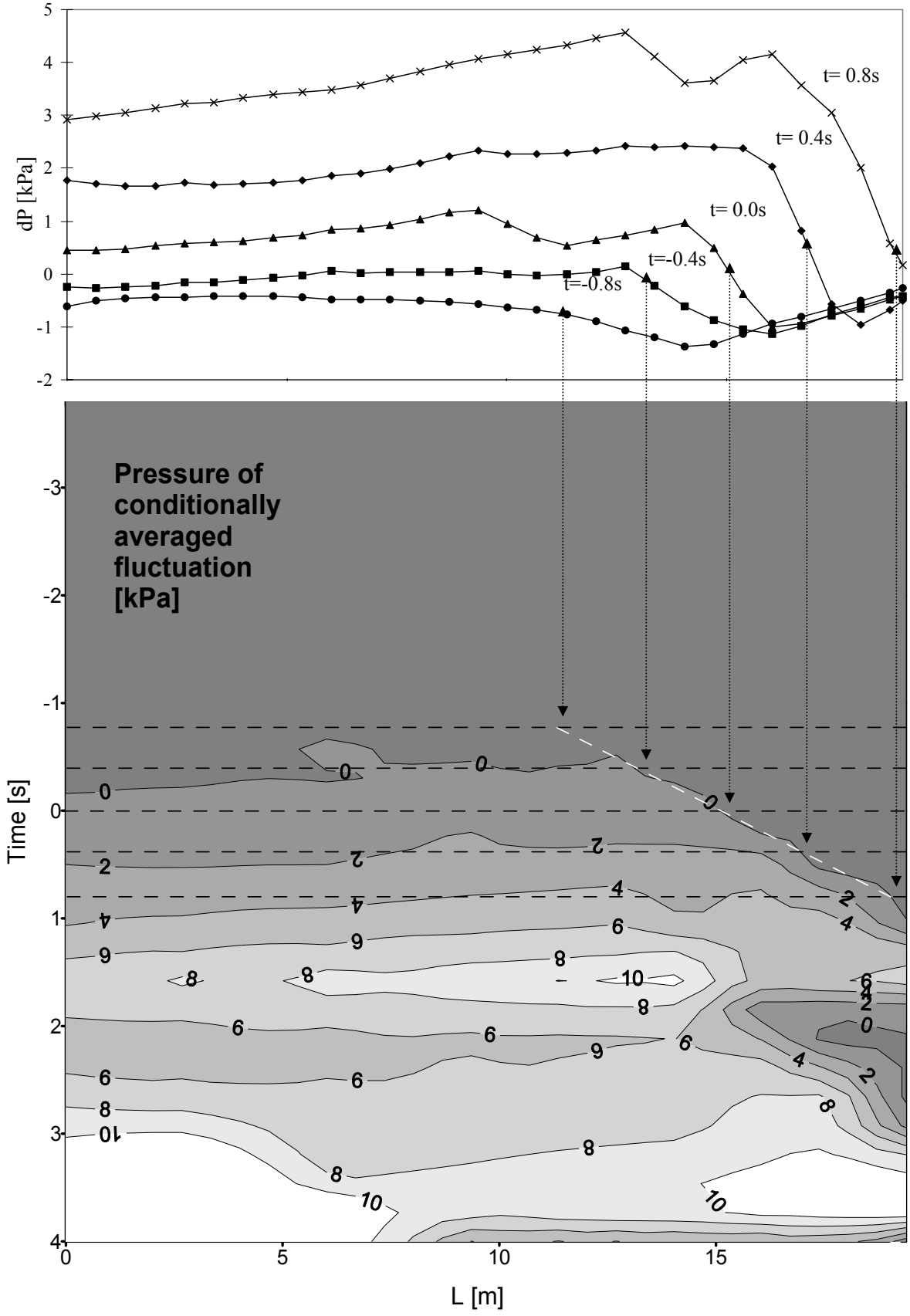

Figure 5.9 Contour plot of conditionally averaged pressure fluctuation at incipient blockage.

The conveying velocity limit for rape seed is increased when introducing a bend. There is one data set, with a bend, that differs from the results without a bend. A conditional averaging of the 6 occurrences of peaks in the pressure on transducer 1, for this data set, clearly shows that the blockage is initiated at the bend section. In Figure 5.9 this can be seen by following the zero pressure line from t=0. This line breaks at transducer 7 indicating a slug or plug occurring at the bend and being transported along the pipeline causing a temporary blockage. Since the observation of a temporary blockage occurring at the bend coincides with the observation of an increased minimum conveying velocity, this clearly shows that the bend has an effect on the minimum conveying velocity for rape seed at low solids feed rates.

Figure 5.9 has been obtained using the conditional averaging scheme described in Section 7.3. Curves of constant pressure have been plotted, and the time developement of a typical pressure fluctuation can be observed.

5.5 The Accuracy of The Conveying Velocity Limits

The accuracy of the conveying limits shown in Figures 5.3 and 5.8 can be estimated by looking at the closeness of the point of stable conveying when approaching the conveying limit. For the pressure minimum the curve has been found by subjectively assessing where the pressure minimum of contours can be found. The assessment of the accuracy of the pressure minimum is therefore more difficult. Table 5.1 lists the estimates of the accuracies obtained in this investigation. These accuracies now give the error bounds that are used in the quantitative comparison in the next chapter, where the reviewed correlations for predicting the limit of stable conveying in suspended or partially suspended flow (which is the main focus of this investigation) have been compared to the experimental data, together with the pressure minimum velocity predictions and the predictions of the limit of stable conveying in plug flow.

Table 5.1 Accuracy of conveying limits

Material	Estimated accuracy of conveying limit [m/s]	Estimated accuracy of pressure minimum [m/s]
Polyethylene pellets	± 0.5	±1
Rape seed	± 1	±1
Sand	± 0.5	±2
PVC granules	± 1 (2 at low mass flow)	±1
Alumina	± 1	±4
Micronized dolomite	±2	±2
Cement	+1 -2	±2

6. Quantitative Comparison Between Data Obtained in the Test Program and Existing Models for Conveying Limits

To carry out the quantitative comparison of the predictions of the different methods for determining characteristic velocity limits, which were listed in Table 2.2, it has been necessary to make several simplifications. All the methods exhibit a dependency either on the terminal velocity of a particle in an infinite expansion of the conveying gas, or on the gas density. Therefore the determination of the conveying limit is an integral part of the design equations, together with the pressure drop computation. It has not been the objective of this investigation to evaluate equations for determining pressure drop. In a real design problem it would be necessary, after an initial estimate, to carry out several iterations computing both pressure drop and minimum conveying velocity, since they are interdependent. To avoid the problem of introducing pressure drop calculations into the evaluation, each method has been compared to the actual operating conditions at which the experimental conveying limit was obtained.

As mentioned previously, the different methods for predicting minimum conveying conditions have been based on observations and measurements that cannot immediately be compared. The investigations by Thomas [7] and Matsumoto [11] show that there is poor correlation between visual observations of saltation and pressure minima, although Matsumoto later chooses to equate the two terms saltation velocity and pressure minimum. Matsumoto and Thomas identify the minimum conveying velocity as the velocity at which a layer forms on the bottom of the pipeline (see Table 2.2). Doig and Roper [10] and Cabrejos et.al. [12] chose to define the saltation velocity as the velocity at which a layer starts to form in the pipeline. In these two cases the visual observation of saltation have both been linked to the pressure minimum and to the limit of stable conveying. This explains some of the problems with definitions that exist in literature about the subject.

The investigations presented in this thesis also show that there is no good correlation between saltation and the limit of stable conveying. As conveying velocity is reduced, a clear layer of solids can be observed to form, before the flow turns unstable, and peaks in the pressure plot can be observed. To be able to compare the models at all, the models that

claim to predict saltation velocity have been compared to the rigorously defined pressure minimum curve in the conveying characteristic.

It is necessary to look at each method to select what characteristic conveying limit it should be evaluated against. Correlations published by Doig and Roper [10], and Zenz [6] give the saltation velocity and are therefore compared to the pressure minimum velocity. Matsumoto et. al. [11] have two correlations to give both the pressure minimum velocity, which is unambiguously defined, and the minimum conveying velocity, which is interpreted as the limit of stable conveying. The correlation published by Rizk [19] also gives the pressure minimum velocity directly. Rose and Duckworth [18], and Thomas[7], compute the minimum conveying velocity, which is interpreted as the limit of stable conveying . Cabrejos et. al. [12,21] compute the minimum pickup velocity of the powder. To evaluate the usefulness of this correlation it has been compared to the limit of stable conveying. Pan [22] and Wirth [16] both give the limit of stable conveying directly.

The different methods are now compared to the experimental results they are expected to predict. Two exceptions have been made. The methods of Wirth and Zenz give predictions that are so poor that they are difficult to plot in the same plots as the other results. Therefore they have not been included in the final evaluation.

Table 6.1 summarizes the results of the evaluation of pressure minimum curve predictions. The methods of Doig & Roper, Matsumoto and Rizk have been included. The range of validity is marked out as areas without shading according to the limits given in Table 2.2.

Table 6.1 The worst case error of pressure minimum curve predictions given in percentage of experimentally obtained value.

	LDPE	R. Seed	Sand	PVC	Alumina	MD100	Cement
Doig & Roper	-25	-55	-76	-85	-95	-87	-91
Matsumoto	48	111	71	16	-70	-4	-82
Rizk	-45	-29	-52	-79	-90	-61	-71

As can be seen from the Figures 6.1, 6.3, 6.5, 6.7, 6.9, 6.10 and 6.11 the ability of each method to predict the pressure minimum curve varies with the solids loading ratio. In

Figures 6.1 through to 6.11 the pressure minimum (pressure minimum curve) and the velocity minimum (the limit of stable conveying in suspended or partially suspended flow) are those obtained in the conveying system described in Chapter 3.

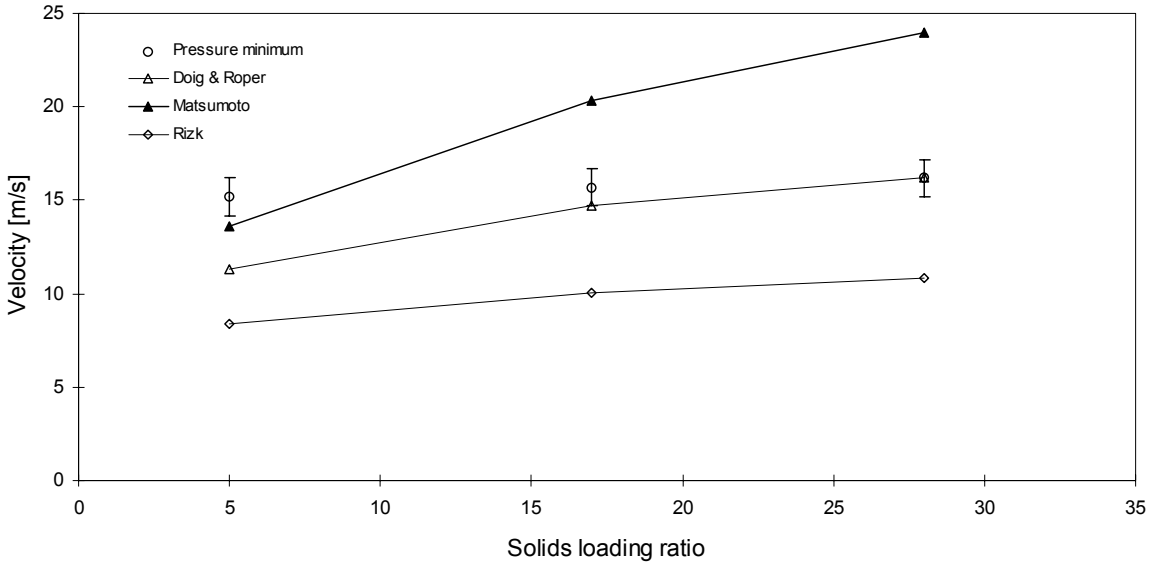

Figure 6.1 Pressure minimum curve compared to predictions for polyethylene pellets

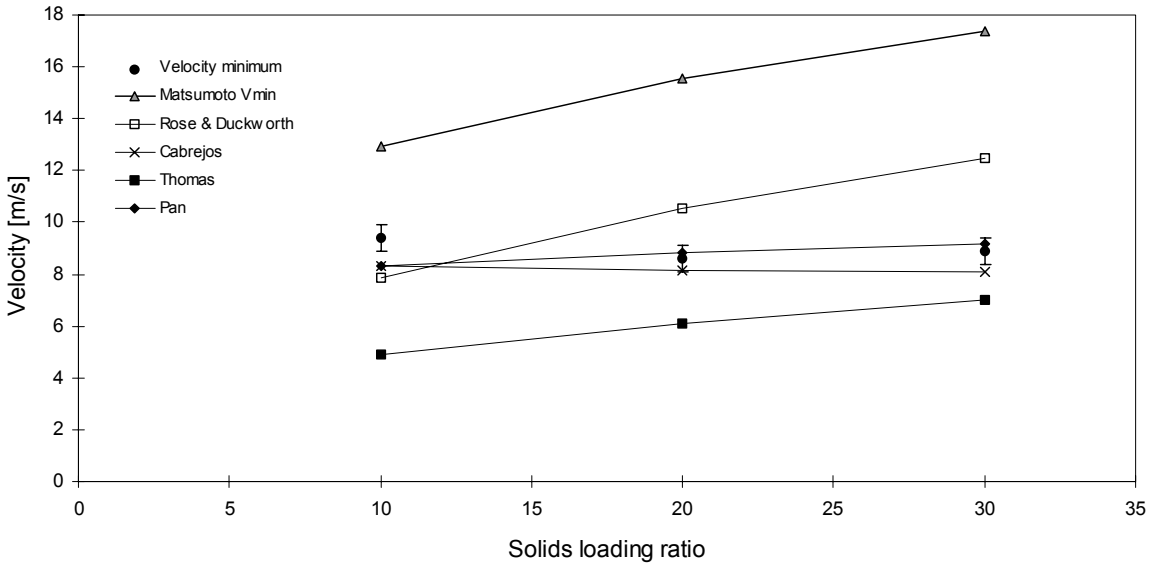

Figure 6.2 Limit of stable conveying (velocity minimum) compared to predictions for polyethylene pellets

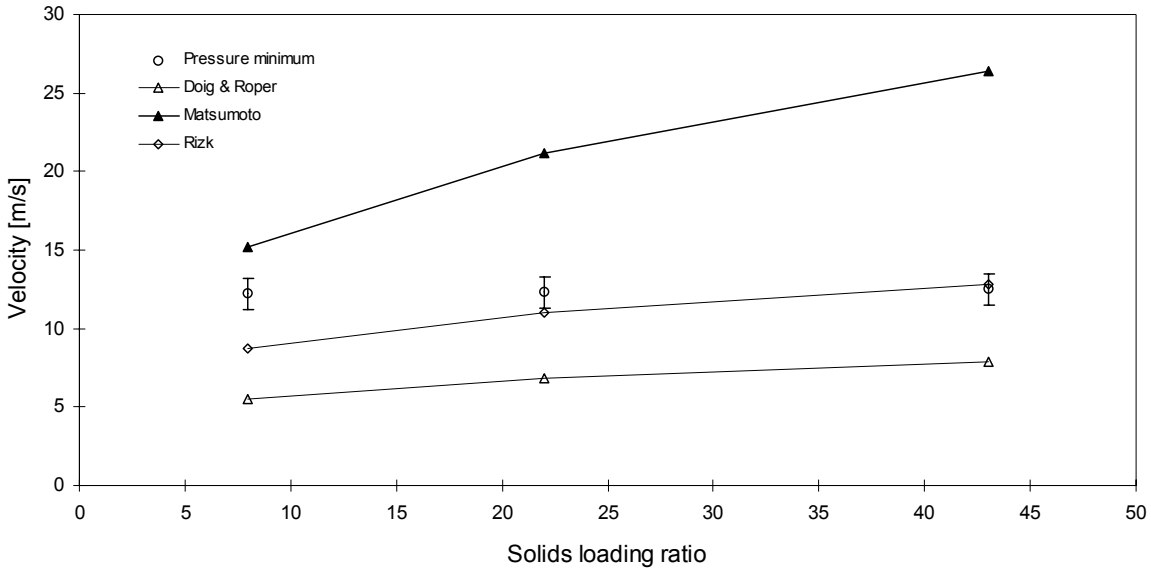

Figure 6.3 Pressure minimum curve compared to predictions for rape seed

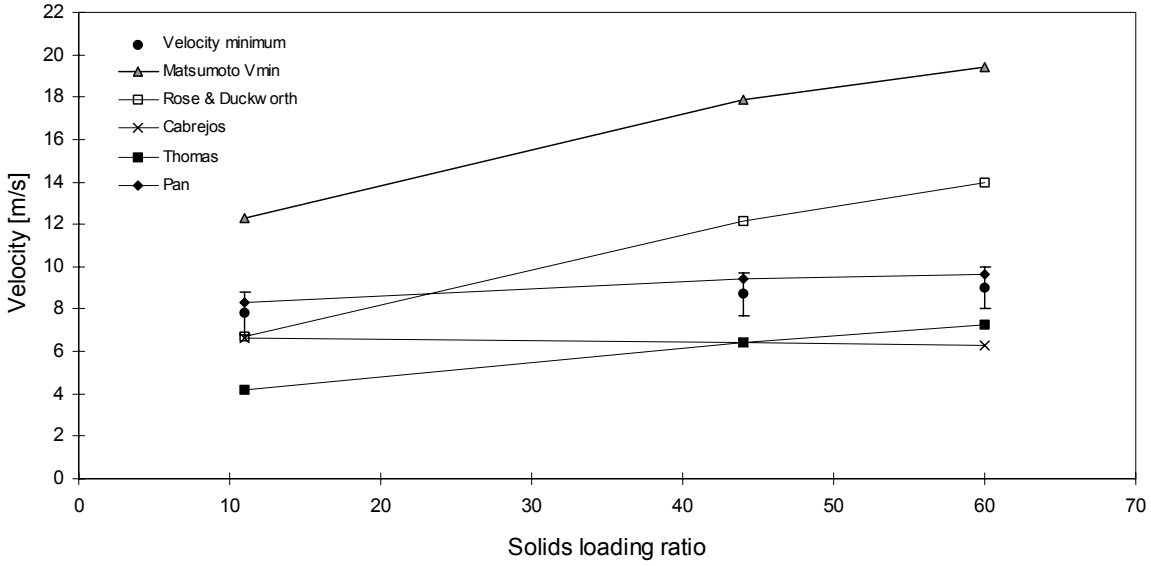

Figure 6.4 Limit of stable conveying (velocity minimum) compared to predictions for rape seed

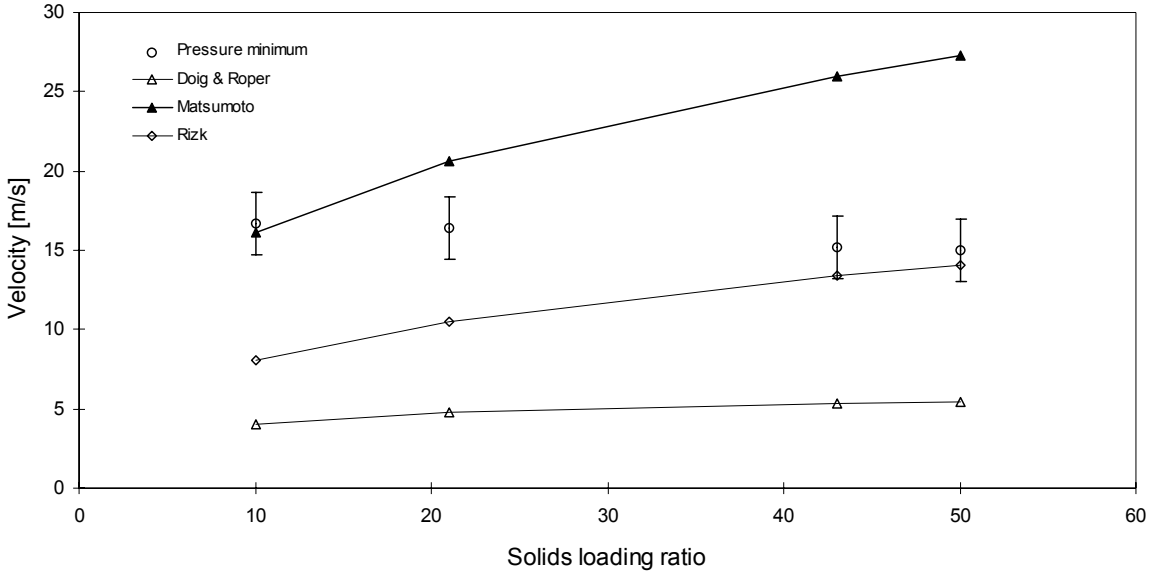

Figure 6.5 Pressure minimum curve compared to predictions for sand

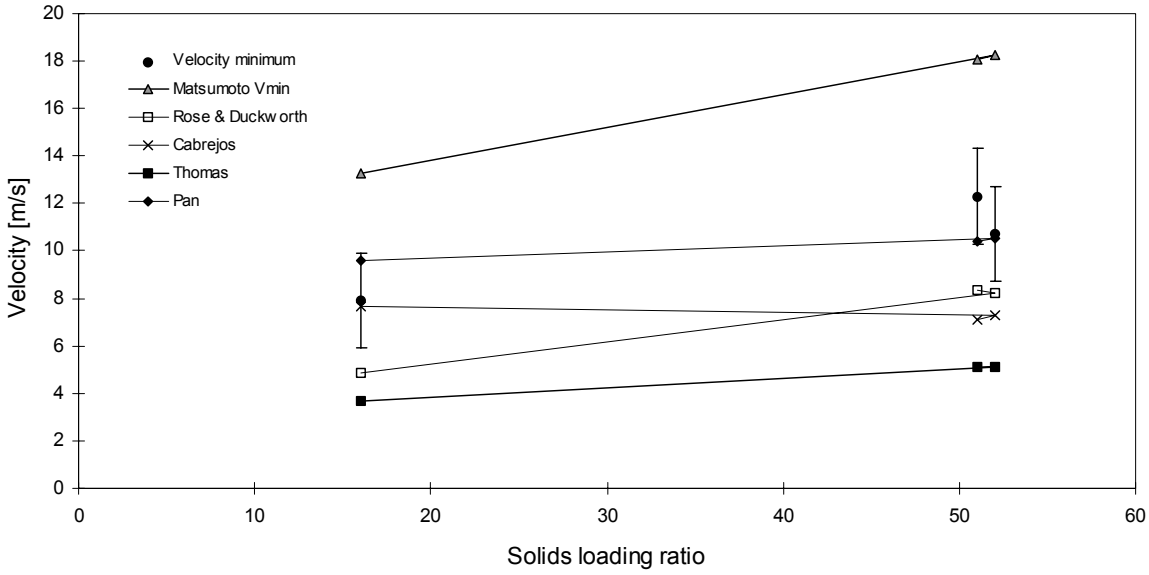

Figure 6.6 Limit of stable conveying (velocity minimum) compared to predictions for sand

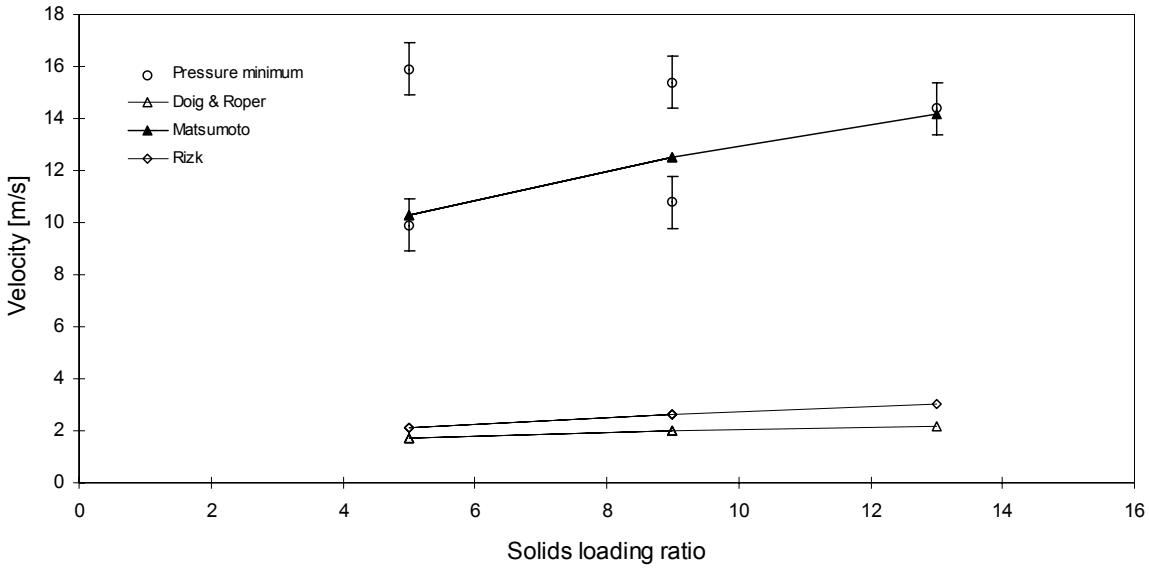

Figure 6.7 Pressure minimum curve compared to predictions for PVC

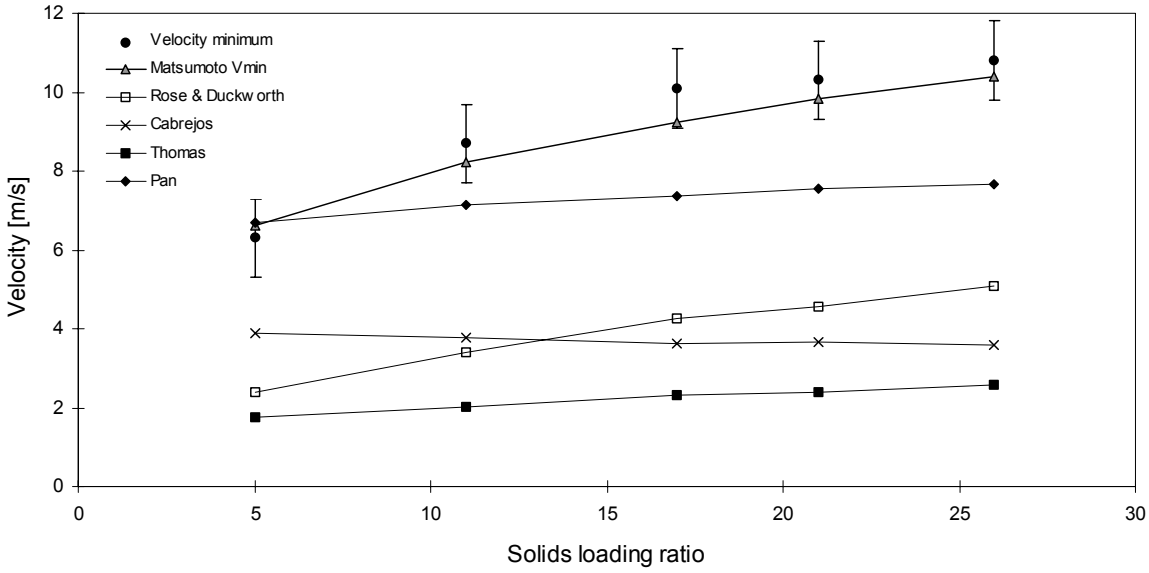

Figure 6.8 Limit of stable conveying (velocity minimum) compared to predictions for PVC

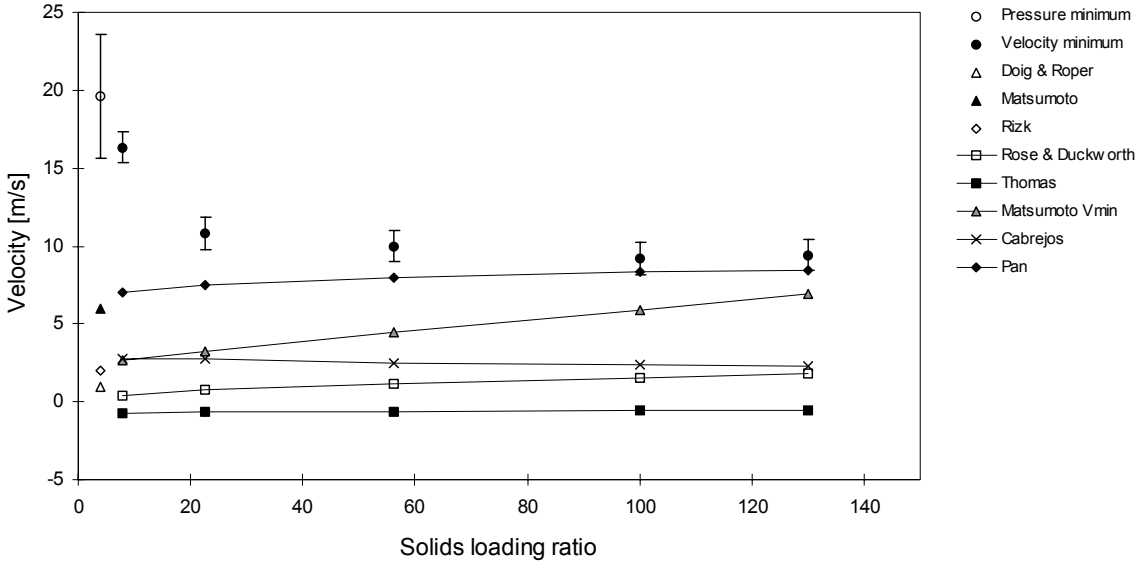

Figure 6.9 Pressure and velocity minimum compared to predictions for alumina

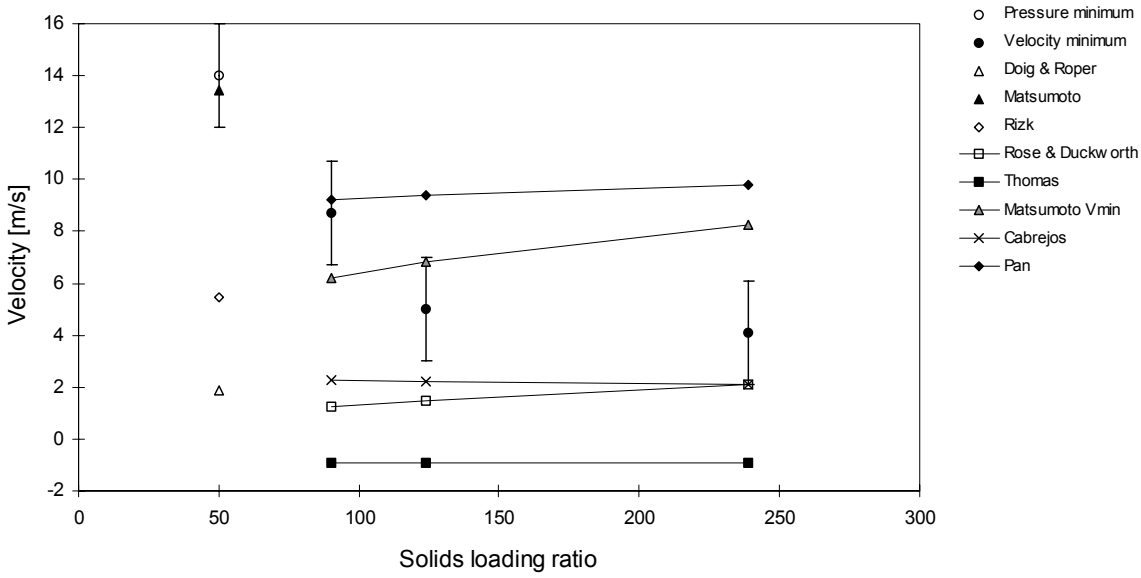

Figure 6.10 Pressure and velocity minimum compared to predictions for micronized dolomite

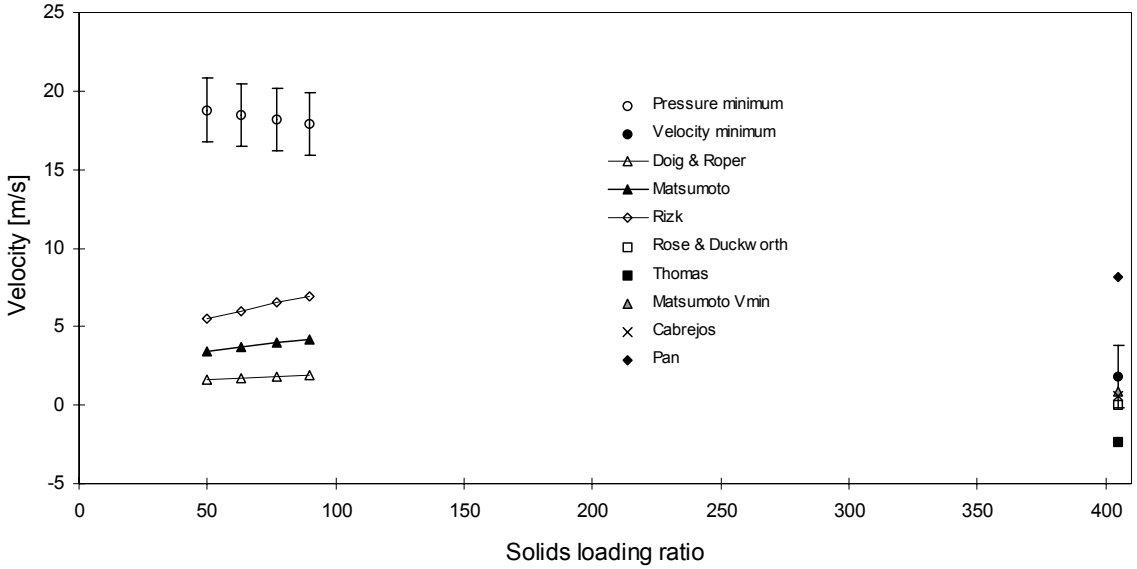

Figure 6.11 Pressure and velocity minimum compared to predictions for cement

The error with which each method predicts the velocity at pressure minimum may in some cases be lower than the values shown in Table 6.1, but since the solids loading ratio will vary from application to application the worst case has been listed. In Table 6.1 the worst case prediction for each material, and model, in percent of the experimentally obtained value, is positive only in the case of the method developed by Matsumoto. Underprediction of conveying limits may cause serious capacity restrictions or pipeline blockage. This means that only the model proposed by Matsumoto gives reliable results, and unless very high safety factors are incorporated, the other two methods should not be used.

The worst case predictions for the limit of stable conveying are shown in Table 6.2. They have been obtained in the same way as for Table 6.1. Again, only one model avoids under prediction of the conveying limit inside the area of validity. This is the model of Rose and Duckworth. The model proposed by Matsumoto underestimates the conveying limit slightly for PVC, and gives large over estimates in the other cases. With an error margin of 31% the model of Pan can be used in the whole area of validity. This model is also attractive because its solids loading ratio dependency is closer to the experimental data than for the other models.

Table 6.2 The worst case error of velocity minimum predictions given in percent of experimentally obtained value.

	LDPE	R. Seed	Sand	PVC	Alumina	MD101	Cement
Pan	-12	8	-31	-29	-57	139	348
Rose & Duckworth	57	56	-44	-62	-98	-86	-98
Matsumoto V_{min}	103	116	71	-8	-80	102	-50
Cabrejos	-17	-30	-53	-67	-83	-74	-67
Thomas	-48	-46	-66	-77	-107	-123	-228

The attempt to evaluate the model proposed by Cabrejos on the basis of the limit of stable conveying, relies on the assumption that the minimum pickup velocity is higher than the saltation velocity. This is stated in his own publication [21]. The limit of stable conveying should, as mentioned earlier, be lower than the saltation velocity. In this case the model should predict minimum pickup velocities that are higher than those at the limit of stable conveying. The model proposed by Cabrejos does not comply with this criterion for any of the materials. It can also be seen that the difference between minimum pickup velocity predicted by his method, and the experimentally obtained limit of stable conveying, is small for the coarse materials and increases for materials with small particles. This is the opposite of what would be expected as the cohesive forces increase and the surface structure of the settled layer is smoothed out for finer materials.

None of the methods for predicting pressure minimum curve or the limit of stable conveying give results for materials with an average particle size below 97μm. The method proposed by Zenz is valid down to 50μm but gives values that are much too high, and is not included in this comparison. The lack of models to predict the behaviour of fine materials is surprising since such materials are frequently encountered in industrial applications.

In Figures 6.1 through to 6.11 the predictions of the pressure minimum curve and the limit of stable conveying have been compared with experimental data. The values plotted in the tables above can be found in these plots as the point along the solids loading ratio axis that deviates the most from the experimental value. In Figure 6.1 this occurs at a solids loading ratio of 5 for the models of Doig and Roper, and Rizk. For the model proposed by

Matsumoto a solids loading ratio of 28 gives the highest deviation. This is a result of the poor correlation with solids loading ratio that can be recognized in all the figures.

Among the methods for pressure minimum curve prediction, the method of Matsumoto is the only one that does not yield underestimates. At low solids loading ratios his method is good. The maximum error of prediction occurs for rape seed, and is 25% of the measured value. The slight under estimate of -10% which this model gives for polyethylene pellets, will have little consequence for design purposes since there is sufficient safety margin in the gap between the pressure minimum curve and the limit of stable conveying. The model proposed by Matsumoto can therefore be recommended for the prediction of the pressure minimum curve. The accuracy of this model is better than 25% for solids loading ratios below 10, and even though it is not equally accurate at higher solids loading ratios it stil does not underestimate the pressure minimum velocity. An obvious flaw in the results of Matsumoto's model is the lack of correlation with experimental data as a function of solids loading ratio. The reason for this could probably be found in the simplifications that are made in the theory behind the model, as mentioned in Section 2.4.7. His original publication also shows that the data have been obtained at very low solids loading ratios (see Table 2.2). The maximum solids loading ratio for the 49mm internal diameter pipeline was approximately 5. The experimental results included in the investigation reported in this thesis incorporate solids loading ratios up to 60 in the region of validity for this model.

The model proposed by Matsumoto for predicting the minimum limit of stable conveying, can also safely be used in the whole area of validity, if a safety factor of 10% is used. This model results, however, in large overestimates of the minimum velocity for stable conveying.

The model of Pan can safely be used in its area of validity if a safety factor larger than 31% is used. This is a larger safety factor, but according to the comparison presented here, the model of Pan will predict the limit of stable conveying more closely at higher solids loading ratios. In addition Pan gives a correlation to compute the maximum velocity of stable conveying in plug flow. In this investigation the correlation can be compared to the two limits obtained for polyethylene pellets and rape seed. As one can see from Figures

6.12 and 6.13, the model predicts values within the error bounds of the experimental results for low solid loading ratios. For higher solids loading ratios the model overestimates the velocity limit. This is unfortunate for this particular conveying limit, since a design based on an overestimate will lead to unstable conveying conditions.

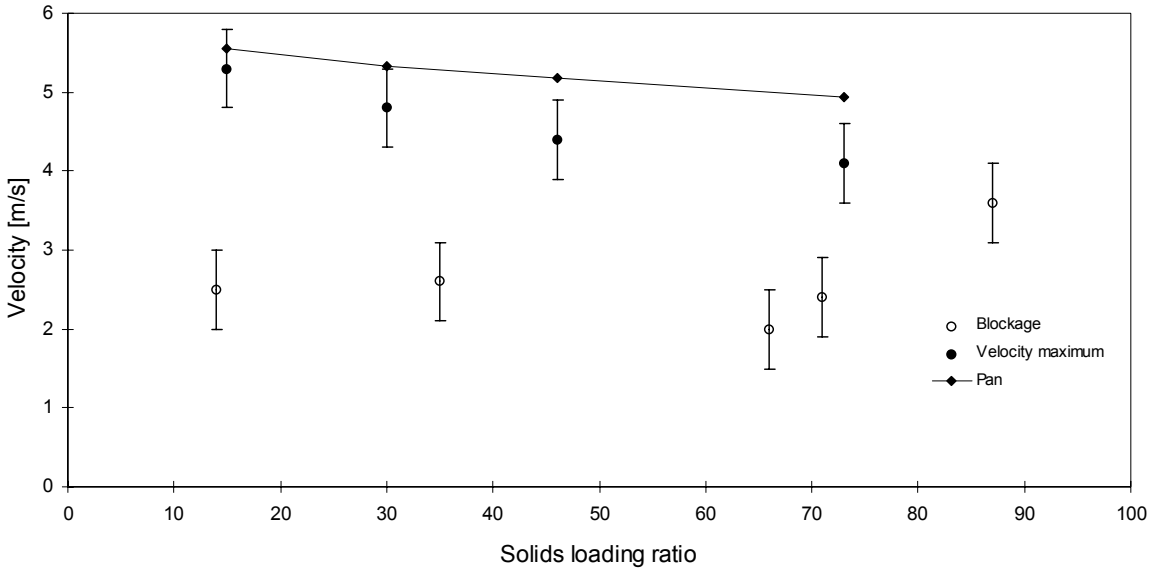

Figure 6.12 Blockage and velocity maximum (maximum limit of stable conveying in plug or slug flow) compared to predictions for polyethylene pellets

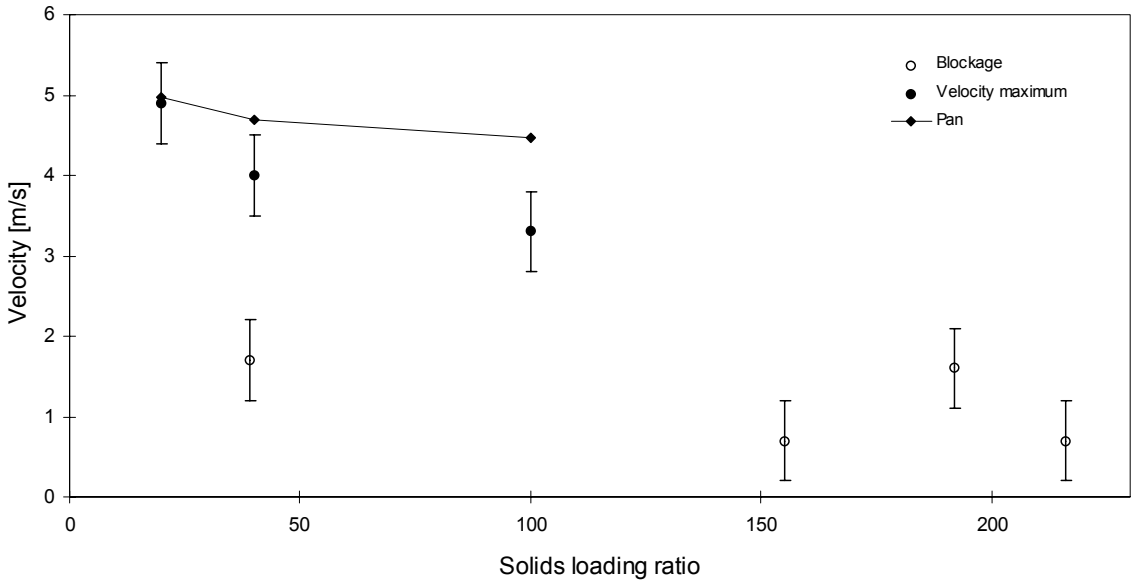

Figure 6.13 Blockage and velocity maximum (maximum limit of stable conveying in plug or slug flow) compared to predictions for rape seed

No models for predicting the blockage limit for plug flow have been found. The two materials in the investigation that exhibit plug flow properties have blockage velocities close to their minimum fluidization velocities, but we have too few data to enable modelling of such a conveying limit.

7. Experimental Observations of the Dynamic Behaviour of Particulate Materials Close to the Conveying Limit

Having conducted a quantitative comparison between existing models and experimental data, in Chapter 6, it is clear that there are severe limitations in applicability and accuracy of the existing models. To try to develop better models, a new approach towards the problem of understanding conveying limits in pneumatic transport systems is necessary. As shown in Chapter 2, the existing models rely on measurement of average values for the flow properties in the pipeline. In Chapter 5 it was pointed out that it is necessary to have some information about the dynamic behaviour of the flow of particulate materials in pneumatic transport systems to enable identification of the conveying limit. Most existing models rely purely on visual observations. Several methods to identify the conveying limit were discussed in Section 5.3. Amongst others, a method based on the registration of pressure fluctuations was discussed, and was applied to identify the conveying limits displayed in Chapter 6.

To get a better understanding of the physics of blockages of pneumatic conveying pipelines we will now use the recordings of pressure fluctuations along the pipeline to identify changes in characteristic frequencies and amplitudes as the conveying limit is approached. It is expected that a better understanding of the dynamics of pipeline blockages will enable mechanistic modelling of conveying limits.

Using pressure measurements, we shall also investigate where the blockage occurs in the pipeline.This was found to be necessary since the literature survey in Chapter 2 did not reveal any information on this subject. Therefore the experiment introducing a bend in the pipeline was included in the program to check if bends have an influence on the location of blockages and the conveying limit, or not.

7.1 The Root Mean Square Values of the Pressure Fluctuations

In Section 5.3 the use of the root mean square (RMS) of the pressure fluctuations to identify conveying limits was discussed. Since it was difficult to select an objective criterion based on these observations, because the amplitudes vary greatly from material to material, the method was not utilized. The information is, however, still interesting with

regard to understanding what happens close to the blockage limit in a pneumatic conveying pipeline.

Information about the pressure fluctuation level is also of interest in itself because pressure fluctuations may add to the average pressure and exceed the maximum pressure available from the air mover. This would cause blockage at higher air velocities than that which would be expected from the average data that constitutes the conveying characteristics.

7.1.1 Mapping of the Root Mean Square Values of the Pressure Fluctuations at the Beginning of the Pipeline Onto the Conveying Characteristics

To obtain a picture of the level of pressure fluctuations at the beginning of the pipeline the root mean square value in % of the average pressure have been mapped onto the conveying characteristics (Figure 7.1). This gives an overview of the level of pressure fluctuations in the pipeline at all conveying conditions covered by the conveying characteristics.

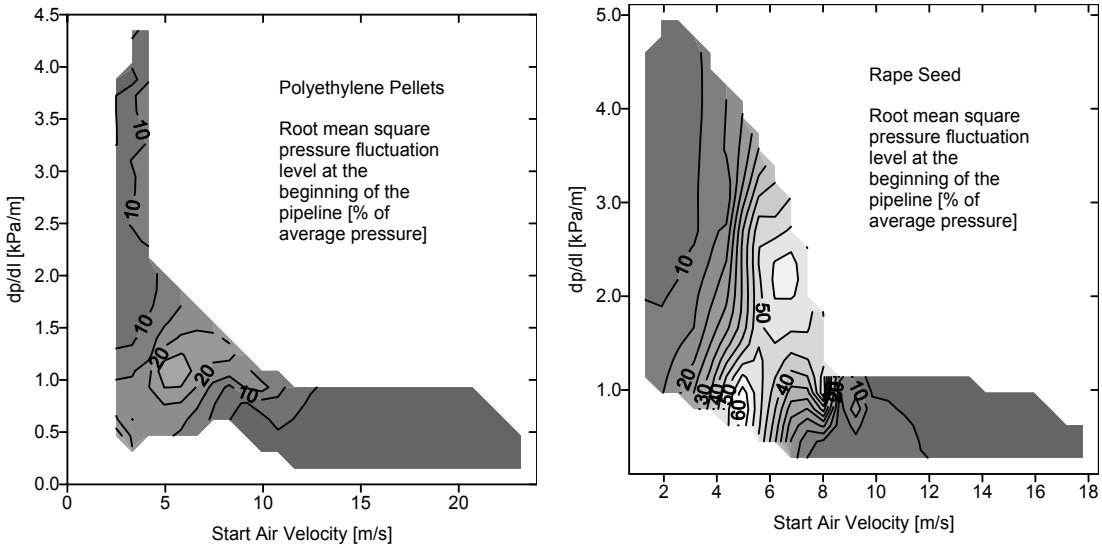

Figure 7.1 RMS maps of pressure fluctuations in the pipeline

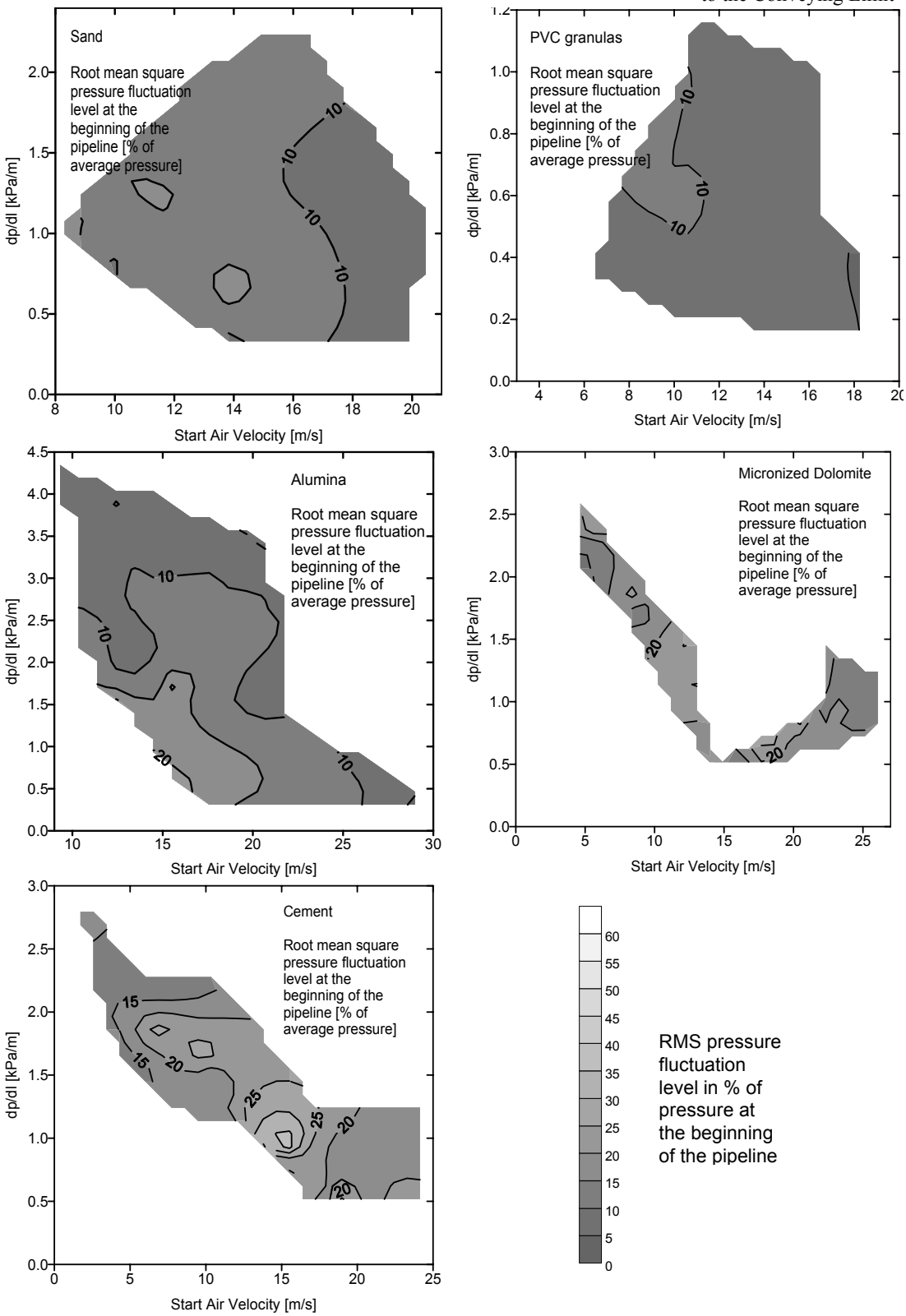

Figure 7.1 (Continued) RMS maps of pressure fluctuations in the pipeline.

As can be seen for all materials, the pressure fluctuations increase towards the conveying limit. For polyethylene pellets and rape seed the pressure fluctuations are, as expected, highest in the unstable region between flow in suspended or partly suspended modes and flow in plug or slug flow.

It should also be noted that the finer materials such as cement and micronized dolomite have a similar region in which the pressure fluctuations are high. Visual observations show that this is not accompanied by a dramatic change in the mode of flow as for the coarser powders like rape seed and polyethylene pellets.

As mentioned in Section 5.2, the conveying characteristics belong to three main categories that can be identified by their shape. These categories of conveying characteristics happen to correspond to the tree main types of materials, A/C, B and D, according to the Geldart [36] classification for fluidisation on which the selection of materials for this experimental investigation was based (see Section 4.4). The pressure fluctuations occuring are also similar for similar materials according to this classification. The rape seed has the same unstable area in the conveying characteristics, shown in Figure 5.3, as the polyethylene pellets. As one may expect the pressure fluctuations (shown in Figure 7.1) and the visual observations of the flow pattern, are also similar for the two materials. The same is also the case for the Geldart type B, and A/C materials. For the remainder of this chapter one representative material from each class (Geldart type A/C, B, and D) has been selected for full investigation using the various methods of analysis. The three materials are micronized dolomite, PVC granules and rape seed.

7.1.2 The Spatial Distribution of the Root Mean Square Value of the Pressure Fluctuations.

The RMS pressure fluctuation maps presented in Figure 7.1 show only the values occurring at the beginning of the pipeline. No information is given with respect to the level of pressure fluctuations along the pipeline. Since it is the dynamic behaviour close to the limit of stable conveying that is of interest, the pressure fluctuations along the pipeline should be monitored as the air velocity approaches the conveying limit.

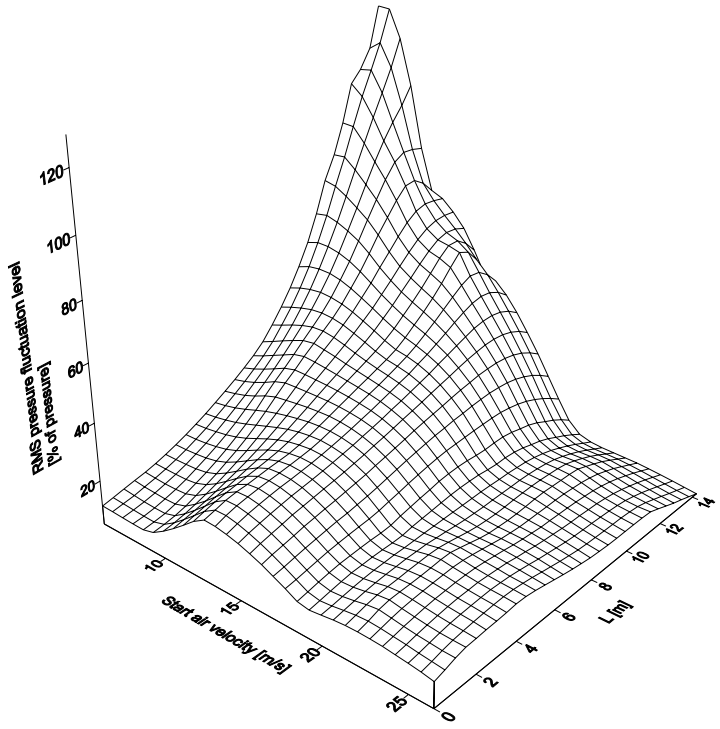

Figure 7.2 Pressure fluctuation level along the pipeline for micronized dolomite, with a fixed solids flow rate of approximately 10 tons/h.

Keeping the solids mass flow constant, the changes in the RMS pressure fluctuation level along the pipeline, when approaching blockage, have been plotted in Figures 7.2 through to 7.4 for micronized dolomite, PVC and rape seed respectively.

Again a similarity between the fine powders capable of fluidized flow and the coarser powders capable of plug or slug flow at low velocities can be seen. They both exhibit high pressure fluctuations in the farmost corner of Figures 7.2 and 7.4, i.e. both towards the end of the pipeline and towards low conveying air velocities. For the PVC granules, in Figure 7.3, the pressure fluctuation level increases gradually towards the limit of stable conveying over the entire conveying line.

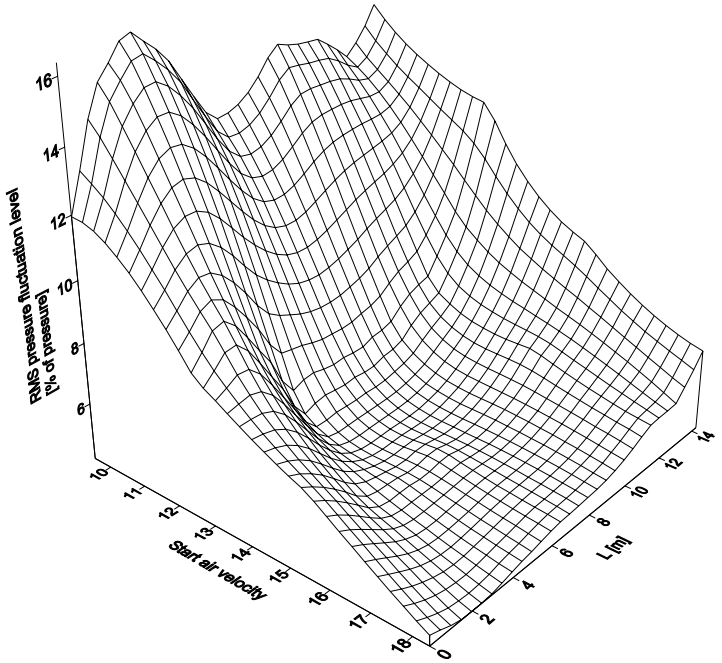

Figure 7.3 Pressure fluctuation level along the pipeline for PVC granules, with a fixed solids flow rate of approximately 1.5 tons/h.

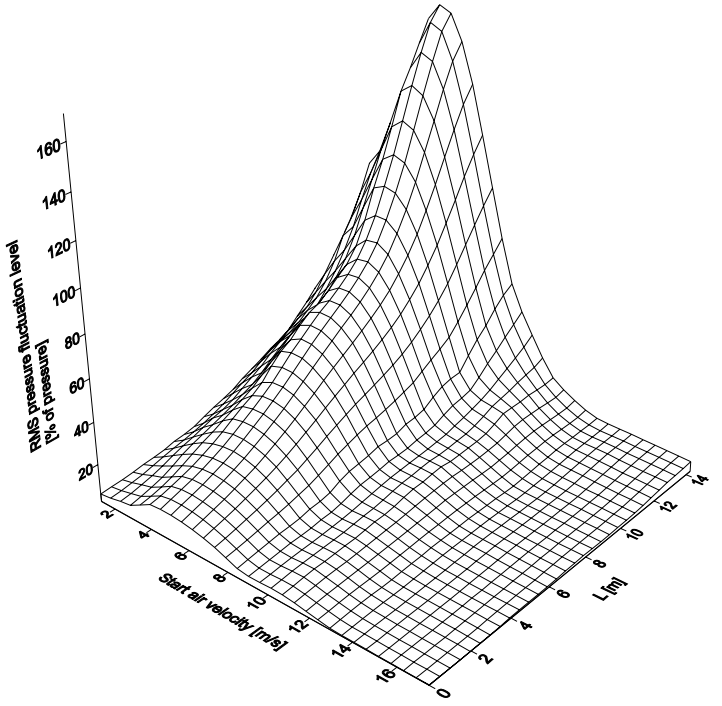

Figure 7.4 Pressure fluctuation level along the pipeline for rape seed, with a fixed solids flow rate between 4 and 5 tons/h.

7.2 The Characteristic Frequencies of the Pressure Fluctuations.

Figure 7.1 gave strong indications that the increase in the RMS values of the pressure fluctuations is linked to the conveying limit. To reveal more information about the nature of these pressure fluctuations, the spatial distribution of the characteristic frequencies, and their dependancy on conveying air velocity can be investigated.

7.2.1 The Spatial Distribution of the Characteristic Frequencies of the Pressure Fluctuations.

Assuming that the occurrence of coherent structures associated with incipient slugging initially takes place as harmonic surface gravity waves on the moving bed of material being transported, one may expect to find characteristic frequencies in the power spectra of the pressure fluctuations. The characteristic frequencies of the pressure fluctuations can be found for each pressure transducer. If these power spectra are stacked side by side, a picture of what characteristic frequencies occur, along the pipeline, emerges. The power spectra of rape seed, PVC granules and micronized dolomite are shown in Figures 7.5 through to 7.7.

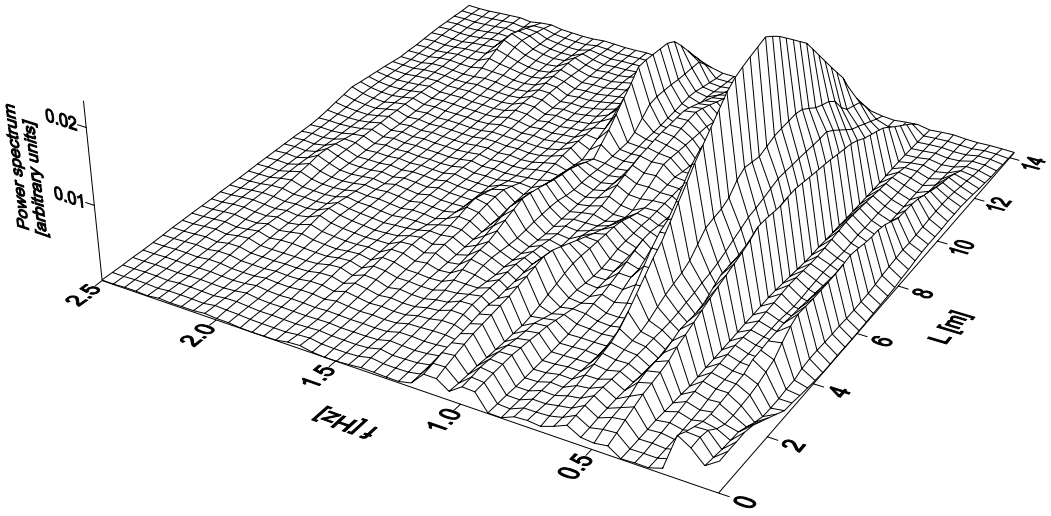

Figure 7.5 Power spectrum along the pipeline for micronized dolomite, with a superficial air velocity of 9.0 m/s at the beginning of the pipeline.

The frequency plot for micronized dolomite in Figure 7.5 shows that the pressure fluctuations which occur just past the middle of the pipeline consist mainly of two frequency bands. One at 0.4 to 0.8Hz and one at 1.3 to 1.5Hz further down the pipeline.

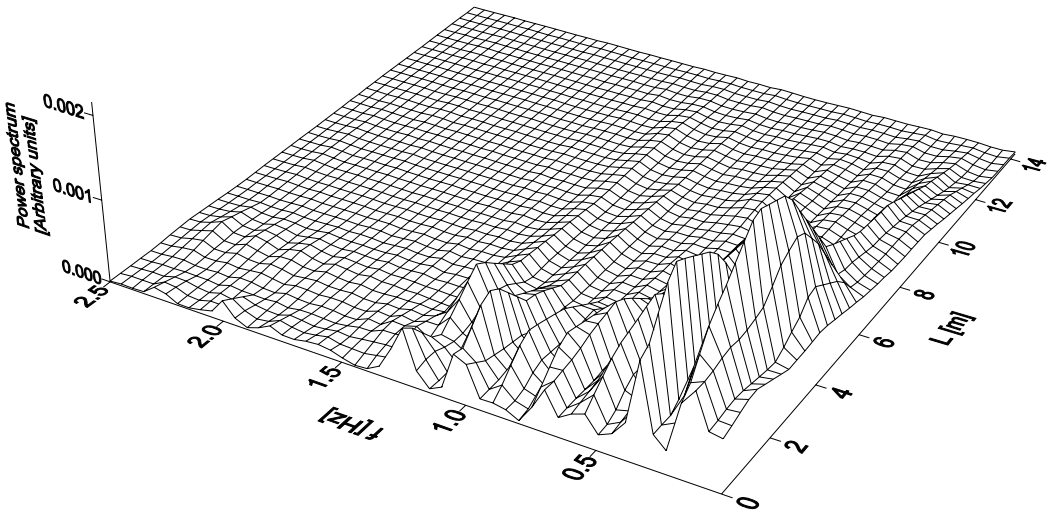

Figure 7.6 Power spectrum along the pipeline for PVC granules, with a superficial air velocity of 9.5 m/s at the beginning of the pipeline.

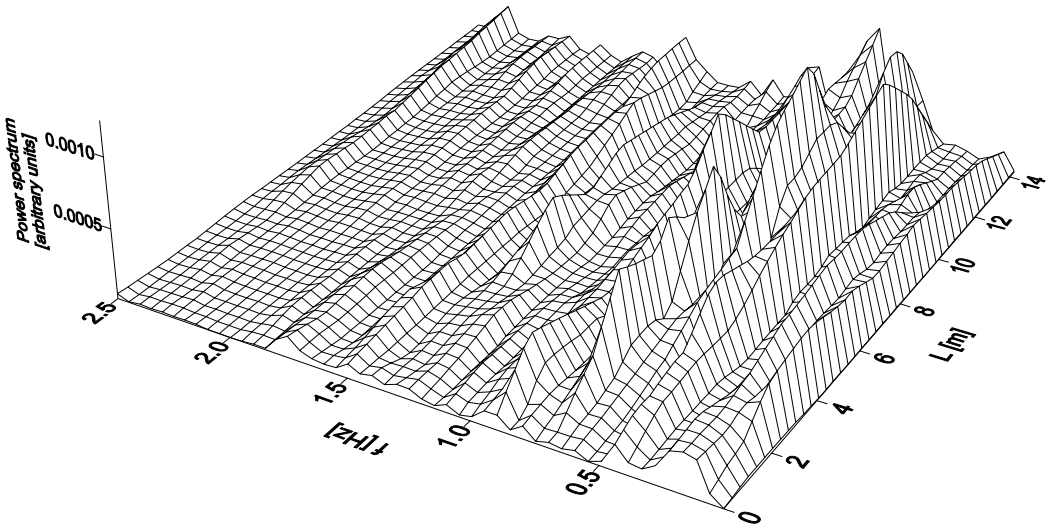

Figure 7.7 Power spectrum along the pipeline for rape seed, with a superficial air velocity of 8.6 m/s at the beginning of the pipeline.

Figure 7.6 shows that the pressure fluctuations when transporting PVC granules close to the limit of stable conveying are predominantly occurring at the beginning of the pipeline, at low frequencies.

For the rape seed, in Figure 7.7, no dominating frequency can be observed. The pressure fluctuations are mainly found at the end of the pipeline at low frequencies.

7.2.2 The Characteristic Frequencies and their Dependancy on the Conveying Air Velocity

As shown in Figure 7.2 through to Figure 7.4 the amplitude of the pressure fluctuations vary along the pipeline for different conveying velocities. The frequencies constituting these pressure fluctuations also vary with the conveying velocity.

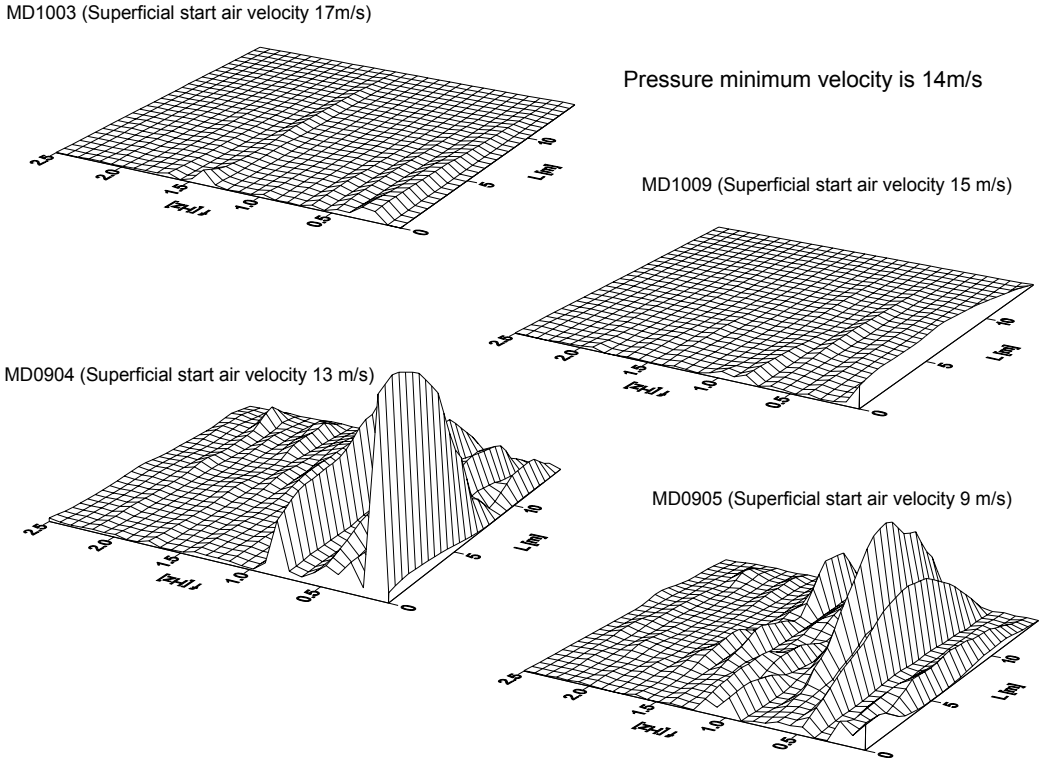

Figure 7.8 Power density spectra for selected test runs with micronized dolomite showing the growth in the low frequencies below pressure minimum.

For the micronized dolomite the low frequencies can be seen to grow dramatically as the superficial air velocity passes the pressure minimum(see Figure 7.8).

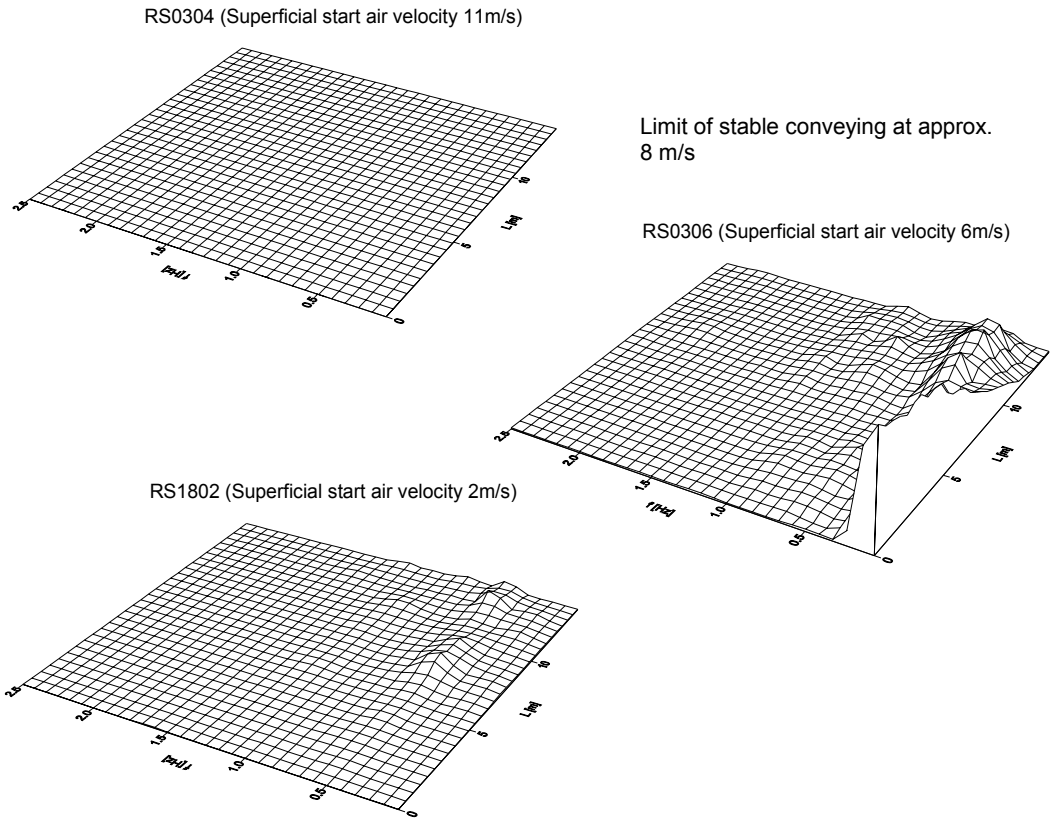

Figure 7.9 Power spectral density for selected test runs with rape seed showing the growth in the low frequencies below the limit of stable conveying.

The same growth in the low frequencies can be seen for rape seed when passing the limit of stable conveying. In Figure 7.9 three frequency spectra representing stable conveying in suspension or partially suspended flow, unstable flow, and stable plug or slug flow, can be seen.

For PVC granules, as one might expect from looking at the pressure fluctuation map in Figure 7.3, there is no dramatic change in the amplitude or the position of the pressure fluctuations as the air velocity is decreased towards the limit of stable conveying. Figure 7.6, which is obtained close to the limit of stable conveying is a good example also for the characteristic frequencies at higher conveying velocities. The amplitude of the power spectral density changes approximately by a factor of two when going from the pressure minimum to the limit of stable conveying while the frequencies remain essentially the same.

7.3 Coherent Structures in the Pressure Fluctuations

The characteristic frequencies that occur in the frequency spectra in Figures 7.5 through to 7.9 are dominated by narrow band components. One possible explanation to this is that these frequencies are associated with harmonic surface gravity waves at incipient slugging. Surface gravity waves on a moving or strongly stratified layer of solids associated with the onset of slugging should cause coherent pressure fluctuations along the length of the pipeline. An investigation has been carried out to look for such pressure fluctuations.

7.3.1 Conditional Averaging of Pressure Fluctuations

To identify coherent pressure fluctuations, a technique known as conditional averaging may be applied [51,52]. As can be seen from Figure 7.1 the pressure fluctuation level increases towards the limit of stable conveying. From Figure 7.2 through to Figure 7.4 it can also be seen that this increased level of pressure fluctuations take place at different places in the pipeline, following clear trends for each material. If coherent structures exist in the pressure signals, originating from incipient slugging, it should be possible to identify them as recognizable pressure variations moving along the pipeline. The simplest way of identifying a coherent structure in such an array of signals is by selecting a condition that describes the structure well, such as amplitude, steepness etc. The condition selected for this investigation, after an initial investigation to identify what conditions display the coherent structures most clearly, is that pressure must be above the average for the selected region for more than 0.4s. In other words pressure peaks above a certain size are picked out.

By using this method it is possible to take the matrix of pressure measurements spanned out by pressure transducer number and time, and search for occurrences of coherent structures being described by the condition selected. At each of the occurrences the pressure profile is taken and included into the average describing the occurrence of the condition selected. By also including an array of pressure profiles just before and after the event, the time development around the occurrence can also be found. If coherent structures exist these should survive the averaging process and leave traces through time

and space in the conditionally averaged representation of the pressure profile time development. In Figures 7.10 through to 7.12 the conditional averaged pressure fluctuations along the pipeline are plotted for micronized dolomite, PVC and rape seed.

From Figure 7.10 one can easily identify coherent structures travelling along the pipeline at a velocity of the order of 15m/s. The coherent structure seems to originate from the beginning of the pipeline, and in this case travels along the whole length of the pipeline.

For the PVC granules, shown in Figure 7.11, coherent structures can be seen travelling along the pipeline only at the beginning of the pipeline, up to approximately 4 to 5 meters from the start of the pipeline. This happens just before the peak value occurs on transducer 5. Peak pressures occur simultaneously along the pipeline when the condition is identified on transducer 5.

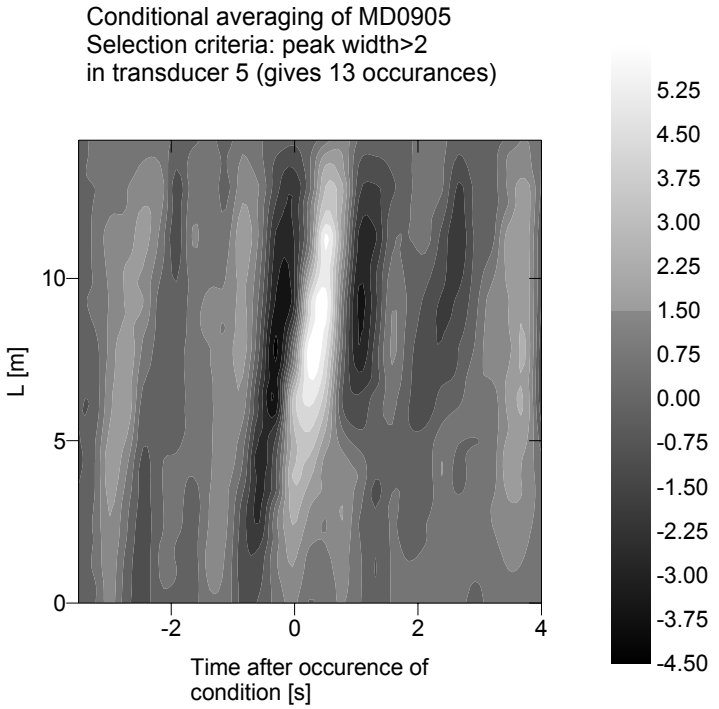

Figure 7.10 Conditionally averaged pressure fluctuation level along the pipeline for micronized dolomite. Gray scale values in kPa.

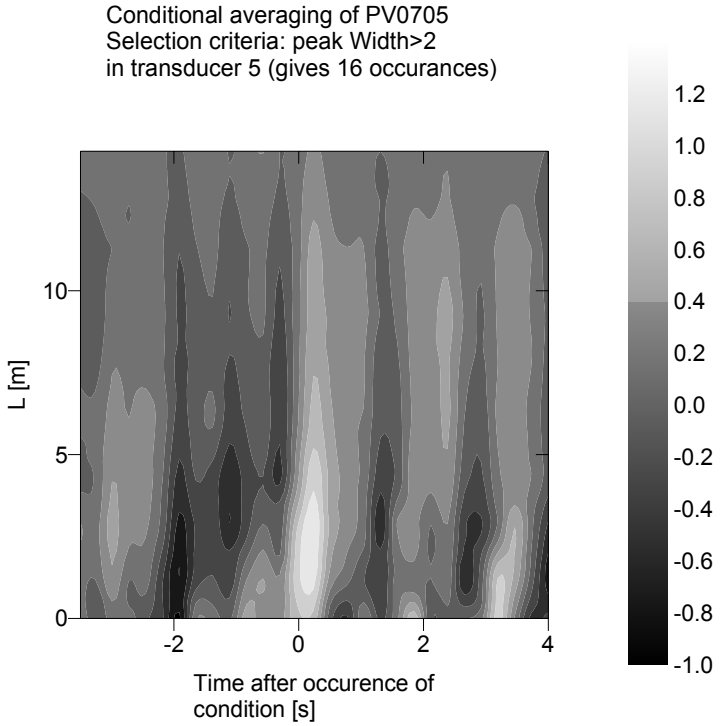

Figure 7.11 Conditionally averaged pressure fluctuation level along the pipeline for PVC granules. Gray scale values in kPa.

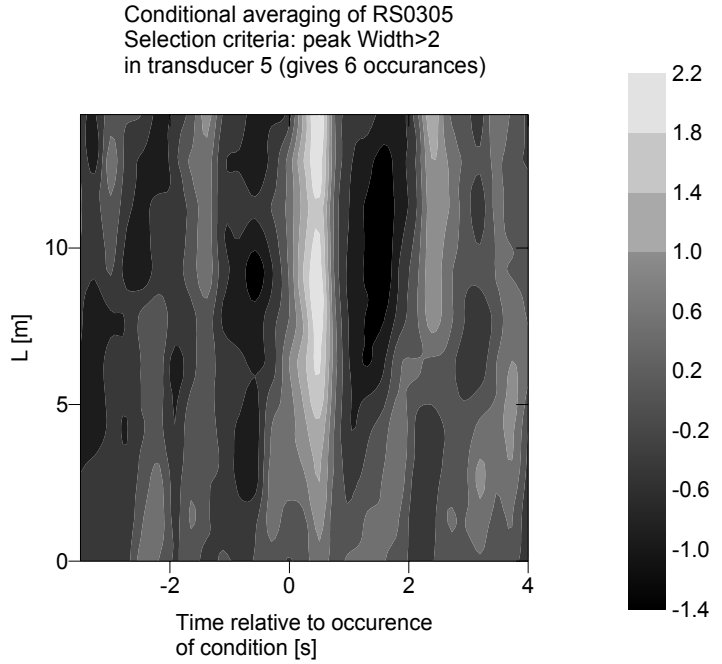

Figure 7.12 Conditionally averaged pressure fluctuation level along the pipeline for rape seed. Gray scale values in kPa.

For the rape seed (Figure 7.12) no clear coherent structure can be identified travelling along the pipeline. There are weak indications of such, but the incoherent fluctuations apparently are dominant and no conclusions can be drawn. It is possible that the high permeability of the coarse materials makes it difficult to detect the pressure difference across plugs as they travel along the pipeline. This should be especially significant at incipient slugging when the slugs are short and weak.

Conditional averaging has detected coherent structures travelling through the pipeline when approaching the limit of stable conveying for the Geldart type A/C materials exhibiting moving bed flow. For the Geldart type B materials, indications of coherent structures can be observed at the beginning of the pipeline. For the Geldart type D materials no coherent structures have been found when approaching the limit of stable conveying.

The positions at which the pressure fluctuations occur in the frequency spectra, in Figures 7.5 through to 7.7, correspond to the positions at which the large pressure fluctuations occur in the conditionally averaged plots (Figure 7.10 through to 7.12). From Figure 7.10 it is clear that the coherent structures observed for the Geldart type A/C can be associated with the dominant characteristic frequency in Figure 7.5 which would be typical for harmonic surface gravity waves.

7.3.2 Measurement of the Velocities of the Coherent Structures by Cross Correlation of Pressure Signals.

The velocity of the coherent structures observed for PVC granules and micronized dolomite, in Section 7.3.1, can be assessed by drawing a line through the ridge traced by the structure. The change in distance per unit of time along the ridge gives the velocity directly. This method however is not very accurate because the temporal resolution is limited to 0.2s due to the sampling rate, and because the ridges traced by coherent structures, due to a low number of conditions satisfied in each signal array, rarely are as clearly defined as is the case for the test run shown in Figure 7.10.

To obtain a better representation of the velocity of the pressure fluctuations travelling along the pipeline, cross correlation of the pressure signals can be used. Because of the low temporal resolution it is not sufficiently accurate to look at the displacement of the peak value of the cross correlation function. By Fourier transforming the cross correlation function, the phase information inherent in the complex result can be used to find the velocity of each of the frequency components [53]. Thus we have:

$$\mathrm{R_{xy}} = \lim_{T\to\infty} \frac{1}{\mathrm{T}} \int_0^{\mathrm{T}} x(\mathrm{t}) y(\mathrm{t}-\tau)\,\mathrm{d}t$$

as the cross correlation function of two pressure signals. If we Fourier transform this cross correlation function, and if the signal is transported unperturbed between the two positions, we can write the transform as the product between the transform of the auto correlation function and a phase component:

$$\mathrm{F_{xy}}(\omega) = \mathrm{F}(\mathrm{R_{xy}}(t)) = \mathrm{A}(\omega)\mathrm{e}^{\mathrm{i}\theta}$$

The phase information can be obtained as

$$\theta_{xy} = \tan^{-1}\left(\frac{\left|\mathrm{Im}(\mathrm{F_{xy}}(\omega))\right|}{\left|\mathrm{Re}(\mathrm{F_{xy}}(\omega))\right|}\right)$$

Each angle represents the phase information for a specific frequency in the discrete Fourier transform. The difference between the angles of the Fourier transform of the auto correlation function of x (θ_{xx}) and the cross correlation function of x and y (θ_{xy}) gives the time delay from transducer x to y for each of the frequency components constituting the Fourier transform of the cross correlation.

$$\Delta\mathrm{t}(\omega) = \left(\frac{\theta_{\mathrm{xy}}(\omega) - \theta_{xx}(\omega)}{\omega}\right)$$

This time delay can be used to compute a frequency specific velocity, and the set of velocities can be selected from frequencies associated with dominant peaks in the power spectrum of the signal.

$$v_{xy}(\omega) = \frac{L_{xy}}{\Delta t(\omega)}$$

The measurement is difficult in the regions outlined in Figure 7.1 where pressure fluctuations were low. In general only a few points have a signal to noise ratio that allows this method to be used. As shown in Figures 7.2 through to 7.4 the level of pressure fluctuations vary along the pipeline, and with the transport air velocity. The method is therefore also sensitive to the positions of the transducers used for cross correlation, and transducer positions corresponding to high amplitudes in the pressure fluctuations should be used.

In Figure 7.13 the power spectral density estimate for the cross correlation between transducer p5 and p7 when conveying micronized dolomite at 4m/s can be seen.

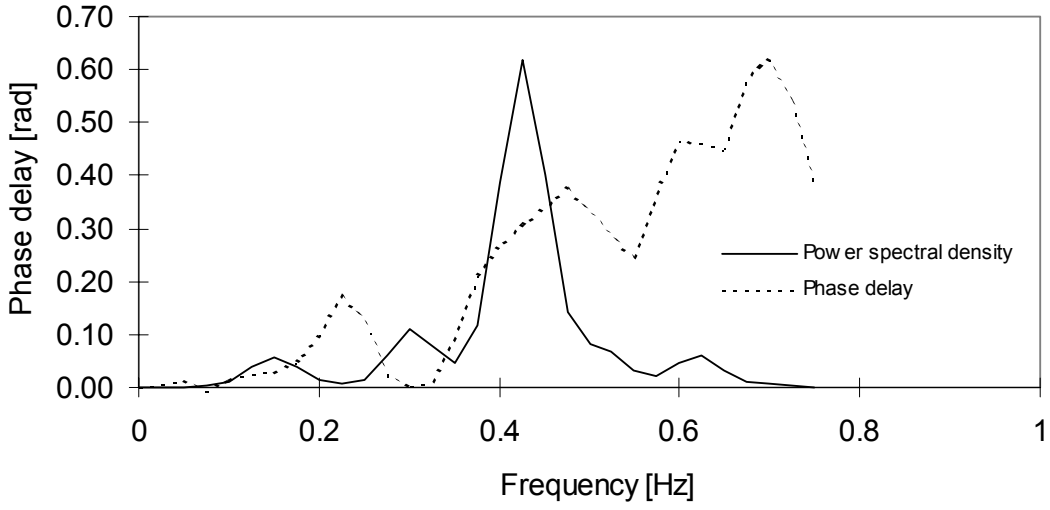

Figure 7.13 Power spectral density and phase delay information for micronized dolomite test run with an air velocity of 4.1m/s.

The phase delay, plotted in Figure 7.13 can now be used to compute the time delay of the coherent part of the signal between the two transducers. The phase delay information selected for computation should be selected in a part of the spectrum with high power density. This is the part one would expect to contain information about coherent structures given that these are dominant in relation to incoherent noise.

The phase information plotted in Figure 7.13 can now be used to compute a specific velocity associated with each frequency in the power spectral density. This narrow band cross correlation is also described by Beck and Plaskowski [54]. The velocities computed can be seen in Figure 7.14. The velocities selected to compute the average have been chosen so that they correspond to the peak in the power spectral density in Figure 7.3, which is expected to be associated with coherent structures.

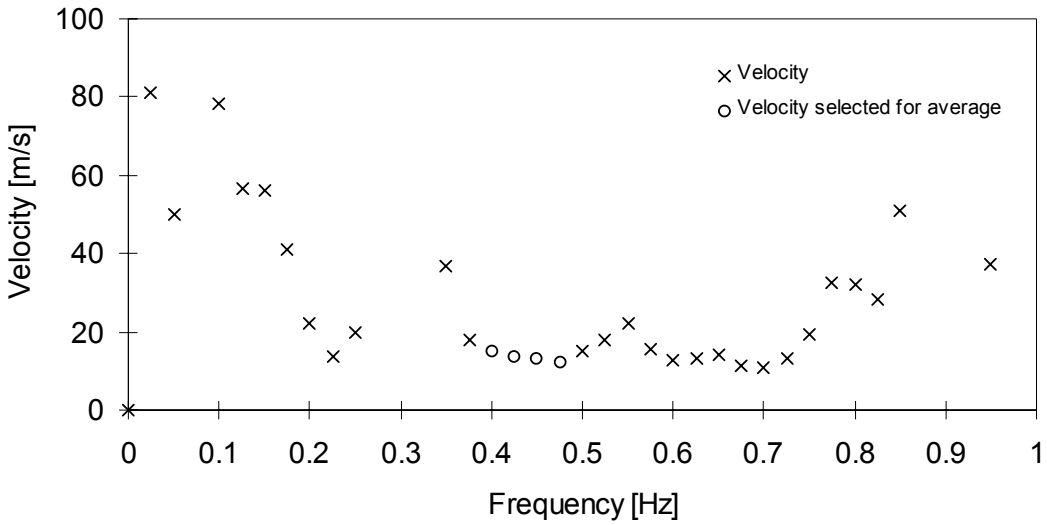

Figure 7.14 Velocities as a function of frequency for the pressure fluctuations with micronized dolomite test run with an air velocity of 4.1m/s.

With the velocities selected one obtains an average velocity of 13.6m/s, and a standard deviation of 1.1m/s. The velocity can consistently be reproduced for all of the pressure transducers following transducer 5. The frequency band in which the data have been obtained corresponds to the peak in the frequency plot of Figure 7.5. The propagation velocity of the coherent structure is considerably higher than the superficial air velocity.

This method has also been applied to obtain velocities for the coherent structures occurring in the data for PVC granules. The most dominant feature of the result of this investigation is the velocity profile for coherent structures for PVC granules shown in Figure 7.15.

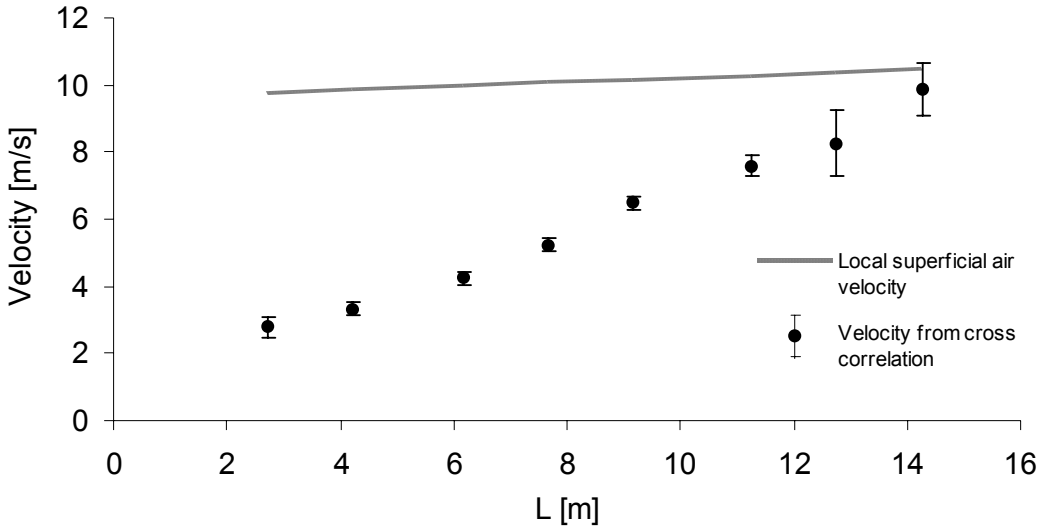

Figure 7.15 Velocity profile for coherent structures in comparison to local superficial air velocity, for PVC granules.

These results have been obtained in the frequency range from 0.05Hz to 0.225Hz which correspond to the highest peaks in Figure 7.6. The average velocity computed for the transition to the last transducer is, within error bounds, equal to the superficial air velocity.

For the three materials, micronized dolomite, PVC granules and rape seed, which have been used for the plotting of conditional averages in Figures 7.10 through to 7.12, the results of the velocity measurements can be summarized as follows:

- The velocities measured for microdol (in Figure 7.13) are generally higher than the superficial air velocity, and the results give consistent values only for the lowest conveying velocity.
- The velocities measured for PVC (in Figure 7.15) show clear acceleration profiles and correlate well with superficial air velocity for the points close to the limit of stable conveying where the pressure fluctuations are high.

- The technique does not work as well for rape seed as for the two other materials, and no consistent results of velocity measurements can be shown. This is also what may be expected since no coherent structures were observed in Figure 7.7.

7.4 Identification of Blockage Point

In the literature survey, no information about the influence of bends on the conveying limit and blockage position was found. Therefore it was decided to carry out an investigation about the influence of bends. In Chapter 5, a small influence of the bend, on the conveying limit, was detected for rape seed at low feed rates. The results of the investigation of blockage point with and without a bend follows below.

7.4.1 Identification of Blockage Point in a Horizontal Pipeline Without a Bend

The same technique used to identify coherent structures in the pressure fluctuations along the pipeline, conditional averaging, can also be used to examine marginally unstable situations giving large peaks in the pressure plots. These peaks represent incipient blockage of the pipeline, and the blockage point can be found by picking out such occurrences and averaging them. Only a few such occurrences are available and as can be seen for Figure 7.16 only one or two occurrences have been found for each material.

The low number of occurrences does not constitute a problem in this case because the incipient blockage causes large pressure variations in relation to steady transport. In the cases where only one occurrence has been found, it may not be justified to call the result a conditional average since no averaging is involved. Even so, the result represents an occurrence of incipient blockage.

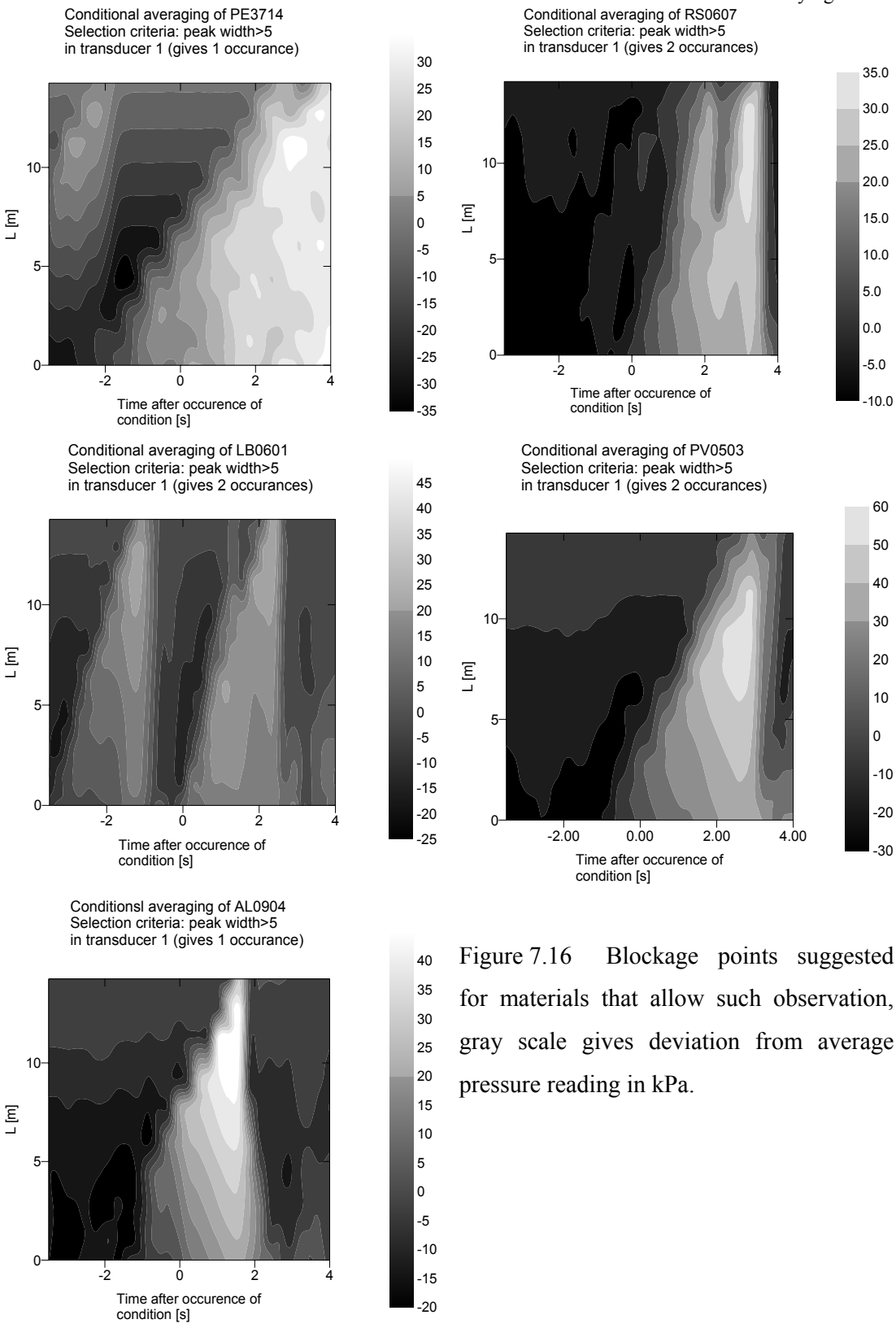

Figure 7.16 Blockage points suggested for materials that allow such observation, gray scale gives deviation from average pressure reading in kPa.

It is suggested from these plots that the pipeline blocks at the beginning. The propagation velocity of the blockage varies slightly from case to case. The blockage point for alumina (AL0904) seems to be at approximately 5m. Others occurences of pressure peaks for alumina, not displayed here, show incipient blockage closer to the beginning of the pipeline.

7.4.2 Identification of Blockage Point with a Horizontal to Horizontal Bend After 15m in the Pipeline

The effect of the bend, on blockage position has been investigated separately. Only minor changes have been detected for the three materials tested. For micronized dolomite and PVC there does not seem to be a change in the blockage position. For rape seed a minor change can be detected. This is also shown in Section 5.3 where the effect on the conveying limit is discussed.

For the pipeline configuration with a bend, the blockage of the pipeline seems to be initiated at the bend position for low feed rates when conveying rape seed. In Figure 7.17 the conditionally averaged map of the deviation from the average pressure reading at occurrences of incipient blockage can be seen for test run RS3208.

In the figure it can clearly be seen that a blockage is initiated at time zero in a position 15m along the pipeline, which corresponds to the start of the bend. Weak indications of the same effect can also be seen in the conditional averages taken at higher feed-rates on the same conveying limit, but the effect is clearly most dominant at low feed rates.

When having a look at each individual occurrence of incipient blockage for this test-run they fall into two categories. One that is initiated at the beginning of the pipeline, and one that is initiated at the bend. This supports the possibility that it is probably a marginal phenomenon, which does not have a large effect on the conveying limit itself, in this case only influencing the conveying limit significantly at low solids feed-rates.

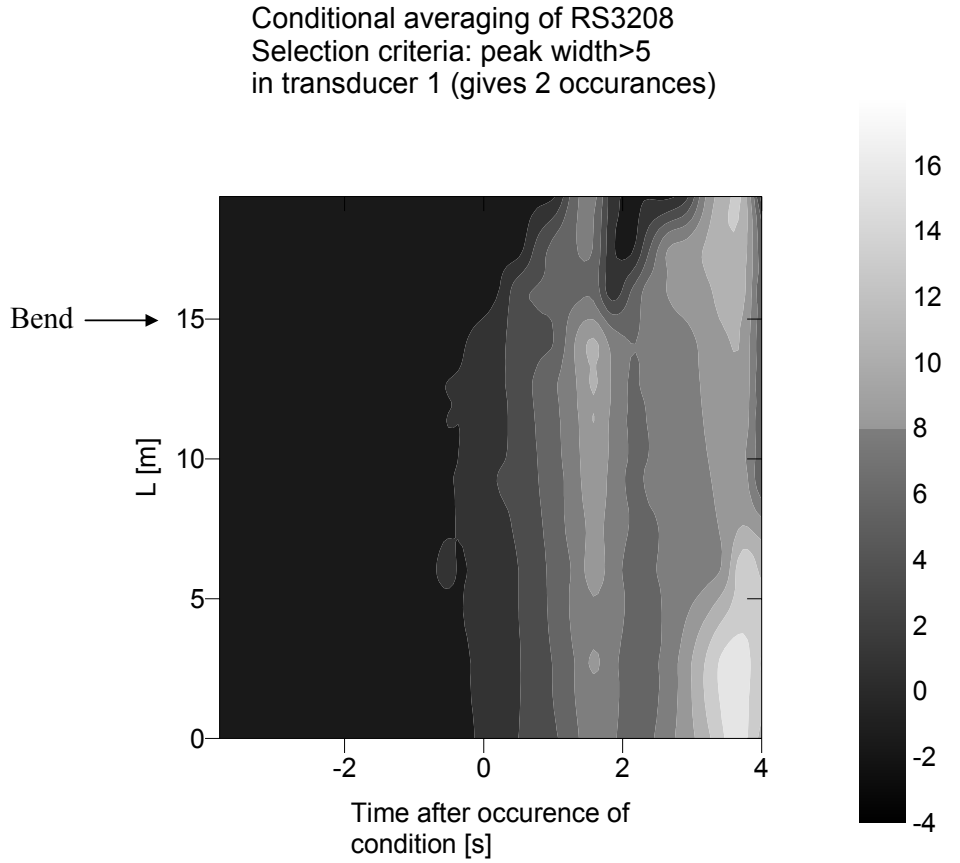

Figure 7.17 Blockage points observed for rape seed with a bend in the pipeline, gray scale gives deviation from average pressure reading in kPa.

7.5 Discussion of the Experimental Observations of Dynamic Behaviour.

The observations of pressure fluctuations at the beginning of the pipeline, as displayed in Figure 7.1 clearly show that an increased level of pressure fluctuations is associated with pneumatic transport close to the conveying limit. The materials tested fall into one of two main groups for which:

- The pressure fluctuations increase monotonously towards the conveying limit.
- The pressure fluctuations increase towards the limit of stable conveying and decrease again after having passed through a region with higher pressure fluctuations.

The first group consists of materials of Geldart type B, with the second consisting of Geldart type A, C and D materials. Figures 7.2 through to 7.4 show the same maximum in the start pressure fluctuations in the intermediate conveying velocity region for the

micronized dolomite and the rape seed. It is also clear from these figures that the change in the pressure fluctuation level is even more pronounced towards the end of the pipeline.

The nature of these pressure fluctuations were then investigated by conditional averaging techniques. Figure 7.10 most clearly shows that the pressure fluctuations in the case of the micronized dolomite are associated with coherent structures moving through the conveying pipeline. An extensive investigation of the use of the conditional averaging technique shows that coherent structures exist in the pressure fluctuation signals from the conveying of micronized dolomite for a large range of operating conditions.

The coherent structures are not as pronounced in the case of PVC granules and rape seed. For the PVC granules coherent structures can be observed at the beginning of the pipeline close to the conveying limit, as shown in Figure 7.11.

An additional piece of information about the nature of these coherent structures can be found from looking at the velocity at which they propagate along the pipeline. The velocity for the coherent structure in micronized dolomite is considerably higher than the superficial air velocity. From Figure 7.10 a velocity of approximately 15m/s can be found. The velocity of the coherent structure at the beginning of the pipeline when conveying PVC granules is approximately 2m/s, which is considerably below the superficial air velocity. This assessment of the propagation velocity of the coherent structure on the basis of the conditionally averaged plots is of limited accuracy, because the temporal resolution is limited to 0.2s due to the sampling rate, and because the ridges traced by coherent structures, due to a low number of conditions satisfied in each test run, are rarely smooth.

The narrow band cross correlation data displayed in Section 7.3.2 show velocities in the same range as those obtained with the crude method of following traces of coherent structures in the conditionally averaged plots. In addition, this method enabled the velocity profile, along the pipeline, for the coherent structures in the PVC data to be found. These velocities increase towards the superficial air velocity at the end of the pipeline.

It is not clear if the velocities observed for PVC granules close to the conveying limit are for coherent structures accelerating through the pipeline, or for different types of pressure

fluctuations travelling at different velocities through the pipeline. The latter view may be favoured from the data shown here as the coherent structures observed at the beginning of the pipeline in Figure 7.11 apparently dies out after approximately 5m. In this case the velocities observed at the beginning of the pipeline are probably associated with the acceleration process of the material, and originate from slugs of material being accelerated and dispersed as they accelerate along the pipeline.

The frequency plots in Figures 7.5 through to 7.7 were vital to the utilization of the narrow band cross correlation. These plots show clearly which frequencies are associated with pressure fluctuations occurring over a large section of the pipeline. This enables the selection of that frequency band when computing the propagation velocity. They also indicate the positions at which the pressure fluctuations are dominant. And as expected the micronized dolomite data set shows the dominant frequency to occur over the whole length of the pipeline, whereas the dominant frequency for the PVC granules is positioned at the beginning of the pipeline, with weak traces along the remaining length. This is all in accordance with the results of the conditional averages and the velocity measurements.

All the data presented above are indications of slugging in the material conveyed. For the micronized dolomite the slugs travel along the pipeline at velocities higher than the superficial velocity. For the PVC granules the slugs only travel along the pipeline at the beginning of the pipeline at low velocities and are then dissolved as they accelerate. In Figure 7.8 it can be seen that the micronized dolomite has a very low frequency component at the beginning of the pipeline, which dies after between 5m and 10m, when being conveyed in the intermediate velocity region (here 13m/s to 15m/s). This is similar to the low frequency component being observed for Geldart type B materials such as PVC and sand. Micronized dolomite is in fact, as shown in Figure 4.2, a borderline A/B material. Similar plots for cement, which is a Geldart type C material show no such low frequency component, and the fact that it occurs for micronized dolomite can probably be attributed to it being a borderline material.

At some stage, when gradually reducing the conveying velocity, the incipient slugs described above turn into temporary blockages in the pipeline, which are blown through the pipeline before it clears. These events may also be observed by using the technique of

conditional averaging. In Section 7.4 such events have been displayed to identify at which position the pipeline initially blocks. In general the pipeline seems to become blocked at the beginning. In Section 7.4.2 one occurrence of blockage at the bend, when introducing a horizontal to horizontal bend after 15m, is displayed. This event is associated with the only change in the limit of stable conveying which was observed as a result of adding the bend, and takes place at low feed rates close to the limit of stable conveying for rape seed.

To sum up, the incipient blockage of a pneumatic conveying pipeline is associated with incipient slugging close to the limit of stable conveying. The incipient slugging occurs at different positions in the pipeline for different materials. For the Geldart type B materials in the test these slugs only exist at the beginning of the pipeline and are dispersed as they accelerate along the pipeline. For the Geldart type A and C materials these slugs can be found travelling along the whole length of the pipeline.

8. Modelling of Flow Close to the Conveying Limit

Having established in Chapter 7 that the change in mode of flow from stable suspension flow or partially suspended flow to unstable flow is associated with a considerable growth in the pressure fluctuations in the pipeline, and with coherent structures travelling through the pipeline, an attempt will now be made to use this information to establish a new approach towards understanding two phase gas-solids flow, based on existing mechanistic models for gas-liquid flows.

In the mechanistic modelling to follow, the fluidized materials will be assumed to be inviscid, even though (as will be shown later) a viscosity can be associated with a fluidized powder. This has also been investigated by several authors previously [55,56]. In one of the models we will assume that the wave propagation velocity in shallow beds is the same for fluidized powders and liquids. This can be justified by the experimental investigation carried out on wave propagation and damping detailed later in Section 8.2.

As mentioned in Section 2.3.1 several methods of modelling may be selected when attempting to predict the conveying limit from the physical characteristics of the materials that are conveyed. When knowledge about mechanisms that control the conveying limit is available, mechanistic modelling may be attempted. Mechanistic modelling in its nature relies on simplifying the problem without losing the essence of the phenomenon to be predicted. The proposed mechanistic models that follow therefore reduce the number of physical characteristics included in the prediction dramatically.

For the prediction of the pressure minimum velocity, no mechanisms have been identified allowing mechanisic modelling. As a complement to the mechanistic modells for maximum mass flow of solids and limit of stable conveying, a model based on multivariate analysis therefore has been developed for the prediction of the pressure minimum velocity. This is included in the last section of this chapter.

8.1 The Proposed Fluid/Powder Analogies.

As mentioned in Section 2.4.2 the Froude number is frequently used in experimental correlations developed for the prediction of conveying limits in pneumatic conveying pipelines. The observations in Chapter 7 generally indicate that the change to unstable flow is associated with the occurrence of surface waves on the partially settled layer of material towards the bottom of the pipeline. This is similar to what happens on a stratified two-phase gas-liquid flow at the onset of Kelvin Helmholz instabilities and, as will be shown later, the Froude number is contained in the stability expression for the flow in the same way as in the existing empirical correlations.

The Froude number also has another application in fluid dynamics. It gives the ratio of flow velocity to wave propagation velocity in shallow ducts. A Froude number equal to one could in this case characterise the conditions just after a hydraulic jump in a pneumatic conveying line, air assisted gravity conveyor or chute. In certain cases this would give a limiting condition for steady mass flow.

To explore the possibility of applying these two analogies with two phase gas liquid flow, some basic properties of the behaviour of fluidized powders need to be investigated. An investigation of wave propagation, viscous damping of waves, and the influence of the bottom and wall friction in a test channel was therefore carried out.

8.2 The Validity of the Fluid/Powder Analogies

The question of the validity of the analogy between a fluid hydraulic jump and a similar event in a fluidized powder has been tested by carrying out surface wave propagation, and viscosity measurements, on a fluidized bed of alumina. The results of these investigations are shown in Sections 8.2.1 and 8.2.2. The surface wave propagation velocity for shallow bed height becomes the denominator of the Froude number, and the direct measurement of the wave propagation velocity determines the validity of introducing this number for a stratified or moving bed flow of solids. This then allows the theory already developed in fluid dynamics to be applied to the flow of fluidized powders (which is the main purpose of including the investigation in Sections 8.2.1 and 8.2.2).

The measurements of surface gravity wave propagation and viscous damping, were carried out in a 4 meter long air assisted gravity conveyor that was closed at both ends and kept horizontal. The width of the conveyor was 210mm. A sketch of the experimental set-up can be seen in Figure 8.1.

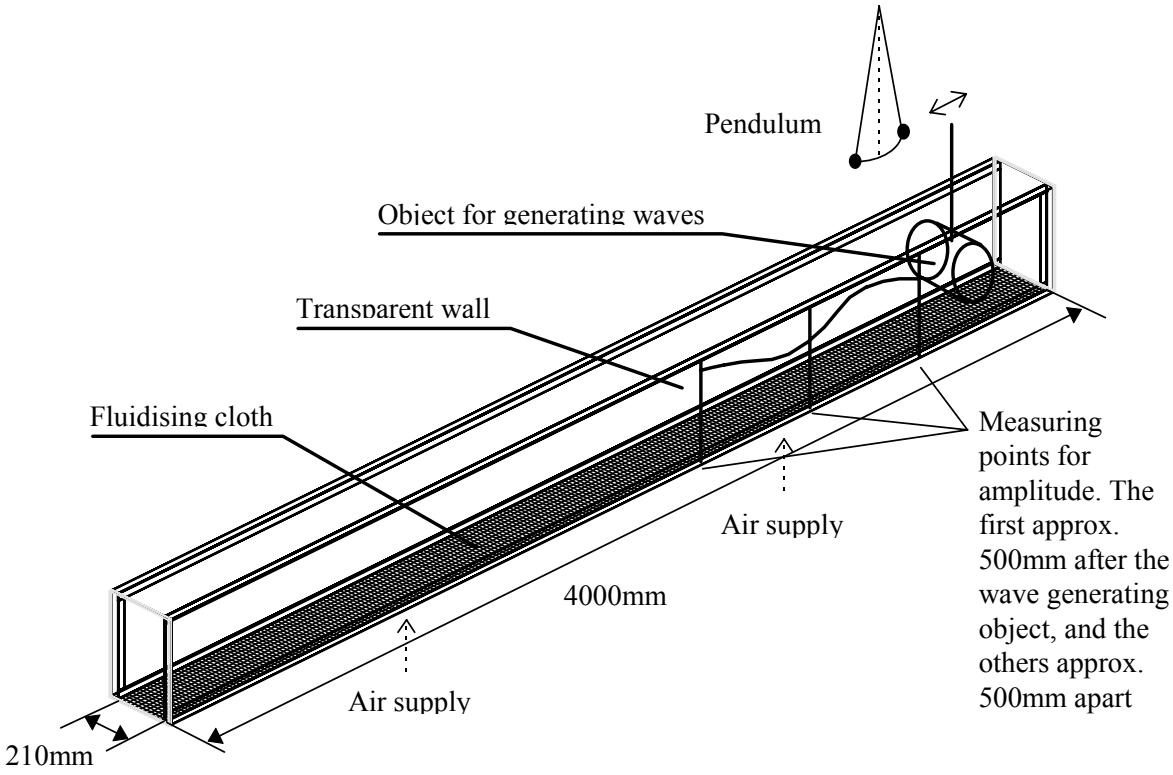

Figure 8.1 Wave tank used for surface gravity wave propagation and viscous damping measurements

This investigation was considered to be preliminary, and simple manual techniques were applied. The waves were generated manually by moving an object back and forth at one end of the tank. Frequencies where kept constant by synchronising the movement of the object to a pendulum. A judgement of when the shape of the waves was sinusoidal was made subjectively. Amplitudes were measured by making video recordings simultaneously at 3 points along the tank. The wave propagation velocity was computed by counting frames in the video recording for a wave peak moving the distance between the first and the last points of measurement (a distance of 1m).

8.2.1 Dispersion Relation for Surface Gravity Waves

The dispersion relation for surface gravity waves on fluidized alumina is shown in Figure 8.2. Compared to linear theory of sinusoidal waves on water, the results for fluidised alumina show a slightly higher propagation velocity at a λ/h ratio of 5. While for a water wave a wave propagation velocity of 0.8 $(gh)^{1/2}$ is expected, the fluidized powder gives a value of 0.9 - 1.0 $(gh)^{1/2}$. This means that the fluidized alumina is close to nondispersive to surface gravity waves, and the wave propagation velocity is close to the shallow duct value for all the λ/h values in the measuring range, which was the basic requirement for the use of the fluid analogy of a hydraulic jump.

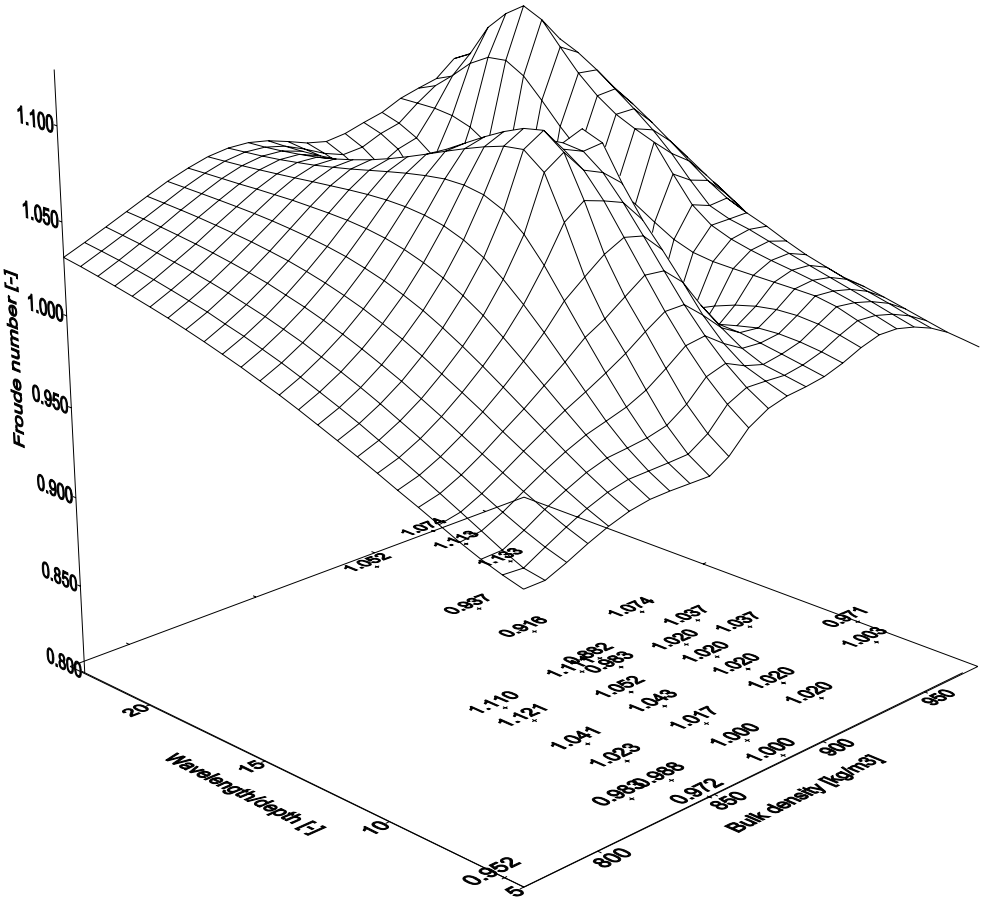

Figure 8.2 Dispersion relation for gravity waves on fluidized alumina.

8.2.2 Viscous Damping of Surface Gravity Waves

The possibility of measuring the apparent viscosity of the fluidized powder, by measuring the viscous damping of a propagating surface wave, has also been investigated. According to Lighthill [57] the total wave energy per unit surface area equals $W=0.5\rho g a^2$ and the proportional internal energy dissipation of a surface wave is $W'/W=4\eta k^2/\rho$, where η is the dynamic viscosity, k is the wave number ($k=2\pi/\lambda$) and ρ is suspension density. If we assume that the density is constant the internal dissipation of energy is also given by $W'=\rho g a(da/dx)(dx/dt)$. By combining these three equations we get an expression for the apparent viscosity:

$$\eta = \frac{\rho c^3}{8\pi^2 a f^2}\frac{da}{dx} \tag{8.1}$$

Where the variables are defined as:

ρ Suspension density.

c Wave propagation velocity.

a Amplitude of the wave.

f Frequency of the occurence of waves.

da/dx Spatial derivative of the amplitude of waves.

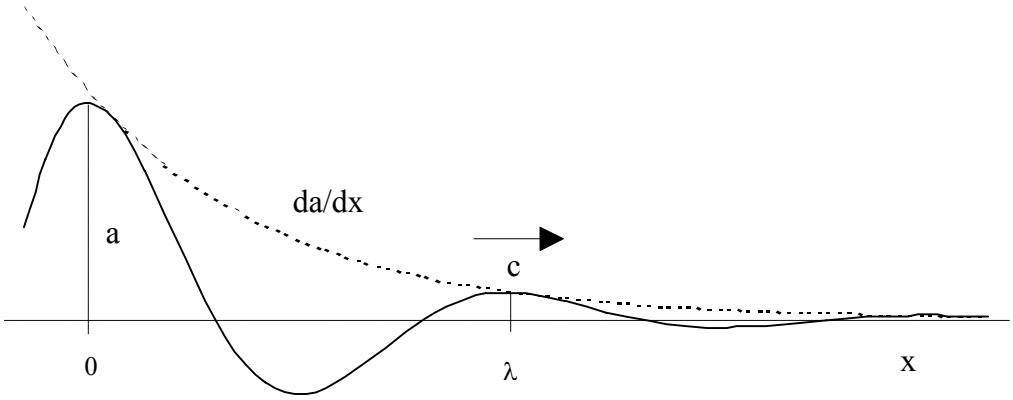

Figure 8.3 Viscous damping of surface waves on water.

The wavelength λ, the propagation velocity c, and the damping of the amplitude per unit length da/dx (see Figure 8.3) can be determined directly from measurements in a long horizontal channel with a fluidized bottom. These measurements were carried out by generating sinusoidal waves on the powder surface in the channel. The wave propagation and damping were measured by close up video recordings of three different sections of the channel.

An investigation of the contribution from the friction at the walls and bottom of the channel to the total dissipation of energy in the wave was also carried out. It is necessary to minimise these contributions to get a reliable measure of the effective viscosity of the fluidized powder. As one can see in Figure 8.4, the apparent viscosity decreases as the ratio of wavelength to the height of filling falls.

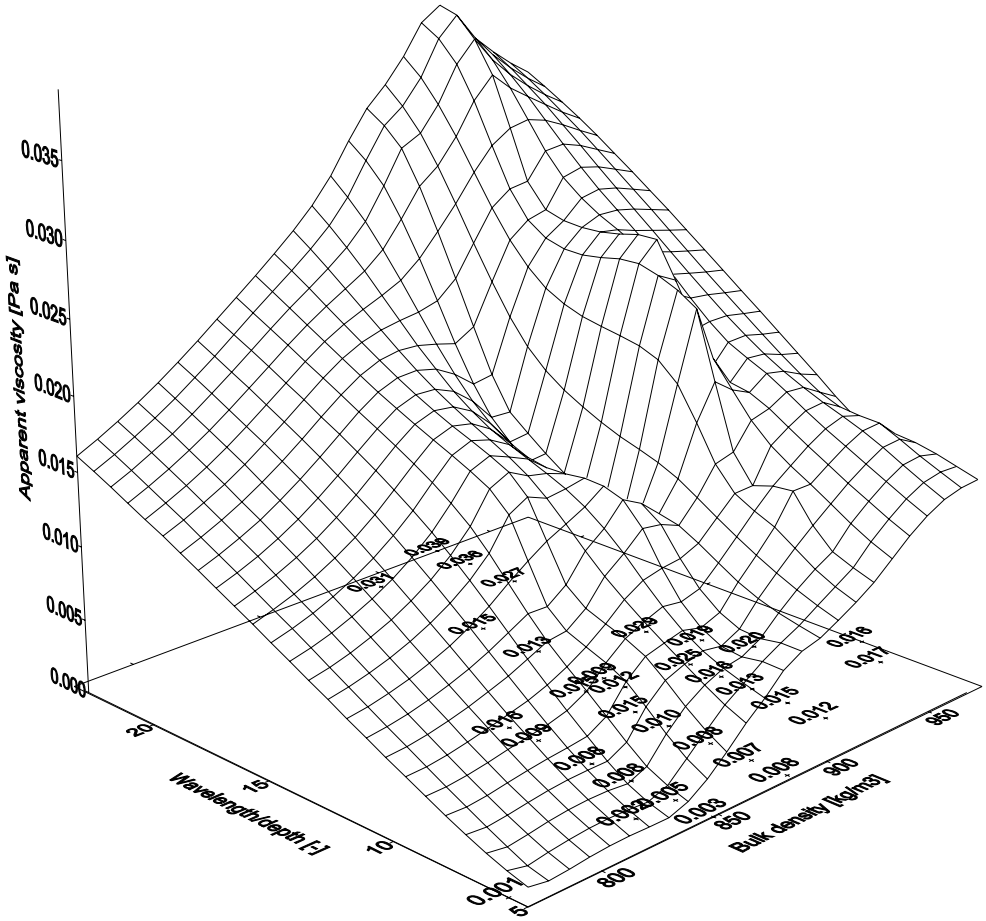

Figure 8.4 Apparent viscosity measured by wave damping and its dependency on λ/h value

This is also what is expected from linear theory of gravity waves on fluids, where the contribution from bottom friction approaches zero at low λ/h values. The value obtained for the viscosity as it approaches zero λ/h value, should therefore be its true value. The values obtained are of the same order of magnitude as those obtained by Botterill et. al. [55] using a 77μm catalyst.

The wall friction influence is shown in Figure 8.5. For alumina there does not seem to be significant effects from wall friction when the width of the channel exceeds 60 to 70 mm.

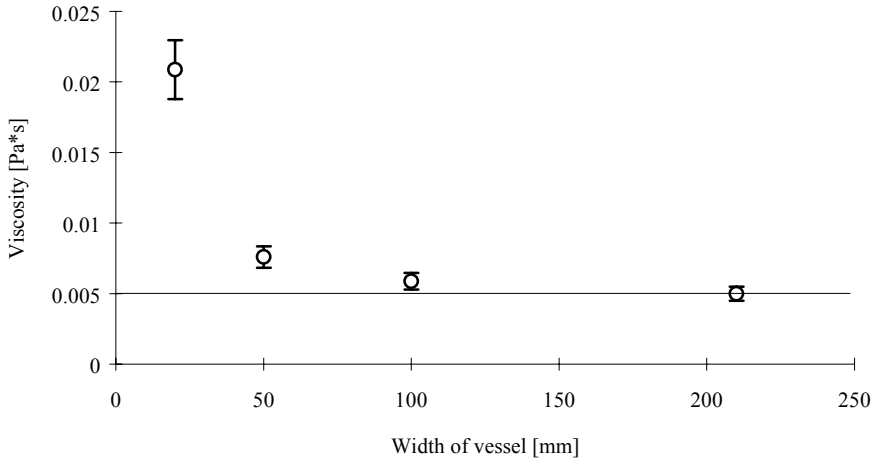

Figure 8.5 Apparent viscosity measured by wave damping, and its dependency on channel width at the same fluidization velocity.

With the model used to compute apparent viscosity from measured values it is possible to obtain an estimate of the accuracy of the computed value through the accuracy of the individual measurements. The estimate of the total experimental error is given as the root of the sum of squares of the rate of change of the viscosity for each measured variable multiplied by the uncertanty of that variable.

$$\Delta\eta \approx \sqrt{\left(\frac{\partial\eta}{\partial\rho}\Delta\rho\right)^2 + \left(\frac{\partial\eta}{\partial f}\Delta f\right)^2 + \left(\frac{\partial\eta}{\partial c}\Delta c\right)^2 + \left(\frac{\partial\eta}{\partial a}\Delta a\right)^2 + \left(\frac{\partial\eta}{\partial\left(\frac{da}{dx}\right)}\Delta\left(\frac{da}{dx}\right)\right)^2} \qquad (8.2)$$

The accuracy of the velocity measurement has a great influence on the total accuracy. Since this is a preliminary investigation we have used simple manual techniques. The waves have been generated manually, and synchronised to a pendulum to give correct frequencies. The shape of the waves has been evaluated subjectively, and amplitudes have been measured by making video recordings of the profile of the powder surface as seen through a transparent side wall in the fluidizing vessel. The accuracy of the computed viscosity is estimated to be ±20%.

8.3 The Hydraulic Jump and the Acceleration of the Solids

Having established that fluidized powders behave similarly to fluids with regard to surface waves and viscosity, we shall proceed by applying the concept of hydraulic jumps to flow of solids. If a stream of particles in a pneumatic transport pipe is slowed down, the change in velocity could lead to an equivalent of a hydraulic jump. The section slowing down the flow could be a bend, a bad weld, a piece of rough pipe wall (Figure 8.6a).

In the feed section the material will initially be moving slowly. Above a certain feed rate this could give rise to a situation, where a short plug builds up at the beginning of the pipeline, limiting the mass flow of solids. This plug would have to be short and permeable enough to allow air to permeate through it to carry off material from its front end. It is expected to dissolve when the Froude number of the flow is above 1 (Figure 8.6b).

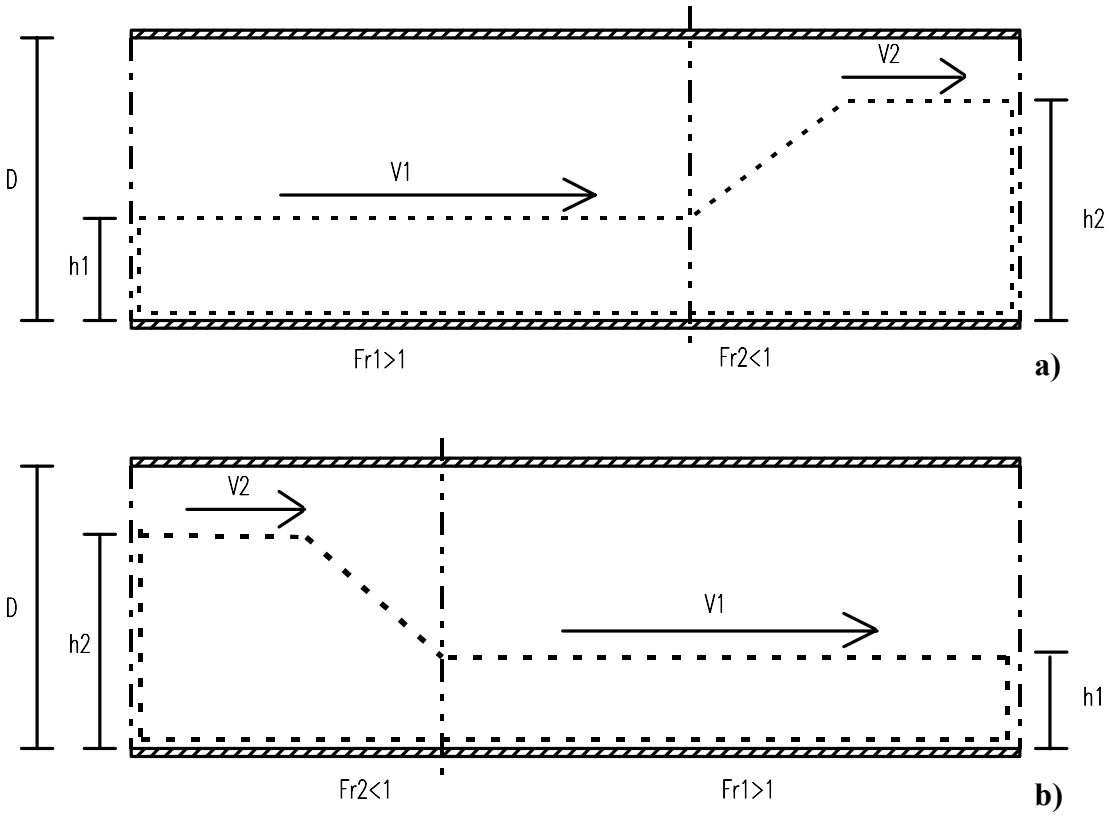

Figure 8.6 Froude numbers for the two cases where, a) the material is slowed down by some obstruction and a phenomenon akin to a hydraulic jump occurs in the pneumatic conveying pipeline, b) the material is accelerated away from the feed section.

In case a) the hydraulic jump will give unstable transport, or pipeline blockage, and in case b) mass flow limitations will occur, if $h_2 \geq D$ and $\rho_2 = \rho_b$, when the material being conveyed is of a type that is likely to block the pipeline at low velocities. These materials are the Geldart type B powders, and to some extent the Geldart type D powders.

8.4 A Model for Maximum Mass Flow of Solids in a Pneumatic Conveying Pipeline

The subcritical velocity section of the flow of a fluidized powder, at which acceleration takes place, will limit the capacity of the transport system by the plugging of the section. The highest obtainable mass flow of solids will be at $Fr \leq 1$ when $h_2 = D$ and $\rho_2 = \rho_b$. It is

assumed that the density of the material falling into the feed section is equal to the poured bulk density. We then have:

$$\dot{m} = \rho_b v_b \pi \frac{D^2}{4} \wedge Fr_b = \frac{v_b}{\sqrt{gD}} \leq 1$$

$$\Downarrow$$

$$\frac{4\dot{m}}{\pi \rho_b D^2} \leq \sqrt{gD}$$

$$\Updownarrow$$

$$\dot{m} \leq m_{max} = \frac{\pi \rho_b g^{1/2} D^{5/2}}{4} \tag{8.3}$$

Where the variables are defined as:

$\dot{m}$	Mass flow of solids.
ρ_b	Poured bulk density.
v_b	Bulk velocity.
D	Pipeline diameter.
Fr_b	Froude number for the flow of the bulk material.
g	Gravitational acceleration.

This should be the maximum flow rate at stable conditions. One may, of course, imagine a plug being pushed through the system at higher feed rates, but this would then cause considerably higher friction forces and unstable flow.

Using the observations of maximum mass flow rate obtained in this experimental investigation it is possible to evaluate the accuracy of this model. When carrying out conveying experiments, some of the materials reached a maximum mass flow before the feeding device was fully open. It is reasonable to assume that this limitation comes from the pipeline itself and not from the feeding device, since increasing the feed rate of the feeding device did not increase the mass flow through the pipeline any further. The opening of the slide valve is 100mm in diameter, which gives a much higher capacity than was observed

as a maximum limiting value. In Figure 8.7 a graph showing the experimentally obtained maximum feed rates in comparison to the limit value predicted by the model is presented.

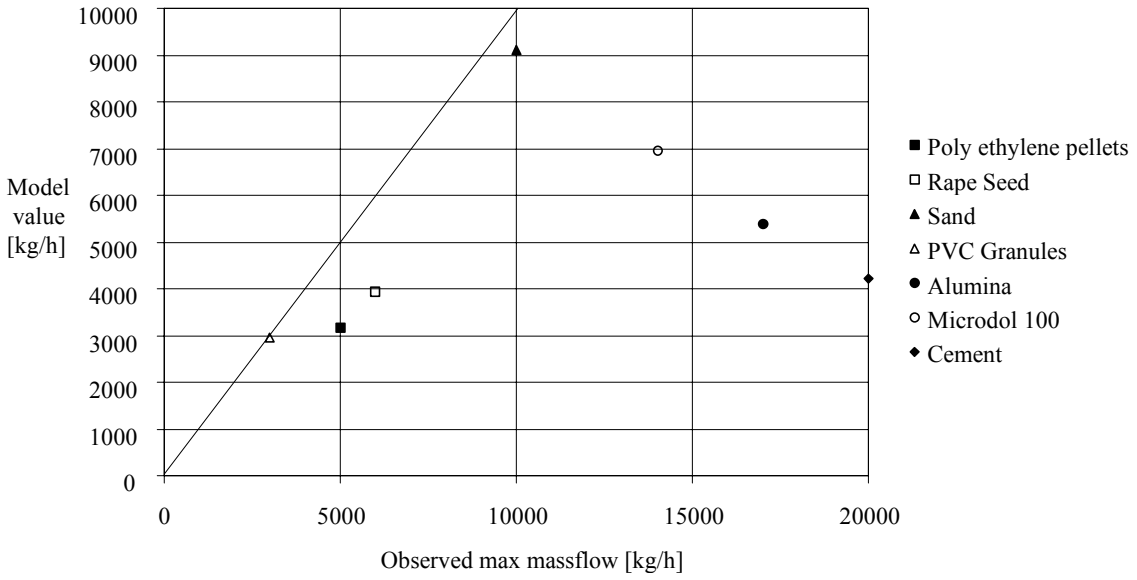

Figure 8.7 Comparison of observed maximum mass flow and predicted value.

As one can see the observed maximum mass flow rate for the Geldart type B materials is close to the limit. The value for PVC granules is identical to the predicted value, whereas sand has a 9% higher mass flow rate than predicted. The type D materials, rape seed and polyethylene pellets, have mass flow rates 34% to 36% higher than the predicted values. The borderline A/B powders and the C powder show much higher discrepancies between measured and predicted maximum mass flow rates.

The prediction of a maximum mass flow rate is thus too conservative for materials other than Geldart type B. It may still be applied for design purposes since it does not under predict the maximum obtainable mass flow rate, and for the materials other than Geldart type B it will work as a worst case estimate.

8.5 The Kelvin Helmholz Instability

We shall now apply the fluid powder analogy, with regards to surface wave propagation, to establish a model for the prediction of flow mode transition from wavy flow to slug flow.

The Kelvin Helmholz instability has been used to explain the transition from wavy flow to slug flow in gas-liquid flows for some years. The corresponding stability criterion, for wavy two phase flow in closed pipelines, was first introduced by Kordyban and Ranov [58] in 1970. Since then a great many papers on the topic have been published, introducing new aspects to the stability criterion such as viscosity [59,60,], filling level [61], and stability of the slug [62].

The Kelvin Helmholz instability may be understood by looking at Bernoulli's equation for steady incompressible frictionless flow along a streamline.

$$\frac{p}{\rho} + \frac{1}{2}v^2 + gz = \text{constant}$$

In a closed horizontal pipeline the gas will flow over a slow moving wavy liquid surface. A wave crest will cause an increase in the local gas velocity. When the pipeline is horizontal, the term gz may be ignored. The local increase in the air velocity will cause a pressure reduction in the gas, which will lift the liquid wave crest. If the lifting force is strong enough to counter gravitational forces, the amplitude of the wave will grow causing instability.

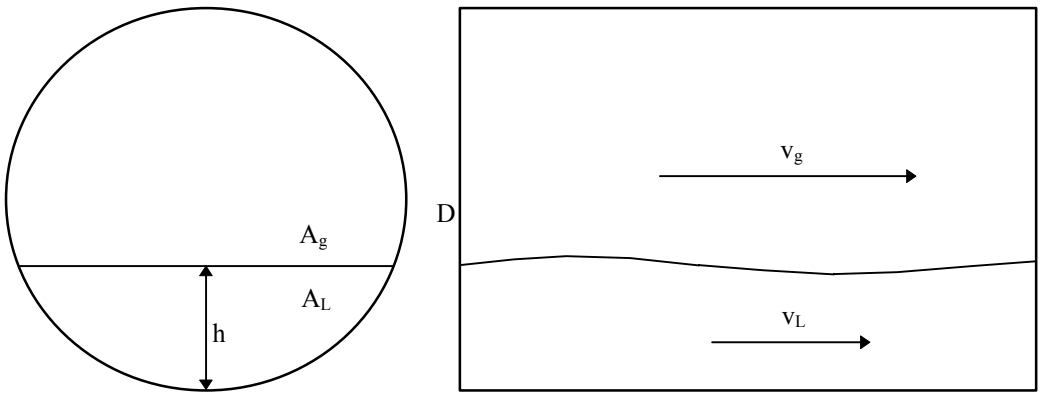

Figure 8.8 The geometry of two-phase Kelvin Helmholz instability.

The geometry of the problem is shown in Figure 8.8. It can be reduced to a problem involving one dimension (along the length of the pipeline) and time.

To adapt the theory of the Kelvin Helmholz instability to two-phase gas-solids flow we shall take the approach of Barnea and Taitel [63] starting with the integral relations for conservation of mass and momentum.

$$\frac{d}{dt}\left(\iiint_{CV}\rho dV\right)+\iint_{CS}(\rho\vec{v}_r\cdot\vec{n})dA=0 \tag{8.4}$$

$$\sum\vec{F}=\frac{d}{dt}\left(\iiint_{CV}\vec{v}\rho dV\right)+\iint\vec{v}\rho(\vec{v}\cdot\vec{n})dA \tag{8.5}$$

The basic assumptions that will be used throughout the derivation of the stability criterion are inviscid flow, no surface tension and incompressible flow.

For a infinitesimally thin control volume covering the cross section of the pipeline this gives.

$$\frac{\partial}{\partial t}(\rho A dx)+\frac{\partial}{\partial x}(\rho v A)dx=0 \tag{8.6}$$

$$-\left(\rho Ag\frac{\partial h}{\partial x}+A\frac{\partial p}{\partial x}\right)dx=\frac{\partial}{\partial t}(v\rho A dx)+\frac{\partial}{\partial x}\left(\rho v^2 A\right)dx \tag{8.7}$$

Which will be valid for each of the two phases. This gives four equations that enable the determination of the dispersion relation for surface perturbations on the layer of liquid towards the bottom of the pipeline. The derivation of the expression is shown in Appendix A. Marginal instability occurs when (see Equation A.27):

$$\frac{A_L'\left(v_g-v_L\right)^2}{Ag}=\frac{\left(R_g\rho_L+R_L\rho_g\right)\cdot\left(\rho_L-\rho_g\right)}{\rho_g\rho_L} \tag{8.8}$$

Where the variables are defined as:

A_L' Shape factor for the pipeline (se Appendix A).

A Pipeline cross section area.

g Gravity acceleration.

v_g Gas velocity.

v_L Liquid velocity.

R_g Ratio between cross section area filled with gas and the total area.

R_L Ratio between cross section area filled with liquid and the total area.

ρ_g Gas density.

ρ_L Liquid density.

8.6 A Model for Predicting The Limit of Stable Conveying in Suspension Flow

The application of the Kelvin Helmholz instability, to predict the limit of stability in suspension flow, rests on the fact that when the conveying limit is approached, the concentration of powder starts to increase towards the bottom of the pipeline, establishing a free surface. Visual observations of the flow pattern indicate that a pulsating flow occurs before a settled layer of material forms in the bottom of the pipeline. This has also been described previously by several authors [64,65,66]. The model proposed here interprets these pulsations as being a result of the Kelvin Helmholz instability, causing a re-suspension of particles from the flowing layer at the bottom of the pipeline. When this re-suspension of particles stops, at the marginal stability limit of the KH instability, conditions for blockage are expected to be fulfilled.

For gas-solids flow the density of the fluid should be equal to the suspension density of the fluidized powder. We shall take the simplest approximation to this and equate it to the bulk density of the powder. We can now adapt Equation 8.8 to apply for fluidized two-phase gas-solids flow. First of all, it has to be simplified to contain superficial gas velocity instead of the velocity difference between the powder and the gas. The filling level of the pipeline also has to be inserted into the expression. In accordance with simplifications introduced by Bendiksen and Espedal [62] one can write this as:

$$v_{sg}^2\left(1-\frac{v_b}{v_g}\right)^2 = KDgR_g^2\cdot\left(R_g+\frac{\rho_g}{\rho_b}\left(1-R_g\right)\right)\frac{\cdot\left(\rho_b-\rho_g\right)}{\rho_g} \tag{8.9}$$

Where the variables are defined as:

v_{sg} Superficial gas velocity.

v_g Gas velocity.

v_b Bulk material velocity.

K Geometrical factor $A/(DA_L')$ equal to $\pi/4$ at a filling level of D/2.

D Pipeline inner diameter.

g Gravitational acceleration.

R_g Ratio between cross section area filled with gas and the total area.

ρ_g Gas density.

ρ_b Poured bulk density of powder.

Given that $v_b << v_g$ and that $\rho_b >> \rho_g$, this can be simplified to:

$$v_{sg}^2 = KDg \cdot R_g^3 \frac{\rho_b}{\rho_g} \tag{8.10}$$

The question of what value to use for K still remains. The factor A_L', which is the rate of change in the cross section area occupied by the "liquid" with filling level, starts out at zero for zero filling level, passes trough a maximum at $\pi/4$, and is equal to zero when the pipeline is filled. The corresponding K factor is contained within the interval $[\infty .. \pi/4]$ at a filling level below D/2. At a filling level above D/2 it is contained within the interval $[\pi/4..\infty]$.

The geometry of the pipeline will contribute to stabilise the flow at a filling level below D/2, because a positive perturbation in the filling level will decrease the energy density per surface area which is proportional to the amplitude of the perturbation to a power of two [57]. At a filling level above D/2 the opposite happens and an increase in the the energy density per surface area due to a positive perturbation in the filling level will contribute to destabilize the flow.

Considering, as stated initially in this section, that it is assumed that the KH-instability causes re-suspension of particles and thereby prevents blockage, the stabilising effect of the pipeline geometry at a filling below D/2 will cause blockages to occur earlier than without the geometrical effect. In short, a flat bottom pipeline should allow conveying to take place at lower air velocities than a circular pipeline. This has been observed experimentally by Wirth and Molerus [67]. For this reason the K factor selected for this model will be $\pi/4$ which corresponds to the highest obtainable filling level without a destabilising effect from the shape of the pipeline cross section.

Before we can use Equation 8.10 for the prediction of stability limits for fluidized powders we must replace the volumetric concentration of gas R_g with an expression containing the solids loading ratio μ. The stability expression incorporates a factor v_L/v_g that has been asumed to be small. To be able to continue the computation, we also have to assume that $v_{sg}/v_b \approx 1$. This means that the expression obtained will only be valid for high solids loading ratios. The last assumption may seem contradictory to the assumption that the local air velocity above the moving bed is much larger than the bulk velocity, but it is important to remember that the bulk material has its own voidage, different from $R_g = A_g/A$, that causes air to flow along inside the bulk of the material. If this fraction of the air flow is large in comparison to the amount of air flowing above the bed, and the slip velocity between the solids and the air flowing inside the bulk of the material is low, the assumption holds. Defining the bulk voidage of the powder as ε_b the expression for the superficial air velocity gives:

$$v_{sg} = \frac{v_b A_b \varepsilon_b + A_g v_g}{A} \approx v_b \Rightarrow \quad v_b A \approx v_b A_b \varepsilon_b + A_g v_g \Rightarrow \quad 1 - \varepsilon_b \approx \frac{A_g v_g}{A_b v_b} \approx R_g \frac{v_g}{v_b}$$

when $A_b \approx A$ which means that the assumptions above are valid when the following condition is satisfied:

$$\frac{v_b}{v_g} \approx \frac{R_g}{(1-\varepsilon_b)}$$

Which also easily complies with the first assumption when the filling level in the pipeline is high:

$$\frac{v_b}{v_g} << 1 \quad \Rightarrow \quad R_g << (1-\varepsilon_b)$$

Using these assumptions we can now write:

$$\mu = \frac{\rho_b A_b v_b}{\rho_g A v_{sg}} = \frac{\rho_b v_b}{\rho_g v_{sg}}\left(\frac{A - A_g}{A}\right) \approx \frac{\rho_b v_b}{\rho_g v_{sg}}\left(1 - R_g\right)$$

$$\Updownarrow \qquad (8.11)$$

$$R_g = 1 - \mu\frac{\rho_g}{\rho_b}$$

which gives:

$$v_{sg}^2 = KDg\frac{\rho_b}{\rho_g}\left(1 - \mu\frac{\rho_g}{\rho_b}\right)^3 \qquad (8.12)$$

Where the variables are defined as:

v_{sg} Superficial gas velocity.

K Geometrical factor $A/(DA_L')$ equal to $\pi/4$ at a filling level of D/2.

D Pipeline inner diameter.

g Gravitational acceleration.

ρ_g Gas density.

ρ_b Poured bulk density of powder.

μ Solids loading ratio.

Equation 8.12 can be used directly to compute the limit of stable conveying in suspension flow. In Figures 8.9 through to 8.15 this model has been compared to the existing models presented in section 6.1.

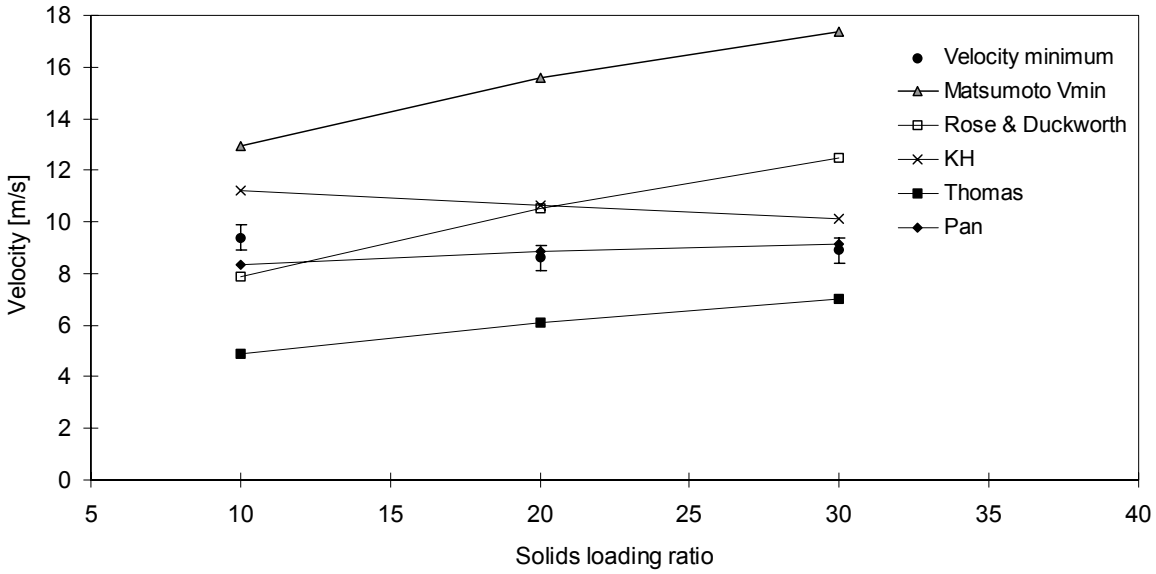

Figure 8.9 Comparison between models to predict limit of stable flow in dilute phase for polyethylene pellets, and experimentally obtained velocity minimum.

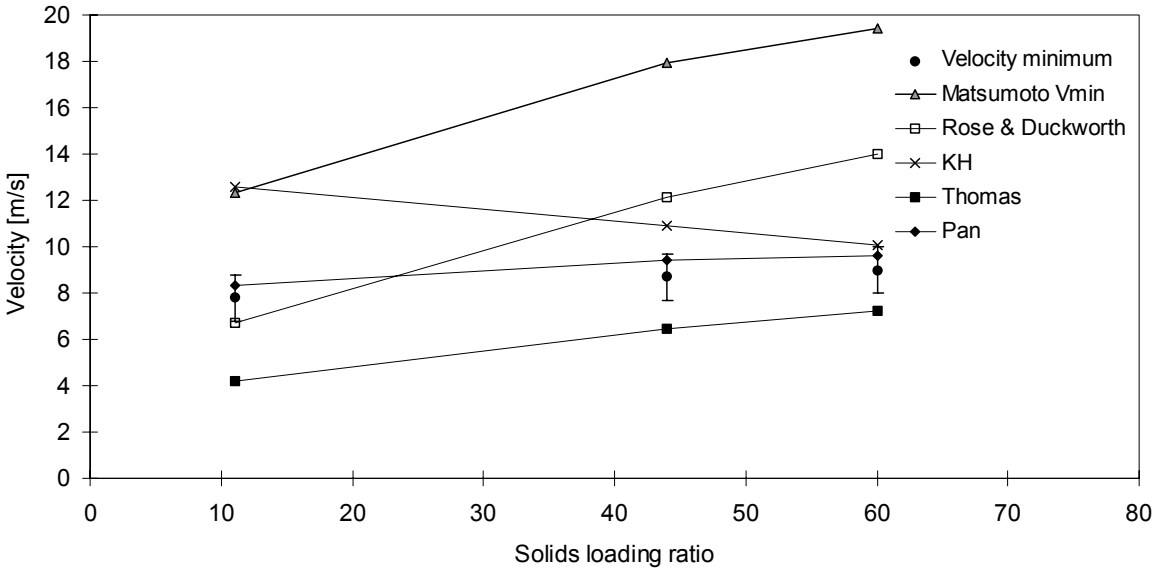

Figure 8.10 Comparison between models to predict limit of stable flow in dilute phase for rape seed, and experimentally obtained velocity minimum.

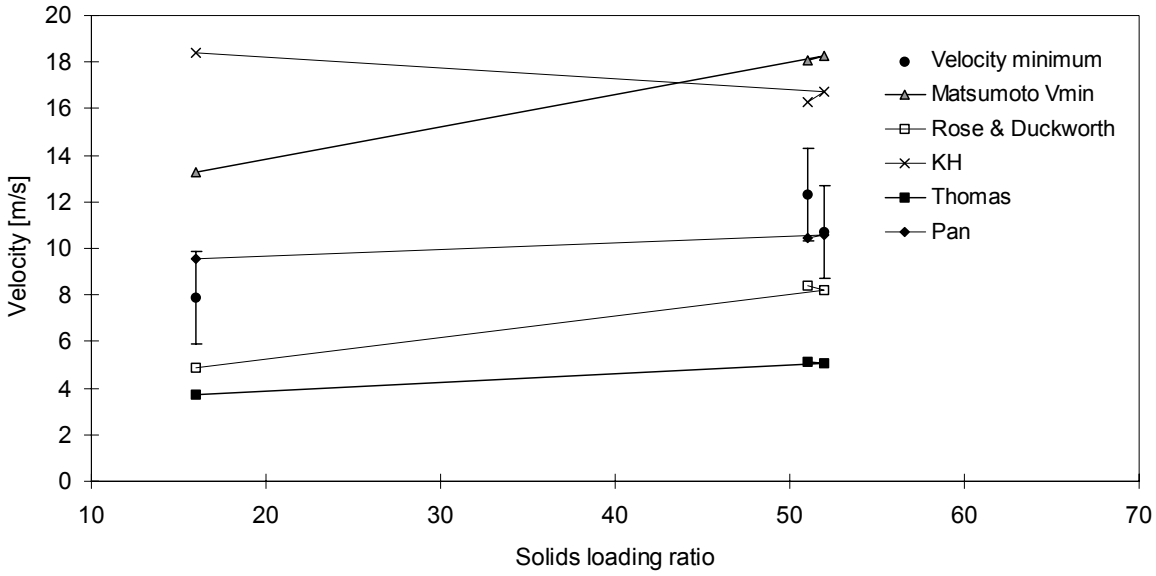

Figure 8.11 Comparison between models to predict limit of stable flow in dilute phase for sand, and experimentally obtained velocity minimum.

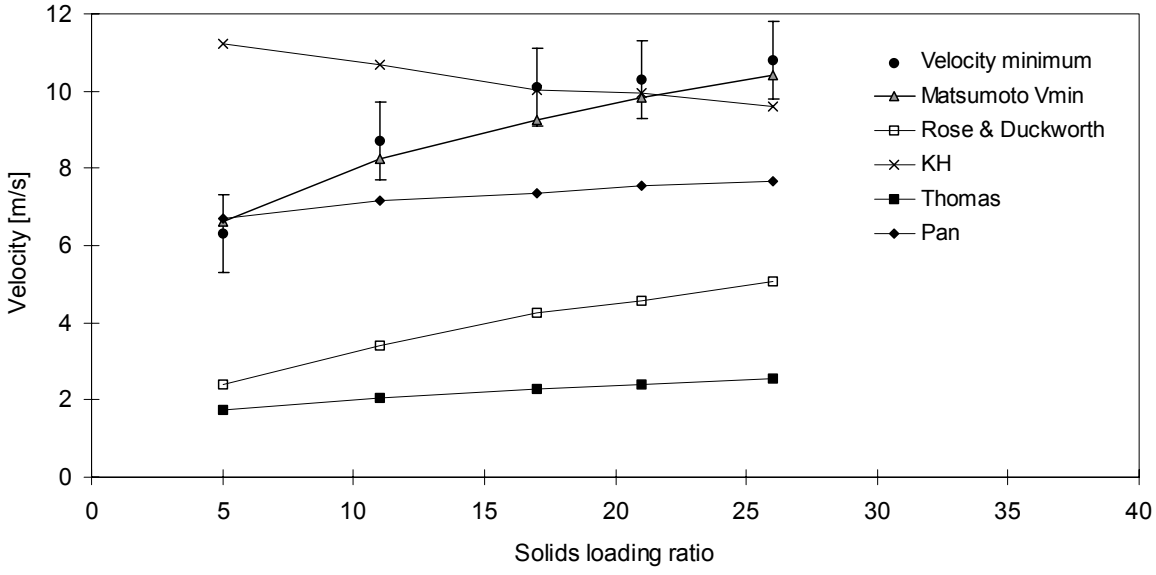

Figure 8.12 Comparison between models to predict limit of stable flow in dilute phase for PVC granules, and experimentally obtained velocity minimum.

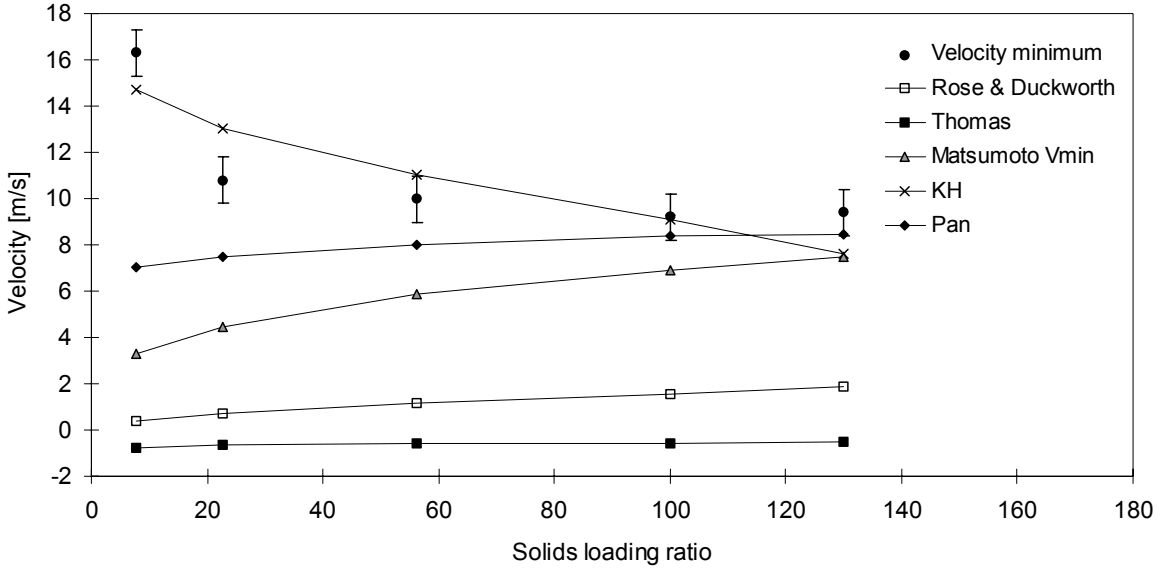

Figure 8.13 Comparison between models to predict limit of stable flow in dilute phase for alumina, and experimentally obtained velocity minimum.

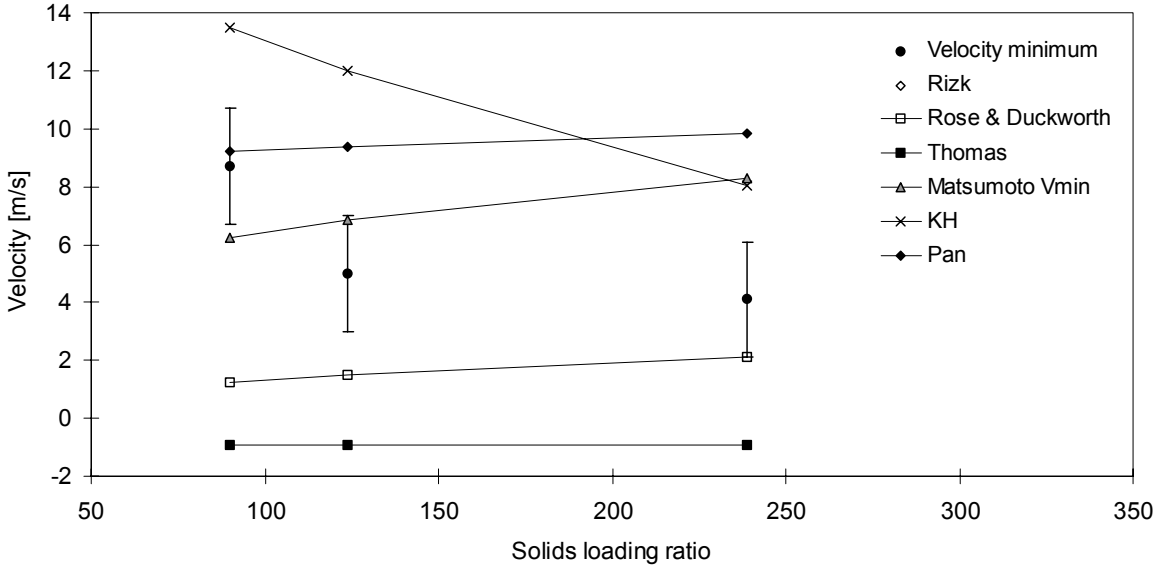

Figure 8.14 Comparison between models to predict limit of stable flow in dilute phase for micronized dolomite, and experimentally obtained velocity minimum.

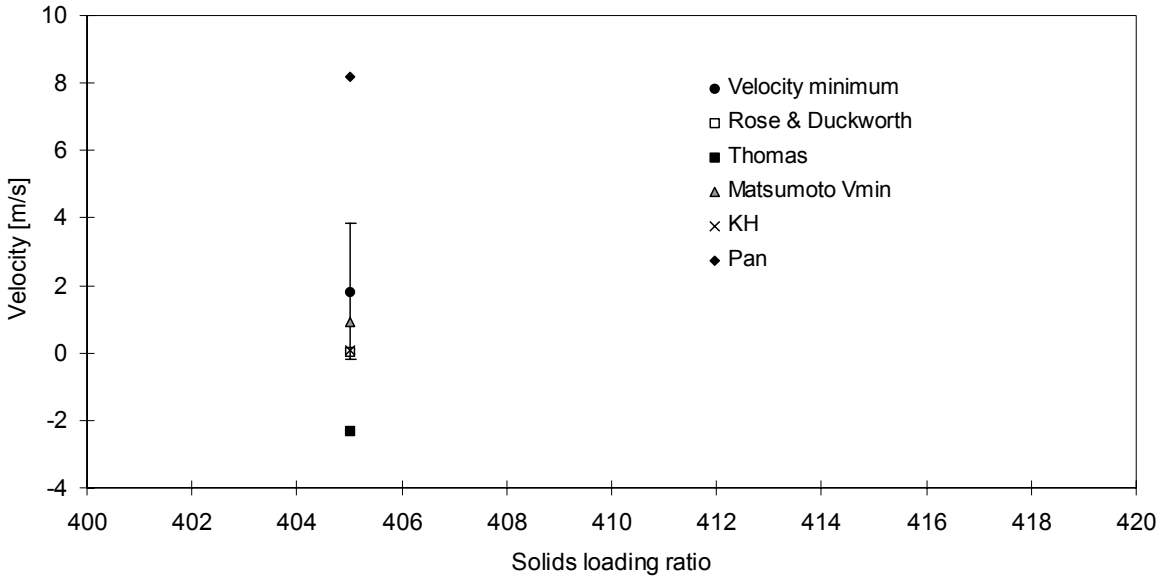

Figure 8.15 Comparison between models to predict limit of stable flow in dilute phase for cement, and experimentally obtained velocity minimum.

As can be seen from Figure 8.9 through to 8.15 the proposed model, with the exception of the cases of high and low solids loading ratio for alumina and high solids loading ratio for PVC, does not underestimate the stability limit. At the points where it does it is just below the error limit of the experimentally obtained value.

In Table 8.1 the results of the comparison above are presented. The worst case prediction errors for all models predicting the limit of stable conveying in suspension flow are shown.

Table 8.1 The worst case error of velocity minimum predictions given in percent of experimentally obtained value.

Model	LDPE	Rape seed	Sand	PVC	Alumina	Micronized dolomite	Cement
Pan	-12	8	-31	-29	-57	139	348
Rose & Duckworth	57	56	-44	-62	-98	-86	-98
Matsumoto V_{min}	103	116	71	-8	-80	102	-50
Thomas	-48	-46	-66	-77	-107	-123	-228
K-H instability	24	61	133	78	21	140	-95

The two most dominant simplifications included in the model are, the assumption of bulk density for the density of the moving concentrated layer of solids occurring close to

blockage or instability, and the assumption of a filling level of D/2. Later improvements to the model should improve on these assumptions and include the effects of the suspension viscosity.

Considering that this model is purely based on theory, and that it has been developed from first principles, without any empirical fitting, it is surprising how well it fits the experimental data.

In Table 8.2 the correlation between model values and experimental data, when varying solids loading ratio μ, is listed for all materials except cement (where we have no observation of blockage). In general, none of the models gives results that correlate well with the experimental data obtained for polyethylene pellets. For the other materials the existing models correlate well with the coarsest materials, while the new model correlates best with the finest materials.

Table 8.2 Correlation with μ for the new and existing models for predicting the limit of stable conveying (negative correlation with μ is shaded).

Model	LDPE	Rape seed	Sand	PVC	Alumina	Micronized dolomite
Matsumoto	0.10	1.00	0.92	0.99	-0.87	-0.85
Rose & Duckworth	0.15	1.00	0.95	0.98	-0.83	-0.84
Thomas	0.16	1.00	0.94	0.98	-0.93	0.18
Pan	0.04	1.00	0.89	0.99	-0.90	-0.84
KH-instability	-0.25	-1.00	-0.98	-0.98	0.83	0.83

It is also possible to evaluate each model's ability to predict the limit of stable conveying for various materials, by computing the correlation coefficient when varying the material type at maximum or minimum solids loading ratio. In Table 8.3 the correlation between model values and experimental data, when varying material type, is listed for all materials. The high correlation coefficient for Rose and Duckworth's model is artificial, since it has a very limited area of validity. Pan's model gives a correlation coefficient of 0.81 inside its area of validity at minimum solids loading ratio. When including all materials the Kelvin-Helmholz instability model gives the best correlation with experimental data. It thus seems as if the K-H instability model has the potential to predict the behaviour also of the coarser

powders, even though it does not predict the correct solids loading dependency for the coarse materials.

Table 8.3 Correlation with material type for the new and existing models for predicting the limit of stable conveying.

Model	At minimum μ, inside area of validity	At minimum μ, for all materials	At maximum μ, inside area of validity	At maximum μ, for all materials
Matsumoto	0.71	0.19	0.37	0.21
Rose & Duckworth	0.97	0.14	0.98	0.15
Thomas	0.52	0.22	0.31	0.24
Pan	0.81	-0.16	0.40	-0.15
KH-instability	0.73	0.56	0.64	0.56

8.7 An Empirical Model for Predicting Pressure Minimum based on Chemometric Analysis

In a collaborative project between the author at Telemark Industrial Research and Development Centre and P.E.Lia and Prof. K.H. Esbensen at Telemark College, a model for predicting the pressure minimum velocity, based on the data presented in this thesis, was developed using multivariate modelling [68].

Multivariate analysis allows complex characteristics to be included in the modelling process. Thus the complete fluidization characteristics have been included directly, not only as single characteristics such as permeability, minimum fluidization velocity and deaeration rate. This allows details in the shape of the characteristics to play a role in the modelling.

As a part of the modelling Lia has carried out a screening of relevant physical characteristics. The results show that particle density, average particle size and permeability play an important role in the prediction of pressure minimum velocity. In addition several interaction effects between different aspects of the fluidization

characteristics also play an important role in the modelling. An overview of the important characteristics and interaction effects is shown in Table 8.4.

Table 8.4 Characteristics that have been identified to be of importance to the prediction of the pressure minimum velocity.

	Description
1	Particle density
2	Mean particle size
3	Permeability prior to fluidization
4	Interaction between median particle size and bed height after 15s deaeration
5	Interaction between mean particle size and bed height after 15s deaeration
6	Interaction between minimum fluidization velocity and total deaeration time
7	Interaction between minimum fluidization velocity and bed height at 45% of the air velocity at maximum bed height
8	Interaction between minimum fluidization velocity and bed height after 15s deaeration
9	Interaction between total deaeration time and air velocity at maximum bed height
10	Interaction between total deaeration time and air velocity at 45% of air velocity at maximum bed height
11	Interaction between air velocity at maximum bed height and air velocity at 45% of air velocity at maximum bed height
12	Interaction between air velocity at maximum bed height and bed height after 15s deaeration
13	Interaction between specific pressure drop at an air velocity equal to 60% of minimum fluidization and bed height after 15s deaeration

It is suprising that neither the wall friction nor the bulk density of the powders play a role in this model. The static and dynamic angle of repose were also found to have no influence.

In Lia's model the polyethylene pellets are identified as a typical outlier. To be able to build a good model, this material had to be left out of the modelling process. LDPE is the material with the largest particle size, so this means that the model established cannot be expected to predict pressure minimum for materials with larger particle size than that of rape seed.

The root mean square value of the error of the prediction (RMSEP) in Lia's model is ±1.16m/s for all 6 materials. The maximum error is -2.2m/s (or -15% of the measured value) and is obtained for PVC. The accuracy has been determined by carrying out cross

validation for all data sets. In Figure 8.16 the comparrison between measured and predicted values is shown. The correlation coeficient beween predicted and measured values is 0.90.

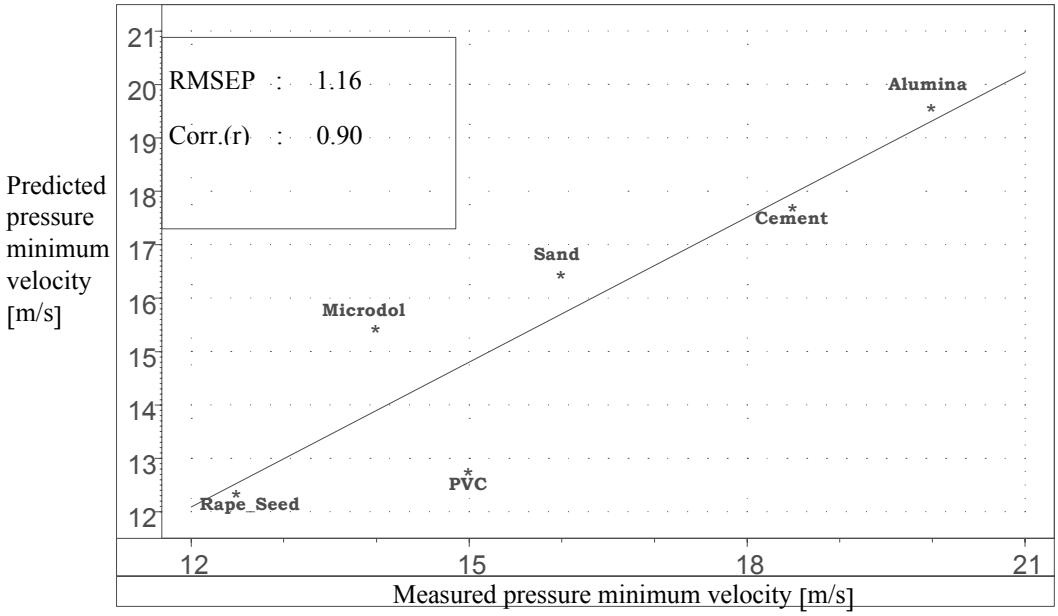

Figure 8.16 Measured versus predicted value for pressure minimum velocity for Lia's model.

A limitation in the work has been the number of materials included in the data set, which is close to the limit of what is possible to use in multivariate analysis. It should also be mentioned that the model, as is the case with all empirical models, is only valid within the area spanned out by the variables associated with the materials and pipelines included in the data set on which it is based. In this case this implies that the model, even though it is valid for a wide range of particle densities and sizes, only can be applied to 53mm diameter pipelines.

9. Discussion of the Effect of Physical Characteristics of Particulate Materials on their Conveyability.

As discussed in Chapter 1, conveyability in pneumatic conveying systems has several aspects. In this investigation, it has been chosen to look at minimum conveying velocities in suspension flow or partially suspended flow. The problem of finding connections between physical characteristics of particulate materials, and their conveyability in pneumatic transport systems can, as shown in Section 2.3.1, be addressed in several ways.

In the process of establishing an understanding of an unexplored phenomenon, the first step is usually to carry out empirical modelling based on dimensional analysis. This method has been applied by many authors investigating conveying limits in pneumatic transport systems, as can be seen in Section 2.4. It requires that a number of relevant physical characteristics is identified, and that these are combined in relevant dimensionless groups.

The next step would be to try to establish a mechanistic model for the prediction of the phenomenon. A mechanistic model has several advantages. It allows extrapolation of the results to new parametric values. It can also result in a simplified description of the phenomenon. And finally it may result in new fundamental understanding of the phenomenon described.

Yet another approach can be taken. By applying multivariate analysis, large sets of data can be incorporated into the search for connections. This method might seem as just another empirical method using curve fitting, but is unique in that it standardizes the identification of important parameters. It is therefore possible to carry out screening tests to find the relevant factors influencing the phenomenon. This method therefore turns out to be an important supplement to the mechanistic approach in that it can identify the relevant physical characteristics.

In this thesis, the focus has been on applying information from existing models for predicting conveying limits, as well as using new experimental observations of the

dynamic behaviour of the materials in the pipeline, to establish a mechanistic model for predicting the conveying limit. Multivariate analysis has also been applied to establish a model for the prediction of pressure minimum velocity, since no plausible mechanisms have been identified for this phenomenon that do not need empirical fitting.

In addition to the modelling work mentioned above, a simple model for the prediction of maximum mass flow of solids in the pipeline has been developed, and some important observations of blockage position has been made. A discussion of these observations is also included in this chapter.

As shown in Section 2.1.1, single particle behaviour is dominant for flow regimes where the mean free path of a particle is larger than the pipeline diameter. Such flow regimes may be expected to occur only at very low solids loading ratios. It has therefore been natural to look into the possibility of establishing models based on the collective behaviour of powders. One such set of possible models is based on an analogy with fluid dynamics. This fluid powder analogy has been applied for both of the mechanistic models described below.

9.1 Prediction of Maximum Mass Flow of Solids

Let us start by looking at the model for predicting the maximum mass flow rate of solids in a pneumatic conveying system (shown in Section 8.4). The model is based on the assumption that a phenomenon akin to the acceleration of a liquid down an inclined slope occurs in the feed section of a pneumatic conveying pipeline.

The material that is to be transported must start out initially at rest. If the feed rate is high enough the initial part of the feed section, or even the pipeline, will be filled in the whole cross section and mechanical locking will take place for types of powders that exhibit high friction forces along the wall when plugging. The point at which the plug breaks up can be characterised by a Froude number of one, given that the analogy with fluid dynamics holds. As a limiting case we will have a powder, with a packing close to bulk density, flowing at a Froude number of one, almost filling the pipeline. This limiting case will

define the maximum mass flow of solids, and the expression is shown in Equation 8.3. The only physical characteristic involved, is the bulk density of the powder.

From the reasoning above it is obvious that materials with physical characteristics associated with Geldart type A/C, when fluidized, will not block a pipeline in the way mentioned. It is also obvious that Geldart type D materials are not likely to be as influenced by this mass flow restriction as Geldart type B materials, because the D type materials do not build strong blockages, due to their high permeability.

In essence the mechanism described can thus be expected to be valid for Geldart type B materials, as is also confirmed by the plot in Figure 8.7. The maximum mass flow of solids for this group of powders is governed by the bulk density of the powder.

9.2 Prediction of the Limit of Stable Conveying in Suspension or Partially Suspended Flow

The next mechanistic model developed is for the limit of stable conveying in suspension flow or partially suspended flow, as described in Section 8.6. The basic assumption is that instabilities on the surface of a partially settled layer of solids contributes to re-suspend particles, and thus to prevent blockage. The instability governing the re-suspension of particles is assumed to be the Kelvin Helmholz instability, which also is applied for the prediction of flow pattern changes in two phase gas liquid flows. For the instability to have any relevance a partially settled layer of solids must exist on which the instability can take place. Visual observations justify the assumption that this layer is always present close to blockage, and that it is the KH instability that is the limiting factor.

An important set of data, supporting the use of KH instability for the prediction of flow transitions for fluidised powders, is the pressure fluctuations that have been observed in Chapter 7. A general growth in the pressure fluctuations can be seen to take place (see Figure 7.1) when approaching the conveying limit. For the fine powders, microdol and cement, the pressure fluctuations pass through a region of high values and are reduced again before blockage. This is exactly what should be expected, since the conveying

velocity has to be low enough to allow a strongly stratified flow to exist, and since this stratified flow will block the pipeline when the surface instability vanishes.

The validity of the fluid powder analogy has been checked for alumina, which is a border line Geldart type A/B powder and is easily fluidized. No information about the validity of the analogy exists for Geldart type B and D materials. Visual observations made by the author indicate that such instabilities exist also for the coarse materials. But even if these materials also exhibit surface instabilities, they will behave differently for these powders due to their relatively higher permeability. The steepening of an unstable surface perturbation for a coarser material may be expected to be slowed down, or even be inhibited, by the constant replacement of conveying air in the volume above the wave crest, permeating through from inside the bulk material.

The model for predicting the limit of stable conveying is therefore thought to be best suited for the Geldart type A/C materials. It is also expected to have a potential to predict the same conveying limit for Geldart type B and D materials, and is expected to perform better when the effect of the permeability of the material is included in the model.

Another physical property that is expected to influence this model, but that has not been included so far, is the viscosity of the suspension. During the investigation of fluid powder analogies in Section 8.2 a method for measuring viscosity, based on damping of surface gravity waves was discovered. This method is non intrusive, and resembles the conditions that may be expected to occur in the conveying line. It will therefore, at a later stage, be possible also to measure, and include, the effect of viscosity. It is known from theory for gas liquid flow that the viscosity has a destabilising effect on the KH instability. This would then result in increased particle re-suspension and lower the conveying velocity limit. As can be seen in Table 8.1 the existing model overestimates the conveying limit, which may be expected, since the proposed model does not yet include the effect of viscosity.

To sum up, the bulk density, the permeability and the viscosity of the powders are expected to govern the limit of stable conveying in suspension flow. The model developed does not yet incorporate the effect of viscosity and permeability, but may be expanded to

do so. Without the inclusion of the effect of permeability the model is expected to fit the fine materials best. Table 8.2 shows that the model has the best correlation with solids loading ratio for the fine materials. Table 8.3 also shows that it has the best overall fit to the whole set of data. This overall fit can be expected to improve once the effect of permeability has been included.

9.3 Prediction of Pressure Minimum Velocity

The multivariate model developed by Lia [65] for the prediction of an average pressure minimum velocity has been based on a set of variables selected from an initial screening of a larger set of variables. Interesting information can be found both from the variables that have not been found to influence the model, and the variables that have been found to do so.

The final model incorporates two particle properties, mean particle size and particle density, in addition to the permeability of the material prior to fluidisation, and various interaction effects between properties of the fluidisation characteristics. The particle density and the mean particle size are included in all the existing model for predicting conveying limits presented in Section 2.4, either directly or indirectly through secondary properties such as terminal velocity in air. No other physical properties of the particulate materials are included, except for the wall friction factor included in Wirth's model [16]. Including fluidisation properties and permeability directly into the model therefore is new to the modelling of the pressure minimum velocity.

It is surprising to notice that the model, in contrast to Wirths model, does not include wall friction. The screening of variables influencing the pressure minimum velocity did not identify this variable as being important. The bulk density and the angles of repose have also been found to be of no influence on the pressure minimum velocity. These results indicate that wall interaction effects, and effects related to internal shear in a material at bulk density, is not important when modelling pressure minimum velocity.

In Lia's model LDPE is identified as an outlier. The observation that it is difficult to model the behaviour of the LDPE has also been made in the section 8.6. In Table 8.2 it can be

seen that the correlation between predicted and measured values for the minimum conveying velocity is very poor for this material. It is difficult to say anything definitive about the reason for this poor correlation, but one possible explanation may lie in the fact that the particle size is much larger in comparison to the pipeline diameter, for this material than for the others.

The model, as all empirical models, is valid inside an area spanned out by the values of the variables associated with the selection of materials on which the model is based. This means that the model is expected to predict the pressure minimum velocity of materials in the size range between 15μm and 1.7mm, for particle densities ranging from 1164kg/m^3 to 3399kg/m^3 and permeabilities ranging from $3.2 \cdot 10^{-5}$ m^2/(Pa s) to $1.0 \cdot 10^{-7}$ m^2/(Pa s). This should cover many of the materials encountered in industry. A limitation of the model is that it is only valid for pipelines with diameter 53mm.

9.4 The Variation of the Pressure Minimum Velocity and the Limit of Stable Conveying in Suspension or Partially Suspended Flow, and the Selection of Relevant Input Parameters.

The question may be raised whether the variations observed in velocities at the pressure minimum, and in the limit of stable conveying in suspension or partially suspended flow, are of any importance or not. As mentioned in Section 2.4, some authors approximate the limit of stable conveying in suspension flow or partially suspended flow to a fixed value. If we look at the experimental observations of the limit of stable conveying in suspension flow, or partially suspended flow, for the materials that exhibit an unstable transition into plug flow, and for the materials that exhibit no low velocity conveying (polyethylene pellets, rape seed, sand, PVC granules and alumina), these limit values range from 6.3m/s to 16.3m/s (se Figures 8.9 to 8.13). The standard deviation of the observations is 2.0m/s and the average value is 9.7m/s. Judging from these statistical data it is apparent that the fixed limit value approximation is unjustified, and that the variations in the experimentally observed velocity limit are significant even for engineering purposes.

The approximation to a fixed velocity limit relies on the assumption that this limit does not change much with mass flow of solids. This is not the case. The effect is most dominant for alumina, for which the limit changes from 16m/s at the lowest observed feed rate, to below 10m/s for the highest observed feed rate. The approximation in question does not take into account any physical characteristics of the materials within this range of materials. Neither does it take into account the diameter effects that have frequently been reported in the literature.

It might be tempting to say that the physical characteristics of the material, such as particle size and particle density, "change much" whereas the conveying limit value does not, and therefore conclude that the limit value is not influenced by these characteristics. This would be a great simplification. Without having any knowledge about the model linking the input parameters (size, density etc.) to an output parameter, which in this case is either the limit of stable conveying in suspension flow or partially suspended flow, or the velocity at pressure minimum, it is impossible to say anything about which parameters influence the output values, and their importance. To do this one would have to be able to compare the variance of completely different sets of data. This would be like comparing the size variations for cats and dogs.

From an empirical point of view, what one has to ask oneself is whether it is of any interest to try to model the variations in the output values at all. If this is the case, and one decides to proceed with the empirical approach, the next step would be to select parameters to go into the model either from experience (dimensional analysis) or from analysis of the direction of maximum variance of the output data in a multidimensional parameter space (multi-variate analysis). The last option was investigated in the modelling carried out by Lia [65] on the superficial air velocity at pressure minimum at the beginning of the pipeline. His work identifies, as shown in Section 8.7, that among the parameters that were considered, the particle density and mean particle size are among the most important parameters for the prediction of the velocity at pressure minimum. The variance of these input parameters is then of no importance. It is the parameters that point out the direction of maximum variance for the output parameters that are of importance. These may, in a more general case, even be the ones having the lowest variance.

For the mechanistic model presented in Section 8.6 it is only the density of the suspension of particles and air towards the bottom of the pipeline close to blockage that is of any importance. The permeability and the apparent viscosity in different states of fluidisation is expected to enter the model when it is refined at a later stage, as a small correction factor. Again the variations in the input parameters necessary for the model are of no importance. The relevant parameters are in this case selected directly from the mechanistic description of the phenomenon.

9.5 The Physical Characteristics of the Materials in Relation to Observations of Blockage

Observations of blockage with and without a horizontal to horizontal bend were included to identify effects of this on the conveying limits for the various materials, since differences in behaviour might be expected for materials with different physical properties.

The observations of blockage described in Section 7.4 shows that blockages are initiated at the beginning of the straight horizontal pipeline for all material types included in the test program.

A set of three materials was selected for investigation in a pipeline with a bend. These were rape seed, PVC granules and micronized dolomite. Among these materials one case was found where the pipeline blocked at the bend. This was for rape seed at low feed rates. The investigation did not take into account the positioning of the bend, and only a horizontal to horizontal bend was investigated. For the case where the bend influence was detected, it only had a small influence on the conveying limit at the lowest solids feed rate.

From the model proposed in Section 8.6 and Equation 8.12 it is clear that the gravity will have a stabilising effect on the flow. An increased apparent gravity due to centripetal acceleration in the bend will therefore, in accordance with the mechanism proposed (also described in Section 9.2), increase the minimum conveying velocity. This is also what is observed. Experiments with pneumatic conveying at Lunar and Mars gravity have been carried out by Sullivan et.al. [69]. These show a reduction in the minimum conveying

velocity at Mars gravity that confirm the relation $v_{sg} \propto \sqrt{g}$ (The experiments at Lunar gravity were inhibited by severe bridging problems in the feeding hopper section.)

The reason why these experiments show no effect of the bend for the other two materials is not known. The experiments were carried out with the bend 15m from the feed section, and more dominant effects might have been detected had the bend been put closer to the feed section. With the bend at least 15m from the feed section the effect on the conveying limit is marginal, and only detectable for the coarsest material at low feed rates.

10. Conclusions

To improve the prediction of conveying limits on the basis of physical characteristics of particulate materials, which was the original objective of this investigation, it was found to be necessary to acquire a large set of data (the conveying characteristics and the characteristics of the particulate materials) to enable evaluation of existing models. This also allowed the evaluation of the new models that have been established.

Existing correlations for predicting the limit of stable conveying in suspension flow or partially suspended flow, as presented in Section 2.4.2, give poor reliability of the predictions even inside their claimed areas of validity. The errors shown in Table 6.2 vary from 116% over prediction to 77% under prediction of the limit of stable conveying. The model that is best suited for the prediction of this conveying limit is Pan's model which, with a safety factor of 31%, has been found not to give under prediction for any of the operating conditions.

Cabrejos' model is the only one for predicting pick up velocity. It has been evaluated together with the models for predicting the limit of stable conveying in suspension flow or partially suspended flow. The results show that Cabrejos' model under predicts this limit for all operating conditions (see Figures 6.2, 6.4, 6.6, 6.8, 6.9 and 6.10). This is in violation of Cabrejos' own description of the pick up velocity as a velocity above the saltation velocity. This concept is therefore not considered to be useful.

The models for predicting the velocity at minimum pressure loss give errors that vary from 111% over prediction to 85% under prediction (see Table 6.1). Matsumoto's model is the only one that does not considerably underpredict this velocity.

Part of the explanation of the poor performance of the existing models mentioned above can be found in the fact that the experimental data, on which the empirical fitting has been based, is limited to solids loading ratios below 5 for relevant pipeline sizes (see Table 2.2).

A simple model has been developed, based on the length of the mean free path for the particles in the suspension, for the prediction of whether single particle behaviour is dominant or not. As Table 2.1 shows, most industrial scale pneumatic transport systems

operate at conditions where single particle behaviour in the pipeline is not dominant. This may be yet another explanation as to why existing models, based on single particle behaviour, do not give reliable predictions of the conveying limit.

To evaluate the possibility of taking another approach towards understanding limitations in the conveying velocity in pneumatic transport systems, based on the collective behaviour rather than the single particle behaviour of the material, a set of wave propagation velocity measurements were carried out. The measurements, which were carried out on fluidized alumina, show that the propagation velocity is equal to that expected from fluid dynamic theory (Figure 8.1) in the large wavelength to bed depth region of the dispersion relation. This explains why the Froude number is relevant for the characterisation of two phase gas solids flow where a stratified flow occurs, since the Froude number characterises such flows. It also justifies applying fluid analogies to flow of fluidized powders.

Based on the fluid analogy, a model was developed (see Section 8.4) that predicts the maximum mass flow of solids in pneumatic conveying pipelines for the Geldart type B materials to within 9 %, and for the Geldart type D materials to within 36%. It is, in all cases, too conservative and can be used for design purposes as a worst case estimate. The model, due to the assumptions on which it is based, cannot be expected to predict the maximum flow of Geldart type A and C materials. The model is purely mechanistic and requires no empirical fitting.

The fluid analogy has also been applied to develop a model for the prediction of when blockage will occur in pneumatic conveying pipelines. The model is based on the assumption that Kelvin-Helmholz instabilities on the partially settled layer of solids close to blockage, contributes to re-suspend particles and thus to prevent blockage. The absence of such instabilities is used as a criterion to identify blockage conditions. The predictions of the model are surprisingly accurate considering that the model is purely mechanistic and does not require any empirical fitting (see Table 8.2). The model, presented in Section 8.6, is expected to give better predictions for fine materials than for coarse ones, because the effect of the permeability, as discussed in Section 9.2, has not been included. It is the first model of its kind that applies to fine powders. The model can probably even be improved further by including the effect of the viscosity of the fluidized powder.

In a collaborative project between the author at Telemark Industrial Research and Development Centre and P.E.Lia and Prof. K.H. Esbensen at Telemark College, a model, based on multivariate analysis, for predicting the pressure minimum velocity has been established (see Section 8.7) that has a root mean square error of prediction of ±1.2m/s on the average. The maximum error is -2.2m/s (or -15% of the measured value) and is obtained for PVC. The model must be validated with many more materials. It probably also needs to be expanded to include the effect of pipeline diameter.

Only marginal effects on the limit of stable conveying have been found after introducing a horizontal to horizontal bend. The bend was positioned after 15m of horizontal pipeline, as shown in Figure 3.4. The only material for which an effect was detected was rape seed. The rape seed data showed an increase in the limit of stable conveying in suspension flow at low feed rates (see Figure 5.8). More pronounced effects of the bend might have been detected had the bend been positioned closer to the feed section.

The models that were available before the completion of this work were based on an understanding of the behaviour of the single particle in the air flow. The experimental data on which they were based, also to a large extent reflects this, because only low solids loading ratios have been considered. By computing the mean free path of the particles and comparing it to the pipeline diameter it has been shown that this approach can be used only at very low solids loading ratios. Realising the shortcomings of the single particle approach, two new mechanistic models have been devised that rely on a fluid dynamic description of the flow. These models require no empirical fitting. No model has been found previously for predicting the maximum mass flow of solids for Geldart type B materials. The predictions of the model for predicting the limit of stable conveying are more accurate than any of those provided by previous models. This model also provides new fundamental understanding of what causes blockages in pneumatic conveying pipelines.

11. Suggestions for Further Work

During the course of finishing this research, several questions have occurred that have not been considered central to the theme of the thesis, and which therefore were not pursued any further. After finishing the current research project, even more questions remain unanswered. These open ends constitute the suggestions for further work. Each individual open end points in its own direction, and may require a separate investigation. Each suggestion is presented as a separate paragraph below.

It was identified in the literature survey that Matsumoto's model fits data well for low solids loading ratios. This model is based on a mechanistic modelling approach with empirical fitting of coefficients. Since it is clear that his model was based on data with very low solids loading ratios, there should be room for improvements of the model, by modifying the empirical fitting to include high solids loading data.

The model for the prediction of the mean free path for the particles in the suspension was based on monosized particles. This can be expanded to be valid for size distributions by introducing a formalism known from kinetic theory of gases, where a collision probability is used. This will then provide a clear definition of dilute and dense phase conveying, and will give information on when pneumatic transport systems operate at conditions where single particle behaviour in the pipeline is dominant, and when they do not.

The investigation of bend effects on the limit of stable conveying should only be considered as preliminary. An investigation of the importance of the distance from the feed section to a bend, or from one bend to another, has not been carried out. No investigation of horizontal to vertical or vertical to horizontal bends have been carried out either. Since a small effect of the bend was found for rape seed, this problem may be worthy of a deeper investigation, which would result in quantifiable guidelines for the positioning of the first bend in the pipeline, and for the minimum separation of subsequent bends.

The surface wave propagation velocity measurements that have been carried out have only included fluidized alumina. The experiments show that the propagation velocity is equal to

that expected from fluid dynamic theory (Figure 8.1), in the large wavelength to bed depth region of the dispersion relation, but this has not been verified for other materials. There is a need for a more thorough investigation of the wave propagation velocities of fluidized powders. This is an investigation of importance to the basic understanding of fluidized powders. No experimental investigations of dispersion relations for surface gravity waves on fluidized powders have been found in the literature. The wave tank that has been developed is also interesting in that it allows non-intrusive measurement of viscosity.

The model for prediction of when slugging will occur on the stratified layer of solids at the bottom of the pipeline, based on the Kelvin Helmholz instability, does not include the effect of the apparent viscosity, and the permeability, of the powder. When information about the viscosity of the powders exists, the model can be modified to include this effect. The inclusion of the effect of permeability probably requires a more basic remodelling, but could improve the model's performance for coarser materials.

The collaborative project between Telemark Industrial Research and Development Centre and Prof. K.H. Esbensen et. al. at the Telemark College, utilising multivariate analysis for predicting the pressure minimum velocity, will continue in the years to come. The plan is to establish a large data base of material characteristics and conveying data, that will improve the reliability and accuracy of the model.

References

1 E.Manger (1996), Modelling and Simulation of Gas-Solids Flow in Curvilinear Coordinates, Dr.Ing. Thesis at Telemark College.

2 F. Rizk (1991), Summary of the Minutes to the 1. Workshop-Meeting on Pneumatic Conveying, Karlsruhe

3 R.A.Bagnold (1941), The Physics of Blown Sand and Desert Dunes, Chapman and Hall, London

4 D.Kobayashi (1972), Studies of Snow Transport in Low Level Drifting Snow. Contrib. Inst. Low. Temp.Sci., Ser.A 24.

5 Y.Shao, M.R.Raupach and P.A.Findlater (1993), Effect of Saltation Bombardment on the Entrainment of Dust by Wind, Journal of Geophysical Research, Vol 98, No D7, 12719-12726.

6 F.A.Zenz (1964), Conveyability of Materials of Mixed Particle Size, Industrial and Engineering Chemistry / American Chemical Society 3, 65-75.

7 David G. Thomas (1962), Transport Characteristics of Suspensions: Part VI. Minimum Transport Velocity for Large Particle Size Suspensions in Round Horizontal Pipes, A.I.Ch.E.Journal 8, 373-378.

8 Donald A. McQuarrie (1976), Statistical Mechanics, Harper & Row, New York.

9 N.J.Mainwarning and A.R.Reed (1987), Permeability and Air Retention Characteristics of Bulk Solid Materials in Relation to Modes of Dense Phase Pneumatic Conveying, Bulk Solids Handling, Volume 7, Number 3, June.

10 I.D.Doig and G.H.Roper (1963), The Minimum Gas Rate for Dilute Phase Solids

Transportation in a Gas Stream, Australian Chemical Engineering 1, 9-19.

11 S. Matsumoto, M Hara, S Saito, S. Maeda (1974) Minimum Transport Velocity for Horizontal Pneumatic Conveying, Journal of Chemical Engineering of Japan 7, 425-430.

12 Francisco J. Cabrejos and George E. Klinzing (1992), Incipient Motion of Solid Particles in Horizontal Pneumatic Conveying, Powder Technology 72, 51-61.

13 B.Singh, T.G.Callocot and G.E.Rigby (1978), Flow of Fluidized Solids and Other Fluids in Open Channels, Powder Technology, 20, 99-113.

14 J.R.Grace (1970), The Viscosity of Fluidized Beds, The Canadian Journal of Chemical Engineering, Vol. 48, February.

15 Frank M. White (1988), Fluid Mechanics, McGraw-Hill International Edition.

16 K.E.Wirth (1980), Theoretische und Experimentelle Bestimmungen von Zusatzdruckverlust und Stopfgrenze bei Pneumaticher Strähnenförderung, Dr.Ing. Dissertation, Der Technishen Universität Erlangen-Nürenberg.

17 B.Mi and P.Wypych (1995), Investigation into Wall Pressure During Slug-Flow Pneumatic Conveying, Powder Technology, 84, 91-98.

18 H.E.Rose and R.A.Duckworth (1969) Transport of Solid Particles in Liquids and Gases, The Engineer 392-483.

19 F. Rizk (1976), Pneumatic Conveying at Optimal Conditions and a Solution of Barth's Equation, Pneumotransport 3 D4, 43-58.

20 F. Rizk (1982), Pneumatic Transport in Dilute and Dense Phase, Bulk Solids Handling 2.

21 Francisco J. Cabrejos and George E. Klinzing (1994), Pickup and Saltation Mechanisms of Solid Particles in Horizontal Pneumatic Transport, Powder Technology 79, 173-186.

22 R. Pan, B. Mi and P.W. Wypych (1994), Design of Pneumatic Conveying Systems for Granular Bulk Solids, Proceedings of International Conference on Advanced Technology and Equipment of Materials Handling. ATEMH'94, Shanghai, 815-820.

23 R.Pan, B. Mi and P.W.Wyppych (1994), Pneumatic Conveying Characteristics of Fine and Granular Bulk Solids, KONA no.12.

24 H.S.Muralidhara, W.J.Rebello, R.P.Krishnan and C.Y.Wen (1979), Saltation Velocity Correlations for the Design of Long Distance Horizontal Pneumatic Coal Transport Systems, Proceedings of the Technical Program, Int. Powd. and Bulk Solids Handling and Processing, Philadelphia, 327-338.

25 H.Arastoopour, M.V.Modi, D.V.Punwani and A.T.Talwalkar (1979), A Review of Design Equations for Dilute-Phase Gas-Solid Horizontal Conveying Systems for Coal and Related Materials, Proceedings of the Technical Program, Int. Powd. and Bulk Solids Handling and Processing, Philadelphia, 339-356.

26 P.C.Arnold, A.R.Reed and P.W.Wypych (1993), Advances in the Design of Pneumatic Transport Systems, Proceedings of the International Symposium Reliable Flow of Particulate Solids II, 451-478.

27 Sir Isaac Newton (1737), De Mundi Systemate, B.Motte and C.Bathurst.

28 Albert Einstein (1933), General Theory of Gravity, Glasgow.

29 K.Esbensen, S.Schönkopf and T.Midtgaard (1994), Multivariate Analysis in Practice, CAMO AS, Trondheim, Norway

30 M.G.Johnes and D.Mills (1990), Product Classification for Pneumatic Conveying, Powder Handling & Processing, Vol.2, No.2, 117-122.

31 Walter Barth (1963), Absetzung, Transport und Wiederaufwirbelung von Staubförmigem Gut im Luftstrom, Chemie-Ing.-Techn. 35, 209-214.

32 B.L.Hinkle (1953), Acceleration of Particles and Pressure Drops Encountered in Pneumatic Conveying, Ph.D. Thesis Georgia Institute of Technology.

33 R. Lilletvedt (1985), Optimal pneumatisk transport med hensyn på minimum hastighet, M.Sc.Thesis, The Norwegian Institute of Technology.

34 Beamex PCS 105 Calibrator, User Guide.

35 G.E.P.Box, W.G.Hunter, J.S.Hunter (1978), Statistics for Experimenters, John Wiley & Sons, Inc.

36 SURFER for Windows User Guide, Golden Software Inc., 809 14th Street, Golden, Colorado 80401 - 1860, USA.

37 Cressie, Statistics for Spatial Data, John Wiley and Sons, Inc., New York, 900pp.

38 D. Geldart (1973), Types of Gas Fluidization, Powder Technology 7, 285-292.

39 SEDIGRAPH 5100, User Manual

40 HELOS, User Manual,Sympatec GmbH, System-Partikel-Technik, Pracherstieg 1, D-38644 Goslar, Germany

41 P.Ibbotson, Fluidisation Testing, POSTEC, Internal Report.

42 G. Enstad, Lecture Notes, Telemark College.

43 P.W.Wypych, P.C.Arnold (1987), On Improving Scale-Up for Pneumatic Conveying Design, Powder Technology, 50, 281-294.

44 M.S.A.Bradley (1990), Prediction of Pressure Losses in Pneumatic Conveying Pipelines, Ph.D. Thesis, Thames Polytechnic.

45 D.Mills (1990), Pneumatic Conveying Design Guide, Butterworth, ISBN 0-408-04719-4

46 G.Dixon (1979), The Impact of Powder Properties on Dense Phase Flow, Int.Conf. on Pneumatic Conveying, 16-18 january, Cafe Royale, London.

47 N. Mainwaring (1989), The Effect of The Physical Properties of Bulk Solid Materials on Modes of Dense Phase Pneumatic Conveying, Ph.D. Thames Polytechnic.

48 M.G. Jones and D. Mills (1990), Product Classification for Pneumatic Conveying, Powder Handling and Processing 2, 117-122.

49 V.Yström (1995), Eksperimentell undersokelse av eksisterende modeller for dimensjonering av pneumatiske transportanlegg, med spesielt hensyn til partikkelhastighet og konsentrasjon ved grensen til pålitelig transport, M.Sc. Thesis, Telemark College.

50 M. Abramowitz and I. A. Stegun (1972), Handbook of Mathematical Functions, Dover Publications, New York.

51 H.L. Pécseli and J. Trulsen, (1991), Analytical Expressions for Conditional Averages: A Numerical Test., Physica Scripta. Vol 43, 503-507.

52 Joseph J.K. Ó Ruanaidh,William J. Fitzgerald (1996), Numerical Bayesian methods applied to signal processing, Springer, New York.

53 H.L. Pécseli and J. Trulsen, (1992) Personal Communication.

54 M.S.Beck and A.Plaskowski (1987), Cross Correlation Flowmeters: Their Design and Application, Adam Hilger, England.

55 J.S.M. Botterill and B.H. Abdul-Halim (1979), The Open Channel Flow of Fluidized Solids, Powder Technology, 23, 67-78.

56 Philip J. Lloyd and Peter J. Webb (1986), The Characterisation of Flow of Aerated Powders, Particle Characterisation, 3, 174-178.

57 J.Lighthill, Waves in Fluids, Cambridge University Press (1978).

58 E.S. Kordyban and T. Ranov (1970), Mechanism of Slug Formation in Horizontal Two-Phase Flow, Journal of Basic Engineering, 92, 857-864.

59 N.Andritsos, L. Williams and T.J. Hanratty (1989), Effect of Liquid Viscosity on The Stratified-Slug Transition in Horizontal Pipe Flow, Int. J. Multiphase Flow, Vol. 15, No. 6, pp. 877-892.

60 Dvora Barnea (1991), On The Effect of Viscosity on Stability of Stratified Gas-Liquid Flow-Application to Flow Pattern Transition at Various Pipe Inclinations, Chemical Engineering Science, Vol. 46, No. 8, pp. 2123-2131.

61 C.J. Crowley, G.B. Wallis and J.J. Barry (1992), Validation of a One Dimensional Wave Model for the Stratified-to-Slug Flow Regime Transition, with Consequences for Wave Growth and Slug Frequency, Int. J. Multiphase Flow, Vol. 18, No. 2, pp. 249-271.

62 K. Bendiksen and M. Espedal (1992), Onset of Slugging in Horizontal Gas-Liquid Pipe Flow, Int. J. Multiphase Flow, Vol. 18, No. 2, pp. 237-247.

63 Dvora Barnea and Yehuda Taitel (1991), Transient-Formulation Modes and Stability of Steady-State Annular Flow, Chemical Engineering Science, Vol. 44, No. 2, pp. 325-332.

64 J.S.Mason, D.Mills, A.R.Reed and C.R.Woodcock (1986), Intensive Short Course Pneumatic Handling of Bulk Materials, Thames Polytechnic (University of Greenwich), London.

65 K.E.Wirth and O.Molerus (1981), Prediction of Pressure Drop in Horizontal Segregated Pneumatic Conveying with Particle Strands Sliding along Bottom of the Pipe, German Chemical Engineering, Vol 4, No5, 278-284.

66 F.J.Cabrejos and G.E.Klinzing (1995), Characterisation of Dilute Gas-Solids Flow Using the Rescaled Range Analysis, Powder Technology, No 84, 139-156.

67 K.E.Wirth and O.Molerus (1985), The Influence of Pipeline Geometry on the Critical Velocity of Horizontal Pneumatic Conveying of Coarse Particles, Powder Technology, No 42, 27-34.

68 P.E.Lia (1996), Modellering av pneumatisk transport i uttynna tilstand ved hjelp av multivariabel dataanalyse - prediksjon av minimum transportluftmengde, M.Sc. Thesis, Telemark College.

69 T.A.Sullivan, E.Koenig, C.W.Knudsen and M.A.Gibson (1992) , Pneumatic Conveying of Materials at Reduced Gravity, Powder Handling and Processing, Volume 4, Number 2, 173-178.

APPENDIX A. DERIVATION OF THE KELVIN HELMHOLZ INSTABILITY.

Starting with the integral relations for conservation of mass and momentum one has:

$$\frac{d}{dt}\left(\iiint_{CV}\rho dV\right)+\iint_{CS}(\rho\vec{v}_r\cdot\vec{n})dA=0 \tag{A.1}$$

$$\sum\vec{F}=\frac{d}{dt}\left(\iiint_{CV}\vec{v}\rho dV\right)+\iint\vec{v}\rho(\vec{v}\cdot\vec{n})dA \tag{A.2}$$

The basic assumptions that shall be used throughout the derivation of the stability criterion are inviscid flow, no surface tension and incompressible flow.

For an infinitesimally thin control volume covering the cross section of the pipeline this gives:

$$\frac{\partial}{\partial t}(\rho A dx)+\frac{\partial}{\partial x}(\rho v A)dx=0 \tag{A.3}$$

$$-\left(\rho Ag\frac{\partial h}{\partial x}+A\frac{\partial p}{\partial x}\right)dx=\frac{\partial}{\partial t}(v\rho A dx)+\frac{\partial}{\partial x}\left(\rho v^2 A\right)dx \tag{A.4}$$

Which will be valid for each of the two phases. This gives the following equations for conservation of mass and momentum for the two phases together.

$$\frac{\partial}{\partial t}(\rho_L A_L)+\frac{\partial}{\partial x}(\rho_L v_L A_L)=0 \tag{A.5}$$

$$\frac{\partial}{\partial t}(\rho_g A_g)+\frac{\partial}{\partial x}(\rho_g v_g A_g)=0 \tag{A.6}$$

$$-\rho_L A_L g\frac{\partial h}{\partial x}-A_L\frac{\partial p}{\partial x}=\frac{\partial}{\partial t}(v_L\rho_L A_L)+\frac{\partial}{\partial x}\left(v_L^2\rho_L A_L\right) \tag{A.7}$$

$$-\rho_g A_g g\frac{\partial h}{\partial x}-A_g\frac{\partial p}{\partial x}=\frac{\partial}{\partial t}(v_g\rho_g A_g)+\frac{\partial}{\partial x}\left(v_g^2\rho_g A_g\right) \tag{A.8}$$

The pressure in the two momentum conservation equations can be eliminated because the assumption of no surface tension implies that the pressure is continuous across the surface interface.

$$\begin{aligned}&\frac{1}{A_g}\frac{\partial}{\partial t}\left(v_g\rho_g A_g\right)+\frac{1}{A_g}\frac{\partial}{\partial x}\left(v_g^2\rho_g A_g\right)+\rho_g g\frac{\partial h}{\partial x}=\\&\frac{1}{A_L}\frac{\partial}{\partial t}\left(v_L\rho_L A_L\right)+\frac{1}{A_L}\frac{\partial}{\partial x}\left(v_L^2\rho_L A_L\right)+\rho_L g\frac{\partial h}{\partial x}\end{aligned} \tag{A.9}$$

The assumption of incompressible flow now gives:

$$\frac{\partial A_L}{\partial t}+v_L\frac{\partial A_L}{\partial x}+A_L\frac{\partial v_L}{\partial x}=0 \tag{A.10}$$

$$\frac{\partial A_g}{\partial t}+v_g\frac{\partial A_g}{\partial x}+A_g\frac{\partial v_g}{\partial x}=0 \tag{A.11}$$

$$\begin{aligned}&\rho_g\frac{\partial v_g}{\partial t}+\frac{1}{A_g}\rho_g v_g\frac{\partial A_g}{\partial t}+\frac{1}{A_g}v_g^2\rho_g\frac{\partial A_g}{\partial x}+2v_g\rho_g\frac{\partial v_g}{\partial x}+\rho_g g\frac{\partial h}{\partial x}=\\&\rho_L\frac{\partial v_L}{\partial t}+\frac{1}{A_L}\rho_L v_L\frac{\partial A_L}{\partial t}+\frac{1}{A_L}v_L^2\rho_L\frac{\partial A_L}{\partial x}+2v_L\rho_L\frac{\partial v_L}{\partial x}+\rho_L g\frac{\partial h}{\partial x}\end{aligned} \tag{A.12}$$

Substituting the spatial derivative of the velocities from the mass conservation equations and defining $A_L'=\frac{dA_L}{dh_L}$ gives:

$$\begin{aligned}&\rho_g\frac{\partial v_g}{\partial t}-\frac{\rho_g v_g}{A_g}\frac{\partial A_g}{\partial t}-\frac{v_g^2\rho_g}{A_g}\frac{\partial A_g}{\partial x}+\frac{\rho_g g}{A_L'}\frac{\partial A_L}{\partial x}=\\&\rho_L\frac{\partial v_L}{\partial t}-\frac{\rho_L v_L}{A_L}\frac{\partial A_L}{\partial t}-\frac{v_L^2\rho_L}{A_L}\frac{\partial A_L}{\partial x}+\frac{\rho_L g}{A_L'}\frac{\partial A_L}{\partial x}\end{aligned} \tag{A.13}$$

The negative part of the expression above can be recognised as the spatial derivative of the gas and liquid velocity from the conservation equations for mass. This gives the following expression:

$$\begin{aligned}&\rho_g\frac{\partial v_g}{\partial t}+v_g\rho_g\frac{\partial v_g}{\partial x}+\frac{\rho_g g}{A_L'}\frac{\partial A_L}{\partial x}=\\&\rho_L\frac{\partial v_L}{\partial t}+v_L\rho_L\frac{\partial v_L}{\partial x}+\frac{\rho_L g}{A_L'}\frac{\partial A_L}{\partial x}\end{aligned} \tag{A.14}$$

Linearisation using the relations $A_L = \overline{A}_L + \widetilde{A}_L$, $v_L = \overline{v}_L + \widetilde{v}_L$, $v_g = \overline{v}_g + \widetilde{v}_g$, where overbar indicates a constant value and tilde a small perturbation, and ignoring the multiples of first order values gives the new set of equations:

$$\frac{\partial \widetilde{A}_L}{\partial t} + \overline{v}_L \frac{\partial \widetilde{A}_L}{\partial x} + \overline{A}_L \frac{\partial \widetilde{v}_L}{\partial x} = 0 \tag{A.15}$$

$$\frac{\partial \widetilde{A}_g}{\partial t} + \overline{v}_g \frac{\partial \widetilde{A}_g}{\partial x} + \overline{A}_g \frac{\partial \widetilde{v}_g}{\partial x} = 0 \tag{A.16}$$

$$\begin{aligned} &\rho_g \frac{\partial \widetilde{v}_g}{\partial t} + \overline{v}_g \rho_g \frac{\partial \widetilde{v}_g}{\partial x} + \frac{\rho_g g}{A_L'} \frac{\partial \widetilde{A}_L}{\partial x} = \\ &\rho_L \frac{\partial \widetilde{v}_L}{\partial t} + \overline{v}_L \rho_L \frac{\partial \widetilde{v}_L}{\partial x} + \frac{\rho_L g}{A_L'} \frac{\partial \widetilde{A}_L}{\partial x} \end{aligned} \tag{A.17}$$

For simplicity, we shall continue by omitting the overbar indicators for constant values. An expression only depending on the cross section area occupied by the liquid can now be found by taking the partial spatial derivative of the equation for conservation of momentum and substituting into it the second order derivatives of velocity from the convective temporal derivatives of the equations for conservation of mass.

$$\frac{\partial^2 \widetilde{A}_L}{\partial t^2} + v_L \frac{\partial^2 \widetilde{A}_L}{\partial x \partial t} + A_L \frac{\partial^2 \widetilde{v}_L}{\partial x \partial t} + v_L \frac{\partial^2 \widetilde{A}_L}{\partial t \partial x} + v_L^2 \frac{\partial^2 \widetilde{A}_L}{\partial x^2} + v_L A_L \frac{\partial^2 \widetilde{v}_L}{\partial x^2} = 0 \tag{A.18}$$

$$\frac{\partial^2 \widetilde{A}_g}{\partial t^2} + v_g \frac{\partial^2 \widetilde{A}_g}{\partial x \partial t} + A_g \frac{\partial^2 \widetilde{v}_g}{\partial x \partial t} + v_g \frac{\partial^2 \widetilde{A}_g}{\partial t \partial x} + v_g^2 \frac{\partial^2 \widetilde{A}_g}{\partial x^2} + v_g A_g \frac{\partial^2 \widetilde{v}_g}{\partial x^2} = 0 \tag{A.19}$$

$$\begin{aligned} &\rho_g \frac{\partial^2 \widetilde{v}_g}{\partial t \partial x} + v_g \rho_g \frac{\partial^2 \widetilde{v}_g}{\partial x^2} + \frac{\rho_g g}{A_L'} \frac{\partial^2 \widetilde{A}_L}{\partial x^2} = \\ &\rho_L \frac{\partial^2 \widetilde{v}_L}{\partial t \partial x} + v_L \rho_L \frac{\partial^2 \widetilde{v}_L}{\partial x^2} + \frac{\rho_L g}{A_L'} \frac{\partial^2 \widetilde{A}_L}{\partial x^2} \end{aligned} \tag{A.20}$$

This gives the following equation:

$$\left(\frac{\rho_L v_L^2}{A_L}+\frac{\rho_g v_g^2}{A_g}-\frac{g}{A_L'}\left(\rho_L-\rho_g\right)\right)\frac{\partial^2 \tilde{A}_L}{\partial x^2}+$$
$$2\left(\frac{\rho_L v_L}{A_L}+\frac{\rho_g v_g}{A_g}\right)\frac{\partial^2 \tilde{A}_L}{\partial t \partial x}+ \qquad (A.21)$$
$$\left(\frac{\rho_L}{A_L}+\frac{\rho_g}{A_g}\right)\frac{\partial^2 \tilde{A}_L}{\partial t^2}=0$$

A dispersion relation for an infinitesimally small surface perturbation can now be found by assuming the perturbation is sinusoidal and substituting it into the equation above.

$\tilde{A}_L = \alpha e^{i(kx-\omega t)}$ where α is a small unspecified cross section area value

This now gives:

$$\left(\frac{\rho_L}{A_L}+\frac{\rho_g}{A_g}\right)\omega^2-$$
$$2\left(\frac{\rho_L v_L}{A_L}+\frac{\rho_g v_g}{A_g}\right)\omega k+ \qquad (A.22)$$
$$\left(\frac{\rho_L v_L^2}{A_L}+\frac{\rho_g v_g^2}{A_g}-\frac{g}{A_L'}\left(\rho_L-\rho_g\right)\right)k^2=0$$

By multiplying through with A and defining $\rho=\rho_g A/A_g+\rho_L A/A_L$ we get:

$$\omega^2-$$
$$\frac{2}{\rho}\left(\frac{\rho_L v_L}{R_L}+\frac{\rho_g v_g}{R_g}\right)\omega k+ \qquad (A.23)$$
$$\frac{1}{\rho}\left(\frac{\rho_L v_L^2}{R_L}+\frac{\rho_g v_g^2}{R_g}-\frac{gA}{A_L'}\left(\rho_L-\rho_g\right)\right)k^2=0$$

Where $R_L=A_L/A$ and $R_g=A_g/A$. The stability of a surface perturbation can be decided by solving Equation A.23 which is of second order in ω, and by looking at the imaginary part

of the solution. When this is negative, the perturbation will grow causing instability. This means that for an instability to occur we must have:

$$\frac{1}{\rho^2}\left(\frac{\rho_L v_L}{R_L}+\frac{\rho_g v_g}{R_g}\right)^2 < \frac{1}{\rho}\left(\frac{\rho_L v_L^2}{R_L}+\frac{\rho_g v_g^2}{R_g}-\frac{gA}{A_L'}\left(\rho_L-\rho_g\right)\right) \Leftrightarrow$$

$$\left(\frac{\rho_L}{\rho R_L}-\frac{\rho_L^2}{\rho^2 R_L^2}\right)v_L^2-2\frac{\rho_g\rho_L v_g v_L}{\rho^2 R_g R_L}+\left(\frac{\rho_g}{\rho R_g}-\frac{\rho_g^2}{\rho^2 R_g^2}\right)v_g^2 > \frac{gA}{\rho A_L'}\left(\rho_L-\rho_g\right) \tag{A.24}$$

And since we have $\rho=\rho_g/R_g+\rho_L/R_L$ which means that:

$$\frac{\rho_g}{\rho R_g}-\frac{\rho_g^2}{\rho^2 R_g^2}=\frac{1}{\rho^2}\left(\frac{\rho R_g\rho_g-\rho_g^2}{R_g^2}\right)=\frac{1}{\rho^2}\left(\frac{\left(\frac{\rho_g}{R_g}+\frac{\rho_L}{R_L}\right)R_g\rho_g-\rho_g^2}{R_g^2}\right)= \tag{A.25}$$

$$\frac{1}{\rho^2}\left(\frac{\rho_g^2}{R_g^2}+\frac{\rho_L\rho_g}{R_g R_L}-\frac{\rho_g^2}{R_g^2}\right)=\frac{\rho_L\rho_g}{\rho^2 R_g R_L}$$

and likewise for the similar liquid density part of the expression. The instability criterion can thereby be simplified to:

$$\frac{\rho_g\rho_L}{R_g R_L}\left(v_g-v_L\right)^2 > \frac{\rho gA}{A_L'}\left(\rho_L-\rho_g\right) \tag{A.26}$$

Marginal instability occurs when:

$$\frac{A_L'\left(v_g-v_L\right)^2}{Ag}=\frac{\left(R_g\rho_L+R_L\rho_g\right)\cdot\left(\rho_L-\rho_g\right)}{\rho_g\rho_L} \tag{A.27}$$

APPENDIX B. RESULTS OF CHARACTERISATION OF THE MATERIALS INCLUDED IN THE TESTWORK

APPENDIX B.1 Size Distributions

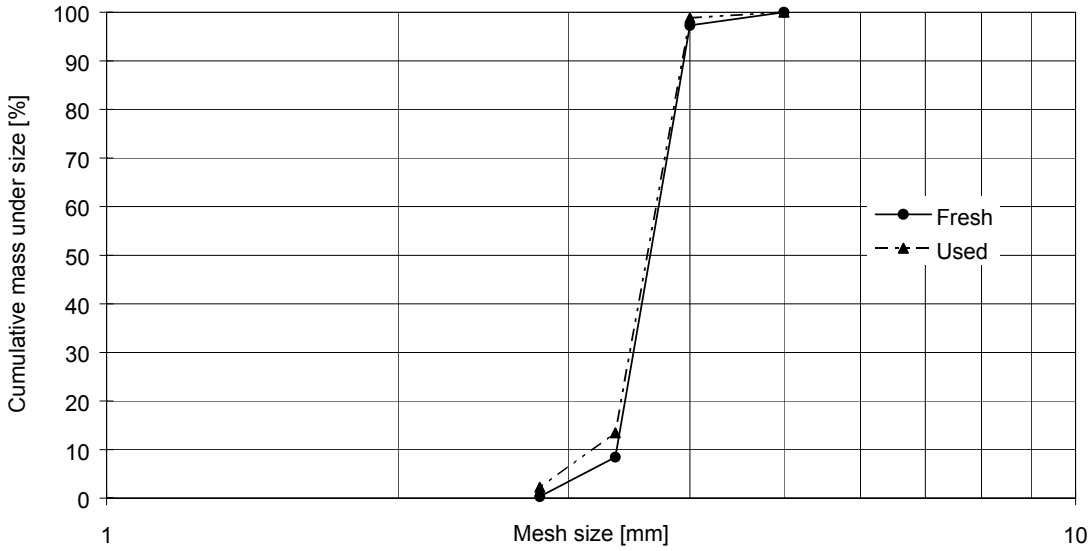

Figure B.1 Size distribution of polyethylene pellets samples taken before starting and after finishing the conveying tests

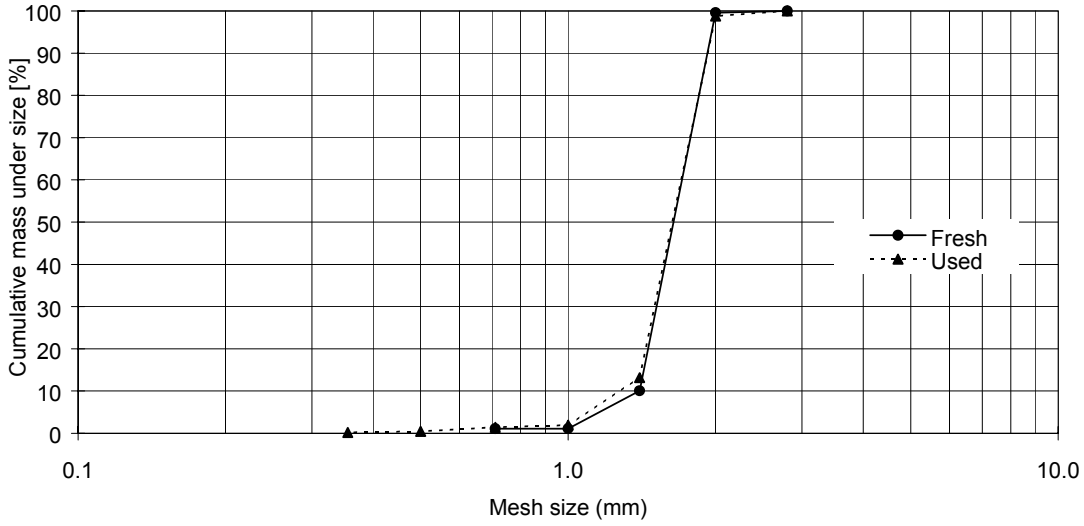

Figure B.2 Size distribution of rape seed samples taken before starting and after finishing the conveying tests

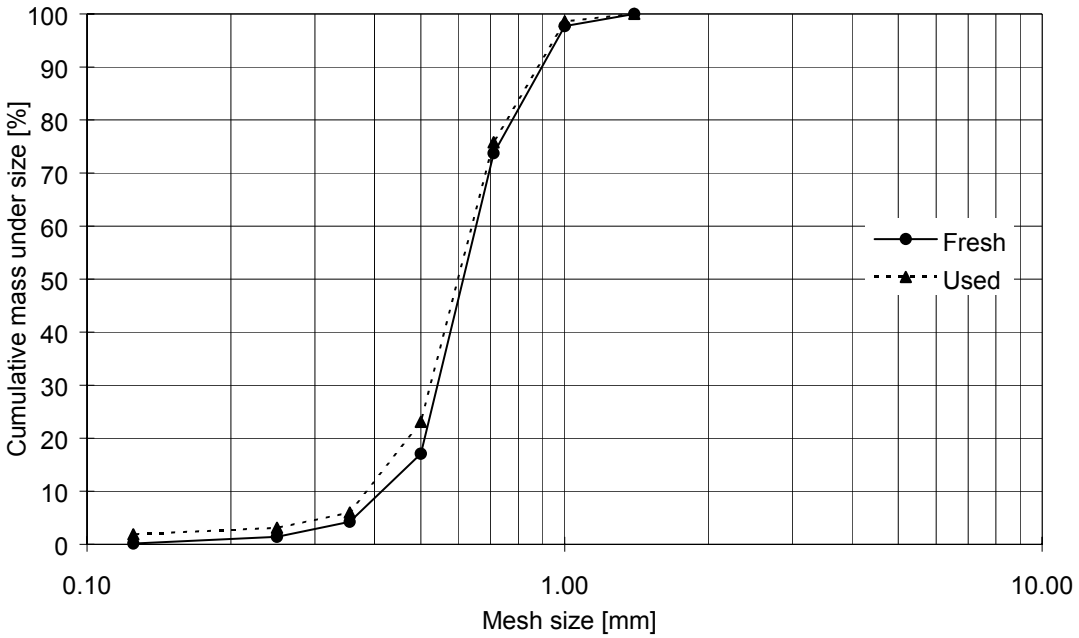

Figure B.3 Size distribution of Leighton Buzzard sand samples taken before starting and after finishing the conveying tests

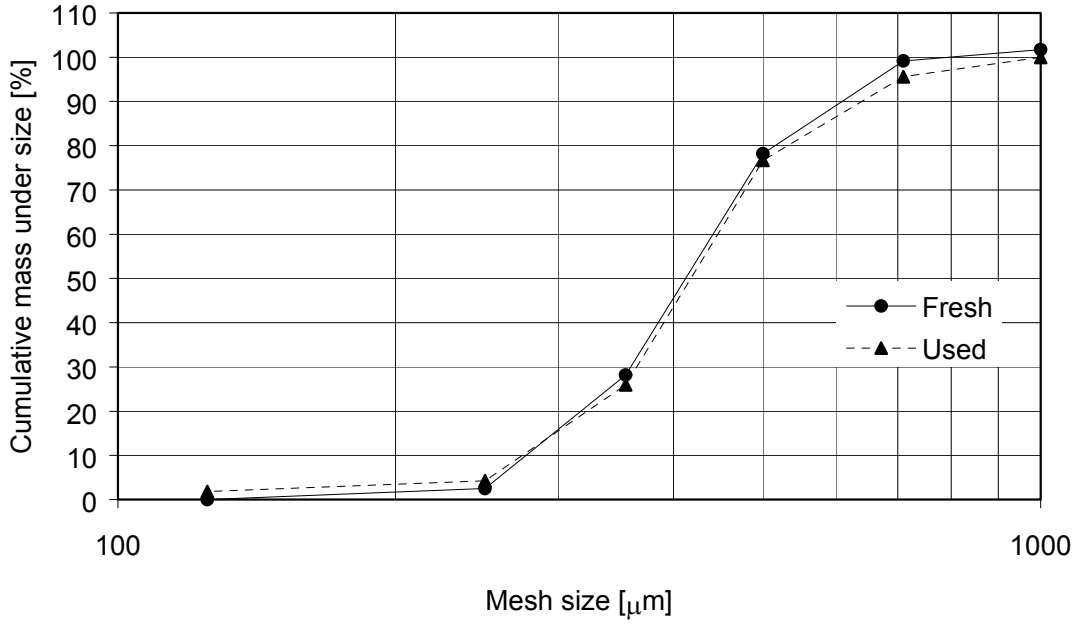

Figure B.4 Size distribution of PVC granules samples taken before starting and after finishing the conveying tests

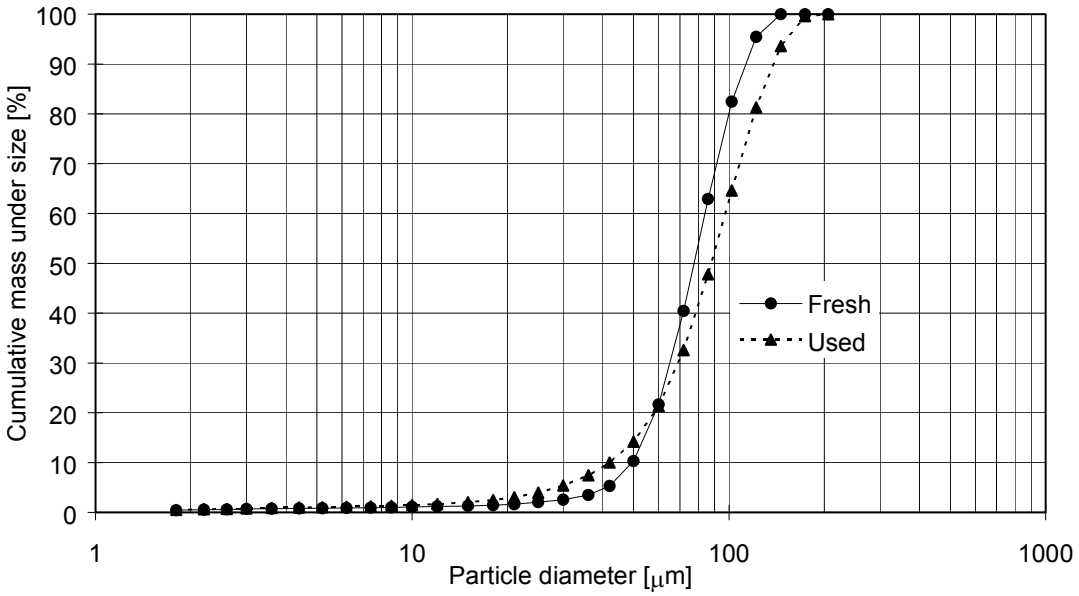

Figure B.5 Size distribution of aluminium oxide samples taken before starting and after finishing the conveying tests

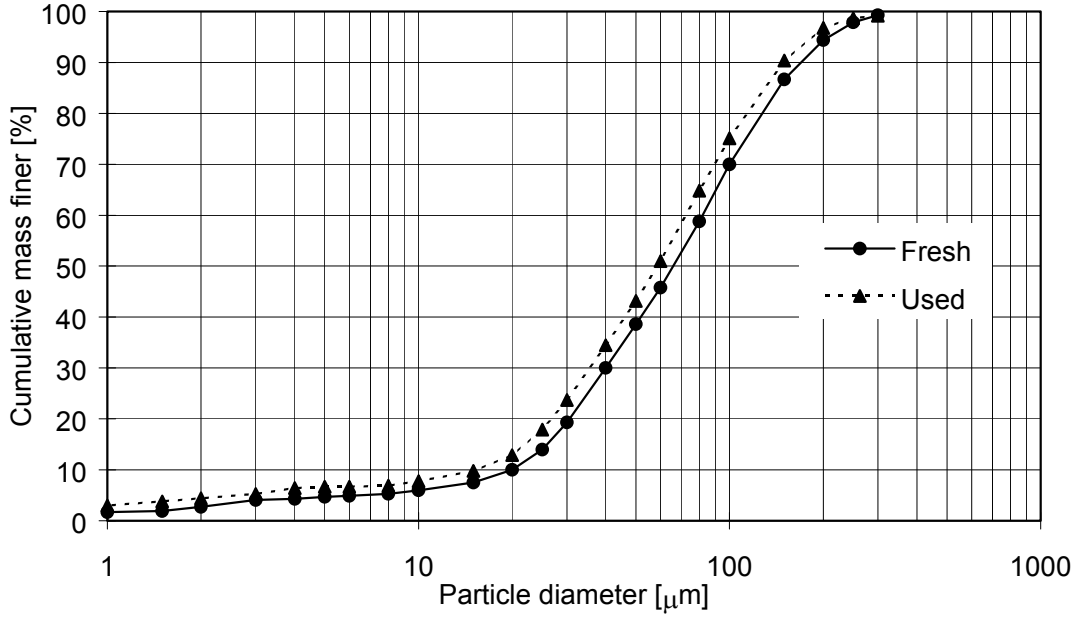

Figure B.6 Size distribution of micronized dolomite samples taken before starting and after finishing the conveying tests

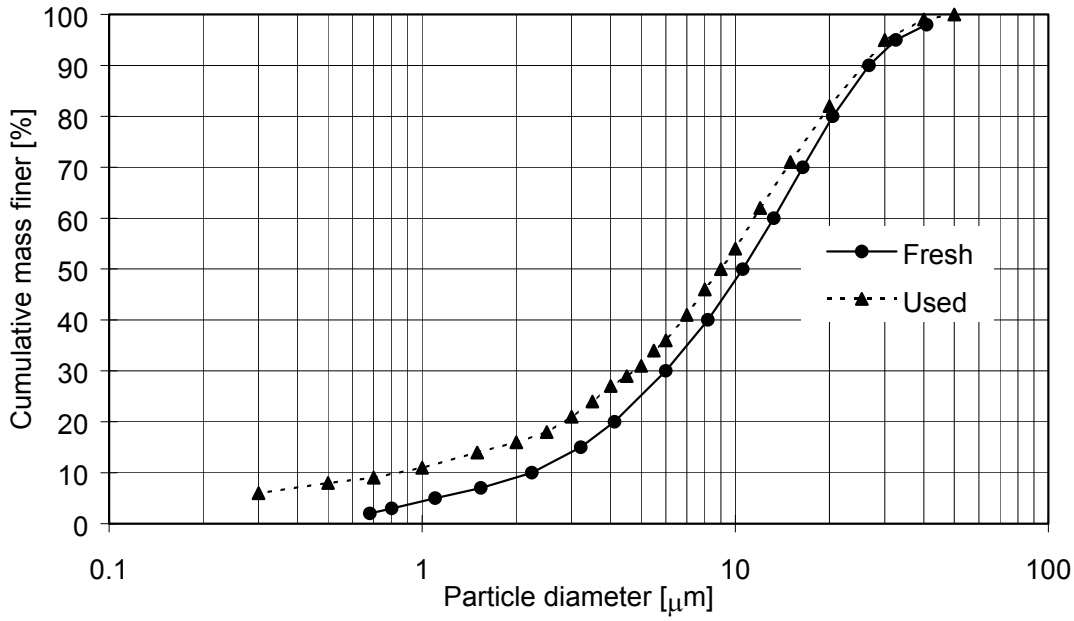

Figure B.7 Size distribution of cement samples taken before starting and after finishing the conveying tests

APPENDIX B.2 Fluidisation Characteristics

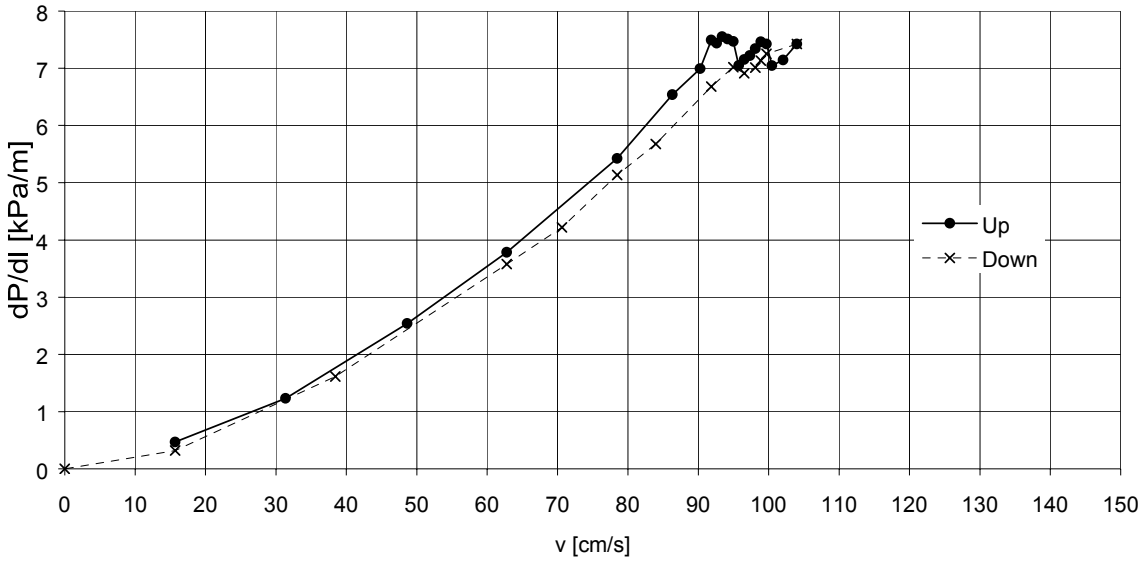

Figure B.8 Fluidization characteristics for polyethylene pellets.

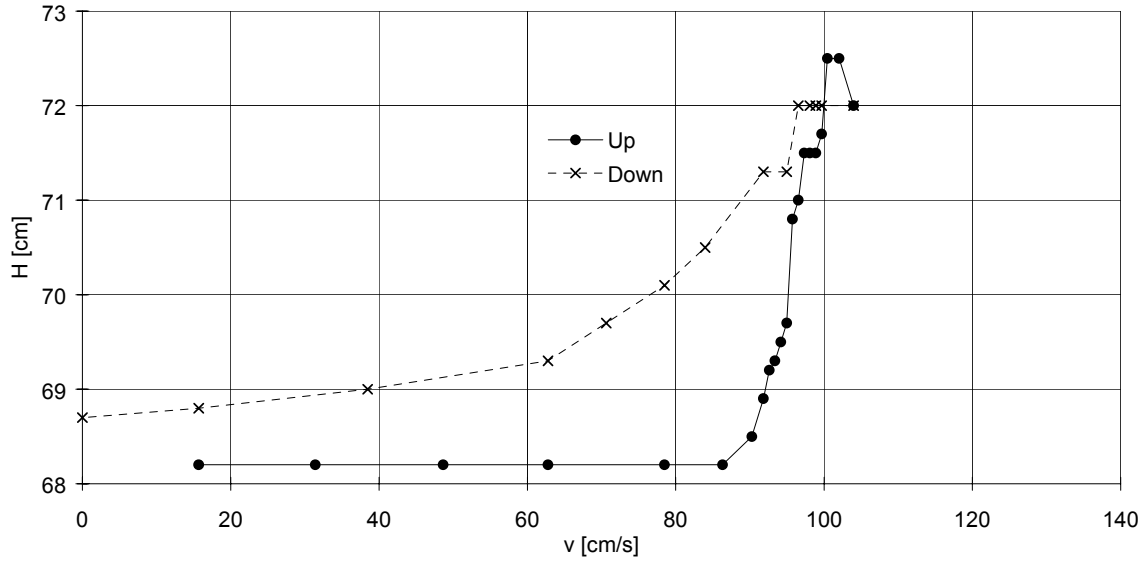

Figure B.9 Bed expansion for polyethylene pellets.

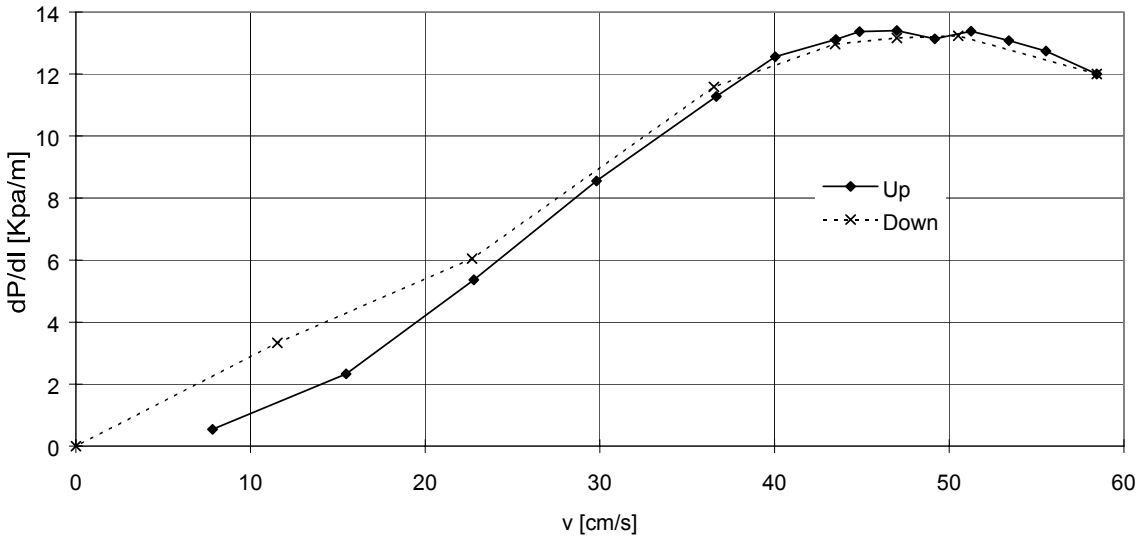

Figure B.10 Fluidization characteristics for rape seed.

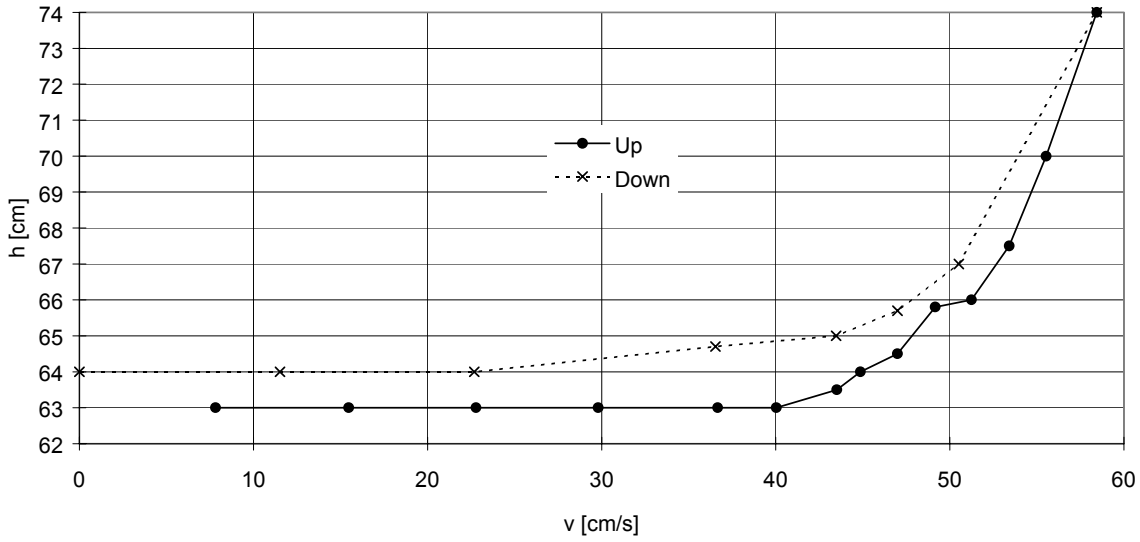

Figure B.11 Bed expansion for rape seed.

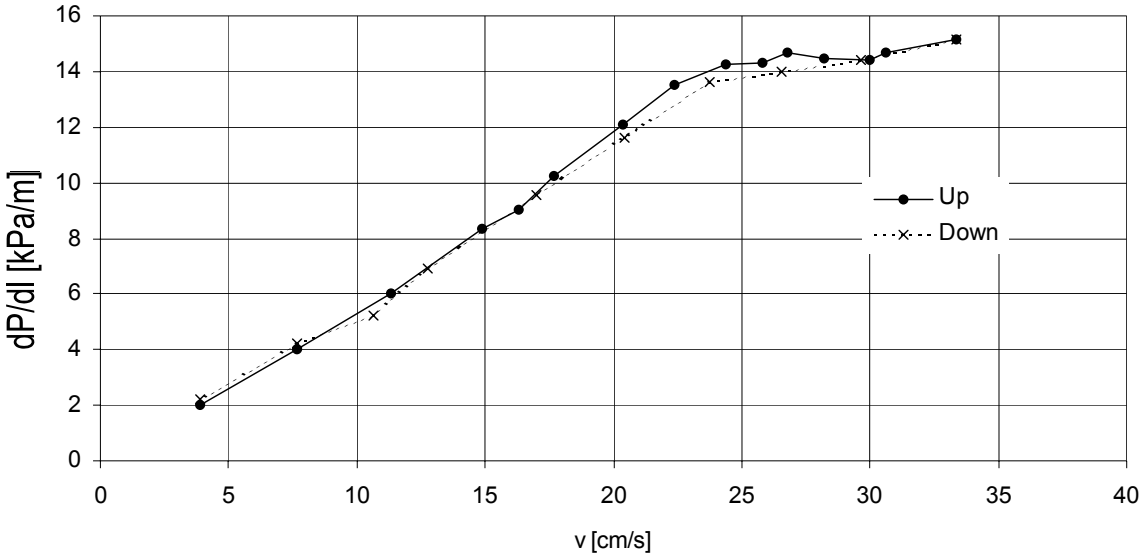

Figure B.12 Fluidization characteristics for sand.

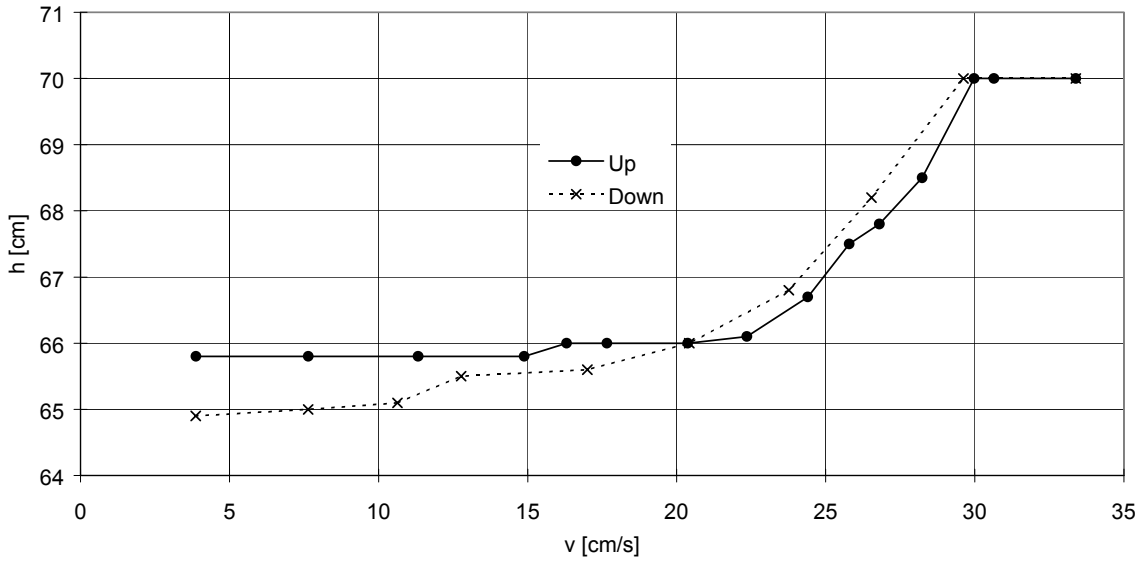

Figure B.13 Bed expansion for sand.

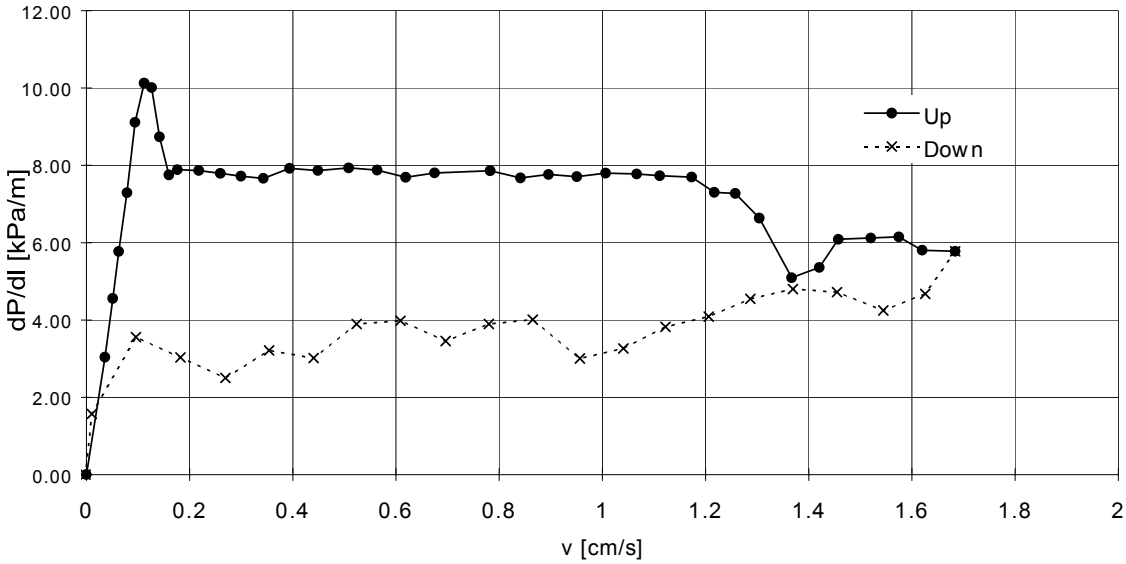

Figure B.14 Fluidization characteristics for PVC granules.

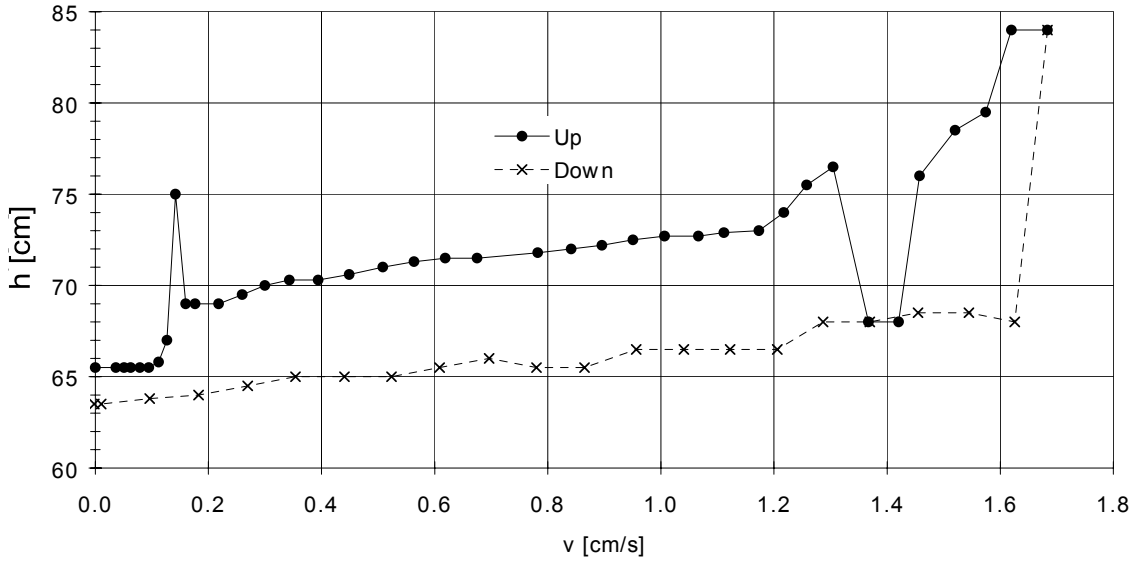

Figure B.15 Bed expansion for PVC granules.

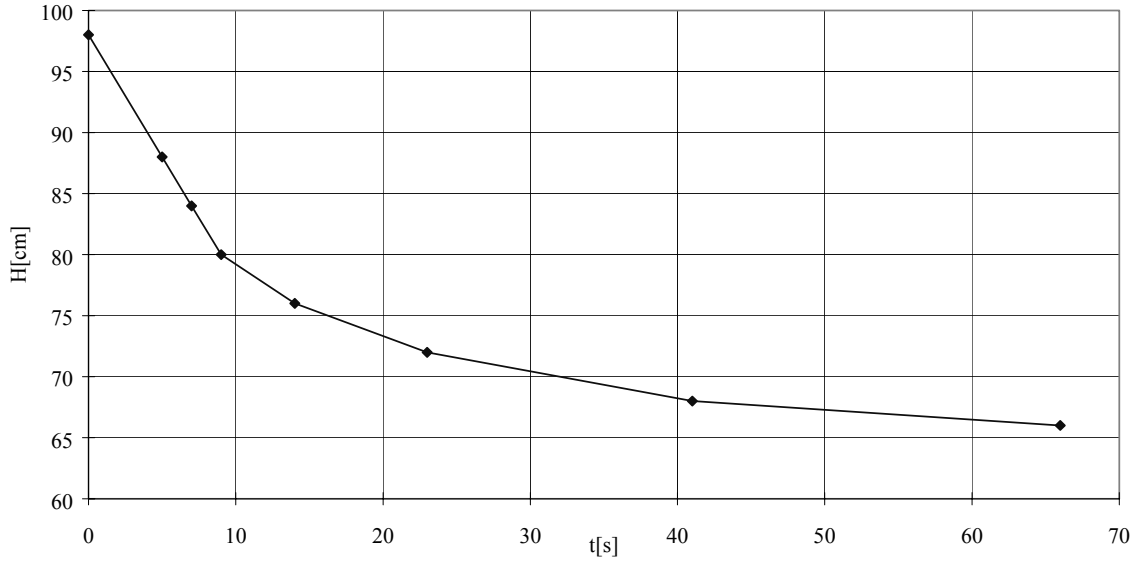

Figure B.16 Deaeration for PVC granules.

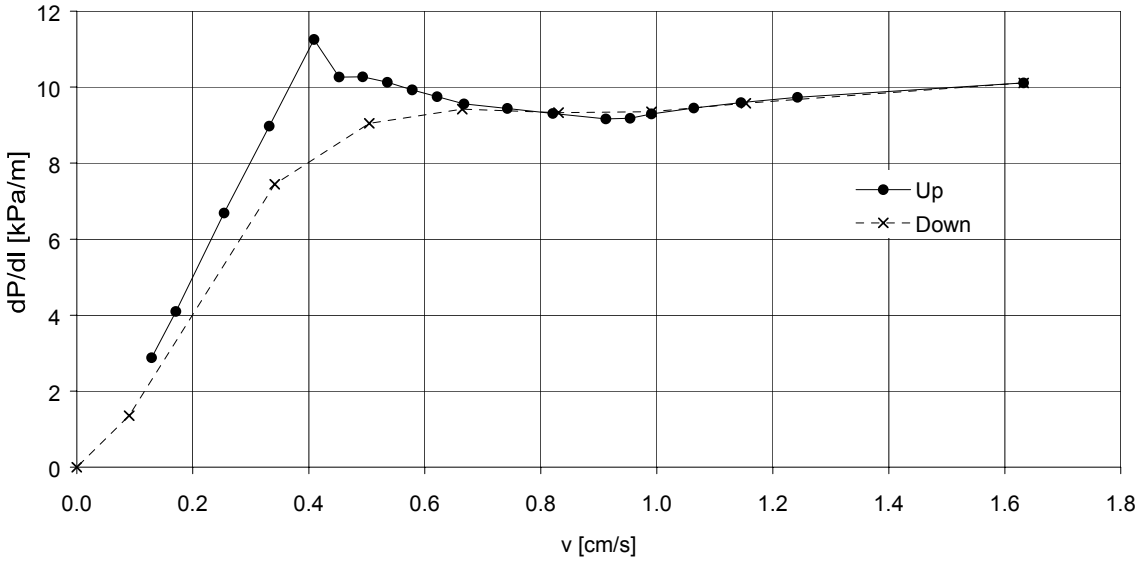

Figure B.17 Fluidization characteristics for alumina.

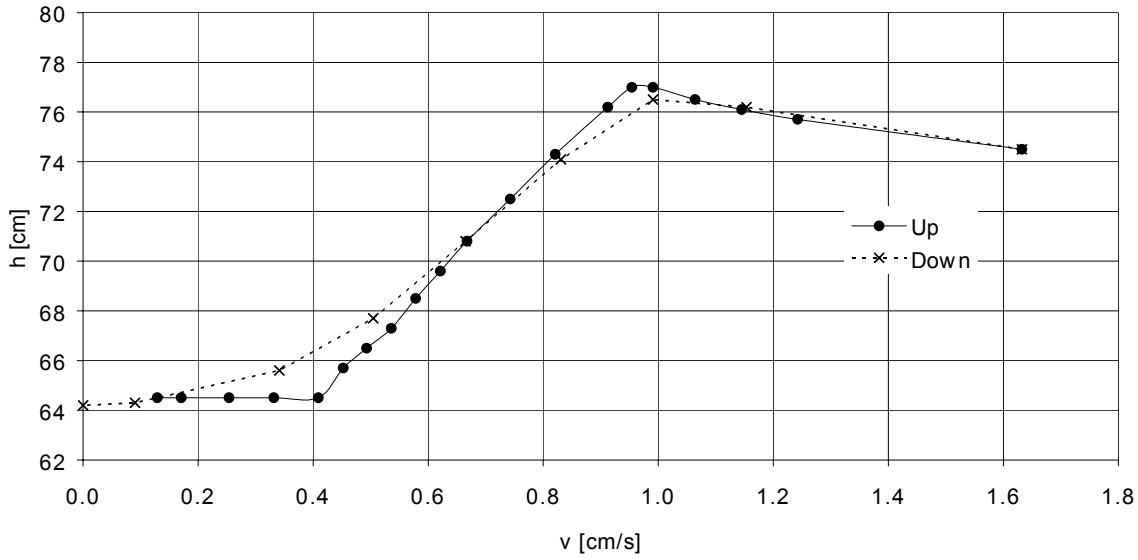

Figure B.18 Bed expansion for alumina.

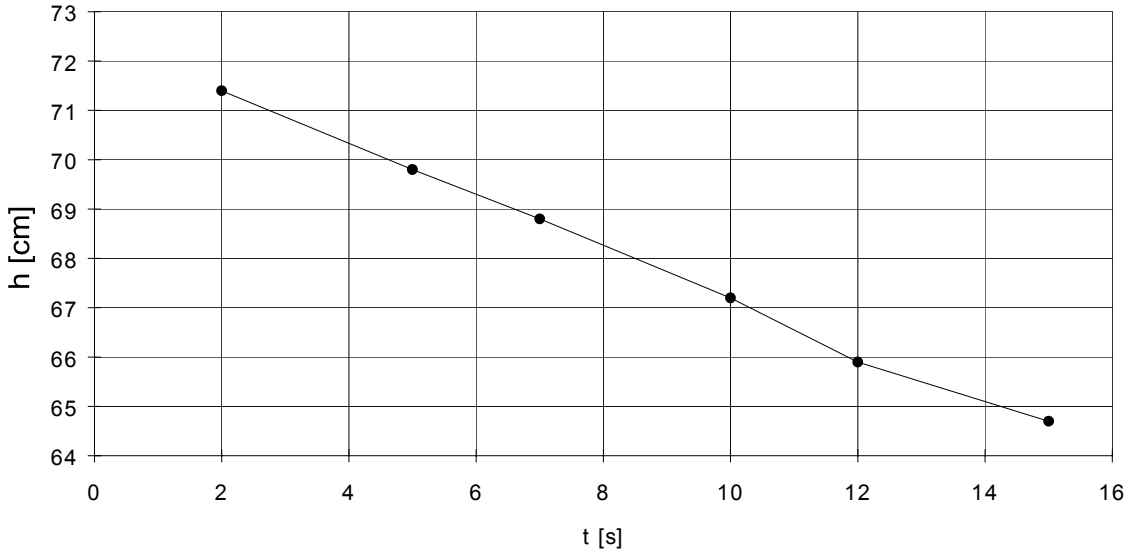

Figure B.19 Deaeration for alumina.

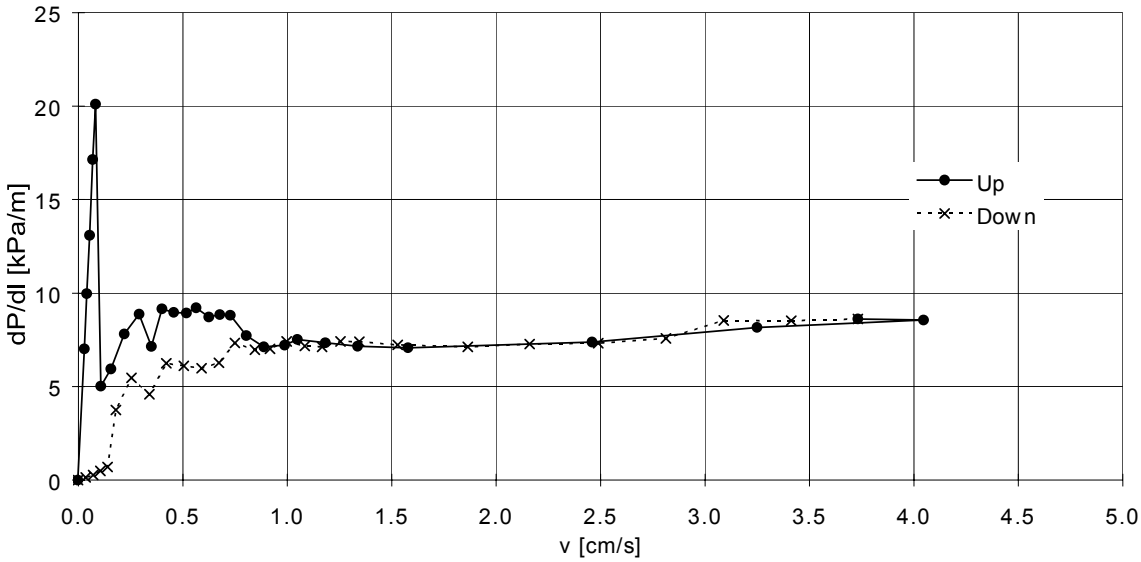

Figure B.20 Fluidization characteristics for micronized dolomite.

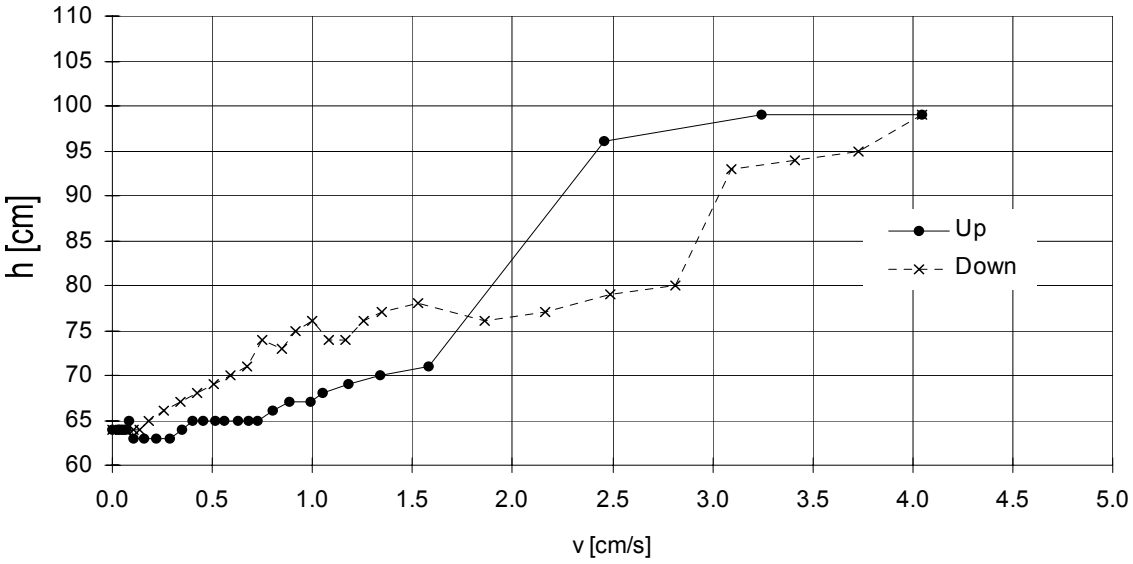

Figure B.21 Bed expansion for micronized dolomite.

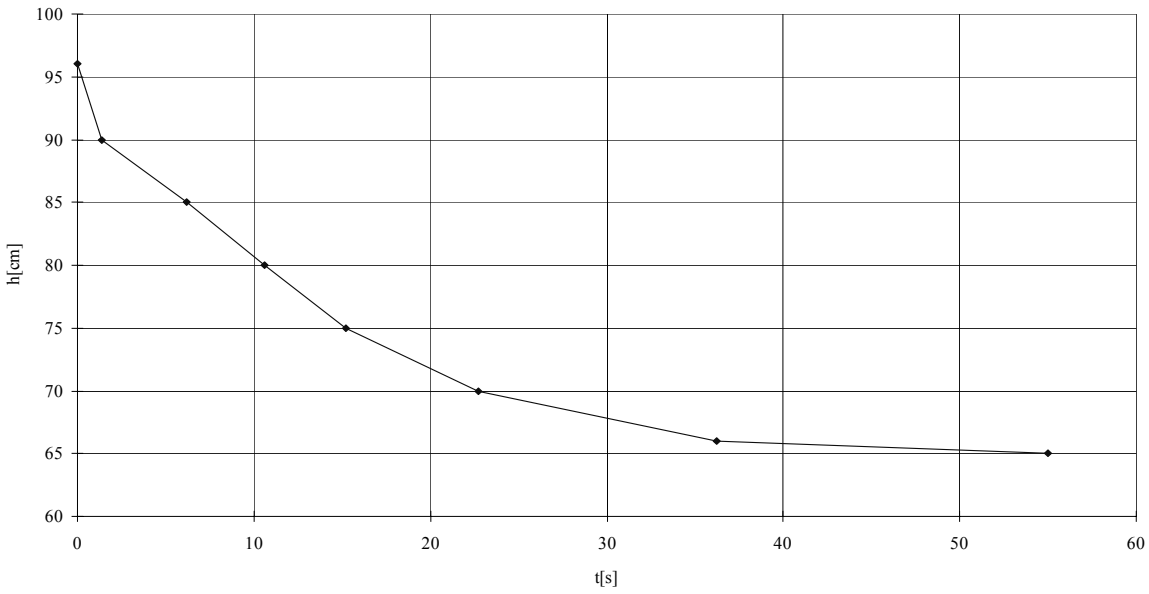

Figure B.22 Deaeration for micronized dolomite

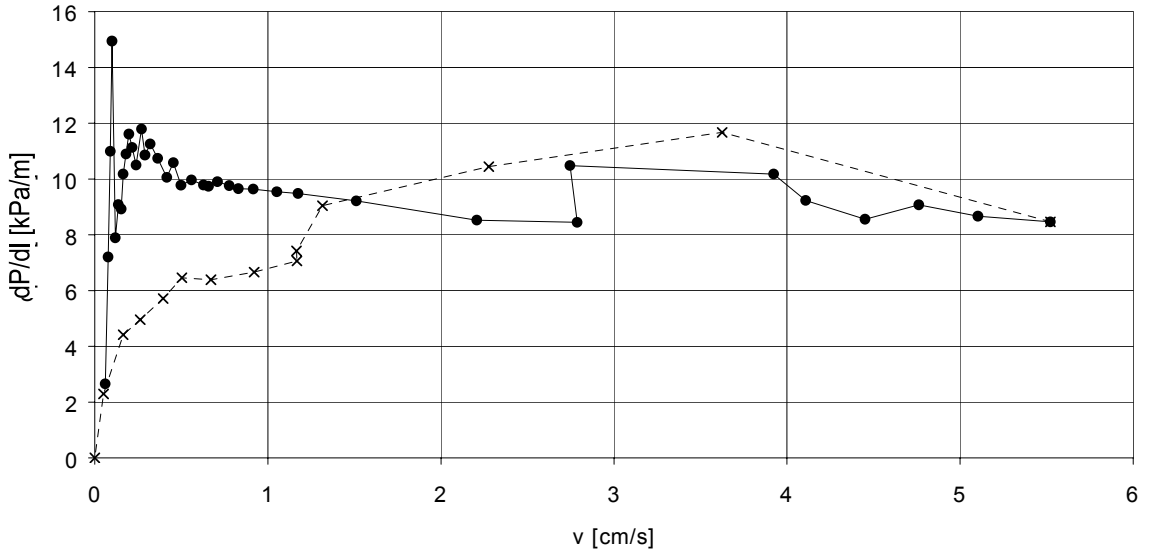

Figure B.23 Fluidization characteristics for cement.

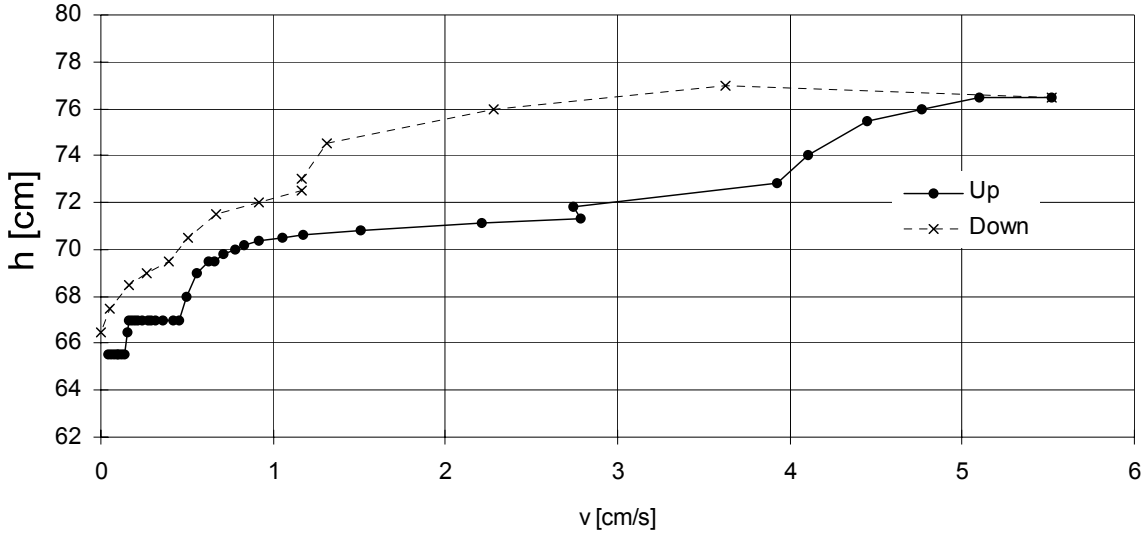

Figure B.24 Bed expansion for cement.

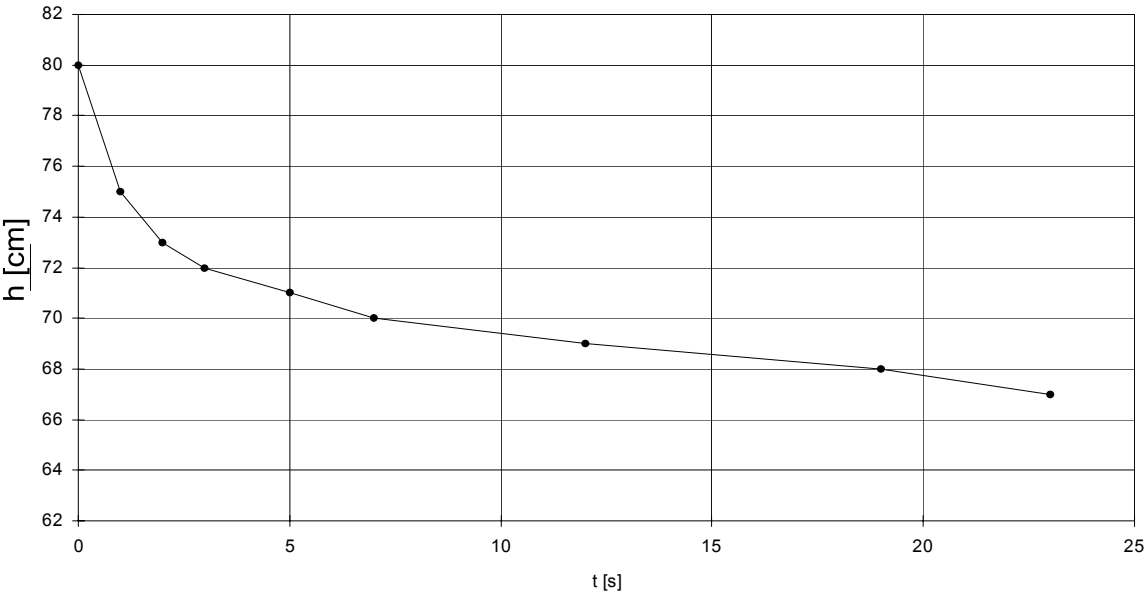

Figure B.25 Deaeration for cement

APPENDIX C. CONVEYING CHARACTERISTICS

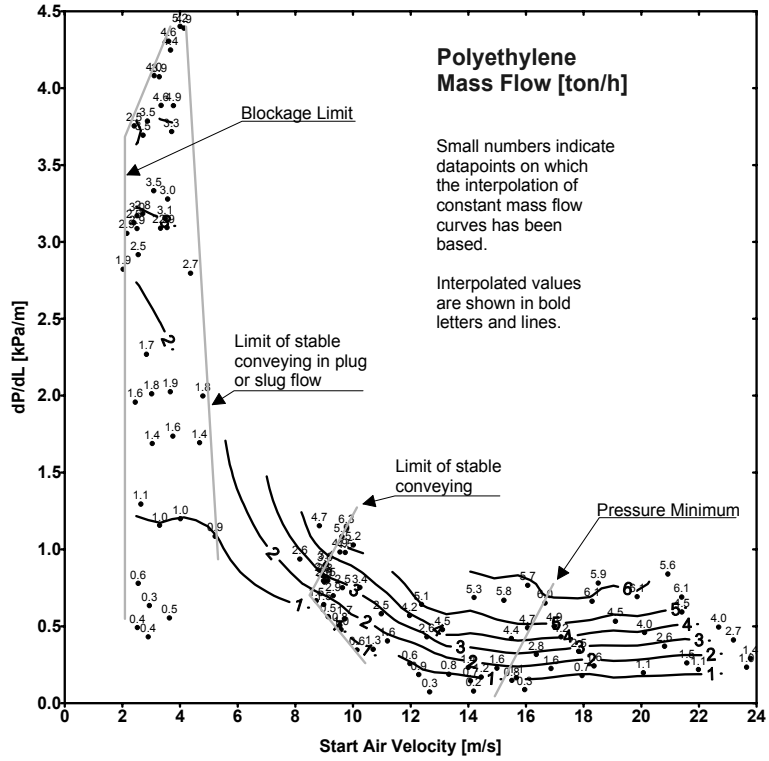

Figure C.1 Conveying characteristic for polyethylene pellets (mass flow of solids).

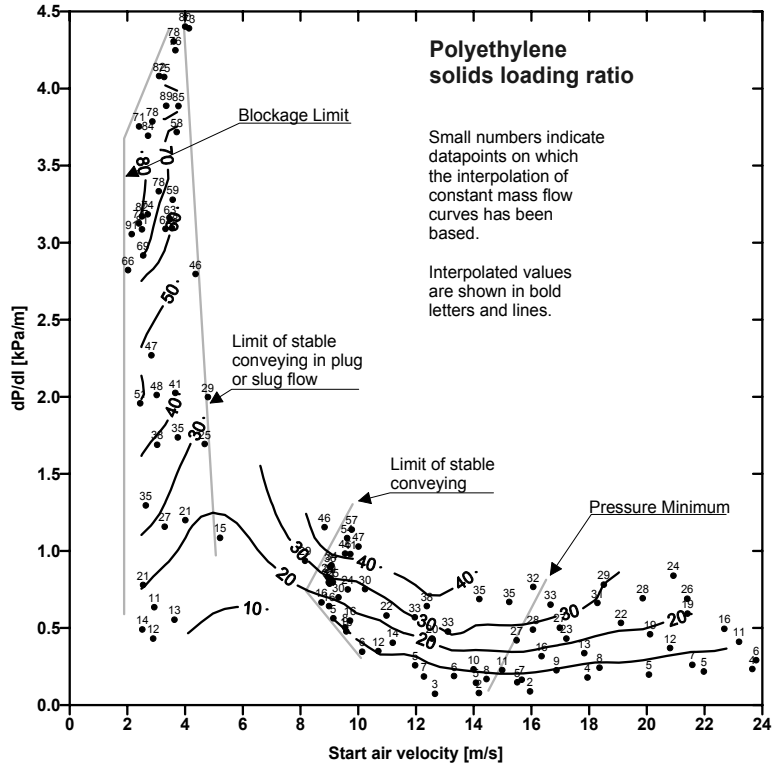

Figure C.1 Conveying characteristic for polyethylene pellets (solids loading ratio).

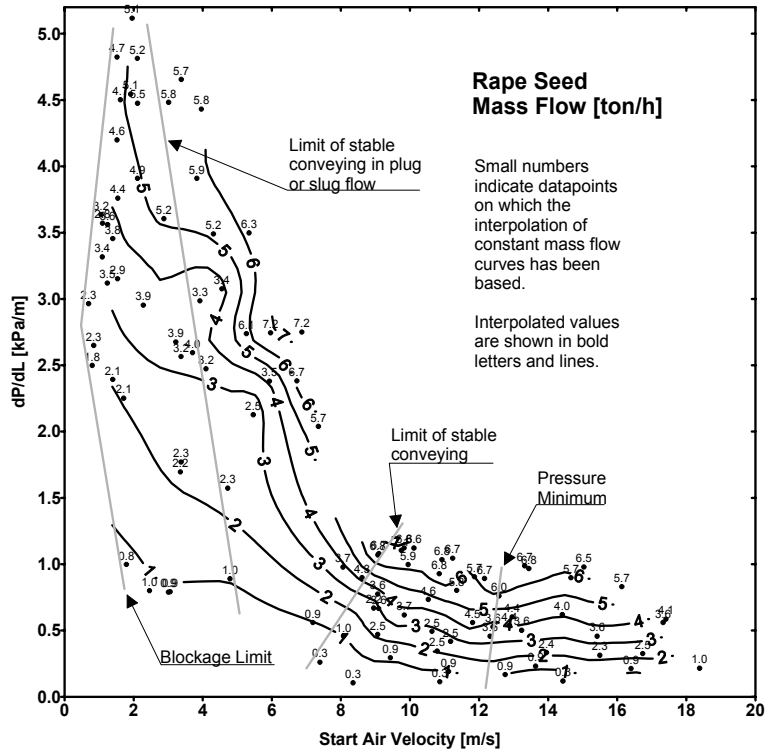

Figure C.2 Conveying characteristic for rape seed (mass flow of solids).

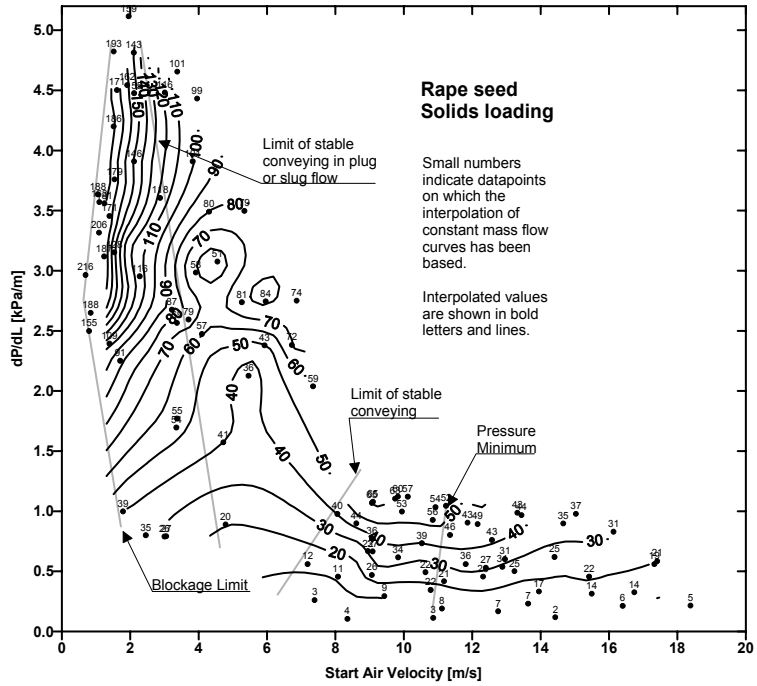

Figure C.3 Conveying characteristic for rape seed (solids loading ratio).

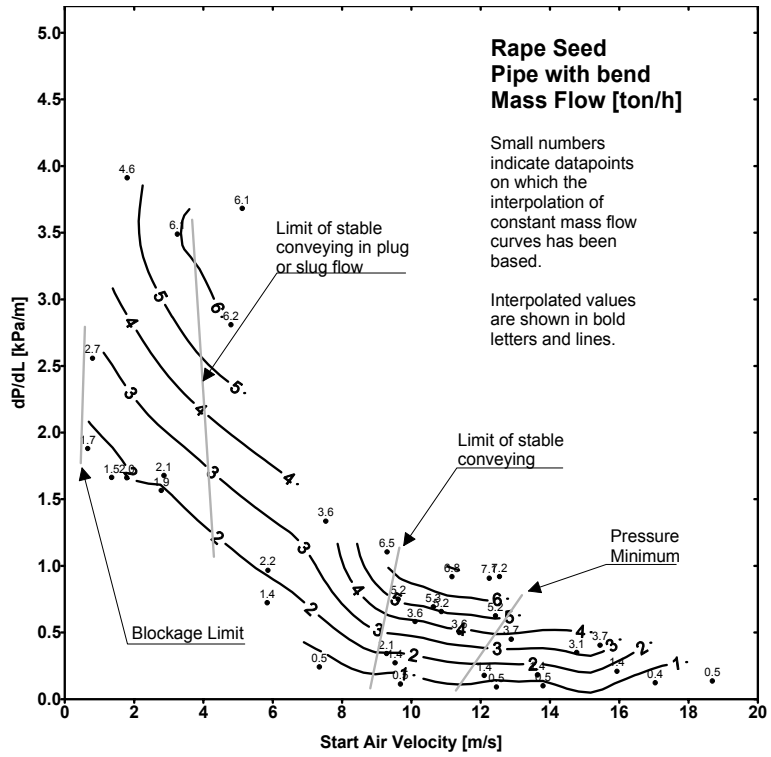

Figure C.4 Conveying characteristic for rape seed with horizontal to horizontal bend (mass flow of solids).

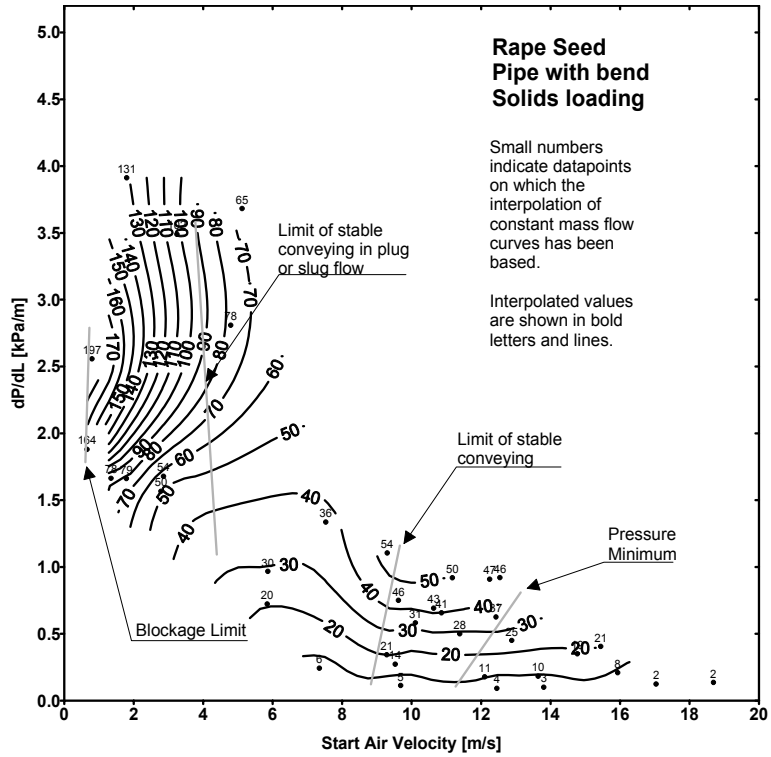

Figure C.5 Conveying characteristic for rape seed with horizontal to horizontal bend (solids loading ratio).

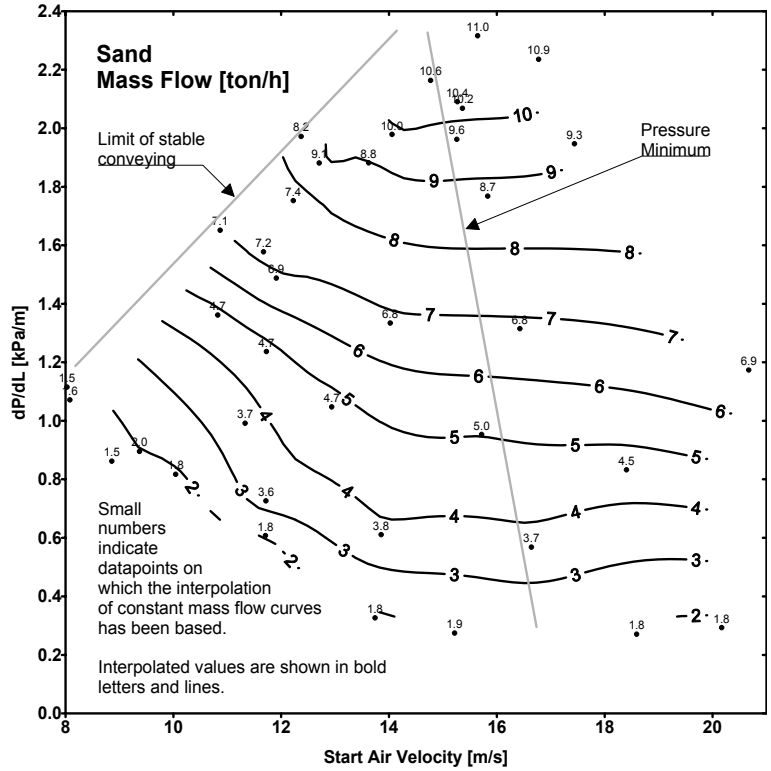

Figure C.6 Conveying characteristic for sand (mass flow of solids).

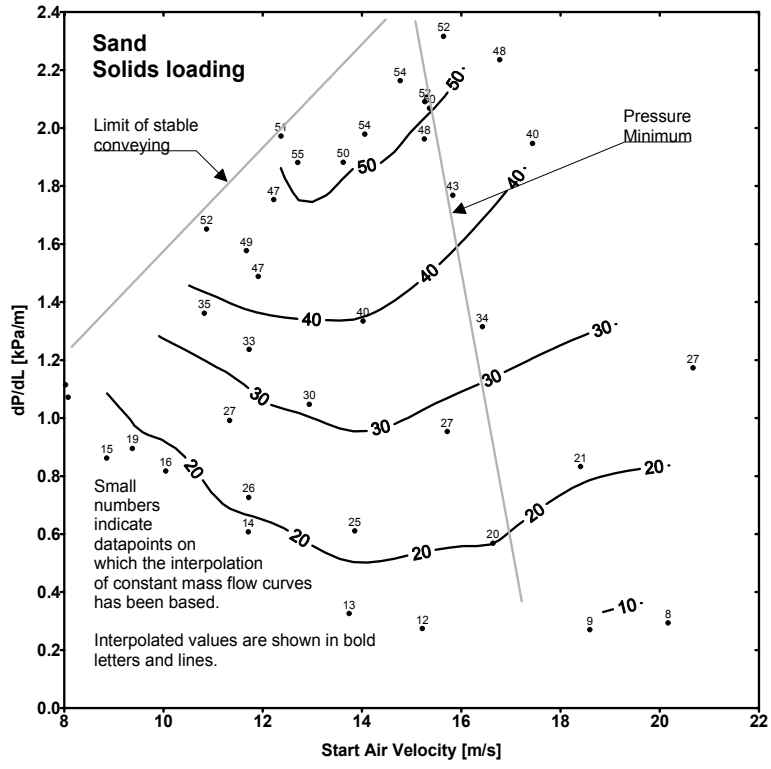

Figure C.7 Conveying characteristic for sand (solids loading ratio).

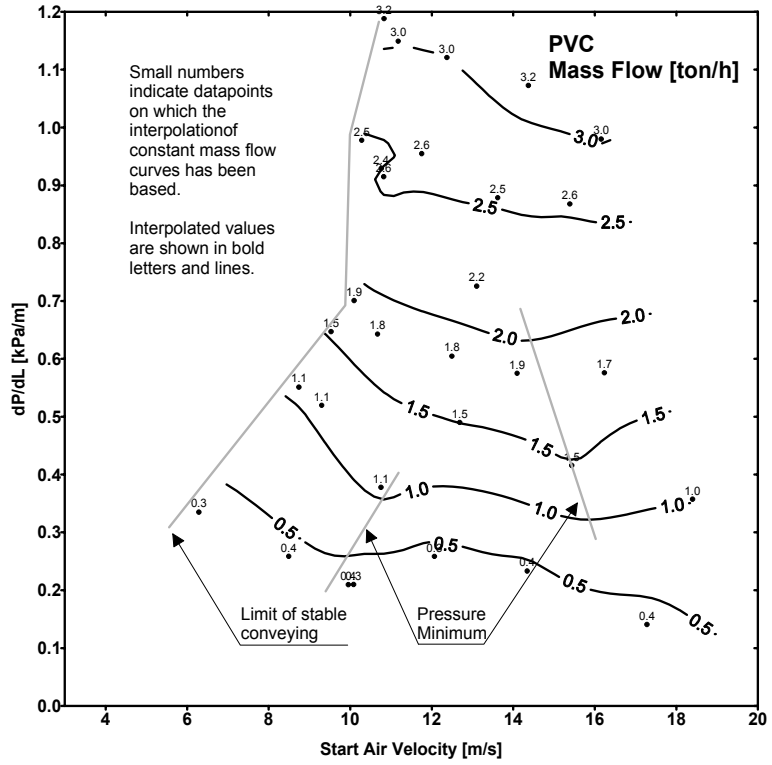

Figure C.8 Conveying characteristic for PVC granules (mass flow of solids).

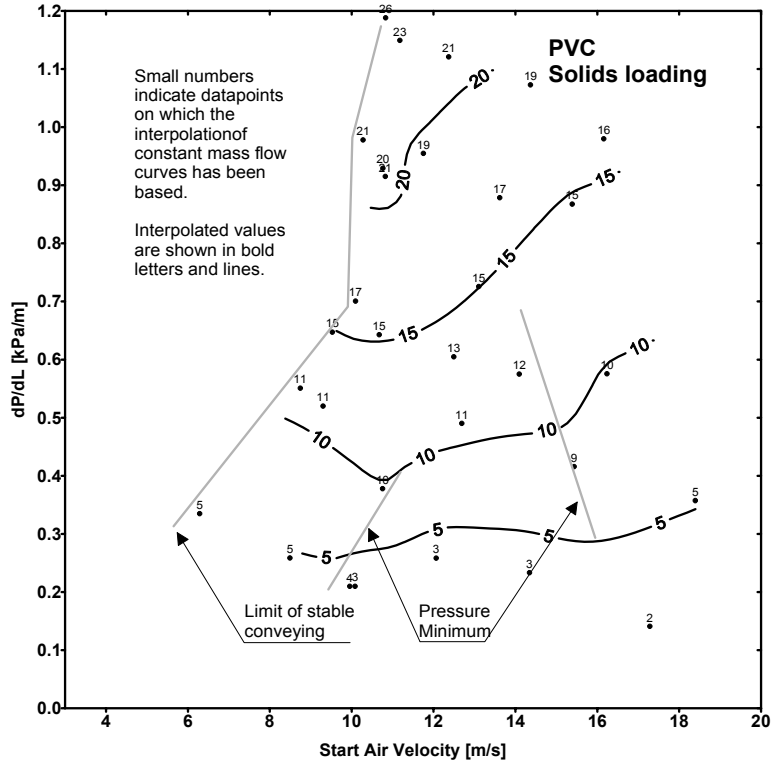

Figure C.9 Conveying characteristic for PVC granules (solids loading ratio).

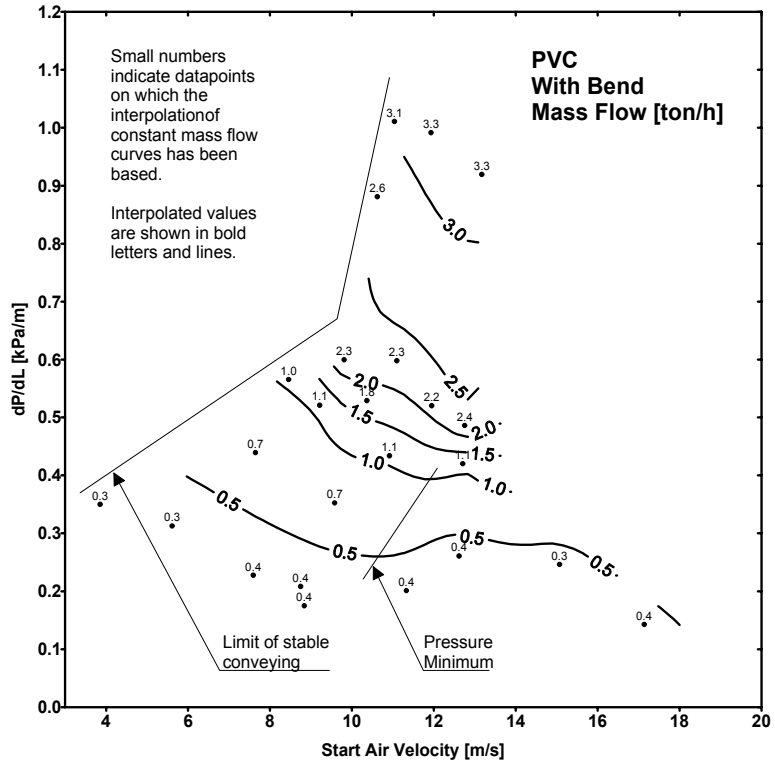

Figure C.10 Conveying characteristic for PVC granules with horizontal to horizontal bend (mass flow of solids).

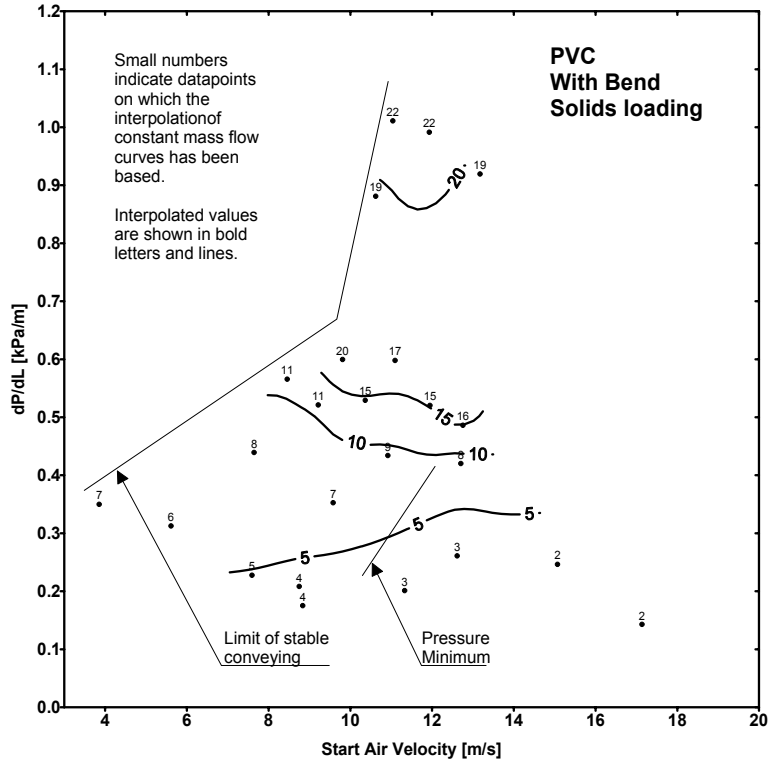

Figure C.11 Conveying characteristic for PVC granules with horizontal to horizontal bend (solids loading ratio).

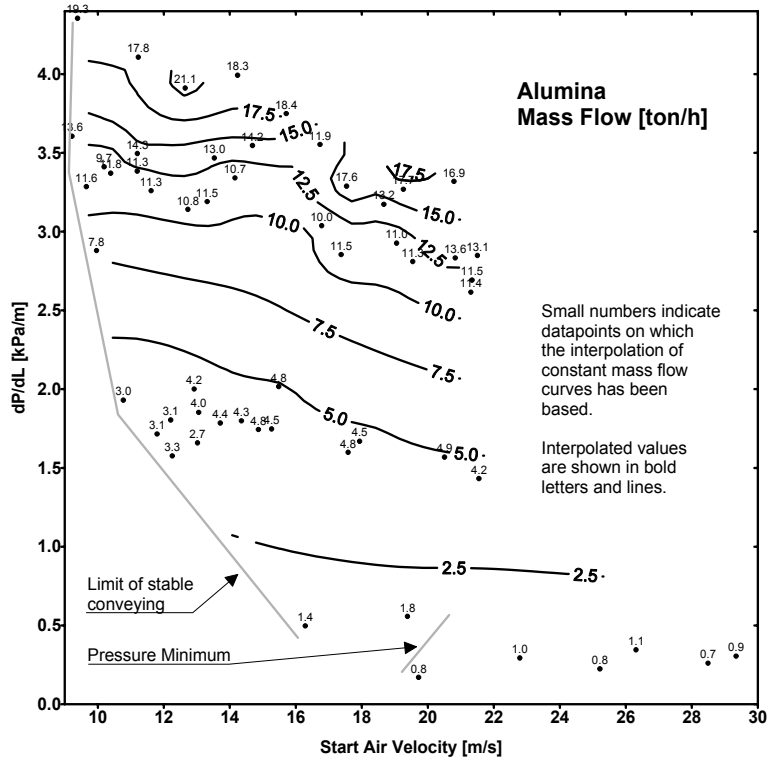

Figure C.12 Conveying characteristic for alumina (mass flow of solids).

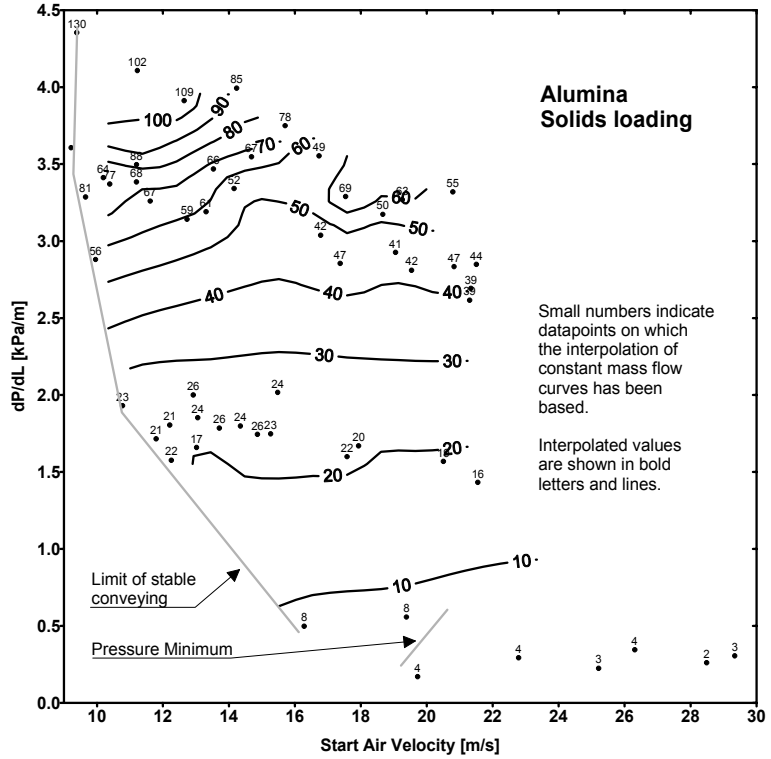

Figure C.13 Conveying characteristic for alumina (solids loading ratio).

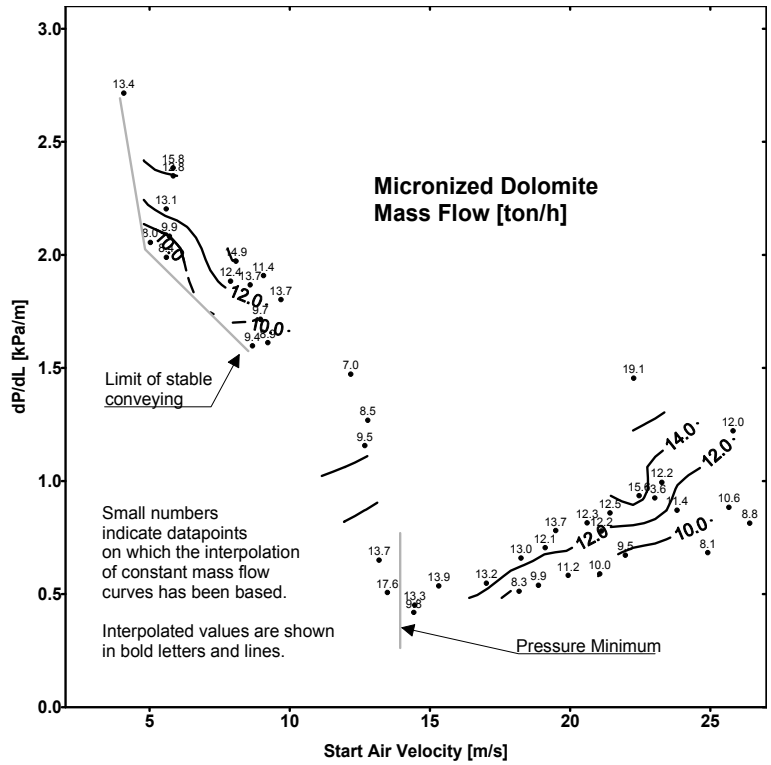

Figure C.14 Conveying characteristic for micronized dolomite (mass flow of solids).

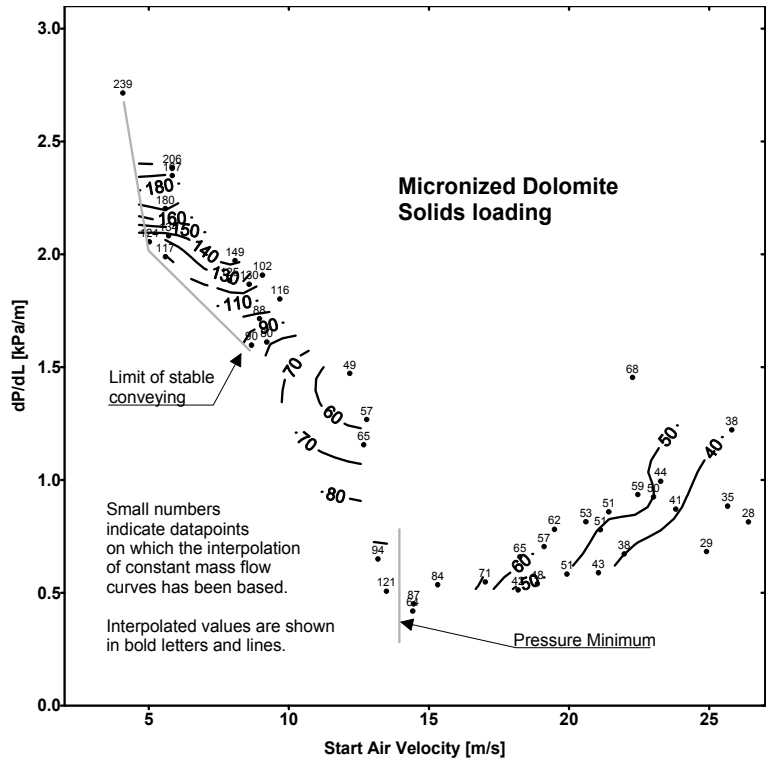

Figure C.15 Conveying characteristic for micronized dolomite (solids loading ratio).

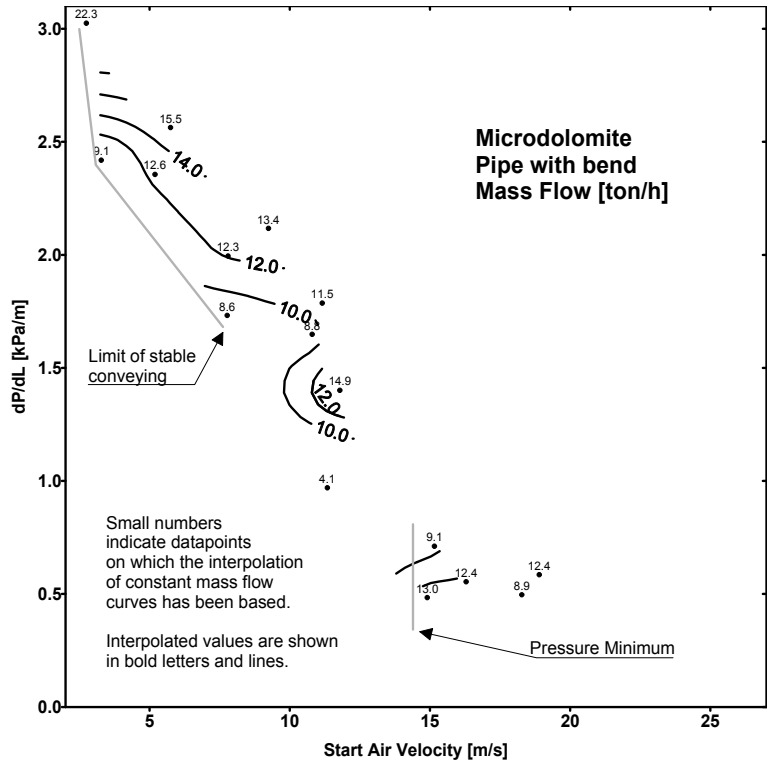

Figure C.16 Conveying characteristic for micronize dolomite with horizontal to horizontal bend (mass flow of solids).

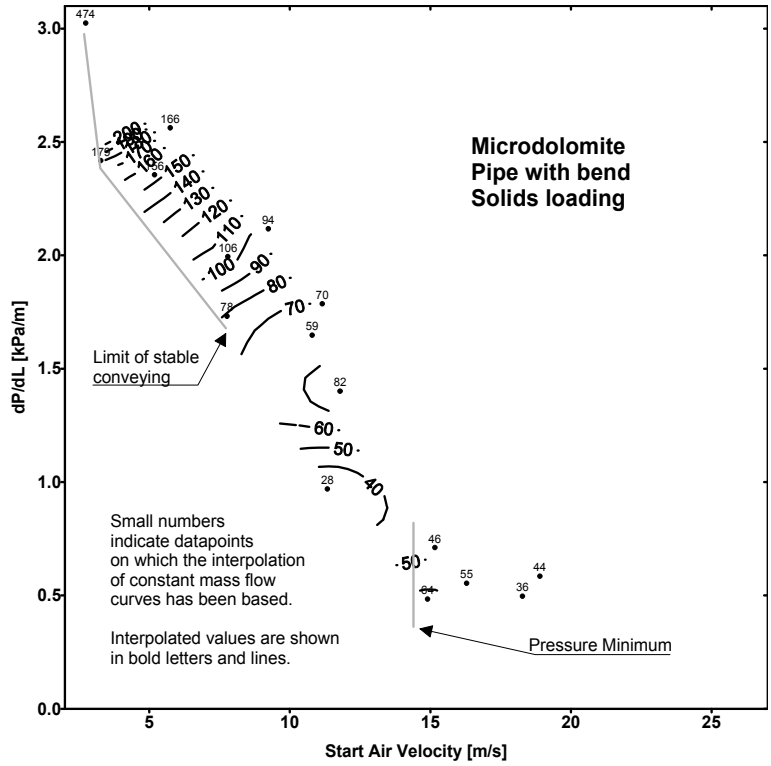

Figure C.17 Conveying characteristic for micronize dolomite with horizontal to horizontal bend (solids loading ratio).

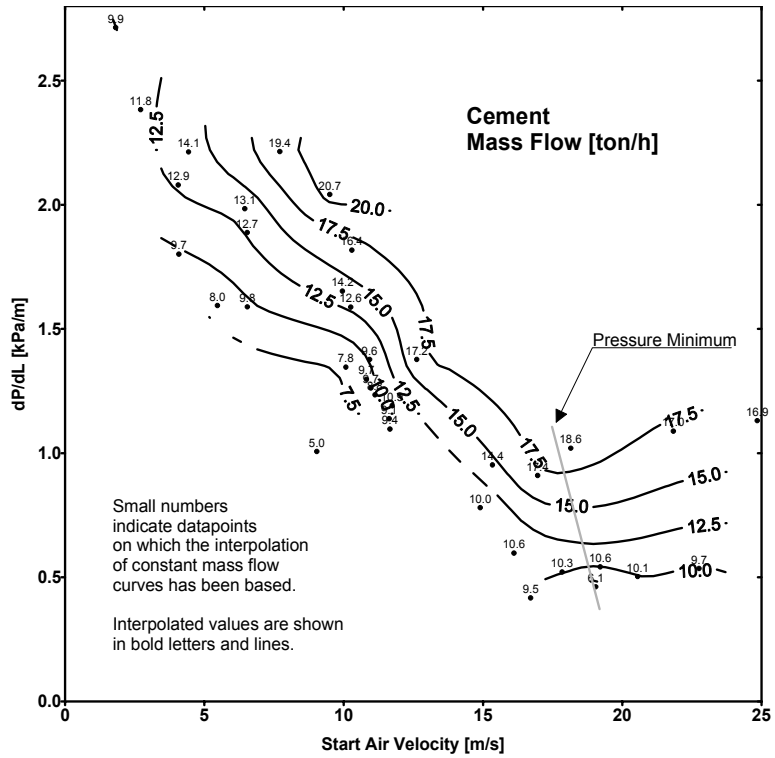

Figure C.18 Conveying characteristic for cement (mass flow of solids).

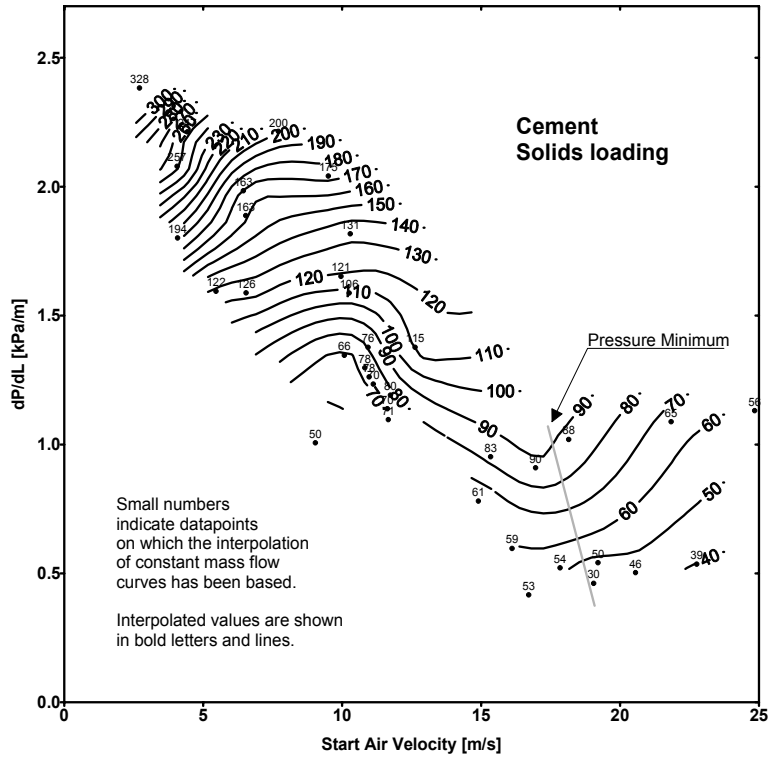

Figure C.19 Conveying characteristic for cement (solids loading ratio).

APPENDIX D. CONVEYING DATA

Each file number has a two letter prefix indicating the type of material:

PE Polyethylene pellets
RS Rapeseed
LB Leighton Buzzard sand
PV PVC granules
AL Aluminium oxide
MD Micronized dolomite
SE Cement

File numbers shown in *italics* contain data obtained for the pipeline configuration with a bend (as shown in Figure 3.4)

File no.	Start air velocity [m/s]	dp/dl [kPa/m]	Solids loading ratio [kg solids/kg air]	Volumetric air flow [Nm3/h]	Mass flow of solids [ton/h]	Average of start pressure [kPa]	Std. dev. of start pressure [% of average]
PE3301	21.4	0.69	25.7	184	6.1	15.8	0.6
PE3302	19.9	0.69	27.6	170	6.1	15.2	0.8
PE3303	18.3	0.66	30.7	155	6.1	13.9	0.4
PE3304	16.7	0.65	33.3	140	6.0	13.2	0.6
PE3305	15.2	0.67	35.2	128	5.8	12.8	0.5
PE3306	14.2	0.69	34.5	119	5.3	12.8	1.7
PE3308	10.0	1.03	46.5	87	5.2	17.2	15.5
PE3310	9.6	1.08	54.5	84	5.9	17.5	8.1
PE3402	22.7	0.49	16.2	191	4.0	12.9	0.7
PE3403	20.1	0.46	18.5	167	4.0	11.2	0.7
PE3404	17.2	0.43	23.1	141	4.2	9.7	1.1
PE3405	15.5	0.42	26.8	126	4.4	9.0	0.6
PE3406	13.1	0.48	32.6	107	4.5	9.1	1.1
PE3407	12.0	0.57	32.9	98	4.2	10.0	2.4
PE3408	10.2	0.75	30.4	86	3.4	13.0	8.4
PE3409	9.0	0.90	36.3	77	3.6	15.2	12.5
PE3411	9.1	0.91	33.9	78	3.4	15.2	13.7
PE3502	23.8	0.29	5.6	194	1.4	9.5	0.9
PE3502	21.6	0.26	6.7	174	1.5	8.2	1.9
PE3503	18.4	0.24	8.4	146	1.6	6.9	1.1
PE3503	16.9	0.23	9.0	133	1.6	6.1	1.1
PE3504	15.0	0.23	10.6	118	1.6	5.6	1.5
PE3504	14.0	0.23	10.2	110	1.4	5.4	0.9
PE3505	11.2	0.40	13.6	90	1.6	7.9	2.5
PE3505	9.7	0.55	16.2	79	1.7	9.9	1.6
PE3506	8.7	0.67	15.8	72	1.5	11.5	3.9
PE3507	9.0	0.64	15.9	74	1.5	11.2	2.8
PE3508	20.9	0.84	24.0	181	5.6	17.7	0.4
PE3509	18.5	0.78	29.0	158	5.9	15.7	0.9
PE3510	16.1	0.77	32.5	136	5.7	14.5	0.5
PE3513	9.8	1.14	57.0	85	6.3	18.7	7.7
PE3602	23.7	0.23	4.1	191	1.0	8.4	0.6
PE3602	22.0	0.22	4.7	176	1.1	7.6	0.8
PE3602	20.1	0.20	5.1	160	1.1	6.6	1.0
PE3602	17.9	0.18	3.7	141	0.7	5.6	0.9
PE3602	15.7	0.16	7.1	122	1.1	4.7	1.0
PE3603	14.4	0.17	8.2	113	1.2	4.4	1.2
PE3603	13.3	0.19	5.9	104	0.8	4.4	0.9
PE3603	12.0	0.26	4.7	94	0.6	5.6	0.9
PE3603	10.7	0.35	11.8	86	1.3	7.1	2.7
PE3603	9.5	0.50	8.3	78	0.8	9.2	1.1
PE3604	9.1	0.56	4.8	75	0.5	9.8	1.7
PE3604	9.6	0.48	10.1	78	1.0	8.7	2.2
PE3701	23.2	0.41	10.7	193	2.7	11.4	0.9
PE3701	20.8	0.37	11.9	171	2.6	9.9	1.9
PE3702	17.8	0.34	13.4	144	2.5	8.3	1.3
PE3702	16.4	0.32	16.2	131	2.8	7.5	0.9
PE3703	12.6	0.43	20.0	101	2.6	8.0	2.3
PE3703	11.0	0.58	21.7	91	2.5	10.6	7.2

File no.	Start air velocity [m/s]	dp/dl [kPa/m]	Solids loading ratio [kg solids/kg air]	Volumetric air flow [Nm3/h]	Mass flow of solids [ton/h]	Average of start pressure [kPa]	Std. dev. of start pressure [% of average]
PE3704	9.6	0.75	23.9	82	2.5	13.4	3.9
PE3704	8.2	0.94	28.7	70	2.6	15.8	8.0
PE3705	9.1	0.80	24.6	78	2.5	13.9	7.8
PE3706	21.4	0.59	19.3	182	4.5	14.0	1.3
PE3707	19.1	0.53	21.9	160	4.5	12.0	1.1
PE3708	17.0	0.50	26.8	141	4.9	10.8	1.0
PE3709	16.1	0.49	27.7	132	4.7	10.3	0.7
PE3710	12.4	0.64	38.0	103	5.1	11.4	2.5
PE3712	9.7	0.98	41.3	85	4.5	16.5	21.7
PE3713	9.5	0.98	45.9	83	4.9	16.3	23.8
PE3714	8.8	1.15	46.1	78	4.7	18.6	23.1
PE3806	15.5	0.15	5.3	119	0.8	4.3	1.8
PE3806	14.1	0.14	5.2	108	0.7	4.0	2.3
PE3806	12.3	0.19	7.4	94	0.9	4.1	2.4
PE3806	10.1	0.35	5.9	80	0.6	6.8	3.7
PE3807	16.0	0.09	1.9	121	0.3	3.5	2.4
PE3807	14.2	0.08	1.5	107	0.2	2.9	3.5
PE3807	12.7	0.07	2.7	96	0.3	2.6	12.0
PE3902	3.7	4.25	75.6	45	4.4	66.1	9.7
PE3903	3.1	4.08	82.5	37	4.0	64.0	6.4
PE3904	2.7	3.69	84.4	32	3.5	59.6	2.8
PE3905	2.5	3.17	82.5	28	3.0	52.1	3.7
PE3907	2.0	2.82	65.8	22	1.9	51.3	8.8
PE4001	9.3	0.70	29.5	76	2.9	12.3	3.5
PE4104	4.7	1.69	25.5	44	1.4	27.6	11.0
PE4105	3.8	1.74	35.1	35	1.6	27.8	7.9
PE4106	3.0	1.69	37.5	28	1.4	27.8	5.7
PE4111	2.4	1.96	50.5	24	1.6	33.3	8.6
PE4201	4.1	4.39	73.2	52	4.9	67.9	6.6
PE4202	3.6	4.31	78.5	45	4.6	68.4	9.8
PE4203	3.3	4.07	75.0	40	3.9	64.5	6.8
PE4204	2.9	3.79	78.0	34	3.5	61.2	2.6
PE4205	2.6	2.92	68.7	28	2.5	48.0	3.9
PE4207	2.4	3.12	73.6	27	2.6	52.3	5.8
PE4304	4.4	2.80	45.6	45	2.7	42.9	14.2
PE4305	3.3	3.09	62.0	36	2.9	49.2	11.7
PE4306	2.7	3.18	73.7	30	2.8	52.4	6.5
PE4311	2.4	3.75	70.5	28	2.5	59.7	6.5
PE4401	3.6	3.28	59.2	40	3.0	51.4	9.9
PE4403	3.5	3.15	63.0	39	3.1	50.6	5.5
PE4404	3.5	3.09	58.1	39	2.9	48.7	10.5
PE4405	9.0	0.79	30.7	75	3.0	13.7	2.8
PE4406	9.0	0.79	30.6	75	2.9	13.8	8.6
PE4407	9.0	0.82	28.7	75	2.8	14.0	9.2
PE4408	8.9	0.83	29.5	74	2.8	14.2	7.4
PE4502	3.7	3.72	58.3	44	3.3	58.6	15.9
PE4505	4.8	2.00	29.5	47	1.8	32.3	11.2
PE4506	3.7	2.02	41.5	36	1.9	32.4	6.0
PE4507	3.0	2.01	48.1	30	1.8	33.3	5.5
PE4509	2.8	2.27	46.6	29	1.7	37.0	9.3

File no.	Start air velocity [m/s]	dp/dl [kPa/m]	Solids loading ratio [kg solids/kg air]	Volumetric air flow [Nm3/h]	Mass flow of solids [ton/h]	Average of start pressure [kPa]	Std. dev. of start pressure [% of average]
PE4512	5.2	1.08	15.4	45	0.9	17.7	33.4
PE4513	4.0	1.20	21.4	35	1.0	19.2	11.8
PE4514	3.3	1.16	27.1	29	1.0	19.0	13.1
PE4601	2.6	1.29	35.4	24	1.1	22.3	9.6
PE4604	3.6	0.55	12.5	29	0.5	9.2	15.3
PE4604	2.9	0.63	11.3	24	0.3	11.1	14.3
PE4605	2.5	0.78	20.7	21	0.6	14.7	17.8
PE4701	4.0	4.40	80.0	50	5.2	71.3	14.8
PE4702	3.8	3.89	85.0	44	4.9	61.2	6.5
PE4703	3.3	3.89	88.9	40	4.6	63.0	2.9
PE4704	3.1	3.33	78.1	35	3.5	54.8	4.5
PE4705	2.5	3.09	80.7	28	2.9	53.2	7.6
PE4706	2.2	3.05	90.7	25	2.9	56.3	15.5
PE4802	2.9	0.43	12.1	23	0.4	7.4	22.2
PE4803	2.5	0.49	14.4	20	0.4	9.6	29.5

File no.	Start air velocity [m/s]	dp/dl [kPa/m]	Solids loading ratio [kg solids/kg air]	Volumetric air flow [Nm3/h]	Mass flow of solids [ton/h]	Average of start pressure [kPa]	Std. dev. of start pressure [% of average]
RS0101	16.7	0.33	14.1	138	2.5	9.1	3.1
RS0102	15.5	0.31	14.3	126	2.3	8.2	2.6
RS0103	14.0	0.33	16.6	113	2.4	7.5	3.7
RS0104	11.2	0.42	20.8	92	2.5	8.4	7.6
RS0105	10.6	0.49	22.0	87	2.5	8.8	7.2
RS0106	9.0	0.67	22.5	75	2.2	11.1	7.8
RS0107	5.5	2.13	36.0	54	2.5	30.9	46.1
RS0201	18.4	0.22	5.0	149	1.0	6.7	3.5
RS0202	16.4	0.21	5.6	131	0.9	5.7	3.3
RS0203	13.6	0.23	6.8	108	0.9	4.5	4.5
RS0204	12.8	0.17	7.3	101	0.9	3.8	5.3
RS0205	11.1	0.19	8.3	88	0.9	4.3	5.1
RS0206	9.4	0.29	9.3	76	0.9	5.5	8.6
RS0207	8.1	0.46	11.1	66	1.0	7.9	6.5
RS0208	7.2	0.56	12.2	59	0.9	9.4	8.7
RS0301	17.4	0.58	21.3	150	4.1	14.0	2.3
RS0302	14.4	0.62	25.1	123	4.0	12.7	2.5
RS0303	13.0	0.60	30.9	110	4.4	12.3	2.7
RS0304	10.5	0.73	39.3	90	4.6	13.4	6.3
RS0305	8.6	0.90	44.5	76	4.3	16.0	5.9
RS0306	5.9	2.38	43.4	63	3.5	40.3	57.1
RS0307	4.6	3.08	51.1	51	3.4	49.3	9.0
RS0308	3.9	2.99	57.9	44	3.3	48.5	15.3
RS0401	16.1	0.83	31.4	142	5.7	16.1	2.0
RS0402	14.7	0.90	34.8	127	5.7	14.5	2.1
RS0403	11.9	0.90	42.9	102	5.7	13.5	2.9
RS0404	9.9	1.00	53.1	86	5.9	13.9	4.3
RS0405	7.4	2.04	59.3	74	5.7	33.7	54.4
RS0406	5.3	2.74	81.5	58	6.1	44.7	49.5
RS0407	4.3	3.49	79.8	50	5.2	54.3	15.5
RS0501	15.0	0.98	37.5	135	6.5	18.3	2.5
RS0502	13.4	0.97	43.8	119	6.8	17.1	1.8
RS0503	11.2	1.04	52.1	99	6.7	16.4	2.5
RS0504	10.1	1.12	57.2	89	6.6	16.6	3.3
RS0505	6.9	2.75	73.8	75	7.2	44.5	49.5
RS0506	6.0	2.74	84.5	66	7.2	45.5	43.3
RS0507	9.8	1.12	59.8	88	6.8	17.2	3.1
RS0508	3.4	4.65	101.4	44	5.7	71.5	10.5
RS0509	2.1	4.81	142.7	28	5.2	77.6	5.1
RS0510	3.0	4.48	115.8	39	5.8	70.8	7.7
RS0511	1.6	4.50	170.8	21	4.7	72.9	4.8
RS0512	1.1	3.63	187.5	13	3.2	63.9	4.4
RS0513	0.7	2.96	215.9	8	2.3	54.8	4.6
RS0601	17.3	0.56	19.1	147	3.6	11.9	2.8
RS0602	15.4	0.46	21.8	128	3.6	10.0	2.5
RS0603	13.2	0.50	25.5	109	3.6	8.8	3.9
RS0604	12.4	0.53	27.4	102	3.6	8.6	4.5
RS0605	9.8	0.62	34.4	83	3.7	11.0	6.6
RS0606	9.1	0.77	35.7	78	3.6	13.3	35.6
RS0607	8.1	0.98	40.3	71	3.7	16.8	56.3

File no.	Start air velocity [m/s]	dp/dl [kPa/m]	Solids loading ratio [kg solids/kg air]	Volumetric air flow [Nm3/h]	Mass flow of solids [ton/h]	Average of start pressure [kPa]	Std. dev. of start pressure [% of average]
RS0608	4.1	2.47	56.7	43	3.2	40.2	15.4
RS0609	1.1	3.57	163.0	13	2.8	62.5	3.5
RS0701	14.4	0.12	1.9	113	0.3	2.9	6.9
RS0702	10.9	0.11	2.7	84	0.3	1.9	9.6
RS0703	8.4	0.10	3.7	65	0.3	2.3	6.8
RS0704	7.4	0.26	3.5	59	0.3	4.7	9.9
RS0802	13.3	0.99	43.5	119	6.7	17.3	1.6
RS0803	10.9	1.03	53.9	97	6.8	16.8	3.0
RS0804	9.7	1.10	63.4	86	7.1	17.5	4.4
RS0805	5.3	3.50	79.4	62	6.3	53.7	27.4
RS0806	9.1	1.07	64.9	81	6.8	18.7	5.4
RS0807	6.7	2.38	71.9	72	6.7	41.7	57.2
RS0811	4.0	4.43	98.6	46	5.8	53.3	12.5
RS0813	2.0	5.12	158.8	25	5.1	68.6	8.0
RS0814	1.5	4.82	192.8	19	4.7	66.3	6.5
RS0904	3.8	3.91	100.7	45	5.9	56.8	11.8
RS0906	1.9	4.54	162.0	24	5.1	70.8	7.2
RS0907	1.5	4.20	185.5	19	4.6	67.8	6.0
RS1102	3.4	2.57	69.5	36	3.2	40.3	13.0
RS1103	1.5	3.15	128.0	18	2.9	53.3	7.6
RS1202	1.2	3.56	180.8	15	3.6	63.3	10.8
RS1204	2.1	4.48	154.6	27	5.5	72.6	6.2
RS1301	4.8	0.89	19.7	41	1.0	13.2	69.3
RS1302	3.1	0.79	27.4	26	0.9	11.8	25.8
RS1303	3.0	0.79	26.2	25	0.9	12.0	29.7
RS1304	2.5	0.80	35.3	21	1.0	12.5	19.4
RS1305	1.8	1.00	38.8	16	0.8	16.7	13.7
RS1501	4.7	1.57	40.7	45	2.3	24.8	30.5
RS1502	3.4	1.77	55.3	33	2.3	28.3	18.1
RS1503	3.4	1.70	53.9	32	2.2	25.9	14.2
RS1504	1.7	2.25	91.0	18	2.1	36.3	8.2
RS1505	1.4	2.39	108.9	15	2.1	40.7	8.9
RS1601	3.7	2.59	79.5	39	4.0	39.7	13.8
RS1602	3.2	2.68	86.9	35	3.9	44.7	8.8
RS1603	2.3	2.95	116.2	26	3.9	50.7	7.5
RS1604	1.4	3.45	171.4	17	3.8	62.6	5.8
RS1605	1.2	3.12	186.5	15	3.5	56.7	5.8
RS1607	0.8	2.65	187.5	10	2.3	51.4	7.7
RS1801	2.9	3.61	118.4	34	5.2	56.6	8.0
RS1802	2.1	3.91	145.6	26	4.9	63.9	8.0
RS1803	1.5	3.76	178.6	19	4.4	64.9	7.0
RS1804	1.1	3.32	205.6	13	3.4	58.1	8.4
RS1805	0.8	2.50	154.9	9	1.8	47.2	10.0
RS2402	9.1	1.08	64.5	80	6.7	17.3	5.9
RS2403	10.8	0.93	55.8	94	6.8	15.5	3.4
RS2404	12.2	0.89	48.8	106	6.7	15.6	2.7
RS2405	9.1	0.67	36.5	77	3.6	12.5	8.2
RS2406	12.3	0.46	27.8	101	3.6	9.1	4.2
RS2407	11.4	0.80	46.3	97	5.8	13.7	4.2

File no.	Start air velocity [m/s]	dp/dl [kPa/m]	Solids loading ratio [kg solids/kg air]	Volumetric air flow [Nm3/h]	Mass flow of solids [ton/h]	Average of start pressure [kPa]	Std. dev. of start pressure [% of average]
RS2408	12.6	0.76	43.3	108	6.0	13.9	3.1
RS2409	11.8	0.56	35.5	98	4.5	10.6	4.1
RS2410	12.9	0.54	31.4	107	4.4	10.7	3.5
RS2411	10.8	0.34	22.3	87	2.5	7.2	7.4
RS2412	9.1	0.47	25.5	75	2.5	9.4	8.5
RS3001	15.4	0.40	21.1	135	3.7	16.2	2.1
RS3101	12.9	0.45	25.5	112	3.7	15.3	3.1
RS3102	11.4	0.50	28.1	99	3.6	16.1	4.0
RS3103	7.5	1.34	36.0	78	3.6	37.2	52.4
RS3104	10.1	0.58	31.4	90	3.6	18.3	9.7
RS3105	12.5	0.92	46.4	119	7.2	26.7	1.7
RS3201	12.3	0.91	47.1	116	7.1	26.0	3.4
RS3202	9.3	1.10	54.4	93	6.5	33.6	21.2
RS3203	11.2	0.92	49.7	106	6.8	26.4	5.1
RS3204	5.1	3.68	65.0	73	6.1	91.2	9.4
RS3205	18.7	0.14	2.4	150	0.5	6.8	2.0
RS3206	17.0	0.12	2.5	136	0.4	5.9	2.4
RS3206	13.8	0.10	3.4	108	0.5	4.4	3.1
RS3207	12.5	0.09	3.7	97	0.5	3.8	3.9
RS3207	9.7	0.11	4.8	76	0.5	4.0	4.8
RS3208	7.3	0.24	6.1	59	0.5	7.4	73.5
RS3302	15.9	0.21	8.1	130	1.4	8.7	2.4
RS3303	13.6	0.18	9.7	110	1.4	7.1	3.1
RS3303	12.1	0.18	10.8	97	1.4	6.5	4.2
RS3304	9.5	0.27	13.6	78	1.4	8.2	6.2
RS3304	5.8	0.72	19.7	53	1.4	21.8	63.3
RS3305	14.8	0.35	19.0	126	3.1	13.4	2.5
RS3401	10.6	0.69	42.9	95	5.3	19.2	5.5
RS3402	9.6	0.75	45.9	88	5.2	21.3	10.3
RS3403	10.9	0.66	41.4	97	5.2	18.4	4.1
RS3404	12.4	0.63	36.6	110	5.2	18.5	2.1
RS3405	9.3	0.34	21.0	78	2.1	11.4	8.5
RS3406	5.9	0.97	29.9	56	2.2	27.9	45.4
RS3407	2.8	1.57	50.1	30	1.9	42.7	11.2
RS3408	1.4	1.66	77.9	15	1.5	47.2	7.6
RS3501	2.9	1.68	53.7	31	2.1	43.5	8.6
RS3502	1.8	1.66	79.5	20	2.0	48.1	5.0
RS3503	0.7	1.88	163.8	8	1.7	59.1	2.5
RS3505	0.8	2.56	196.9	11	2.7	75.1	2.7
RS3506	1.8	3.91	131.5	27	4.6	101.2	1.9
RS3507	3.2	3.49	101.7	46	6.1	90.1	5.5
RS3508	4.8	2.81	77.5	61	6.2	70.7	9.8

File no.	Start air velocity [m/s]	dp/dl [kPa/m]	Solids loading ratio [kg solids/kg air]	Volumetric air flow [Nm3/h]	Mass flow of solids [ton/h]	Average of start pressure [kPa]	Std. dev. of start pressure [% of average]
LB0402	20.7	1.17	26.8	200	6.9	28.3	6.4
LB0501	16.4	1.31	33.9	156	6.8	25.7	8.7
LB0502	11.9	1.49	47.0	114	6.9	26.9	11.2
LB0601	10.9	1.65	52.0	106	7.1	29.2	13.2
LB0604	14.0	1.33	39.8	133	6.8	25.1	11.5
LB0606	11.7	1.58	49.2	113	7.2	28.5	11.2
LB0607	18.4	0.83	21.1	166	4.5	19.3	8.4
LB0701	15.7	0.95	27.3	142	5.0	19.4	12.6
LB0702	12.9	1.05	30.4	119	4.7	21.5	13.2
LB0704	11.7	1.24	32.8	111	4.7	25.0	15.9
LB0705	10.8	1.36	35.2	104	4.7	27.2	15.3
LB0706	15.3	1.96	47.9	155	9.6	34.5	11.4
LB0801	12.7	1.88	55.2	128	9.1	33.7	13.4
LB0802	14.1	1.98	54.0	143	10.0	34.6	14.0
LB0804	14.8	2.16	53.9	153	10.6	37.2	11.3
LB0805	17.4	1.95	40.3	178	9.3	35.6	10.8
LB0806	16.8	2.24	47.9	176	10.9	39.7	12.6
LB0807	20.2	0.29	8.3	167	1.8	9.9	7.8
LB0807	18.6	0.27	9.0	152	1.8	8.6	7.7
LB0903	12.2	1.75	47.0	121	7.4	31.9	13.1
LB0904	15.2	0.27	11.6	124	1.9	7.6	10.7
LB0904	13.7	0.33	12.7	113	1.8	8.7	8.3
LB0905	11.7	0.61	14.4	99	1.8	12.1	11.1
LB0905	10.0	0.82	16.2	88	1.8	15.8	9.6
LB1002	15.4	2.07	50.4	157	10.2	36.4	11.2
LB1003	16.6	0.57	20.2	143	3.7	14.0	12.5
LB1003	13.9	0.61	25.0	119	3.8	14.2	16.4
LB1004	15.8	1.77	42.9	157	8.7	32.3	11.1
LB1101	11.7	0.73	26.1	106	3.6	19.7	13.6
LB1103	11.3	0.99	27.3	104	3.7	21.7	13.4
LB1104	13.6	1.88	49.8	137	8.8	34.0	12.9
LB1106	12.4	1.97	50.8	125	8.2	35.2	10.8
LB1107	15.3	2.09	51.7	156	10.4	37.7	11.6
LB1108	15.6	2.32	52.4	163	11.0	40.1	11.7
LB1201	9.4	0.90	18.6	83	2.0	17.6	11.1
LB1202	8.9	0.86	14.6	77	1.5	16.1	12.6
LB1202	8.1	1.07	17.2	72	1.6	18.7	20.9
LB1203	8.0	1.11	15.9	72	1.5	19.2	12.7

File no.	Start air velocity [m/s]	dp/dl [kPa/m]	Solids loading ratio [kg solids/kg air]	Volumetric air flow [Nm3/h]	Mass flow of solids [ton/h]	Average of start pressure [kPa]	Std. dev. of start pressure [% of average]
PV0304	10.8	0.38	9.9	88	1.1	8.5	9.6
PV0401	9.3	0.52	11.2	77	1.1	9.9	9.7
PV0404	8.7	0.55	11.4	72	1.1	9.9	10.9
PV0405	18.4	0.36	5.2	150	1.0	8.6	4.5
PV0406	16.2	0.98	16.3	145	3.0	19.4	6.8
PV0501	14.4	1.07	19.2	129	3.2	19.6	6.8
PV0502	12.4	1.12	21.0	111	3.0	19.2	8.3
PV0503	10.8	1.19	25.8	97	3.2	19.4	10.8
PV0504	11.2	1.15	23.3	100	3.0	19.2	7.7
PV0505	15.4	0.87	14.6	135	2.6	17.4	6.7
PV0506	16.2	0.58	9.7	138	1.7	13.0	5.7
PV0507	17.3	0.14	2.0	136	0.4	4.5	5.5
PV0507	14.3	0.23	2.7	113	0.4	5.1	6.8
PV0507	12.1	0.26	2.8	95	0.3	4.7	5.2
PV0507	10.1	0.21	2.6	79	0.3	3.8	6.6
PV0508	10.0	0.21	3.8	78	0.4	3.8	5.4
PV0601	8.5	0.26	4.7	67	0.4	4.4	4.9
PV0601	6.3	0.33	5.1	50	0.3	5.4	6.3
PV0603	13.6	0.88	16.5	119	2.5	16.5	7.4
PV0604	11.8	0.95	19.4	103	2.6	16.5	9.5
PV0605	10.8	0.93	19.6	94	2.4	15.8	9.9
PV0606	10.3	0.98	21.3	90	2.5	16.2	10.6
PV0608	14.1	0.57	12.2	119	1.9	12.2	7.6
PV0609	12.5	0.60	13.5	105	1.8	11.8	8.6
PV0610	10.1	0.70	17.0	86	1.9	13.1	9.7
PV0612	10.7	0.64	15.3	90	1.8	12.2	10.8
PV0701	13.1	0.73	15.0	112	2.2	14.1	7.7
PV0702	10.8	0.91	21.3	94	2.6	15.4	9.6
PV0703	15.4	0.42	9.1	128	1.5	10.0	6.9
PV0704	12.7	0.49	11.1	105	1.5	10.1	8.7
PV0705	9.5	0.65	14.8	80	1.5	12.0	12.0
PV1401	12.8	0.49	16.0	117	2.4	22.4	6.2
PV1402	12.0	0.52	15.3	110	2.2	22.4	5.6
PV1403	9.8	0.60	19.9	91	2.3	23.8	5.1
PV1501	11.1	0.60	16.9	103	2.3	23.4	5.8
PV1502	13.2	0.92	19.4	130	3.3	31.1	5.7
PV1503	11.9	0.99	21.5	118	3.3	31.6	5.2
PV1505	11.0	1.01	22.0	108	3.1	31.0	5.2
PV1601	17.1	0.14	2.2	137	0.4	6.6	2.9
PV1601	15.1	0.25	2.0	121	0.3	7.3	6.5
PV1602	12.6	0.26	2.7	101	0.4	6.4	3.6
PV1603	11.3	0.20	3.4	90	0.4	5.3	3.8
PV1603	8.8	0.21	4.3	69	0.4	5.2	3.5
PV1604	8.8	0.18	4.2	69	0.4	4.8	4.2
PV1605	7.6	0.23	4.9	60	0.4	5.9	3.7
PV1606	5.6	0.31	5.9	45	0.3	7.6	4.4
PV1607	3.9	0.35	6.5	31	0.3	7.9	5.0
PV1609	10.4	0.53	14.5	93	1.8	19.9	6.0
PV1701	12.7	0.42	7.6	108	1.1	13.0	4.1

File no.	Start air velocity [m/s]	dp/dl [kPa/m]	Solids loading ratio [kg solids/kg air]	Volumetric air flow [Nm3/h]	Mass flow of solids [ton/h]	Average of start pressure [kPa]	Std. dev. of start pressure [% of average]
PV1702	10.9	0.43	8.8	93	1.1	13.8	4.5
PV1703	9.2	0.52	10.6	80	1.1	15.2	5.4
PV1704	8.5	0.57	10.8	74	1.0	15.8	5.6
PV1705	10.6	0.88	19.4	102	2.6	28.1	5.6
PV1802	9.6	0.35	6.6	79	0.7	9.2	4.2
PV1803	7.6	0.44	8.3	64	0.7	11.0	5.3

File no.	Start air velocity [m/s]	dp/dl [kPa/m]	Solids loading ratio [kg solids/kg air]	Volumetric air flow [Nm3/h]	Mass flow of solids [ton/h]	Average of start pressure [kPa]	Std. dev. of start pressure [% of average]
AL0101	19.7	0.17	3.7	160	0.8	7.3	11.3
AL0102	16.3	0.50	7.8	137	1.4	11.1	20.7
AL0105	19.4	0.56	8.3	165	1.8	12.6	17.8
AL0106	22.8	0.29	4.1	190	1.0	10.1	12.5
AL0204	10.0	2.88	56.3	107	7.8	45.6	9.2
AL0301	29.3	0.31	2.8	250	0.9	13.2	4.9
AL0302	28.5	0.26	2.3	240	0.7	11.7	3.9
AL0303	26.3	0.35	3.9	224	1.1	12.8	10.7
AL0304	25.2	0.22	2.8	208	0.8	9.7	9.6
AL0306	11.2	3.38	68.4	128	11.3	52.1	6.4
AL0307	10.2	3.41	64.4	116	9.7	51.8	6.1
AL0401	21.3	2.62	38.7	227	11.4	42.0	10.6
AL0402	19.5	2.81	41.5	210	11.3	43.0	10.7
AL0403	17.4	2.85	47.4	188	11.5	44.1	13.5
AL0404	14.2	3.34	51.5	161	10.7	51.4	7.4
AL0501	21.3	2.69	38.8	229	11.5	43.4	6.4
AL0502	19.1	2.93	41.3	206	11.0	44.4	8.0
AL0503	16.8	3.04	42.2	184	10.0	46.4	10.1
AL0504	13.3	3.19	61.1	146	11.5	46.2	10.2
AL0505	12.7	3.14	59.2	141	10.8	47.3	9.5
AL0506	11.6	3.26	67.5	130	11.3	49.1	7.9
AL0507	10.4	3.37	77.0	119	11.8	52.2	7.4
AL0508	9.7	3.29	81.5	110	11.6	51.7	5.9
AL0601	21.6	1.43	15.9	205	4.2	28.5	9.6
AL0602	20.5	1.57	19.0	199	4.9	30.6	7.3
AL0603	17.6	1.60	21.8	170	4.8	30.3	9.5
AL0604	14.9	1.74	25.8	144	4.8	30.6	9.5
AL0605	13.1	1.85	24.4	127	4.0	31.1	9.1
AL0606	12.2	1.80	20.7	118	3.1	29.9	11.6
AL0701	21.5	2.85	43.8	232	13.1	45.4	6.5
AL0702	20.8	2.83	46.8	224	13.6	45.2	9.8
AL0703	18.7	3.17	50.3	203	13.2	46.9	9.9
AL0704	16.7	3.55	48.8	188	11.9	51.8	5.9
AL0705	14.7	3.55	66.8	165	14.2	51.5	8.8
AL0706	13.5	3.47	66.0	152	13.0	51.9	5.4
AL0707	11.2	3.50	87.9	126	14.3	52.3	6.6
AL0708	9.2	3.61	100.0	105	13.6	54.3	6.3
AL0801	20.8	3.32	55.0	237	16.9	52.9	4.9
AL0802	19.3	3.27	62.8	218	17.7	51.2	6.6
AL0803	17.5	3.29	69.4	196	17.6	49.7	6.3
AL0804	15.7	3.75	78.0	182	18.4	55.1	7.7
AL0805	14.2	3.99	84.8	167	18.3	56.8	6.1
AL0806	12.6	3.91	109.0	149	21.1	57.9	11.1
AL0807	11.2	4.11	102.2	135	17.8	60.4	6.4
AL0808	9.4	4.35	130.0	115	19.3	63.8	8.7
AL0901	15.3	1.75	23.4	147	4.5	30.2	22.9
AL0902	13.7	1.78	25.9	131	4.4	29.0	12.2
AL0903	13.0	1.66	16.9	123	2.7	27.9	13.2
AL0904	11.8	1.71	21.5	111	3.1	28.1	14.5

File no.	Start air velocity [m/s]	dp/dl [kPa/m]	Solids loading ratio [kg solids/kg air]	Volumetric air flow [Nm3/h]	Mass flow of solids [ton/h]	Average of start pressure [kPa]	Std. dev. of start pressure [% of average]
AL1001	15.5	2.02	24.5	152	4.8	33.3	11.1
AL1002	17.9	1.67	20.1	172	4.5	30.1	12.2
AL1003	14.4	1.80	23.9	139	4.3	31.1	10.8
AL1004	12.9	2.00	25.7	127	4.2	33.3	8.8
AL1005	12.3	1.58	22.4	114	3.3	26.5	21.4
AL1006	10.8	1.93	22.7	103	3.0	30.2	13.4

File no.	Start air velocity [m/s]	dp/dl [kPa/m]	Solids loading ratio [kg solids/kg air]	Volumetric air flow [Nm3/h]	Mass flow of solids [ton/h]	Average of start pressure [kPa]	Std. dev. of start pressure [% of average]
MD0202	14.4	0.42	63.9	118	9.8	8.8	20.2
MD0202	12.2	1.47	48.8	111	7.0	20.6	25.8
MD0203	19.9	0.58	50.9	170	11.2	13.1	17.1
MD0204	4.1	2.71	238.9	43	13.4	41.6	11.7
MD0205	25.7	0.88	35.1	234	10.6	20.9	11.5
MD0301	8.1	1.97	149.0	77	14.9	27.3	19.0
MD0302	13.5	0.51	121.0	113	17.6	11.0	22.4
MD0303	18.2	0.66	64.5	156	13.0	13.6	31.0
MD0304	23.0	0.92	50.1	210	13.6	21.2	21.5
MD0502	8.7	1.60	90.3	81	9.4	24.0	15.6
MD0504	14.5	0.45	86.5	119	13.3	9.8	27.4
MD0601	5.8	2.38	205.7	60	15.8	35.9	27.8
MD0602	7.9	1.88	124.7	77	12.4	29.6	20.0
MD0603	8.6	1.87	130.1	81	13.7	25.9	22.8
MD0604	22.3	1.45	67.8	218	19.1	30.8	15.6
MD0605	25.8	1.22	38.2	243	12.0	25.8	12.7
MD0607	20.6	0.81	53.0	180	12.3	17.4	26.5
MD0608	19.1	0.70	57.1	164	12.1	15.5	23.4
MD0701	22.5	0.93	58.7	205	15.6	21.3	12.5
MD0702	24.9	0.68	28.6	218	8.1	16.2	18.1
MD0703	21.1	0.59	43.0	180	10.0	13.7	18.8
MD0704	18.2	0.51	42.3	152	8.3	10.6	22.0
MD0705	12.8	1.27	57.0	115	8.5	19.3	20.9
MD0706	9.2	1.61	80.2	86	8.9	24.0	15.5
MD0707	5.6	1.99	117.2	55	8.4	31.2	9.3
MD0708	5.0	2.05	124.1	50	8.0	31.3	8.3
MD0901	26.4	0.81	28.5	238	8.8	19.6	13.7
MD0902	22.0	0.67	38.3	191	9.5	15.0	16.2
MD0903	18.9	0.54	48.0	159	9.9	11.5	14.5
MD0904	12.7	1.16	64.5	114	9.5	19.1	26.1
MD0905	9.0	1.71	88.5	85	9.7	26.0	10.8
MD1001	23.8	0.87	40.9	215	11.4	19.9	12.8
MD1002	21.1	0.78	50.6	186	12.2	17.0	13.8
MD1003	17.0	0.55	71.3	143	13.2	11.6	15.4
MD1004	13.2	0.65	93.9	113	13.7	13.5	16.5
MD1005	9.1	1.91	102.3	86	11.4	26.3	15.2
MD1006	23.3	0.99	44.4	213	12.2	21.6	15.1
MD1007	21.4	0.86	50.8	191	12.5	18.3	17.0
MD1008	19.5	0.78	62.0	170	13.7	16.2	20.2
MD1009	15.3	0.54	83.7	128	13.9	11.5	10.5
MD1010	9.7	1.80	116.0	91	13.7	25.5	16.7
MD1011	5.8	2.35	167.0	59	12.8	35.4	16.3
MD1101	5.6	2.20	179.8	56	13.1	33.7	10.1
MD1102	5.7	2.08	134.5	57	9.9	32.4	11.2
MD1201	14.9	0.48	64.0	157	13.0	40.5	9.6
MD1301	11.2	1.79	70.3	126	11.5	50.6	8.5
MD1302	7.8	1.99	105.9	90	12.3	53.6	8.2
MD1303	5.2	2.36	155.7	62	12.6	60.4	7.0
MD1501	18.3	0.50	36.4	188	8.9	36.4	8.3

File no.	Start air velocity [m/s]	dp/dl [kPa/m]	Solids loading ratio [kg solids/kg air]	Volumetric air flow [Nm3/h]	Mass flow of solids [ton/h]	Average of start pressure [kPa]	Std. dev. of start pressure [% of average]
MD1601	15.2	0.71	46.1	153	9.1	34.6	12.3
MD1602	10.8	1.65	58.7	116	8.8	42.7	6.6
MD1603	7.8	1.73	77.9	85	8.6	46.3	9.4
MD1604	3.3	2.42	178.7	40	9.1	60.9	3.8
MD1801	16.3	0.55	54.6	176	12.4	44.1	9.1
MD1802	18.9	0.58	44.0	218	12.4	54.2	5.7
MD1803	11.8	1.40	82.5	140	14.9	58.5	5.0
MD1804	9.2	2.12	94.5	110	13.4	58.3	10.7
MD1805	2.7	3.02	473.9	36	22.3	76.8	9.7
MD1806	5.7	2.56	166.0	72	15.5	67.5	3.5
MD1807	11.3	0.97	27.6	114	4.1	34.1	11.8

File no.	Start air velocity [m/s]	dp/dl [kPa/m]	Solids loading ratio [kg solids/kg air]	Volumetric air flow [Nm3/h]	Mass flow of solids [ton/h]	Average of start pressure [kPa]	Std. dev. of start pressure [% of average]
SE0101	11.1	1.23	70.2	97	8.8	20.5	17.1
SE0201	11.0	1.26	77.6	97	9.7	20.4	21.8
SE0202	10.3	1.59	106.0	92	12.6	22.8	20.4
SE0203	10.0	1.65	121.0	91	14.2	24.5	27.7
SE0204	6.5	1.89	162.7	60	12.7	27.2	28.1
SE0205	4.1	2.08	256.6	39	12.9	32.0	15.0
SE0206	1.8	2.71	404.5	19	9.9	42.8	17.5
SE0302	4.1	1.80	194.0	39	9.7	28.6	13.0
SE0303	6.5	1.59	126.1	60	9.8	24.2	16.1
SE0306	10.8	1.30	78.2	96	9.7	20.3	13.7
SE0307	16.7	0.42	53.3	139	9.5	12.0	22.4
SE0401	9.5	2.04	174.8	92	20.7	30.3	16.6
SE0402	10.9	1.38	76.1	98	9.6	20.8	15.3
SE0403	7.7	2.21	200.0	75	19.4	31.9	9.9
SE0405	5.5	1.59	122.0	51	8.0	25.6	13.3
SE0406	9.0	1.01	50.1	78	5.0	16.9	19.3
SE0407	19.1	0.46	30.0	156	6.1	11.5	31.1
SE0501	6.5	1.98	163.4	62	13.1	30.1	19.3
SE0502	4.4	2.21	247.3	44	14.1	34.0	11.2
SE0503	2.7	2.38	328.2	28	11.8	38.0	13.1
SE0601	10.3	1.82	131.2	97	16.4	28.2	23.7
SE0602	12.6	1.38	115.5	115	17.2	24.2	23.2
SE0701	15.3	0.95	82.8	135	14.4	19.7	40.6
SE0702	17.0	0.91	89.9	150	17.4	20.4	22.4
SE0703	18.2	1.02	87.6	164	18.6	23.4	20.0
SE0704	21.8	1.09	65.3	201	17.0	26.1	18.7
SE0705	24.8	1.13	56.5	231	16.9	27.6	15.1
SE0801	11.6	1.14	69.8	101	9.1	19.4	9.2
SE0802	14.9	0.78	60.9	127	10.0	16.7	14.6
SE0803	17.8	0.52	53.5	149	10.3	14.0	16.9
SE0804	20.6	0.50	45.6	172	10.1	13.9	17.2
SE0805	22.8	0.54	39.3	191	9.7	14.5	22.3
SE0902	11.7	1.10	70.8	103	9.4	17.9	26.8
SE0903	11.7	1.19	79.6	106	10.9	19.8	24.0
SE0904	16.1	0.60	59.0	139	10.6	14.2	26.5
SE0905	19.2	0.54	49.6	165	10.6	14.1	24.0
SE0906	10.1	1.35	66.1	91	7.8	19.9	16.8

APPENDIX E. DRAWINGS OF THE FLUIDISATION RIG

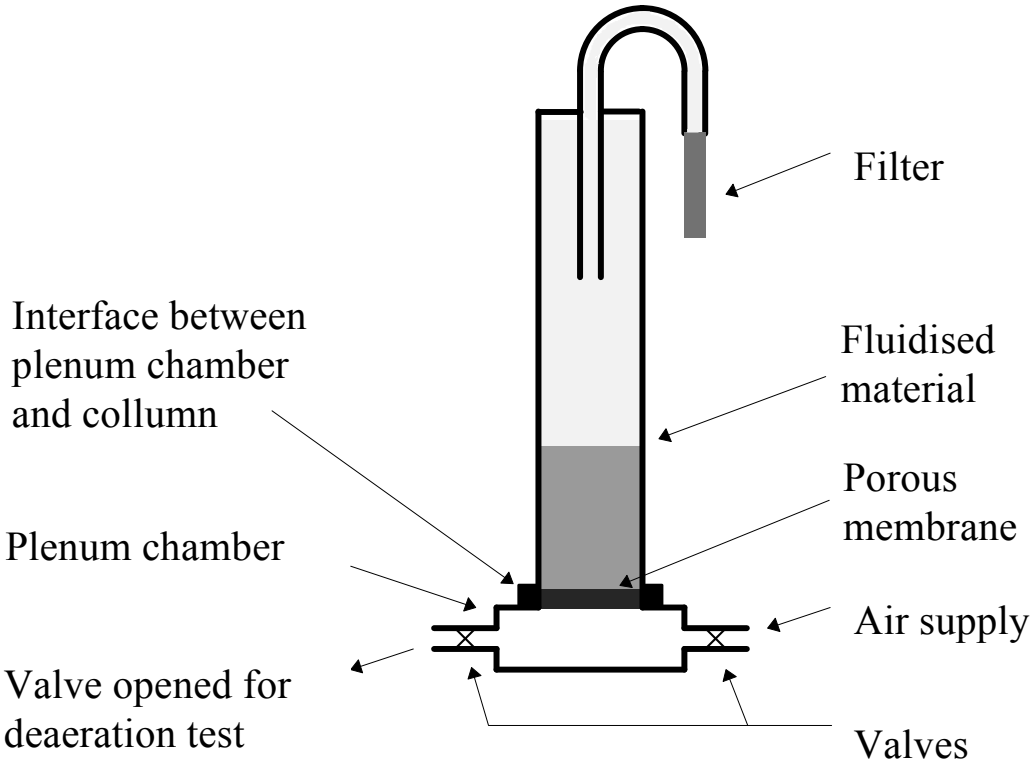

Figure E.1 Sketch of the fluidisation rig (POSTEC Marketing document).

Tree column widths available (50mm, 80mm and 110mm in diameter). The columns are made of perspex. The fluidisation cloth that has been used is a woven Polyester cloth (Aeroslide Fabric 4-5/FLUITEX E350) with a thickness of 4 to 5 mm supplied from Johannes Möller, Hamburg. The permeability of the cloth is $8.8 \cdot 10^{-3}$ Nm3/(Pa·s·m^2). Details of plenum chamber and column interfaces can be seen in the figures below.

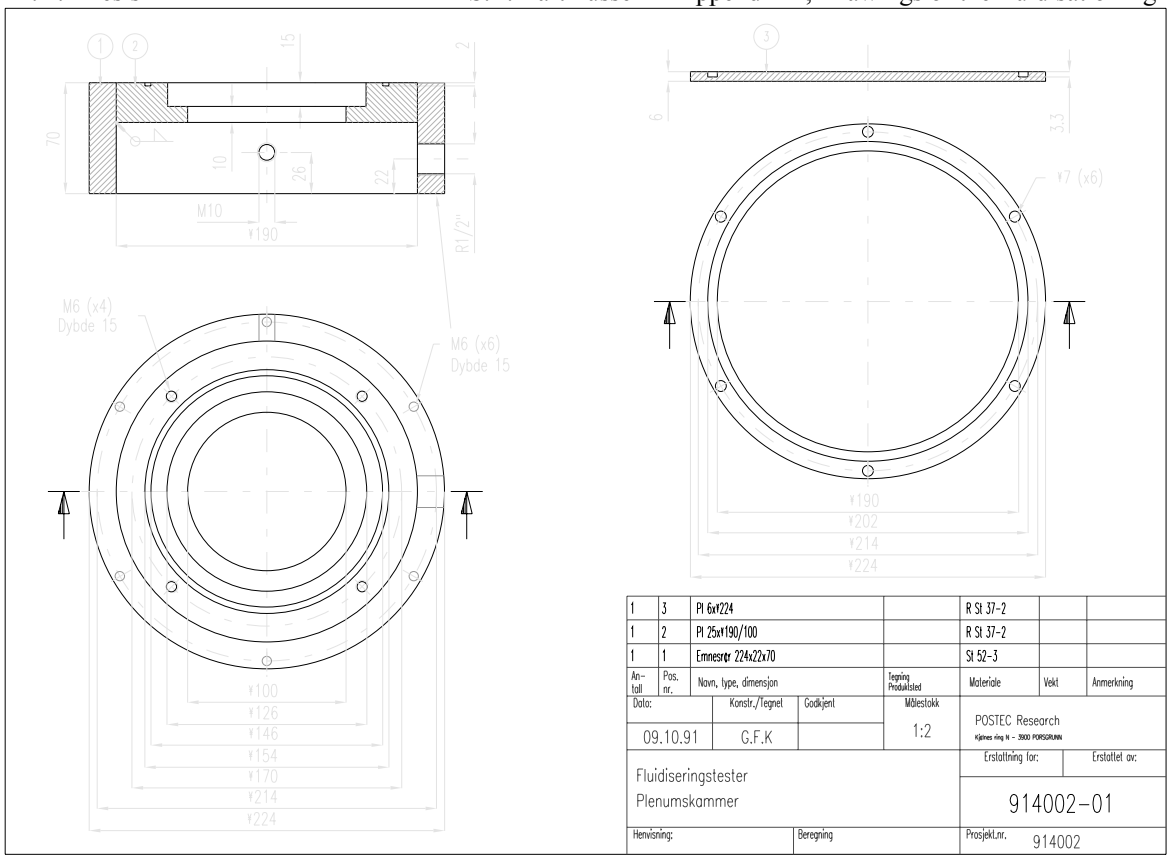

Figure E.2 Details of the plenum chamber. Total volume is $1.36 \cdot 10^{-3}$ m^3.

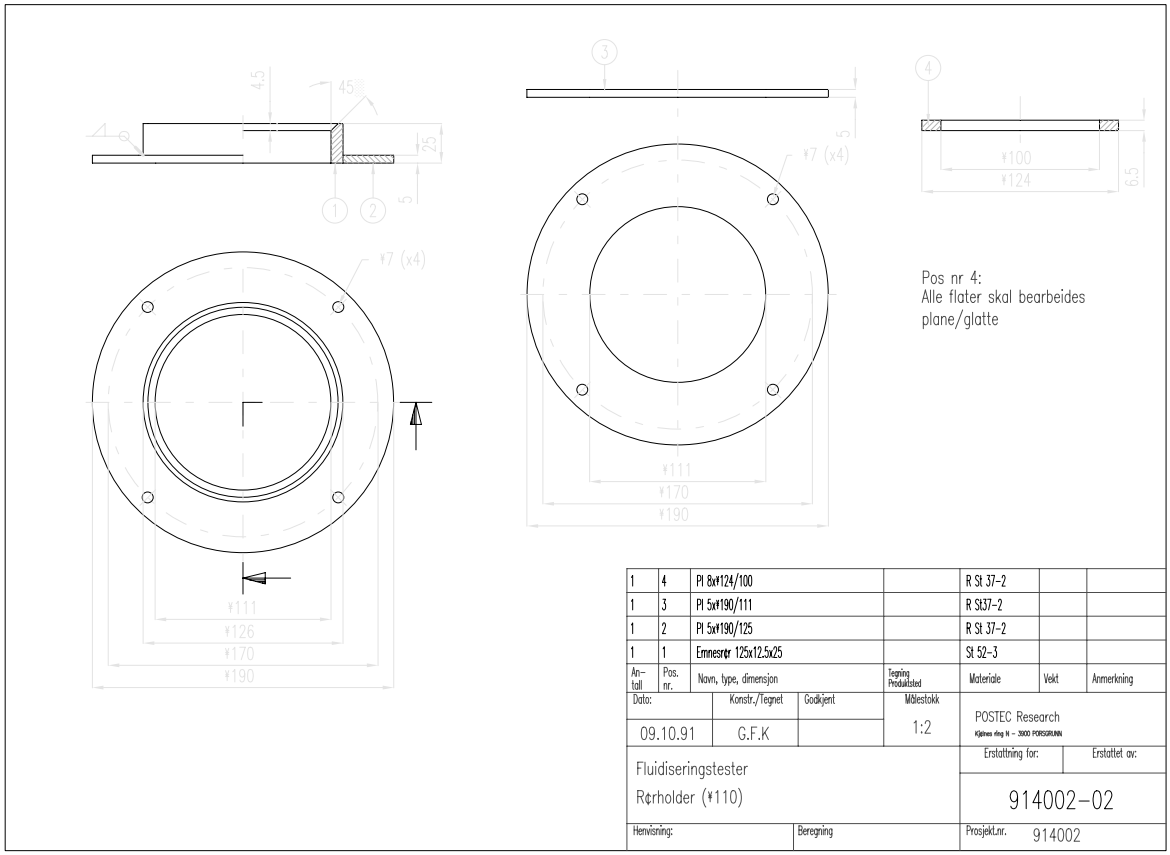

Figure E.3 Details of the 110mm column interface

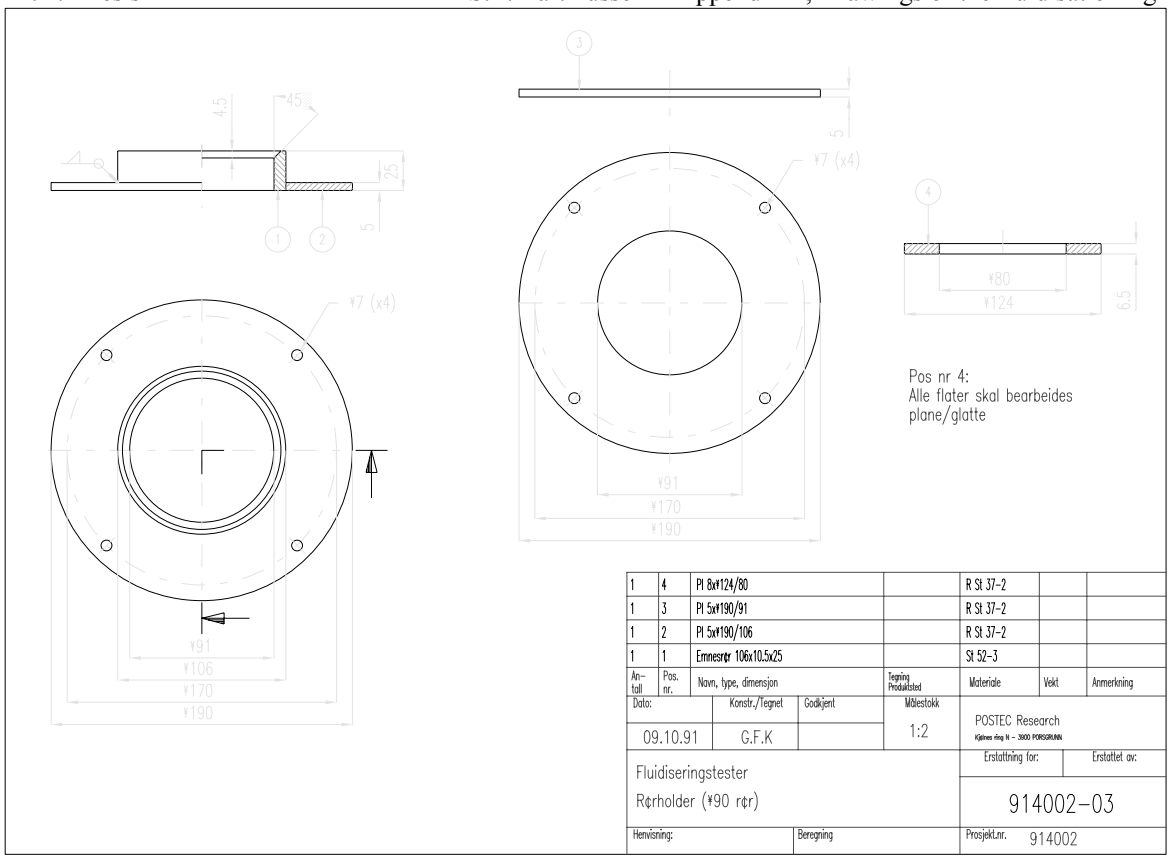

Figure E.4 Details of the 80mm column interface.

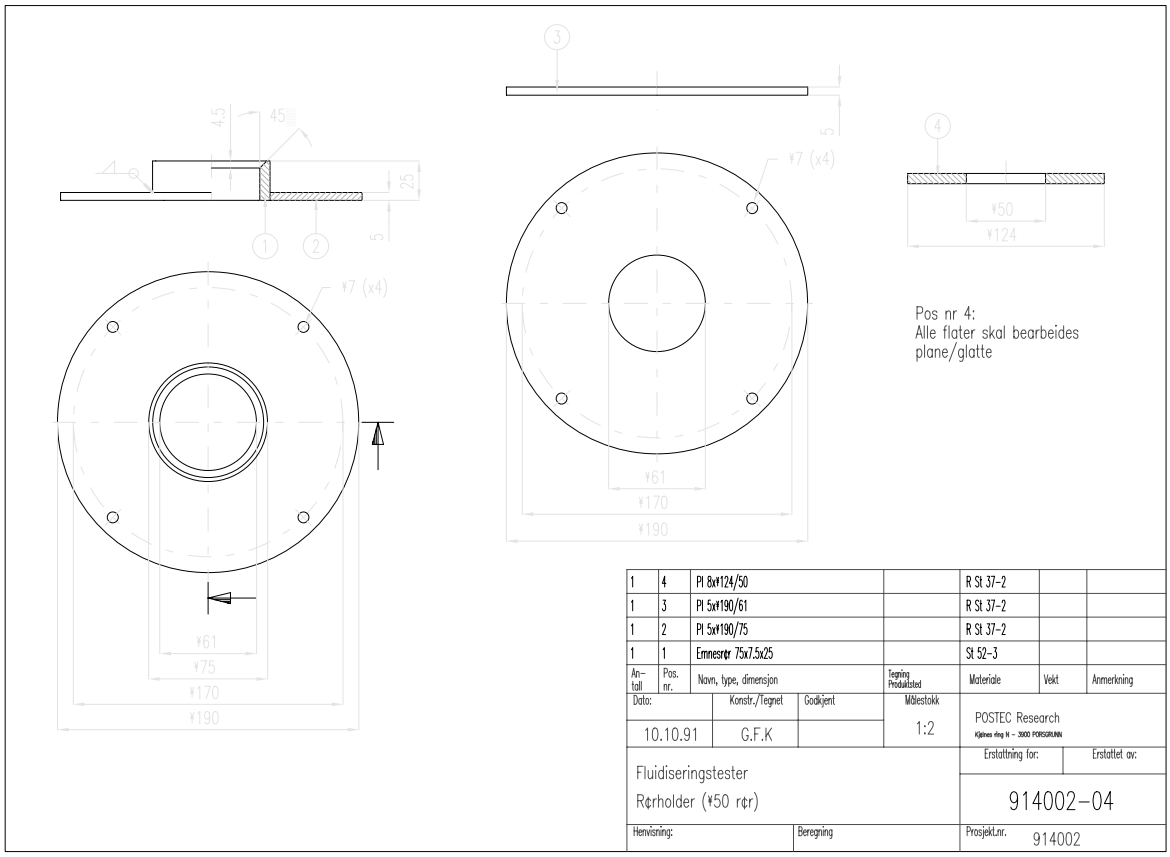

Figure E.5 Details of the 50mm column interface

5th Int. Conf. on Bulk Materials Storage, Handling and Transp., Newcastle , Australia10-12 July 1995

Reliable Conveying Conditions and Transitions Between Flow Regimes in Pneumatic Conveyors

S.E.Martinussen[1)] , S.R.Woodhead[2)] , S.R.deSilva[1)] , A.R.Reed[2)]

1) TEL-TEK, Dept. of Powder Science and Technology Research, Kjølnes Ring,
3914 PORSGRUNN, NORWAY
2) The Wolfson Centre for Bulk Solids Handling Technology, University of Greenwich,
London, SE18 6PF, UK

Pneumatic conveying is used in a wide variety of industries. Several important aspects of the performance of a pneumatic conveying system, such as energy consumption, stable operation, pipeline wear, and product degradation, are linked to the problem of finding the conveying limit of the powder in the actual pipeline. Because it has been identified that this is an important problem, a special test rig has been developed. All conveying characteristics obtained so far are presented. The analysis of the data focuses on conveying limits and changes in the mode of flow. Frequency analysis of the pressure fluctuations along the pipeline are also presented. A quantitative way of identifying the limits of stable conveying is developed. All the results have been obtained using a straight, horizontal, 15.9m long, 2" pipeline, with no flow hindrances or deviations.

1. NOTATION

g	Standard gravity acceleration.
ρ_b	Bulk density
ρ_p	Particle density
d_p	Particle diameter.
D	Pipeline diameter.
v_s	Superficial air velocity.
μ	Solids loading ratio.
m	Mass flow of solids.
x_{50}	Median particle size
u_{mf}	Minimum fluidization velocity
dP/dl	Pressure drop per unit length.
C_x	Discrete cross correlation function.

2. INTRODUCTION

The flow of particulate materials in a pneumatic conveyor will, at certain operating conditions, undergo a transition between flow regimes with dramatically different pressure gradients in the conveying line. This transition is described as a saltation limit by Rizk (1), or as a minimum velocity limit for safe conveying by Matsumoto et. al. (2). Cabrejos (3), (4) has addressed this problem by investigating pickup velocities of particles on a settled bed of material, which is similar to Barths (5) experiments. Rose and Duckworth (6) recognise the conveying limit to be a stability limit, and more recently Pan et. al. (7) give correlations for the limits at which the flow turns unstable.

As part of an investigation to identify the conveyability of particulate materials, and the dependency on their physical properties, we have carried out conveying tests close to the limits of stable conveying. The first region of stable conveying, at low air velocities, has a maximum velocity limit of stable conveying. The second region of stable conveying, at higher air velocities, has a minimum velocity limit of stable conveying. In between these two regions there is a region where the mode of flow switches between two regimes with different total pressure drop. The investigation described below will show that we consider the stability of the flow to be a more useful means of characterising the flow in the conveyor, both for engineering purposes, and for the fundamental understanding of what is happening when the flow of solids stops.

To characterise the stability of the flow, the standard deviation or the kurtosis of the pressure fluctuations may be used. The stability of the flow of solids must be visualised as a function of the operating parameters of the conveyor. This is done by plotting the standard deviation or the kurtosis as a function of superficial air velocity and pressure drop, in the same way as in a conveying characteristic. This way of displaying the data provides the possibility of identifying the limit of stable conveying quantitatively. For instance, a certain level of pressure fluctuations in the pipeline might be selected as a suitable limit. This would, of course, depend on the characteristics of the air supply to be used in the actual conveying rig.

3. THE EXPERIMENTAL SETUP

The main components of the test rig are the blow tank, the pipeline and the receiving tank. The recharging of the blow tank is taken care of by a movable silo carried by an overhead crane. The solids feed rate is either controlled by the bypass to transport air ratio or by a knife valve at the bottom of the blow tank. Air flow rate is controlled by globe valves, and monitored by turbine flow meters. Humidity, temperature and pressure are also monitored on the air supply side. The conveying line

used for these experiments is 15.9m long, with no bends or other flow hindrances, and the inner pipeline diameter is 53mm. Along the conveying line 10 pressure transducers are positioned, as can be seen in Figure A13 in the Appendix. Flow rate, temperature and humidity of the exhaust air from the receiving tank are also measured. The receiving tank itself is placed upon three load cells enabling average mass flow rate measurements to be made. All signals from the different instruments are sampled, digitised and stored in a computer.

4. TEST PROGRAM

The characteristic values obtained for the test materials used so far are listed in Table 1. When selecting test materials it was decided to choose from common materials used in the process industry.

Table 1. Characteristics of the test materials

Material	LDPE	Sand	Cement	Rape Seed
ρ_p (kg/m^3)	920	2650	3124	1113
x_{50} (μm)	3700	600	10	1660
u_{mf} (cm/s)	120	25	<0.1	80
Permeability [m^2*Pa^{-1}*s^{-1}]	1.8 10^{-3}	1.7 10^{-4}		6.8 10^{-4}

For each of the test materials, the conveying characteristics have been found. The characteristic for Leighton Buzzard sand is displayed in Figure 1. The conveying characteristics for all the powders investigated can be found in the Appendix.

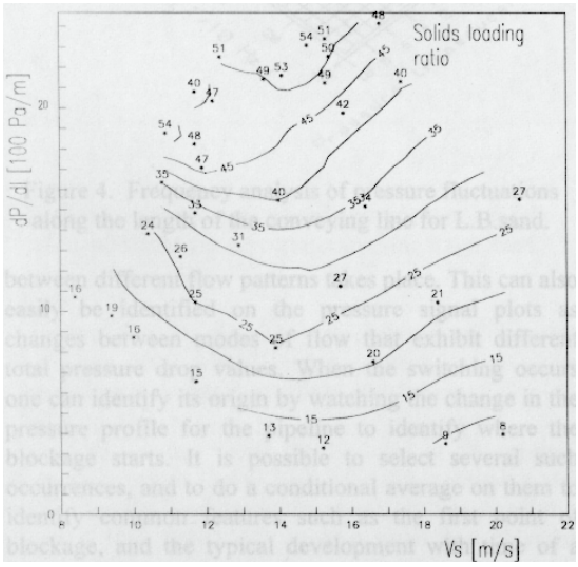

Figure 1. Conveying characteristic for Leighton Buzzard sand.

The data were sampled at a rate of 5Hz, and each test run lasts between 30s and several minutes.

5. ANALYSIS OF THE DATA

Because it was found to be difficult to identify the transition in the flow pattern by means of observing saltation of particles in the pipeline, it was necessary to find a new and objective way of determining the conveying limit. The pressure fluctuations in the pipeline was found to be useful for identifying the limits of stable conveying. Therefore an analysis of the pressure fluctuation level in the pipeline was made. The result for Leighton Buzzard sand is shown in Figure 2.

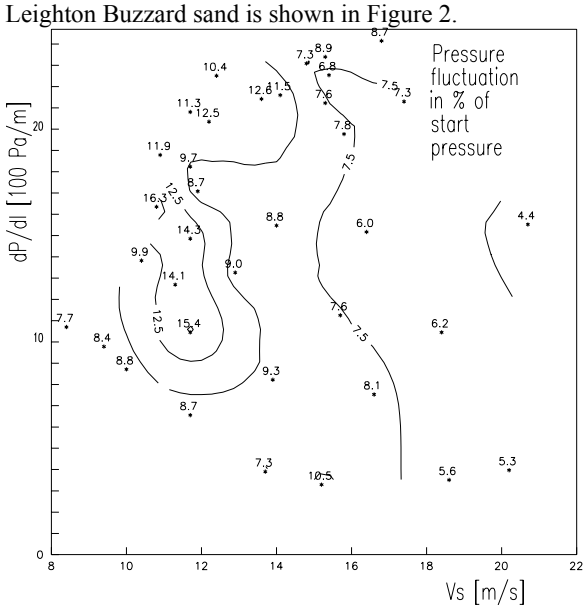

Figure 2. Pressure fluctuation level in % of start pressure

The average of the rms values of the signals on all transducers are plotted in percent of the total pressure drop in the pipeline. The pressure fluctuation analysis for all the powders investigated can be found in the Appendix. As one can see the pressure fluctuation level grows rapidly towards the limit of stable conveying. In the case of rape seed and LDPE (polyethene pellets) the pressure fluctuation level also grows towards low solids feed rates. The cement displays an intermediate region where the pressure fluctuations are higher, but no clear conveying limit.

The frequency spectrum of the signals along the pipeline is shown in Figure 3 through Figure 6 for all materials tested. All the frequency spectra have been obtained close to the limit of stable conveying in the second region of stable conveying. As one can see the low frequency component dominates.

When the operating point of the pneumatic conveyor is brought beyond the limit of stable conveying, switching

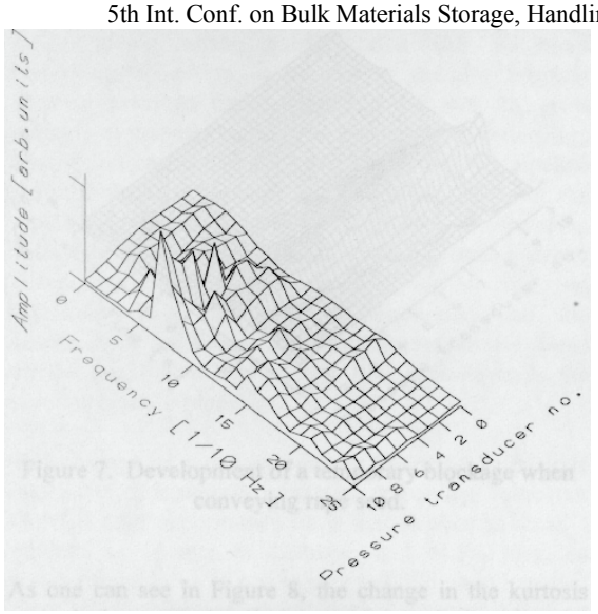

Figure 3. Frequency analysis of pressure fluctuations along the length of the conveying line for rape seed.

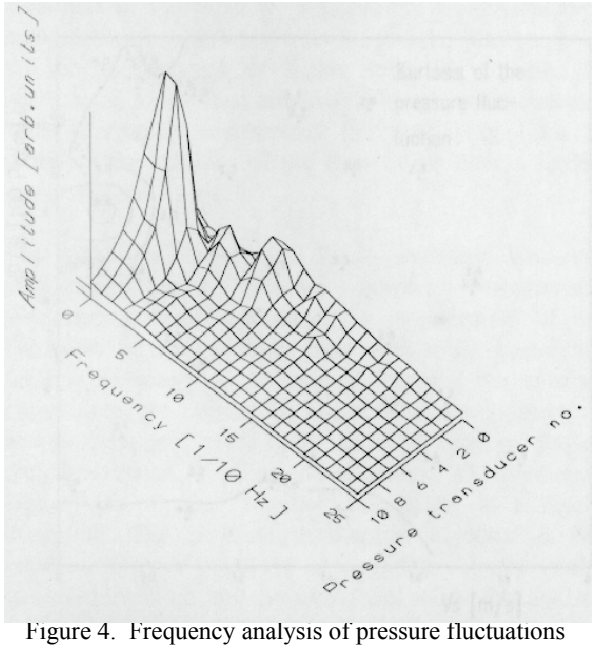

Figure 4. Frequency analysis of pressure fluctuations along the length of the conveying line for L.B.sand.

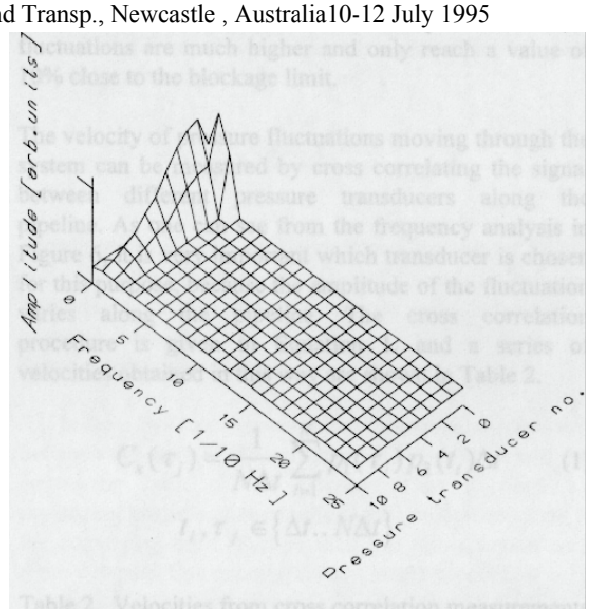

Figure 5. Frequency analysis of pressure fluctuations along the length of the conveying line for polyethene pellets.

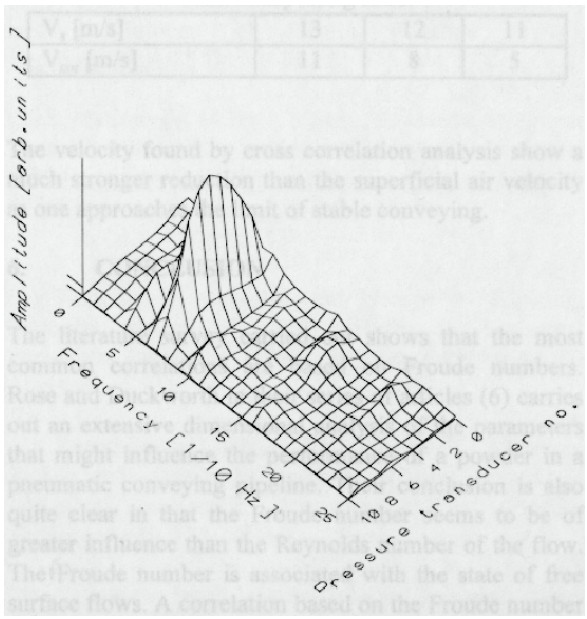

Figure 6. Frequency analysis of pressure fluctuations along the length of the conveying line for cement.

between different flow patterns takes place. This can also easily be identified on the pressure signal plots as changes between modes of flow that exhibit different total pressure drop values. When the switching occurs one can identify its origin by watching the change in the pressure profile for the pipeline to identify where the blockage starts. It is possible to select several such occurrences, and to do a conditional average on them to identify common features such as the first point of blockage, and the typical development with time of a temporary blockage. Sand, LDPE and rape seed consistently show that the pipeline blocks at the beginning. Figure 7 shows a temporary blockage that emerges at the beginning of the pipeline and moves through the system. The switching in the mode of flow associated with the temporary blockages mentioned above, suggests that the kurtosis of the pressure signal, as defined by Abramowitz and Stegun (8), could be used to determine the stability of the flow. A map of the kurtosis of the signal from the pressure transducers can be displayed in a similar way as for the pressure fluctuation maps shown in Figure 2, and in the Appendix.

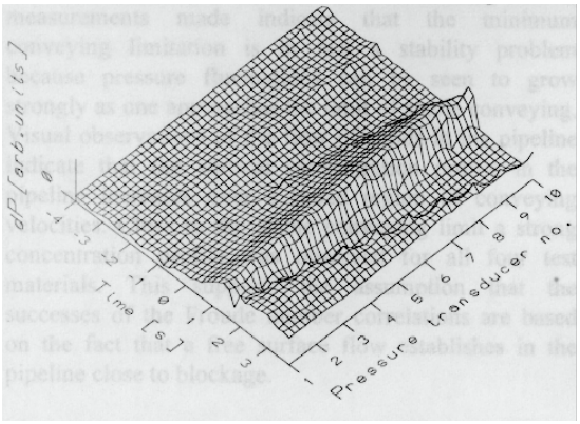

Figure 7. Development of a temporary blockage when conveying rape seed.

As one can see in Figure 8, the change in the kurtosis towards the conveying limit is much less distinct than the change in the pressure fluctuation maps as shown in Figure 2 and in the Appendix. Figure 8 can be compared directly with Figure A4 in the Appendix.

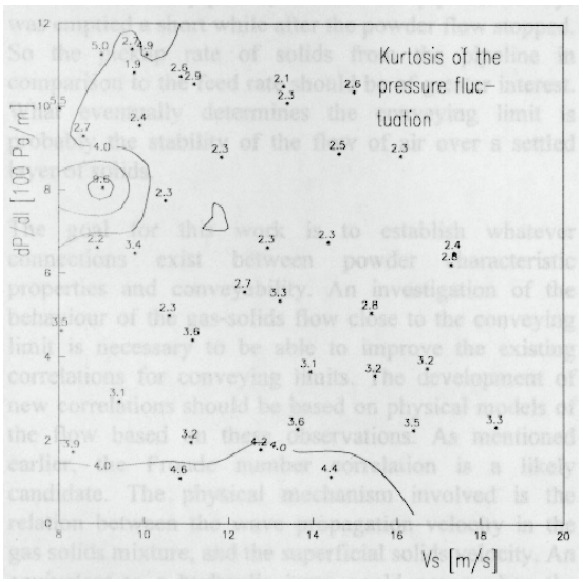

Figure 8. The Kurtosis of the pressure signal for the second stable region when conveying Rape Seed.

It seems that the method of plotting the pressure fluctuation level identifies the conveying limit more clearly than the method of plotting the kurtosis.

To set an absolute value for the level of the pressure fluctuations close to the limit of stable conveying one might, for the four materials shown in the Appendix, select a 10% limit. This gives a good and objective identification of the conveying limit of the second stable region. For the first stable region of conveying as found for rape seed and polyethene pellets the pressure fluctuations are much higher and only reach a value of 10% close to the blockage limit.

The velocity of pressure fluctuations moving through the system can be measured by cross correlating the signal between different pressure transducers along the pipeline. As one can see from the frequency analysis in Figure 6, it is very important which transducer is chosen for this purpose, because the amplitude of the fluctuation varies along the pipeline. The cross correlation procedure is given in Equation 1. and a series of velocities obtained in this way are shown in Table 2.

$$C_x(\tau_j) = \frac{1}{N\Delta t}\sum_{i=1}^{N} p_1(\tau_j)\, p_2(t_i)\Delta t \qquad (1)$$

$$t_i, \tau_j \in \{\Delta t .. N\Delta t\}$$

Table 2. Velocities from cross correlation measurements in comparison to superficial air velocity close to the limit of stable conveying, at a solids loading ratio of $3 \cdot 10^1$, when transporting sand.

V_s [m/s]	13	12	11
V_{cor} [m/s]	11	8	5

The velocity found by cross correlation analysis show a much stronger reduction than the superficial air velocity as one approaches the limit of stable conveying.

6. CONCLUSION

The literature survey carried out shows that the most common correlations are based on Froude numbers. Rose and Duckworth in their series of articles (6) carries out an extensive dimensional analysis of the parameters that might influence the performance of a powder in a pneumatic conveying pipeline. Their conclusion is also quite clear in that the Froude number seems to be of greater influence than the Reynolds number of the flow. The Froude number is associated with the state of free surface flows. A correlation based on the Froude number of the concentrated area of solids towards the bottom of the pipeline close to blockage, might prove to be a good candidate for predicting minimum conveying velocity. If it is the transition from supercritical to sub critical flow in the concentrated layer of solids that governs the transition from stable to unstable conveying, it would be necessary to predict bed height to get a useful correlation.

Observations carried out during experimental test runs indicate that there exists no clearly defined saltation velocity at solids loading ratios relevant to industrial applications. Only when a partial blockage occurs, and the mode of flow switches, can a rapid saltation of powder be observed. This phenomena is of course lost in experiments if one does not monitor the flow pattern or the pressure drop along the whole pipeline. The pressure measurements made indicate that the minimum conveying limitation is in fact a stability problem because pressure fluctuations can be seen to grow

strongly as one approaches the limit of stable conveying. Visual observations of the flow of solids in the pipeline indicate that the vertical concentration profile in the pipeline increases over a broad region of conveying velocities. Close to the stable conveying limit a strong concentration profile was observed for all four test materials. This supports the assumption that the successes of the Froude number correlations are based on the fact that a free surface flow establishes in the pipeline close to blockage.

The concept of a pickup velocity seems to be of little interest in determining minimum conveying velocities. Our LB sand experiments show that in even as small a pipeline as 50 mm in diameter, and 14.5m long, an instability takes up to one minute to build up at low feed rates. This happens in a region of the transport characteristics where only a small fraction of the particles in the pipeline are suspended in the air. The pickup velocity of the powder was well below the actual velocities in the pipeline, because the pipeline always was emptied a short while after the powder flow stopped. So the pickup rate of solids from the pipeline in comparison to the feed rate should be of greater interest. What eventually determines the conveying limit is probably the stability of the flow of air over a settled layer of solids.

The goal for this work is to establish whatever connections exist between powder characteristic properties and conveyability. An investigation of the behaviour of the gas-solids flow close to the conveying limit is necessary to be able to improve the existing correlations for conveying limits. The development of new correlations should be based on physical models of the flow based on these observations. As mentioned earlier, the Froude number correlation is a likely candidate. The physical mechanism involved is the relation between the wave propagation velocity in the gas solids mixture, and the superficial solids velocity. An equivalent to a hydraulic jump could occur when the superficial solids velocity is too low. A consequence of this possible Froude number limitation is that there should exist a maximum flow rate of solids in the pipeline, under stable flow conditions. Since there are always places in the pipeline where the transported material is slowed down, as for instance at the material inlet or in a bend, a pipeline operating close to maximum feed rate should contain one or several sections in which the concentration of solids is close to bulk density, and the superficial solids velocity is close to a value giving a critical Froude number of one. These slow sections will now limit the mass flow of solids because a density perturbation in the solids suspension in this case would be allowed to travel faster than the superficial solids velocity, to create temporary or permanent blockages in the pipeline. The simple expression for the maximum mass flow of solids for stable conveying obtained from this chain of thought

$$\dot{m}_{\max} = \frac{\pi \rho_b g^{1/2} D^{5/2}}{4} \qquad (2)$$

correlates reasonably well with data obtained for LDPE and sand. By pursuing this line of thought it may be possible to obtain new correlations based on simple physical models instead of, or in addition to, experimental correlations.

At present we are investigating possible connections between the state of the settled or flowing layer and the conveying limit of the powder. This is done by measuring particle concentrations and velocities close to the conveying limit. Further tests are also planned with more complex line geometries and larger pipe sizes.

7. REFERENCES

(1) F. Rizk, Pneumatic Conveying at Optimal Conditions and a Solution of Barth's Equation (1976), Pneumotransport 3 D4, 43-58.

(2) S. Matsumoto, M Hara, S Saito, S. Maeda, Minimum transport velocity for horizontal pneumatic conveying (1974), Journal of Chemical Engineering of Japan 7, 425-430.

(3) Francisco J. Cabrejos and George E. Klinzing, Incipient motion of solid particles in horizontal pneumatic conveying (1992), Powder Technology 72, 51-61.

(4) Francisco J. Cabrejos and George E. Klinzing, Pickup and saltation mechanisms of solid particles in horizontal pneumatic transport (1994), Powder Technology 79, 173-186.

(5) Walter Barth, Absetzung, Transport und Wiederaufwirbelung von Staubförmigem Gut im Luftstrom (1963), Chemie-Ing.-Techn. 35, 209-214.

(6) H.E.Rose and R.A.Duckworth, Transport of Solid Particles in Liquids and Gases (1969), The Engineer 392-483.

(7) R. Pan, B. Mi and P.W. Wypych, Design of Pneumatic Conveying Systems for Granular Bulk Solids, Proceedings of international conference on advanced technology and equipment of handling (1994), ATEMH'94, Shanghai, 815-820.

(8) M. Abramowitz and I. A. Stegun, Handbook of Mathematical Functions (1972), Dover New York.

APPENDIX

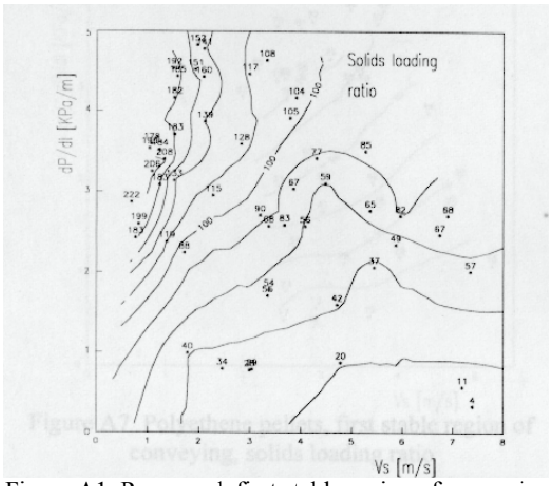

Figure A1 Rape seed, first stable region of conveying, solids loading ratio

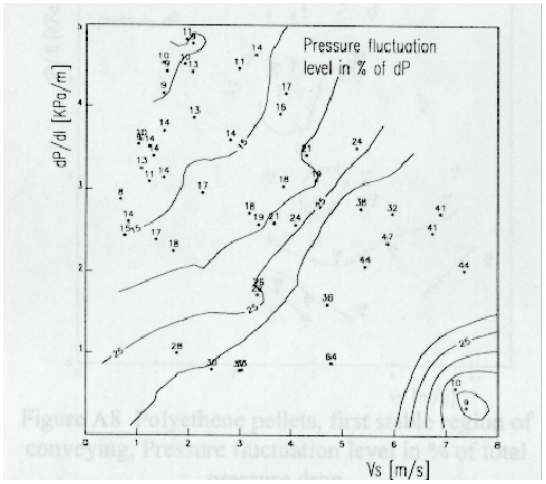

Figure A2 Rape seed, first stable region of conveying, Pressure fluctuation level in % of total pressure drop

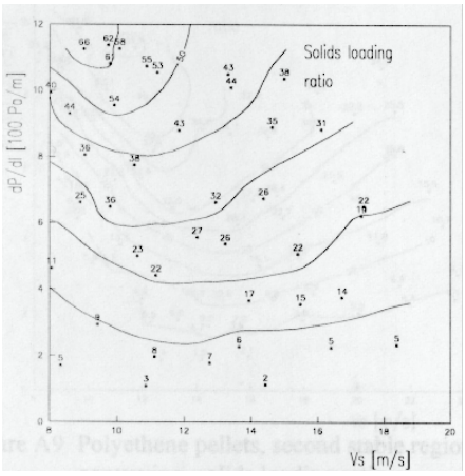

Figure A3 Rape seed, second stable region of conveying, solids loading ratio

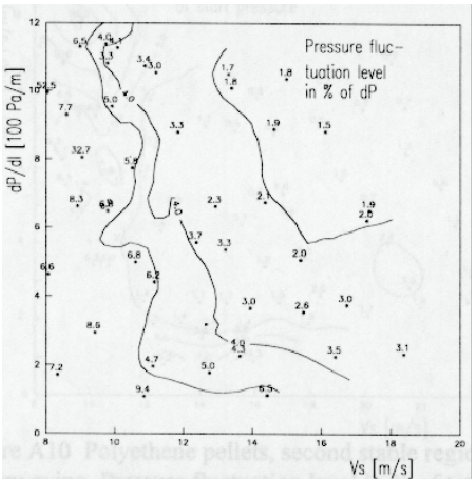

Figure A4 Rape seed, second stable region of conveying, Pressure fluctuation level in % of the total pressure drop

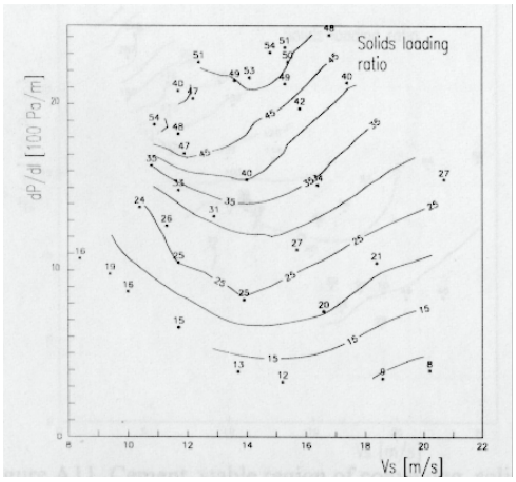

Figure A5 Leighton Buzzard sand, stable region of conveying, solids loading ratio

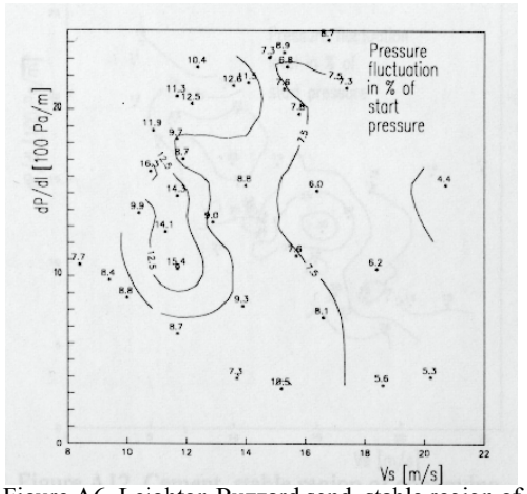

Figure A6 Leighton Buzzard sand, stable region of conveying, Pressure fluctuation level in % of the total pressure drop

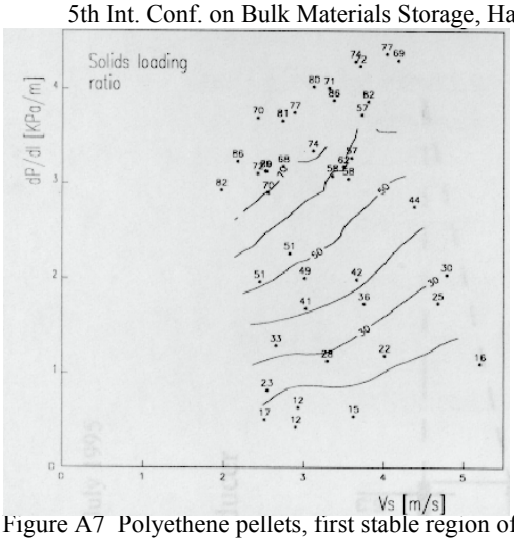

Figure A7 Polyethene pellets, first stable region of conveying, solids loading ratio

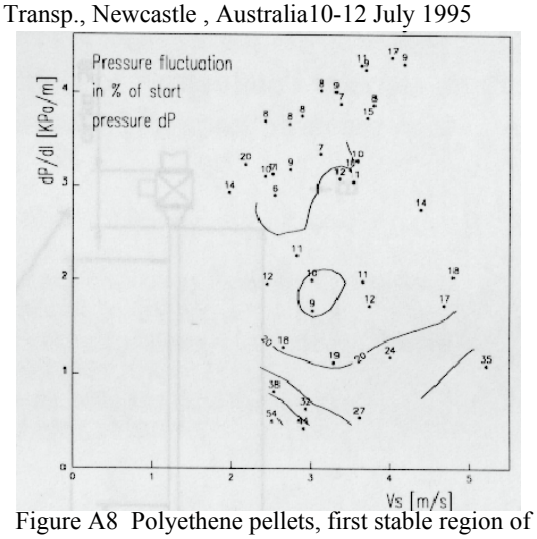

Figure A8 Polyethene pellets, first stable region of conveying, Pressure fluctuation level in % of total pressure drop

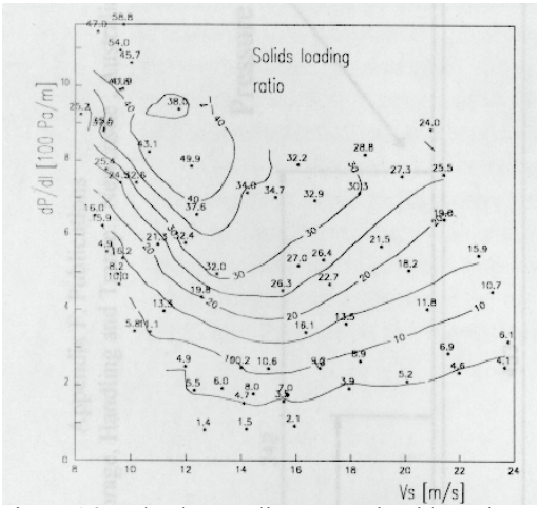

Figure A9 Polyethene pellets, second stable region of conveying, solids loading ratio

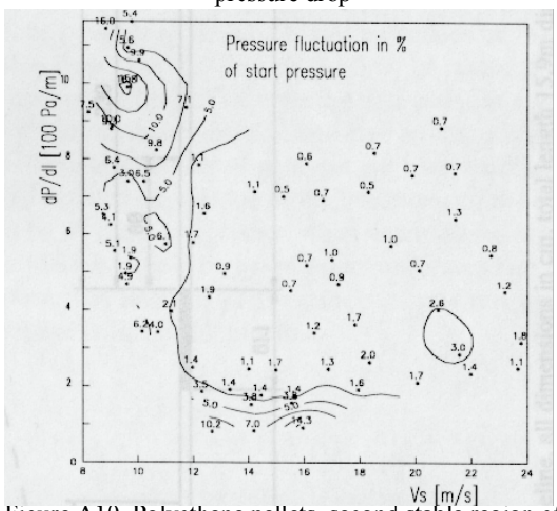

Figure A10 Polyethene pellets, second stable region of conveying, Pressure fluctuation level in % of total pressure drop

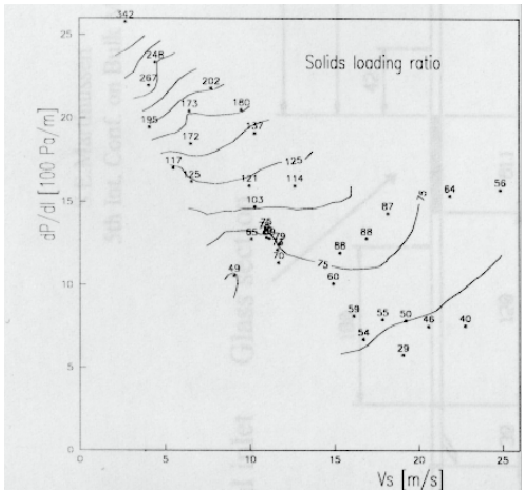

Figure A11 Cement, stable region of conveying, solids loading ratio

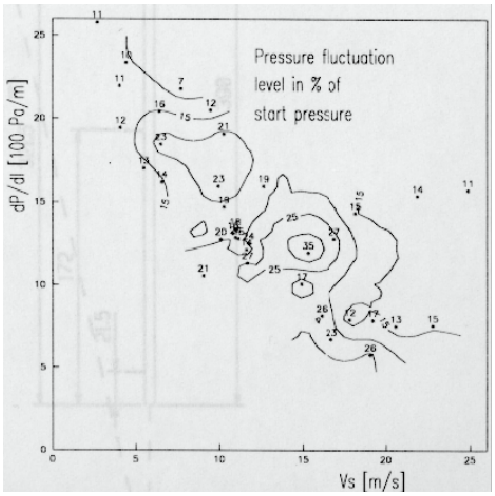

Figure A12 Cement, stable region of conveying, Pressure fluctuation level in % of the total pressure drop

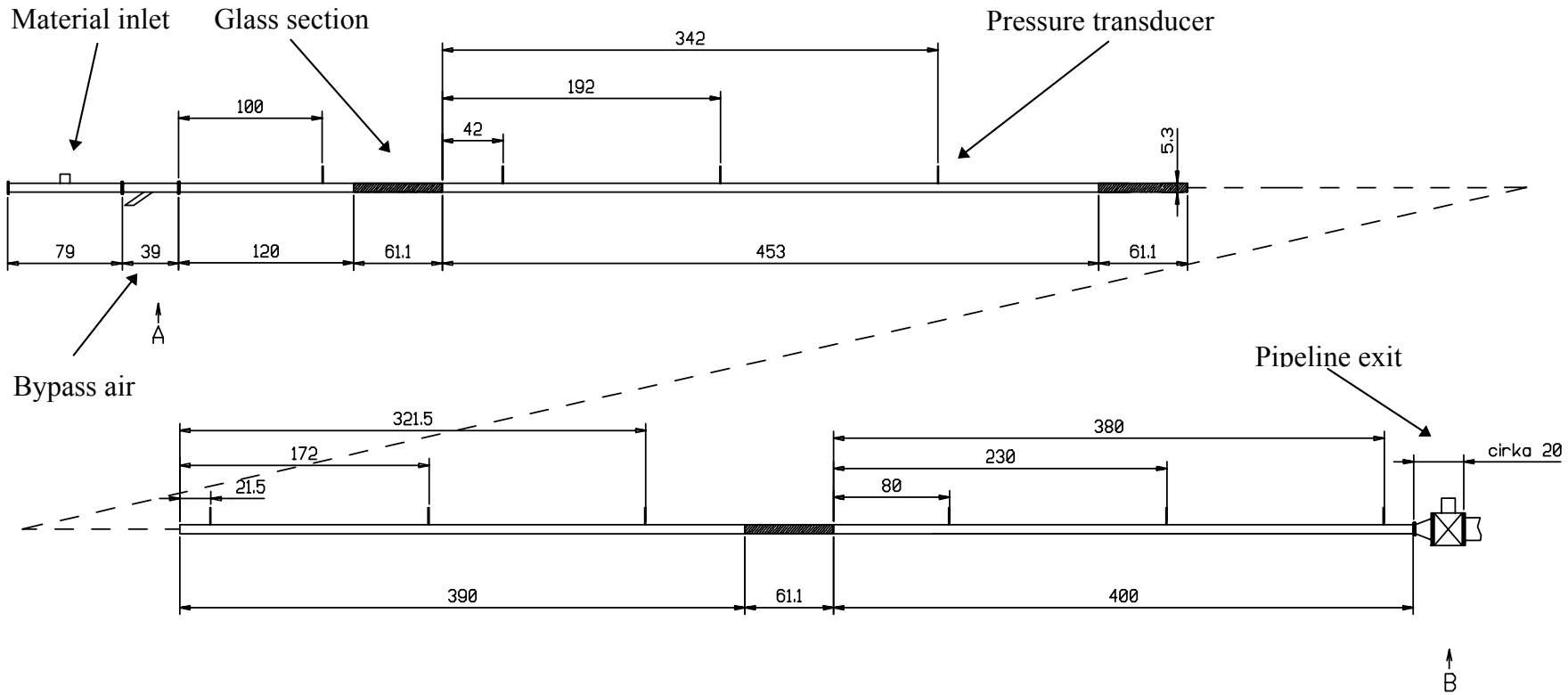

Figure A13 The layout of the pipeline, all dimensions in cm, total length 15,9m diameter 53 mm.

5th World Congress of Chem. Eng.,San Diego, California,, U.S.A.14-18 July 1996

The Effect of Physical Characteristics of Particulate Materials on their Conveyability in Pneumatic Transport Systems

S.E.Martinussen[1)], S.R.Woodhead[2)] , S.R.deSilva[3)] , A.R.Reed[2)]

1) TEL-TEK, Dept. of Powder Science and Technology Research, Kjølnes Ring, 3914 PORSGRUNN, NORWAY
2) The Wolfson Centre for Bulk Solids Handling Technology, University of Greenwich, London, SE18 6PF, UK
3) Telemark College, Department of Technology, Kjølnes Ring, 3914 PORSGRUNN, NORWAY

The results of an experimental investigation to establish a link between the physical characteristics of a powder, measurable on small samples in a laboratory, and the conveyability of a material in a pneumatic conveying line, will be presented. The investigation focuses on the limit between stable "suspension" flow, and unstable flow. The stability of the flow of material in the pipeline is used as a criterion to identify the conveying limit. The investigation includes a variety of common particulate materials with widely differing characteristics, and also an investigation of the effects of horizontal to horizontal bends. Several methods of analysis are used to determine what happens close to the conveying limit. The detailed knowledge of the behaviour of the system close to the conveying limit is considered to be of great importance when establishing new and better models for minimum conveying limits. Models should be based on an understanding of the basic physics of a blockage or of unstable flow. The analysis of the data confirms this point of view, and focuses on the identification of blockage points in the pipeline.

5th World Congress of Chem. Eng.,San Diego, California,, U.S.A.14-18 July 1996

INTRODUCTION

When designing new, or modifying the use of existing pneumatic conveying systems one of the main factors that has to be taken into consideration is the conveying limit of the transported material. Several correlations exist for predicting the conveying limit [1 - 8]. To evaluate and improve these correlations, an investigation of the conveying properties and physical characteristics of seven powders, that are frequently transported pneumatically, has been initiated. The point of departure has been that an improved understanding of what happens just before a pipeline is blocked is of great importance. This will make it possible to establish models based on physical understanding of blockages.

PREVIOUS WORK

Evaluations of existing models [9 - 10] show that they at best can predict the conveying limit of a material to within ±30%. Some of the models are in error by several hundred percent when compared to experimental observations. The inaccuracy of these models might come from the limited amount of data included in the test work. A serious flaw with many of the test rigs used is that they are too short, and do not allow high feed rates. A list of existing models can be found in Table 1. The work of Rizk is considered to be the best, and in this investigation it has proved to give conveying limit values correct to within ±30% of the measured value.

Table 1 Extracts of information about different models for determining conveying limits.

Author	Type of model	Area of validity [particle diameter, or as specified]	Materials tested	Length of test pipeline [m]	Diameter of test pipeline [mm]
Thomas	Dimensional analysis and experimental correlation	97 - 2000 μm	From other authors : rape seed, glass beads, sand, cress seed, mustard seed, own water/glass bead experiments	N.A.	16 - 44
Doig and Roper	Comparison of existing models and data, which leads to a new correlation.	150 μm - 6 mm	From other authors : rape seed, glass beads, salt, sand, wheat, tenite, soya beans.	N.A.	N.A.
Matsumoto et. al.	Pressure drop model and minimisation	290 - 2600 μm $1.0 \leq \rho_p \leq 8.7$, $5 \leq Fr \leq 30$	Spherical particles of: glass, copper and polystyrene	11 and 26	26 and 49
Rose and Duckworth	Dimensional analysis and experimental correlation	0.96 - 3.2 mm	Mustard seed, glass, steel and lead	3.66 and 9.75	32
Rizk	Experimental correlation.	0.7-6 mm $\rho_p \approx 1000$ kg/m^3	Polystyrol and styropor.	N.A.	50-400
Zenz	Analogy to free fall velocity, experimental correlation.	50 μm - several mm	Rice Krispies, rape seed, glass beads, sand, salt, cracking catalyst, soybeans, tenite.	4.6 and 2.7	32 and 63

THE TEST PROGRAM

The test program devised to address this problem establishes conveying characteristics and characteristic properties for all the powders. The conveying tests have been carried out in a 15m long pipeline with an internal diameter of 53mm. This pipeline has also been extended to 21m including a long radius bend, with a diameter ratio of 30, positioned 13m after the start of the pipeline.

The physical characteristics of the powders included in the test can be found in Table 2. Only the physical characteristics that were determined for all materials have been included. This is to enable

a comparison of characteristic properties, that are obtainable for all of the materials, with conveying properties.

Table 2 Physical characteristics of materials.

	Particle density [kg/m3]	Poured density [kg/m3]	Median particle size [μm]	Mean particle size [μm]	Minimum fluidisation velocity [m/s]	Permeability prior to fluidisation [m2/(Pa*s)]	Wall friction angle against ST37 [Deg]	Static angle of repose [Deg]	Dynamic angle of repose [Deg]
Polyethylene Pellets	913	555	3654	3667	$1.2*10^{0}$	$1.6*10^{-3}$	14.8°	38°	37°
Rape Seed	1164	687	1660	1650	$8.0*10^{-1}$	$6.5*10^{-4}$	18.7°	30°	30°
Sand	2645	1590	622	687	$2.7*10^{-1}$	$2.0*10^{-4}$	16.3°	36°	33°
PVC Granules	1414	518	296	472	$1.2*10^{-1}$	$7.5*10^{-4}$	19.7°	37°	35°
Alumina	3399	939	78	87	$3.6*10^{-3}$	$4.2*10^{-6}$	22.8°	47°	34°
Microdol 100	2865	1212	66	91	$3.2*10^{-4}$	$4.3*10^{-7}$	26.1°	63°	39°
Cement	3095	734	11	15	$1.0*10^{-3}$	$3.6*10^{-6}$	29.3°	65°	33°

For each of the conveying characteristics that have been obtained, the conveying limits have been identified. Several limitations on conveyability may be considered. The two limits that can easily be identified by objective measures are minimum pressure drop limit and blockage limit. By watching the pressure at the starting point of the pipeline, the limit of stable conveying in suspension flow, and the maximum limit of plug flow, can also be found. Instabilities show as peaks in the pressure plot.

The conveying characteristics and the conveying limits are shown in Figure 1 a) through to g). The Polyethylene and Rape Seed show typical conveying characteristics for coarse materials with high permeability. They have two separate regions of stable conveying, and four conveying limits are present. For the other materials only blockage limit and minimum pressure drop limit are present.

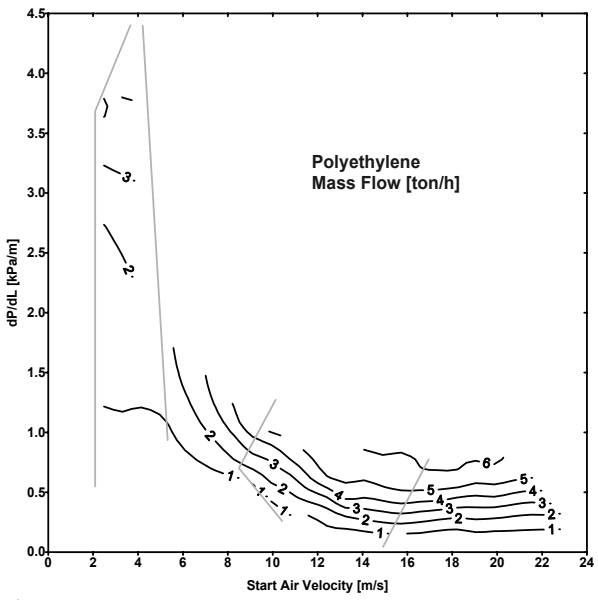

a)

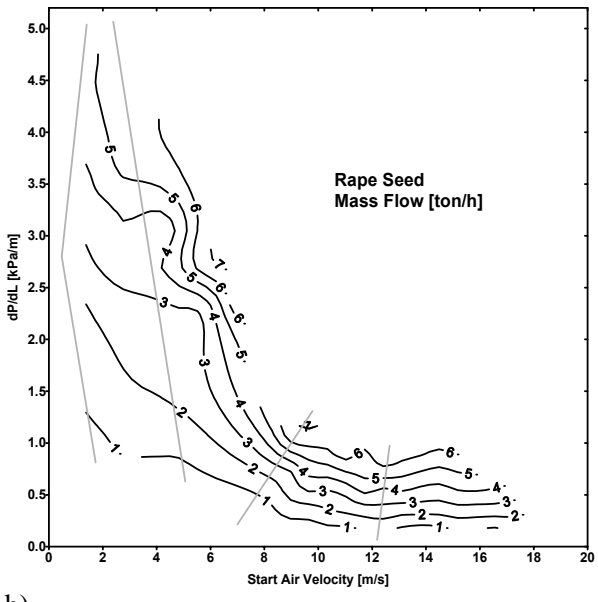

b)

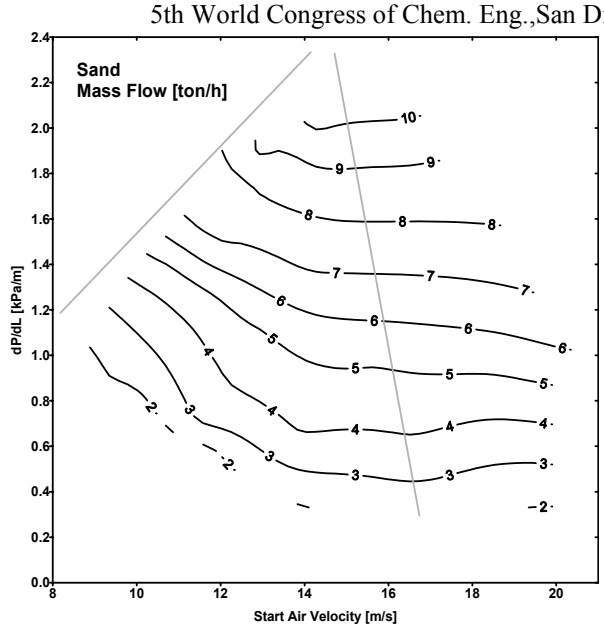

c)

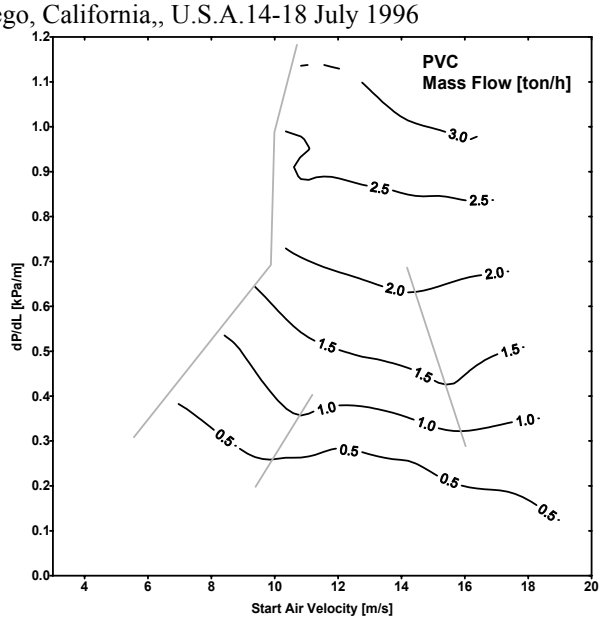

d)

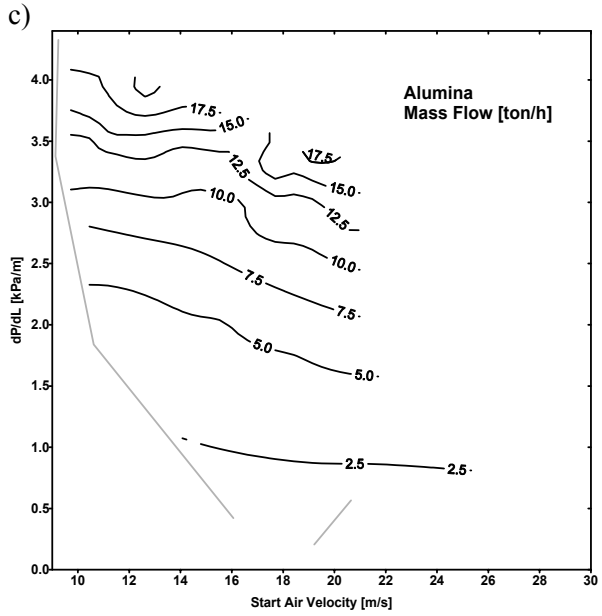

e)

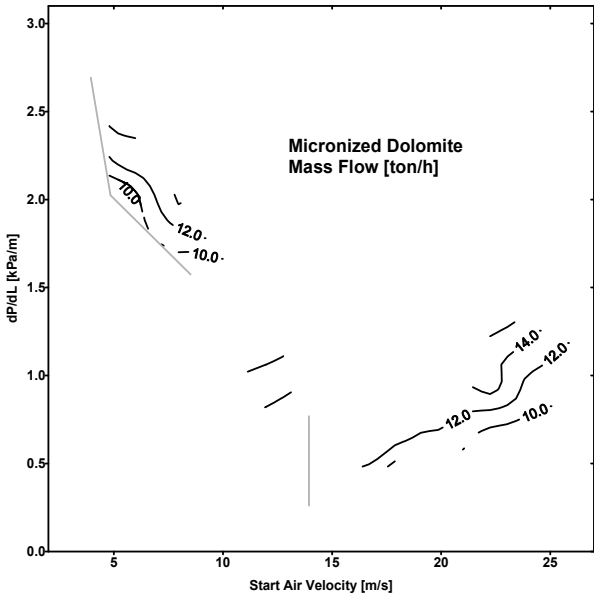

f)

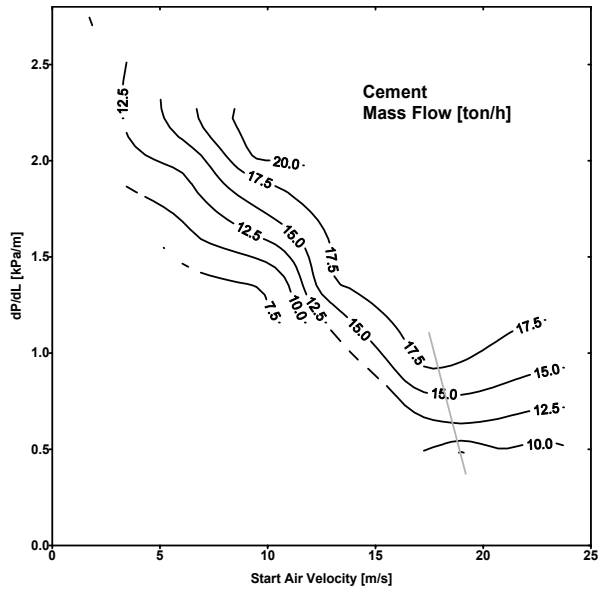

g)

Figure 1 Conveying characteristics and limits for the materials that have been tested in a 53 mm diameter pipeline, showing blockage boundaries and minimum pressure drop

ANALYSIS OF THE DATA

Visual observation of saltation, that has been used by some authors [1, 3, 4, 5, 8] to identify conveying limits, does not correspond to the blockage limits or to the pressure drop minima. For the PVC material, saltation was only observed at very low feed rates and air velocities. Saltation was only observed when the mass flow rate of solids was below 0.5ton/h and when the air flow velocity was below 10m/s. The same is the case for sand, which showed saltation when the mass flow rate of solids was below 7.5ton/h and when the air flow velocity was below 13m/s.

Blockage points can easily be identified by carrying out conditional averaging of pressure profiles along the pipeline. By selecting a trigger condition that identifies early stages of blockage, several events can be selected and a typical pressure profile can be identified. Frequency analysis of the pressure signal along the pipeline shows that these blockage events correspond to high pressure fluctuations at the beginning of the pipeline. The materials that show a smooth transition into moving bed flow, in this case cement and micronized dolomite, exhibit pressure fluctuations with a maximum in the middle of the pipeline.

The observations of pressure fluctuations and blockage suggests that the mass flow is limited by blockages occurring at the beginning of the pipeline. According to basic texts on fluid dynamics, the Froude number can be used to characterise the state of flow in open channels [11]. Flow with Fr=1 corresponds to critical flow, and is the limit case for when hydraulic jumps can occur. In a closed duct, the section where Fr<1 (Fr is the Froude number of the flow of solids) will give unstable transport if h≥D and $\rho=\rho_b$ (h is the height of the moving layer of solids, D is pipeline diameter, ρ is density, and subscript b indicates that it is the bulk density that is to be used). This low velocity section will limit the capacity of the transport system. The highest obtainable mass flow of solids will be at Fr<1 when h=D and $\rho=\rho_b$. We then have :

$$\dot{m} = \rho_b v_b \pi \frac{D}{4} \;\wedge\; Fr = \frac{v_b}{\sqrt{gD}} \le 1$$

$$\Downarrow$$

$$\frac{4\dot{m}}{\pi \rho_b D^2} \le \sqrt{gD}$$

$$\Updownarrow$$

$$\dot{m} \le \dot{m}_{max} = \frac{\pi \rho_b g^{1/2} D^{5/2}}{4}$$

which should be the maximum flow rate of solids at stable conditions (g is the acceleration due to gravity). It is possible to imagine a plug being pushed through the system at higher feed rates, but this would then cause considerably higher friction forces and unstable flow. The validity of the fluid powder analogy used above rests on the assumption that surface gravity waves propagate on fluidized powders in the same way as on liquids. This is being investigated separately [12]. The expression should be valid for the type of powders that can not be extruded as a single plug through the pipeline, and show almost perfect correlation with values obtained for PVC and sand.

The use of the fluid powder analogy above, to obtain mass flow limitations in pneumatic conveying systems, motivates further investigation of its validity. The next natural step would be to use it to characterise the stability of the flow of particulate material in the pipeline in the same way as in two phase liquid gas flows [13].

CONCLUSION

The visual observations of saltation show that this way of identifying conveying limits is not correlated to pressure minima or blockage. At very low feed rates it corresponds to flow between pressure minima and blockage for sand and PVC. The identification of the pressure minima can be achieved with no problems related to the objectivity of the observer.

All analyses carried out so far show blockages occurring at the beginning of the pipeline. Introducing a bend downstream does not change this. An expression for the maximum flow of solids in the pneumatic transport system can be found. The expression is based on a fluid-powder analogy where the surface gravity wave propagation velocity limits the mass flow of solids. It correlates well with observed values for PVC and sand. Other materials, that are capable of being extruded, will not have a maximum mass flow limited in the same way.

The intention is now to use the data obtained to proceed with multi-variable data analysis to identify correlations between physical characteristics and conveying limits. The necessity for the determination of other characteristics than those listed in Table 2 will, it is hoped, also emerge as a result of such an analysis.

REFERENCES

1 David G. Thomas (1962) Transport Characteristics of Suspensions: Part VI. Minimum Transport Velocity for Large Particle Size Suspensions in Round Horizontal Pipes. A.I.Ch.E.Journal 8, 373-378.
2 Walter Barth(1963) Absetzung, Transport und Wiederaufwirbelung von Staubförmigem Gut im Luftstrom. Chemie-Ing.-Techn. 35, 209-214.
3 F.A.Zenz (1964) Conveyability of materials of mixed particle size, Industrial and Engineering Chemistry / American Chemical Society 3, 65-75.
4 I.D.Doig and G.H.Roper (1963) The minimum Gas Rate for Dilute Phase Solids Transportation in a Gas Stream. Australian Chemical Engineering 1, 9-19.
5 H.E.Rose and R.A.Duckworth (1969) Transport of Solid Particles in Liquids and Gases. The Engineer 392-483.
6 F. Rizk (1976) Pneumatic Conveying at Optimal Conditions and a Solution of Barth's Equation. Pneumotransport 3 D4, 43-58.
7 F. Rizk (1982) Pneumatic Transport in Dilute and Dense Phase. Bulk Solids Handling 2.
8 S. Matsumoto, M Hara, S Saito, S. Maeda (1974) Minimum transport velocity for horizontal pneumatic conveying. Journal of Chemical Engineering of Japan 7, 425-430.
9 H.Arastoopour, M.V.Modi, D.V.Punwani and A.T.Talwalkar (1979) A review of design equations for dilute-phase gas-solid horizontal conveying systems for coal and related materials. Proceedings of the Technical Program, Int. Powd. and Bulk Solids Handling and Processing, Philadelphia, 339-356.
10 S.E.Martinussen (1995) The Effect of Physical Characteristics of Particulate Materials on their Conveyability in Pneumatic Transport Systems. Document to support an application for transfer of registration from MPhil to PhD, University of Greenwich.
11 F.M.White, Fluid Mechanics, McGraw-Hill, 1988
12 Svein E.Martinussen, Mitsuhiro Wada, Sunil R.deSilva, Surface gravity waves on fluidized powders. Fluid Particle Interactions IV, 12-17 May 1996, Davos Switzerland.
13 D.Barnea and Y.Taitel, Kelvin-Helmholz stability criteria for stratified flow: viscous versus non viscous (inviscid) approaches. International Journal of Multiphase Flow, 19, 4, pp639-650, 1993